UNIVERSITY OF ICELAND

Modeling of energy and mass balance using remote sensing for seasonal snow and glaciers in Iceland

Andri Gunnarsson

2022

FACULTY OF CIVIL AND ENVIRONMENTAL ENGINEERING

Modeling of energy and mass balance using remote sensing for seasonal snow and glaciers in Iceland

Andri Gunnarsson

Dissertation submitted in partial fulfillment of a
Philosophiae Doctor degree in Civil Engineering

Supervisor
Sigurður M. Garðarsson

Doctoral Committee
Sigurður M. Garðarsson
Jessica D. Lundquist
Óli G. B. Sveinsson
Tómas Jóhannesson

Opponents
Jason E. Box
Peter L. Langen

Faculty of Civil and Environmental Engineering
School of Engineering and Natural Sciences
University of Iceland
Reykjavik, September 2022

Modeling of energy and mass balance using remote sensing for seasonal snow and glaciers in Iceland

Dissertation submitted in partial fulfillment of a *Philosophiae Doctor* degree in Civil Engineering

Faculty of Civil and Environmental Engineering
School of Engineering and Natural Sciences
University of Iceland
Hjarðarhaga 2- 6
107 Reykjavík Reykjavik
Iceland

Telephone: 525-4000

Bibliographic information:
Andri Gunnarsson (2022) *Modeling of energy and mass balance using remote sensing for seasonal snow and glaciers in Iceland*, PhD dissertation, Faculty of Civil and Environmental Engineering, University of Iceland, 195 pp.

ISBN 978-9935-9647-7-9

Author ORCID: orcid.org/0000-0002-9041-8763

Printing: Háskólaprent
Reykjavik, Iceland, September 2022

Abstract

Snow and glacier research is important in Iceland for a variety of reasons. Water resource forecasting for hydro-power production is important and monitoring of long-term changes and trends provide guidance for adoption strategies due to climate change. Activity in glacier-covered volcanoes can cause volcanic ash and tephra deposits leading to enhanced melt or in some cases glacier surface isolation reducing melt significantly. The high natural climate variability can pose a risk to the reliability of the energy production and delivery systems as drought conditions, low-flow periods, and years with low summer melt are challenging to predict. Many Earth observing satellites provide data that can improve estimations of physical processes that can be challenging to model accurately, such as snow cover and surface albedo of snow and ice-covered surfaces.

In this research, satellite data were used to create gap-filled products of daily snow cover and surface albedo in Iceland from 2000 to 2021 at a 500 m horizontal resolution. The products relied on data collected from the two satellites carrying the MODIS sensor, Aqua and Terra, providing sub-daily overpass. A process pipeline was developed to merge the daily data and apply temporal aggregation to reduce the high number of cloud-obscured pixels. Due to high cloud cover, yielding many pixels obscured by clouds even after merging and temporal aggregation, machine learning models were further developed to fully reclassify the remaining unclassified data. The output from this process was a spatio-temporal product with capabilities for further analysis and extraction of various statistical parameters describing snow cover and albedo properties in Iceland. To better understand the seasonal and inter-annual variability and possible trends, a surface energy balance model was developed utilizing remotely sensed snow cover and albedo as prognostic variables. Surface albedo was used to constrain net shortwave radiation forced at a snow-covered surface and fractional snow cover provides an aerial constraint for seasonal snow outside of glaciers by estimating the fractional snow cover of pixels, scaling the calculated melt energy accordingly. Large-scale atmospheric circulation anomalies and surface energy balance were analyzed to study relationships of the data and understanding the drivers of variability.

The results show high seasonal and inter-annual variability in surface energy balance, snow cover and surface albedo for snow- and ice-covered surfaces in Iceland. The high variability in surface energy balance reflects the high variability of albedo, especially for glaciers. The impacts of light-absorbing particles (LAPs), both from tephra deposits due to volcanic eruptions and dust deposits from airborne dust, were estimated to provide understanding of the extent, magnitude and impact on surface energy balance and showed a significant melt enhancement for years with high LAPs deposits. Sea

surface temperature impacts cloud cover in Iceland during the melting season. Recent abrupt changes in the sea surface conditions near Greenland and SST south of Iceland correlate strongly with cloud cover in Iceland during the melt season. Cloud cover acts as a modulator on the incoming short-wave radiation available for surface forcing, i.e., surface energy balance. Large-scale patterns such as the Greenland Base Index (GBI) and the North Atlantic Oscillation (NAO) also showed significant correlation to controlling parameters relating to the surface energy balance.

Útdráttur

Fjöldi gervitungla á sporbraut um jörðu gera athuganir af yfirborði jarðar sem geta bætt mat og aukið skilning á eðlisfræðilegum ferlum í vatna- og jöklafræði. Mörg þessara ferla er krefjandi að skilja og herma rétt með reiknilíkönum, eins og snjóhula og endurkastsstuðul yfirborðs hulið snjó og ís, en þar geta fjarkönnunargögn bætt skilning og aukið gæði hermanna.

Í verkefninu voru fjarkönnunargögn notuð til að búa til samfelldar tímaraðir í tíma og rúmi fyrir daglegt mat á snjóhulu og endurkastsstuðli fyrir yfirborð hulið snjó og ís fyrir tímabilið 2000 til 2022 á Íslandi. Afurðirnar nýttu gögn úr MODIS skynjara tveggja gervihnatta sem dagleg fóru yfir Ísland frá 2000. Þróuð var úrvinnsluaðferð sem nýtti gögn skynjaranna og tók tillit til mikillar skýjahulu á Íslandi. Tölfræðilegar aðferðir voru þróaðar til að sía villur í gögnunum og aðferðir vélræns náms nýttar til að flokka óflokkaða myndreiti. Afurð þessara úrvinnsluaðferðar voru samfelld gögn í tíma og rúmi sem bjóða upp á frekari greiningar, vöktun á breytingum og sem inntak í frekari líkangerð af snjó og jöklum á Íslandi. Gæði afurðana voru sannreyndar með mönnuðum athugunum, athugunum úr veðurstöðum utan og á jöklum en einnig fjarkönnunargögn úr öðrum gervihnöttum í hærri upplausn. Til að skilja betur breytileika innan árs, sem og milli ára, var þróað orkuskiptalíkan sem nýtir mat á snjóhulu og endurkastsstuðli til að meta betur orkuskipti yfirborðs hulið snjó og ís. Endurkastsstuðull var nýttur sem inntak til að skorða magn stuttbylgjugeislunar sem nýtist til leysingar og hlutfallstala snjóhulu innan myndreits utan jökla gefur skorður á magni leysingarorku tiltækri fyrir árstíðarbundin snjó. Niðurstöðurnar voru settar í samhengi við stórskala breytileika í loftslagi og veðri á og við Ísland, til að skilja betur drifkrafta breytileika fyrir árstíðarbundin snjó og jökla.

Niðurstöðurnar staðfesta mikinn breytileika innan árs og milli ára fyrir snjóhulu, endurkastsstuðul og orkuskipti yfirborðs á Íslandi. Mikill breytileiki í orkuskiptum yfirborðs endurspeglast sérstaklega í breytileika endurkastsstuðuls en ljósgleypnar agnir (ryk og aska) í yfirborði höfðu mikil áhrif. Áhrif ljósgleypinna agna, með uppruna í eldgosum eða frá óstöðugum yfirborðum utan jökla (sandfok), voru metin til að skilja betur umfang og áhrif þeirra á orkuskipti. Niðurstöðurnar sýna umfangsmikil áhrif fyrir ár þar sem mikið magn agna sest í yfirborð, sérstaklega jökla, t.d. þegar eldgos eiga sér stað að vori og sumri til. Einnig komu í ljós tengsl sjávarhita í kringum og við Íslandstrendur við skýjahulu á landi. Sjávarhitafrávik sunnan Grænlands og Íslands hafa sterk vensl við skýjahulu á Íslandi yfir vor og sumar. Skýjahula mótar magn innfallandi stuttbylgjugeislunar frá andrúmslofti sem er tekin upp af yfirborði til leysingar á snjó og íss, þ.e. orkuskipti yfirborðs. Önnur stórskala ferli eins og Greenland Base Index

(GBI) og North Atlantic Oscillation (NAO) sýndu einnig marktæk vensl við lykilbreytur í orkuskiptum yfirborðs.

"I want to thank me for believing in me, I want to thank me for doing this hard work, I want to thank me for having no days off. "
Snoop Dogg

Contents

List of Figures

List of Tables

List of Original Publications

I: Gunnarsson, A., Garðarsson, S. M., and Sveinsson, Ó.G.B.: Icelandic snow cover characteristics derived from a gap-filled MODIS daily snow cover product, Hydrol. Earth Syst. Sci., 23, 3021–3036, https://doi.org/10.5194/hess-23-3021-2019, 2019.

II: Gunnarsson, A., Gardarsson, S. M., Pálsson, F., Jóhannesson, T. and Sveinsson, Ó.G.B.: Annual and inter-annual variability and trends of albedo of Icelandic glaciers, The Cryosphere, 15, 547–570, https://doi.org/10.5194/tc-15-547-2021, 2021.

III: Gunnarsson, A., Gardarsson, S. M., Pálsson, F.: Modeling of surface energy balance for Icelandic glaciers using remote sensing albedo, manuscript in preparation, to be submitted.

IV: Gunnarsson, A., Gardarsson, S. M.: Spatial estimation of snow water equivalent by modeling of the seasonal snow and glaciers in Iceland, manuscript in preparation, to be submitted.

Acknowledgments

This dissertation would never have materialized without the support of numerous people, academics, professionals as well as friends and family.

First, to my advisor, Sigurður M. Magnússon, I am very grateful for the opportunity to undertake this dissertation with me and for a fruitful and enjoyable collaboration, frequent motivation, and the right amount of "push". I am thankful for the flexibility he has shown me as well as supporting every step of this journey.

To Óli G. B. Sveinsson at Landsvirkjun, I am especially thankful. Óli has supported many of the overly ambitious ideas I have proposed, including perusing this dissertation. I am very thankful for the flexibility and support he has shown towards the work and for believing in that the final product will have value.

I am ever thankful to Jessica D. Lundquist, professor at the University of Washington, for supporting my Valle Scholarship application leading to the opportunity for me and my family to spend a year in the US. I am also very gratuitous for the warm welcome into Jessica's Snow Hydrology Group at UW and for all the discussion and time allocated to me. The time in the US was not only valuable for me in an educational and networking aspect but also for my wife and kids who built friendships with many people which we still reminisce about. Our time at our US home at 119 Northwest 55th Street was unforgettable.

I am very gracious to Tómas Jóhannesson at IMO for taking time from his schedule to participate in this with me. I have been lucky to work with Tómas in many other aspects besides this dissertation but in all cases I have learnt a lot. I will never make the mistake between the en dash (-) and the em dash (–) again.

I am very thankful to all the people I meet at the year spent in Seattle, people at the Snow Hydrology Group, David Shean, Faisal Hossain, Ed Waddington who all impacted me and, in some way, had a contribution to all of this. David Shean being extremely motivational in remote sensing aspects and Faisal Hossain for the fun talks and insights. Our landlord Jim who enabled us to have an amazing family experience while in Seattle will never be forgot.

Landsvirkjun receives a special thanks for the indirect funding of the project and allowing work flexibility to pursue the project.

I would like to thank Finnur Pálsson, which is not only a good colleague, but I feel lucky to call him my friend. You have motivated me more than you know, a kinder, better person is hard to find.

All my family and friends, wife Guðfinna, kids Bergsteinn and Elísabet, mom and dad you know your part, you are the most important piece in this dissertation. I love you all.

The opponents for the dissertation defense, Jason E. Box and Peter L. Langen, also receive thanks for reserving time and interest in the work.

1 Introduction

Snow is a crucial component of the global climate and hydrological system,regulating surface energy budgets, modulating temperatures and driving atmospheric systems (Barry, 2002; Henderson et al., 2018). Estimations show that one-sixth of the global population lives in areas where streamflow is dominated by snow melt runoff (Barnett et al., 2005; Biemans et al., 2019). This demonstrates that information about water stored annually as snow, as well as onset of melt in spring, is crucial information to understand and predict climate variability and change,flooding, avalanches, forecasting water resources and estimating ecological interactions among other important processes (Mote et al., 2005; Jóhannesson et al., 2007; Acevedo et al., 2010; Fischer et al., 2011).

Generally, in the northern hemisphere, the development of seasonal snowpack and glacier mass balance is divided in two main phases, snow accumulation during winter and snow/ice melt in the spring and summer depending on the extent, elevation and climatic controls (Marks et al., 1998). During the accumulation period, precipitation mostly falls in solid form building up the snow pack. With warming temperatures in spring, average snow pack temperatures increases steadily until the point where the cold content of the snow pack has been absorbed and melt occurs within the snowpack leading to runoff. The main control on snowpack accumulation and timing of snow melt, when the snow pack starts to release melt water, is the snow pack energy balance. The energy balance is controlled by energy fluxes between the snow surface and the atmosphere controlling the evolution and intensity of the snow melt.

During melt season in the Northern Hemisphere absorbed solar energy by snow- and ice-covered surfaces is mainly constrained by surface albedo controlling the radiative forcing of seasonal snow, glaciers, ice caps and the associated ice-albedo feedback (Male and Granger, 1981; Fernandes et al., 2009; Guðmundsson et al., 2009; Hudson, 2011; Box et al., 2012; Chen et al., 2016). Surface albedo is defined as the unitless ratio of the radiant flux reflected from Earth's surface to the incident flux. It is a controlling parameter which governs the portioning of the short-wave radiative energy between the atmosphere and surface and therefore a control of the surface energy balance modulated by the solar zenith angle, cloud optical thickness, cloud cover and transmission properties of the atmosphere (Klein and Stroeve, 2002; Gardner and Sharp, 2010; Donohoe and Battisti, 2011). Changes in snow- and ice-cover duration and extent can magnify the effect on climate for warming and cooling due to the complex and self-enhancing ice-albedo feedback with temperature (Barnett et al., 2005; Adam et al., 2008; Choi et al., 2010; Hudson, 2011; Flanner et al., 2011; Box et al., 2012). Due to the importance of snow and ice albedo properties, as an amplifier of climate change,

surface albedo has been defined as an Essential Climate Variable and a requirement for climate monitoring (WMO, 2011; Bojinski et al., 2014).

Iceland is a small island located in the North Atlantic Ocean with an area of 103. 000 km^2 close to the Arctic Circle, between 63–67° N and 18–23° W. Climate in Iceland is driven by oceanic and atmospheric circulations. The North Atlantic Current, a branch of the Gulf Stream towards north-east, transports warm ocean water to the North Atlantic Subpolar Gyre, explaining milder climates at higher latitudes (Lozier et al., 1995; Rossby, 1996; Ólafsdóttir et al., 2010; Knudsen et al., 2012). Flowing along the southern and western Icelandic coast the Irminger Current brings relatively warm Atlantic water towards Iceland moderating climate. In the north and east, the cold East Greenland Current, originated in cold Polar waters, and the cold East Icelandic Current, a branch of the East Greenland Current, bring cold water masses towards the Icelandic coast in the north and east, respectively (Renner et al., 2018; Zhao et al., 2018).

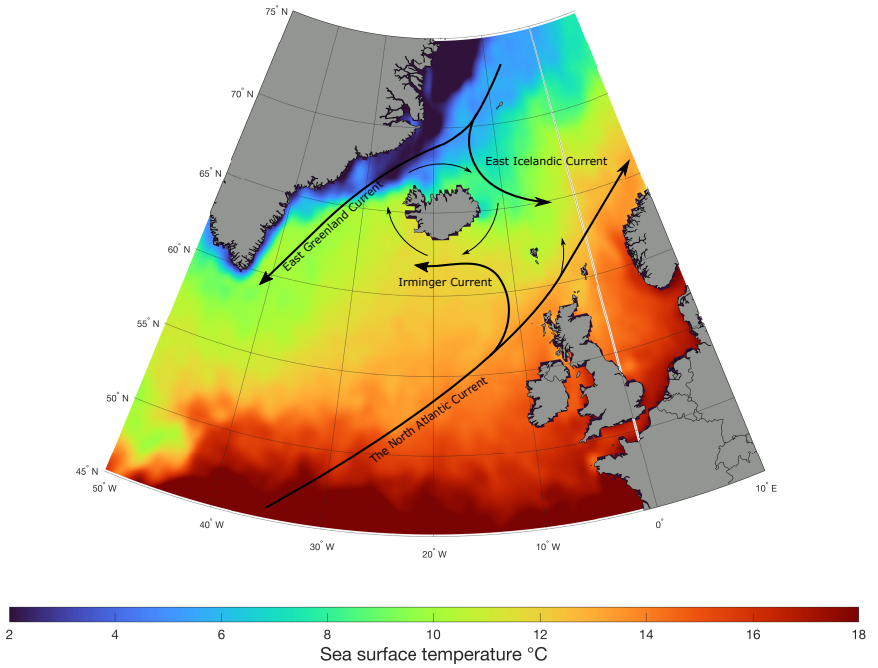

Figure 1.1. Location of Iceland in the North Atlantic Ocean. Color represent ocean surface temperature and arrows show the main surface current branches. NOAA High Resolution SST data provided by the NOAA/OAR/ESRL PSL, Boulder, Colorado, USA, shown for August 2020.

These oceanic and atmospheric circulation systems lead to a temperate maritime climate

with mild summers and winters with small variations in temperature between seasons. During summer, the average temperature at lower elevations (less than 400 m a. s. l.) ranges from 8–10°C, with a country-wide average of 7°C. In winter, the average temperature is 0–3°C at lower elevations and about −5°C for the whole island (Björnsson, 2003; Henriksen, 2003).

Precipitation is frequent with lows and storm systems passing the North Atlantic Ocean, characterized by a general precipitation reduction with increase in latitude forced by the orographic generation of precipitation in mountainous regions parallel to the dominating SE-to-SW wind direction (Crochet et al., 2007; Björnsson et al., 2018). Area average precipitation is 1.7 m (of water equivalent) with the highest values at glacier peaks in the south (up to 10 m). During winter, heavy snowfall is frequently induced by cyclones crossing the North Atlantic, where air and water masses of tropical and Arctic origins meet (Einarsson, 1984; Ólafsson et al., 2007). In the highlands, this leads to the formation of a seasonal snowpack and the sustainment of glaciers. Icelandic glaciers span an elevation range from sea level up to 2110 m a. s. l. in a maritime climate, with large mass turnover and high variability in annual mass balance. Seasonal snow in Iceland is classified as a combination of taiga, tundra and maritime types with overall shallow snowpack with high density, frequent melt and wind-blown features (Jóhannesson and Sigurðsson, 2014; Sturm et al., 1995, 2010).

At present, about 10% of the country is covered by glaciers (10.300 km^2) storing about 3400 km^3 ($\sim$3100 Gt) of water as ice, totaling about 20 years worth of annual accumulated precipitation (Björnsson and Pálsson, 2008; Hannesdóttir et al., 2020). Since the end of the Little Ice Age ($\sim$1890 in Iceland), Icelandic glaciers have gradually been losing area and mass with a decrease in area by 750 km^2 since 2000, and by approximately 2100 km^2 since the end of the 19th century. The associated mass change has been estimated for the entire period 1890–2019 as -4.2 ± 0.7 Gt a^{-1} and -9.2 ± 0.7 Gt a^{-1} for the more recent period 1994–2019 (Aðalgeirsdóttir et al., 2020).

Snow and glacier research is important in Iceland for many of reasons, including but not limited to, civil protection, monitoring of active natural hazards, volcanic activity, water resource forecasting and long-term changes due to climate changes. Activity in glacier-covered volcanoes can cause volcanic ash and tephra fall-outs on glaciers during explosive eruptions leading to enhanced melt or in some cases glacier surface isolation reducing melt significantly (Warren and Wiscombe, 1980; Möller et al., 2014; Wittmann et al., 2017; Möller et al., 2019; Gunnarsson et al., 2021). Other derivative impacts include health hazard due to inhaling volcanic ash (Damby et al., 2017), influence on civil infrastructures due to tephra fallout hazard such as transportation, airports, transmission lines and other vital infrastructure in modern societies (Barsotti et al., 2018). Glacier-covered volcanoes can also produce large glacier outburst floods (jökulhlaups) associated with eruptions and rapid melt of ice that can threaten municipalities downstream as well as civil infrastructure (Björnsson, 1975, 1992, 2010). The recent volcanic eruptions in Eyjafjallajökull and Grímsvötn, 2010 and 2011, disrupted civil aviation by airborne ash upsetting travels of thousands of air passengers (Úlfarsson and Unger, 2011; Bolić and Źarko Sivčev, 2011; Alexander,

2013).

1.1 Motivation

To date in Iceland, limited research efforts have been allocated to investigate near-real-time monitoring of various key cryosphere variables using remote sensing. Developing a product that is continuous in time and space opens opportunities to understand and put in historical perspective ongoing events but also enables applications to provide insights into interaction between the cryosphere and the climate system by improved understanding of various essential climate variables, such as snow cover and albedo.

The motivation of the PhD dissertation was to utilize different data sources that individually provide partial description or information on a dynamic hydrological system but when combined improve understanding of the system being investigated. Figure 1.2 presents a conceptualization of how remote sensing, modeling and in-situ observations can support and validate one and another in context. Remote sensing and earth system modeling can augment sparse ground observations providing a more complete spatio-temporal coverage and permitting reconstruction of historical conditions as well as predictions of future developments. It is important to realize that no single method is flawless and without uncertainty but by integration they can provide a more complete representation of earth systems.

1.2 Objectives

The aim of this PhD dissertation was to derive a better understanding of the spatio-temporal signatures of snow and glacier related properties such as snow cover, snow surface albedo, snow water equilivent, timing of melting, surface energy balance and changes and trends of those properties over time. The process pipelines and methods developed were aimed at being adoptable to new or alternative data streams, such as new satellite sensors or climate forcing, to support ongoing near-real-time monitoring and understanding of snow and glaciers.

Hence the objectives were:

- Develop a method to create a gap-filled snow surface properties product for Iceland and extract spatio-temporal characteristics using optical remote sensing and provide detailed validation of the product.

- Address some of the shortcomings and challenges for remotely sensed products for glaciers and seasonal snow in Iceland and derive products suitable for operational use as well as a scientific study.

- Study the spatial and temporal variations in snow cover and albedo utilizing the

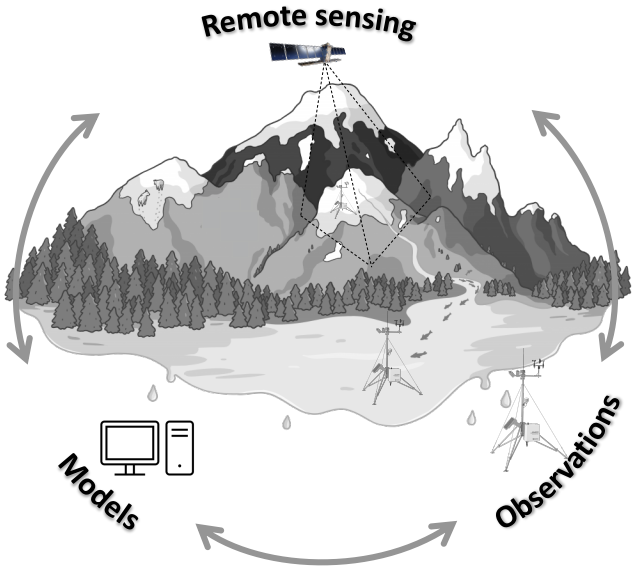

Figure 1.2. Conceptualization of the possible synergy of remote sensing, modeling and in-situ observations.

spatio-temporal products created and investigate recent changes and trends, and how various processes such as volcanic eruptions and light-absorbing particle deposits on snow and glacier surfaces, had impact on snow cover and albedo.

- Develop a modeling framework to reconstruct the surface energy balance of major Icelandic glaciers and seasonal snow in the highlands to extract spatio-temporal characteristics using fractional snow cover and albedo from remote sensing and high-resolution climate forcing.

- Investigate the relations between surface energy balance and large-scale atmospheric circulation patterns to provide better insight into drivers of recent changes in surface energy balance.

2 Background

In a rapidly changing world, the immense amounts of satellite imagery, high spatio-temporal resolution and availability of climate reconstruction products and in-situ observations, often with a long temporal record, offer possibilities to understand complex hydrological problems by innovative use of these data-sets combined (Martinec and Rango, 1981; Box et al., 2012; Guan et al., 2013; Yang et al., 2013; Rittger et al., 2016).

Data on snow cover, depth, density, snow water equivalent and energy balance of the snowpack are critical to efficiently estimate timing and the amounts of snow melt at a given location (Lundquist et al., 2005). Other properties contribute to the understanding of the evolution of the snowpack (strength, grain shape/size, stratigraphy, surface roughness, etc.) but are not dominant controls on mass changes nor timing of melt. To monitor and estimate these processes, various methods are applied and generally rely on the geographic scale on the information required (Nolin, 2010; Nolin et al., 2021). Geographic scale ranges from global down to sub-catchment scales where global and continental scales ($>10^6$ km^2) have characteristic distances of 1000s of km where dynamic meteorological effects are important (Ford et al., 2013). Remote sensing and global weather/climate models often describe the processes at these scales better than observations although observations are often used for data assimilation and model state variable updating (Dong, 2018). For catchment (10^3–10^2 km^2) and sub-catchment scales (10^1–10^2 km^2), remote sensing products and climate models often are produced at too coarse spatial resolution to resolve details in the snow hydrological processes, especially in complex terrain. At these scales (and smaller), in-situ observations often provide good estimates of snowpack mass, especially for sites that have been operated over long periods where statistical relations can be found between years (Pomeroy et al., 2004; Skaugen, 2007). Estimates of seasonal snow and onset of melt may be found efficiently by hydrological modelling, remote sensing and by in-situ observations, both fixed and continuous in time. Either by fusing the different information streams together in a modelling framework (data assimilation), utilizing the best available information, or by using relevant remote sensing and/or in-situ observations to calibrate and constrain hydrological models' parameters and state variables (Barrett, 2003; Andreadis and Lettenmaier, 2006; Oaida et al., 2019; Smyth et al., 2019; Largeron et al., 2020). Remote sensing offers data collection over large areas with repetitive coverage at a variety of scales and resolutions with a wealth of new sensors in the past two decades, together with existing satellite data archives, gives opportunities to monitor and understand various cryospherical processes (Raup et al., 2015; Lettenmaier et al., 2015; Taylor et al., 2021). Various challenges remain for remote sensing, such as pixel obstruction due to cloud cover for optical sensors (Marshall et al., 1993), repetitive spatio-temporal

coverage to sense and describe dynamic features and processes, handling of large data volumes and retrieval and processing algorithm development and improvements (Gomes et al., 2020; Taylor et al., 2021).

Earth system models generally offer spatio-temporal continuous data for the model time and grid resolution which relates to the computational cost of the model. Headway in knowledge and computational power means models become more sophisticated as they are constantly being revised and improved, with capabilities to solve more complex calculations at a higher spatial and temporal resolution (Weyn et al., 2020). This leads to scientists generating more and more accurate representation of the dynamic problems around us but with a never-ending quest for greater precision (Hannah et al., 2020).

In-situ data often provide high quality information that is lacking spatial overage as they represent a point and its nearest surrounding, often over a wide range of parameters. In-situ data, both point collections made manually or by the operation of stations, such as gauging- or weather stations, come at an operation- and maintenance cost, especially in remote, complex and harsh environments (Bair et al., 2018b). Historically, in-situ observations have been extensively used to calibrate, validate, and provide parameter estimates for remote sensing sensors or products and earth system models. Recent advances in computational resources and model development now allow for more complex data assimilation schemes to update model state variables and make various corrections and bias adjustments (Oaida et al., 2019). Remote sensing has been used in a similar manner with earth system models, to validate, calibrate and provide parameter estimates, but with recent increase in sensors and more frequent repeat times to allow for near-real-time usage in modeling frameworks, improving modeling output (Bair et al., 2016; Rittger et al., 2016; Bair et al., 2018a, 2019).

An example combining ground observations and satellite data from microwave and visible sensors is the Interactive Multisensor Snow and Ice Mapping System (IMS) operated by the National Oceanic and Atmospheric Administration's National Environmental Satellite Data and Information Service (NOAA/NESDIS). Daily operational snow and sea ice coverage data are issued for the Northern Hemisphere at 1, 4 and 25 km spatial resolution (Ramsay, 1998). The product is made by fusing multi-satellite sensor data sources including NOAA polar orbiters and geostationary data (POES/GOES), Japanese geostationary meteorological satellites (GMS), European geostationary meteorological satellites (METEOSAT), US Department of Defense (DOD) polar orbiters, and Defense meteorological satellite program (DMSP) as well as indirect in-situ observations such as daily snow depth Helfrich et al. (2007). The data are important for climate monitoring, improved snow parameterization, weather forecast modeling and they guide marine traffic in sea ice as an example (Key et al., 2001).

NOAA's National Operational Hydrologic Remote Sensing Center Snow Data Assimilation System (SNODAS) is similar to the IMS system. A modeling and data assimilation framework provides real-time estimates of snow cover and associated variables (state and diagnostic variables) to support hydrological modeling and analysis, based on satellite, airborne platforms, and ground stations, with model estimates of snow cover over

the U. S. (Barrett, 2003). The core of the system is a multi-layered, spatially distributed snow mass and energy balance model based on the one-dimensional temperature index model SNTHERM. 89 (Jordan, 1991). Usage of the data is both from a research and scientific perspective, but also supports near-real-time operational users such as river flow forecast centers with the potential to improve hydrological forecasts and water resource estimates (Andreadis and Lettenmaier, 2006; Lv et al., 2019).

Remote sensing generally offers a powerful way to quantitatively assess the physical properties of the cryosphere in remote locations which often are inaccessible and where in-situ observations would be expensive (Pope et al., 2014; Raup et al., 2015). The global coverage and frequent overpasses of satellite remote-sensing instruments allows scientist and relevant institutions to quantify cryosphere properties at local, regional, and global spatial and temporal scales (Tedesco, 2015). In recent years, the availability of free and open-source Earth observing satellite products have changed the remote-sensing community. Satellite and satellite sensor technological advances and computational resources allow for more data to be collected at higher spatial and temporal resolutions (Pope et al., 2014).

Figure 2.1 shows the evolution of optical or multispectral satellite platforms with fully or partial open-source data since 1960, frequently used in cryospheric research and monitoring. Slow steady growth is observed in the first decades, from 1972 through the 1990s with accelerating rapid growth since 2000. Currently, the private sector drives the rapid growth in earth observation satellites spearheaded with the development of smaller satellites (smallsats/cubesats < 500 kg) and a growing launch opportunity. Planet Labs currently operates the largest constellation of earth imaging smallsats and has deployed over 450 satellites with 200 in orbit collecting data. They have the capabilities to imaging the entire land mass of the Earth every day at a high spatial resolution, emerging as a key resource for the remote-sensing community as they enable monitoring and observing various surface processes daily at a high resolution. The disadvantage comes at the cost of radiometric and geometric quality between different smaller platforms compared with the traditional platforms (TERRA/AQUA, Landsat, Sentinel) meaning the images need further post-processing for many analysis applications (Frazier and Hemingway, 2021). Another consideration comes from the constantly evolving technology of smallsats, which improves product quality, but can create discrepancies across sensor generations, limiting long-term and historical observational records.

The United States Geological Survey (USGS) Landsat program initiated the Earth remote sensing revolution for Earth Science in moderate resolution in the 1970s. Today, it represents the world's longest continuously acquired collection of spaced-based, moderate resolution land remote-sensing data and therefore provides vital information for a rapidly changing world (Emery and Camps, 2017; Zhu et al., 2019). The launch of Landsat 1 (Earth Resources Technology Satellite, ERTS-1) in 1972 marked the first imaging platform dedicated to support a wide range of applications in such areas as global change, agriculture, forestry, geology, resources management, geography, mapping, water quality and oceanography. In September 2021, the Landsat legacy was carried on by the launch of Landsat 9, joining its sister satellite in orbit, Landsat 8.

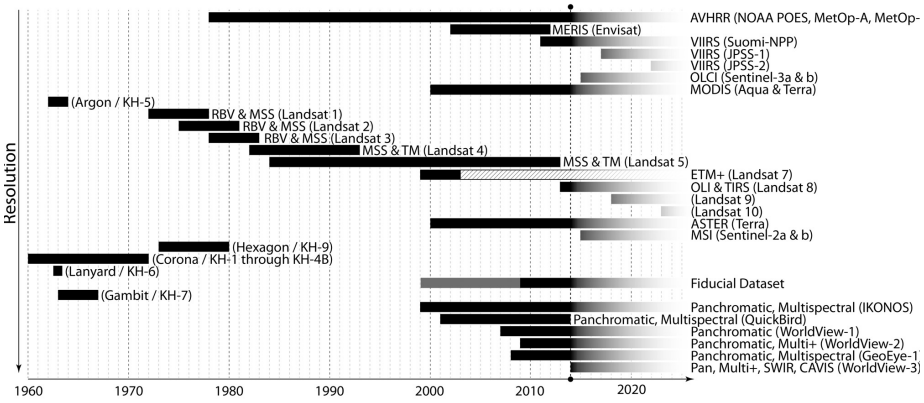

Figure 2.1. Overview of historical, ongoing and future proposed optical and multispectral satellites with fully or partially open-source data. Figure from Pope et al. (2014).

For the first decades of the Landsat program, data were not publicly available free of charge, but revenue by the user community did not exceed the cost of fulfilling user requisitions. In 2008, the USGS adopted a free and open Landsat data policy leading to a considerable increase in the use of Landsat data benefiting many operational and scientific studies and applications (Wulder et al., 2016a,b; Zhu et al., 2019).

Figure 2.2 shows the first nearly cloud-free image of Vatnajökull from Landsat 1 (ERTS-1) MSS imager on 31 January 1973 revealing many glaciological, structural and volcanic features, clearly visible for the first time in a comprehensive way (Williams and Þórarinsson, 1973; Williams, 1983, 1987). Under the ERTS-1 program, Iceland was one of the 327 experiments conducted, supported by NASA, directed at analysis of MSS imagery from ERST-1 to study a variety of geologic, hydrologic, oceanographic and agricultural phenomena (Williams, 1974, 1973a,b; Williams and Pálmason, 1973; Williams et al., 1973). This first extensive satellite remote sensing effort in Iceland led to further analysis and extension of knowledge in many fields such as revealing detailed surface morphology of glaciers, distribution and size of subglacial volcanic calderas, cauldron subsidence caused by subglacial geothermal activity, delineation of the probable surface ice divides and estimation of glacier surface area in Iceland (Þórarinsson et al., 1973; Björnsson, 1978).

The Copernicus program (European Union's Earth Observation and Monitoring Program) headed by the European Commission (EC) in partnership with the European Space Agency (ESA) operates several Earth Observation missions in recent years with similar open data policies as the Landsat program benefiting societies, research, and operational goals. The ESA Sentinel program is a series of next-generation Earth observation missions aimed to replace the older Earth observation missions which have retired or are nearing the end of their operational life with a range of technologies,

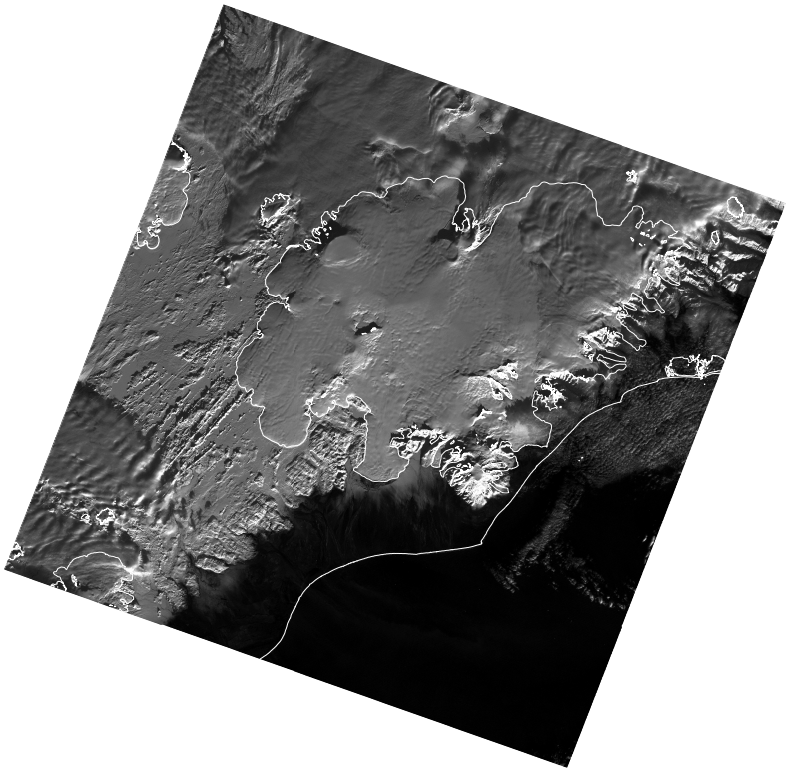

Figure 2.2. One of the first nearly cloud-free image of Vatnajökull from Landsat 1 MSS imager on 31 January 1973. The image shows digitally enhanced band 7 at 60 m ground resolution. Glacier outlines from Hannesdóttir et al. (2020).

such as multispectral and radar imaging instruments for land, ocean and atmospheric monitoring. The newly launched satellites, Sentinel-1, Sentinel-2 and Sentinel 3 provide extensive amounts of free and open optical and synthetic aperture radar (SAR) remote sensing imagery (Drusch et al., 2012; Torres et al., 2012; Donlon et al., 2012). These satellites, among others, have improved significantly the spatio-temporal resolution of satellite data acquisitions in the world, not least in Arctic regions, as they are polar orbiting.

2.1 Remote sensing of snow and ice

Earth observation satellites offer a wide range and a variety of image data with different characteristics. Remote sensing data domains are generally described with four resolution domains, spatial, temporal, spectral (wavelengths) and radiometric (signal to noise) resolution. Each remote sensing sensor designed for a certain application, has its own resolution requirements in the four domains mentioned above creating trade-offs between spatial and temporal coverage of the sensor and spectral and radiometric resolutions of the remotely-sensed products. Therefore, the resolution of the satellite sensor must be balanced against the desired capabilities and objectives of the sensor and the applications that it serves.

2.1.1 Spatio-temporal properties of snow and ice

Spatial resolution defines the smallest possible feature detectable and is defined by the angular cone of visibility of the sensor that sees the surface being observed at a given altitude. Global and continental scales (>10^6 km^2) have characteristic distances of 1000s of km where dynamic meteorological effects are important. Remote sensing and global weather/climate models often describe processes at these scales better than observations although observations are often used for data assimilation and model state variable updating. For catchment (10^3–10^2 km^2) and sub-catchment scales (10^1–10^2 km^2), remote-sensing products and climate models often are produced at spatial resolution too coarse to resolve details in the snow hydrological processes, especially in complex terrain. Figure 2.3 shows an example of different spatial resolutions from different satellite sensors all showing snow covered surfaces in Iceland. The MODIS sensor carried by the Aqua and Terra satellites has a spatial resolution of 250 m to 1000 m, depending on which spectral bands are used, with a swath width of 2400 km. The satellite constellation is sun-synchronous crossing the same location of the Earth at about the same local time every day, enabling almost the entire Earth's surface to be observed daily, pending cloud cover. Figure 2.3 (left) shows a 500 m MODIS image using bands 7-2-1 to exaggerate snow covered surface in Iceland detailing various synoptic patterns such as topographic and elevation snow distribution. Figure 2.3 (center) shows optical data from Sentinel 2 at a 20 m spatial resolution showing more details at a basin or catchment scale, where processes such as detailed elevation distribution of snow cover and influence of aspect on snow distribution become important. Figure 2.3 (right) shows data from Maxar World View 3 at a 0.3 m pixel resolution emphasizing details at the

sub-catchment (hill slope) scale where effects of blowing snow, canopy interception and impacts of local topography, small-scale aspect, melt ponds and other small scale-effects can clearly been seen.

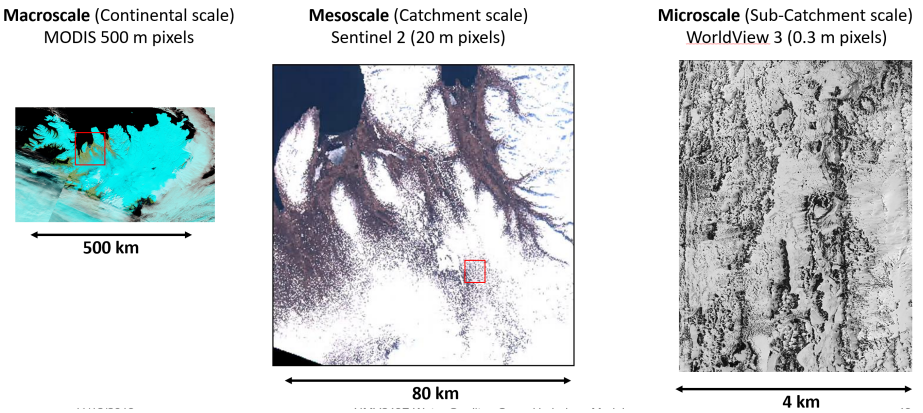

Figure 2.3. Snow cover from different satellite platforms and sensors showing different level of detail.

Temporal resolution is the time between two satellite sensor acquisitions. For dynamic systems, such as evolution of seasonal snow cover, glacier bare-ice extent or surface-albedo changes the temporal resolution needs to be sufficient to describe these processes correctly. For snow-cover or sea-ice analysis of the Northern Hemisphere weekly data might be sufficient to describe the system sufficiently while for catchment or sub-catchment details weekly data might be too coarse. Other factors can influence the temporal resolution of surface processes, such as cloud cover obscuring the surface at the satellite over-pass time for optical sensors. In some applications, processing methods are applied to increase data availability per pixel.

For optical remote sensing, the two major limiting factors are cloud cover and forest canopy/vegetation (Nolin, 2010). High average cloud cover limits the satellite during overpass to capture valid surface reflectance for further processing. In Iceland, average cloud cover ranges from 72–78% depending on location, limiting the capabilities to use daily products without further processing, such as temporal aggregation and gap filling with statistical methods (Gascoin et al., 2017; Gunnarsson et al., 2019). Higher spatial-resolution optical data have been obtained from the Landsat constellation (30 m spatial resolution) for snow cover and albedo retrievals with capabilities to further resolve smaller scale patterns, more detailed variability of albedo and for sub-pixel variability of large footprint satellite sensors (Winther, 1993; Reijmer et al., 1999; Gascoin et al., 2017; Naegeli et al., 2017, 2019). The general downside of higher spatial resolution data is lower temporal resolution.

Figure 2.4 shows an example of a processing method for snow-cover analysis in Iceland for MODIS data from Paper I. Since average cloud cover is about 75% in Iceland, a single MODIS acquisition only provides limited information about the surface con-

ditions such as snow cover. By merging daily data acquisitions from both Aqua and Terra satellites, cloud obscured pixels were reduced by 7% since clouds move over land between the respective satellite overpasses. By further daily aggregation of data, data from neighboring dates were used to further gap-fill areas with missing data. The example in Figure 2.4 shows a daily data aggregation of 6 days contributing data to the center day being analyzed. By this, further 60% of cloud obscured pixels were reclassified within the aggregation window. Finally, a supervised classification model was applied to classify the remaining 9% of unclassified pixels. Various other processing methods have been applied to gap-fill satellite sensor data.

Box et al. (2012) used similar methods to increase data availability for MODIS albedo retrivals over Greenland during the melt season by applying a 11-day running statistical filter to identify and reject values contributing to daily estimates of surface albedo. Dozier et al. (2008) proposed a time trajectory interpolation of daily maps of fractional snow cover and albedo from MODIS to create time–space continuity of data that has been applied in many studies (Rittger et al., 2016; Morriss et al., 2016; Redpath et al., 2019; Tran et al., 2019; Ackroyd et al., 2021).

Temporal resolution, without reducing spatial resolution, can also be increased by operating satellite sensors in the same orbits but at different overpass times, so the sensors are observing the same surface areas but at different times. An example is ESAs Copernicus satellite constellation where Sentinel 2A and Sentinel 2B carrying the same sensor setup, are occupying the same orbit, but separated by 180 degrees. Each overpass is repeated in a 10-day interval for each satellite sensor resulting in a 5 day repeat coverage. NASA's recently launched Landsat 9 operates in a similar fashion with Landsat 8 and work on fusing Sentinel-2 data with Landsat data is undergoing, generating an harmonized surface reflectance product with unprecedented opportunities for moderate-to-high spatial resolution multispectral satellite imagery, providing timely and accurate observation of Earths status and dynamics (Claverie et al., 2018).

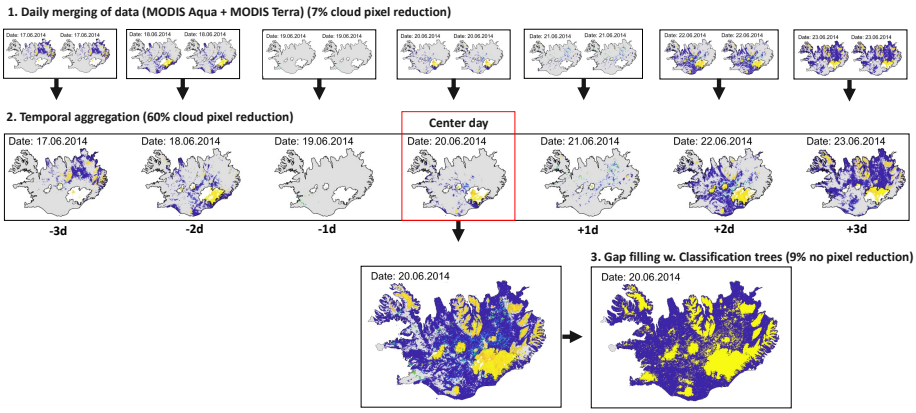

Figure 2.4. Example of temporal aggregation, from Paper I,for binary snow cover from MODIS to increase data coverage. The first step was daily merging of the two overpasses by the MODIS sensor, second to aggregate forward and back in time data under the assumption that no major changes take place for the aggregation period in snow-cover extent and finally classification of missing pixels using classification trees. The processing pipeline reduces cloud obscured pixels by 7% for daily merging, further 60% reduction was achieved by temporal aggregation leaving 9% of pixels needing classification with classification trees.

2.1.2 Spectral properties of snow and ice

Satellite sensors have spectral bands that are sensitive to the properties of ice and snow. The properties of the surface, and in some cases the subsurface, influence the reflectance observed in each sensor spectral band. The spectral response allows for discrimination of various properties by applying thresholds, band math or simple to complex computational methods. Optical sensor rely on daylight to make observations as they are passive systems that collect electromagnetic energy reflected from the Earth's surface and its atmosphere.

Figure 2.5 shows radiometric characteristics and spectral bands for a selection of optical earth observing satellite sensors over atmospheric transmission. Atmospheric transmission varies by wavelength in the atmosphere as gasses, water vapor, dust and particles influence the absorption of electromagnetic energy. By designing satellite sensors and their representative wavelengths in context with atmospheric transmission, the information collected can be used in an efficient manner emphasizing the features investigated. The spectral resolution of a sensor describes the ability to define fine wavelength intervals which again can influence the capabilities of the sensor product to discriminate between detected features. Spectral signatures of surface features are emphasized and mapped using the spectral properties of optical multispectral and hyperspectral sensors.

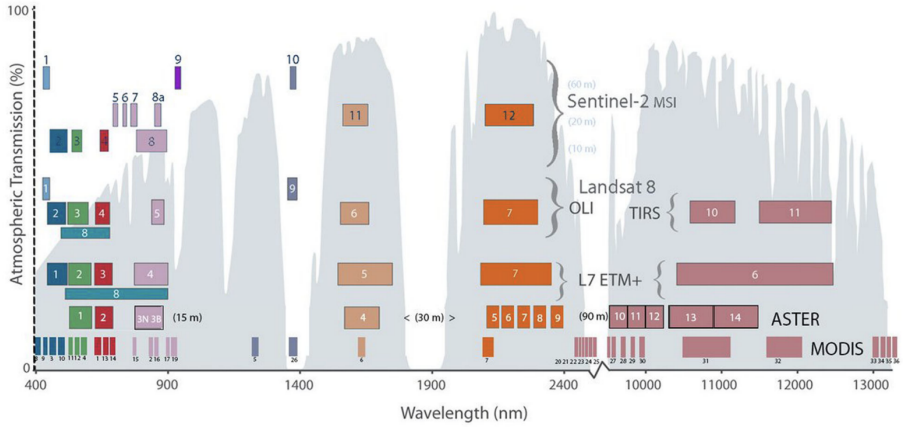

Figure 2.5. Spectral wavelengths and band properties of selected optical satellite sensors frequently applied in cryospheric research. In the background (grey), the atmospheric transmission for a range of wavelengths is shown with spectral bands and their spectral width for various satellite sensors. Each overlaying box represents a sensor aboard the representative satellite, its locations show the wavelength range and the width of the box represents the spectral resolution of the band. Figure adapted from Ustin and Middleton (2021).

Snow cover extent is observed using optical satellite sensors because the unique and spectral varying reflectance of snow in the visible, near-infrared and infrared spectral

range (Dozier, 1989; Painter et al., 2012). There are two main methods for mapping snow-covered area (SCA), binary classification of snow cover (bSCA) and fractional snow cover (fSCA). Binary classification provides pixel classification as snow or non-snow while fractional snow cover classification aims at estimating the fraction within a pixel covered with snow (Nolin, 2010).

Dozier (1989) introduced the discrimination of snow and land based on the Normalized Difference Snow Index (NDSI) which utilizes the spectral signature of snow being highly reflective in the visible spectral range (VIS) and very low reflectance in the short-wave infrared spectral ranges (near-infrared, NIR) by analyzing spectral signatures of the Landsat Thematic Mapper.

NDSI is a simple band math method and an computationally efficient way to estimate binary snow cover widely used and validated in many studies, especially from the MODIS mission, where daily snow-cover estimations are provided worldwide (e.g., MODIS MOD10A1, MYD10A1, MOD10A2, MYD10A2 products) (Hall et al., 2002; Klein and Barnett, 2003; Parajka and Blöschl, 2006; Hall and Riggs, 2007; Dietz et al., 2012; Rittger et al., 2013; Gascoin et al., 2015; Gunnarsson et al., 2019). Fractional snow-cover mapping has been developed using two main methods. Salomonson and Appel (2004) developed a method based on correlation of MODIS NDSI binary SCA (500 m pixels) and Landsat EMT+ binary SCA (30 m pixels) to empirically estimate fSCA for MODIS pixels at 500 m spatial resolution.

Painter et al. (2009) developed a multiple-end-member method for fSCA mapping (MODSCAG) using spectral mixture models providing a more reliable snow cover mapping method better accommodating the spatial heterogeneity of different land-cover types (rock, vegetation, forest). In addition to subpixel snow covered, area it provides estimates of snow grain size and albedo which can then be used to further model snow cover. Information of snow grain size is used to estimate clean snow albedo using and evolution and estimate radiative forcing of the snow due to light-absorbing particles (LAPs) such as dust. Unlike other snow cover products from MODIS, MODSCAG is not produced globally but has been adopted and used in many applications investigating snow properties but also incorporated in models for parameter validation or direct insertion to constrain snow and ice models (Micheletty et al., 2014; Rittger et al., 2016; Hao et al., 2019; Bair et al., 2019).

Optical satellite remote sensing offers a way to observe surface albedo continuously at large spatio-temporal scales but are limited to times of clear sky overpasses. Various studies have shown that surface albedo over snow and ice can be derived successfully from visible and near infra-red satellite sensors (Stroeve et al., 1997; Reijmer et al., 1999; Stroeve, 2001; Klein and Stroeve, 2002; Liang et al., 2005; Stroeve et al., 2005, 2013). Since October 1978, regular polar coverage has been provided by the National Oceanographic and Atmospheric Administration (NOAA) satellites carrying the Advanced Very High Resolution Radiometers (AVHRR) (Stroeve et al., 1997; Xiong et al., 2018).

Surface albedo is dependent on the properties of the snow cover, but as well the solar zenith angle and proportions of direct and diffuse solar radiation. Reflected irradiance from a snow-covered surface is anisotropically scattered mostly in the forward direction meaning albedo is not directly measured by remote sensing instruments (Warren and Wiscombe, 1980; Warren, 1982; Skiles et al., 2018a). To account for anisotropic scattering a bidirectional reflectance distribution function (BRDF) is applied factoring in grain size, surface roughness, local angle of illumination and proportion of direct and diffuse radiation providing estimations of broad- and narrowband albedo from the MODIS sensor (Schaaf et al., 2002).

Figure 2.6 shows spectral characteristics for different snow grain effective radius and light-absorbing particles content (dust loading) resulting in different spectral responses of the surface and albedo response using the Snow, Ice, and Aerosol Radiative (SNICAR) model (Flanner et al., 2021). Figure 2.6 a to c shows visual examples of snow resulting in various spectral responses (Figures 2.6 d to f). Figure 2.6d shows a typical spectral response for clean fresh new snow, it has the highest albedo of any naturally occurring Earth surface. In the visible and near-UV wavelengths, snow albedo is >0.9 (Grenfell et al., 1994) and near 0.82 averaged over the full wavelength spectrum (0.3–4 μm) (Warren, 1982). Initially, new snow has high specific surface area (SSA) scattering light by the numerous snow crystal surfaces (Keegan, 2021). Snow metamorphism, driven by lowering of snowpack surface energy, reduces the SSA of the snow crystals by internal snowpack processes such as grain growth, sublimation and sintering that change the snow crystal structure and physical properties of the snowpack. This results in snow grain-size reduction with reduction in albedo (Adolph et al., 2017). Figure 2.6e shows how the spectral response of impurity-free snow evolves with changes in snow grain effective radius, from an broadband albedo of 0.82 for new snow with 50 μm grain radius to an 1000 μm radius with a albedo reduction to 0.66, primarily happening in the near infrared and short-wave infrared wavelengths.Figure 2.6f show how the spectral response changes for a range of now grain effective radius and various loading from dust or carbonaceous particles (light-absorbing particles). When LAPs are present, snow albedo decreases primarily in the visible wavelengths dramatically reducing broadband albedo absorbing more incoming radiation, causing the snowpack to warm and or melt (Warren and Wiscombe, 1980; Warren, 1982; Painter et al., 2012).For snow- and glacier-covered surfaces, light-absorbing particles deposited in the surfaces can dramatically increase short-wave radiative energy forcing, enhancing melt intensity. The dust loading to a surface often happens through processes that conventional hydrological, snow and glacier models are not set up to simulate, therefore underestimating the melt enhancement (Skiles et al., 2012; Wittmann et al., 2017; Schmidt et al., 2017; Skiles et al., 2018a,b; Skiles and Painter, 2018).

Surface albedo for snow has successfully been retrieved by TERRA and AQUA carrying the MODIS sensor since early 2000, both as a daily product, (MOD10A1, MYD10A1) and a 16-day composite generally of higher quality due to a more robust processing and quality assurance (MCD43A3). MCD43A3 provides daily albedo using 16 days of Terra and Aqua MODIS data at 500-meter (m) resolution. Data are temporally weighted to the ninth day of the 16 days (Schaaf and Wang, 2015; Stroeve et al., 2013). The

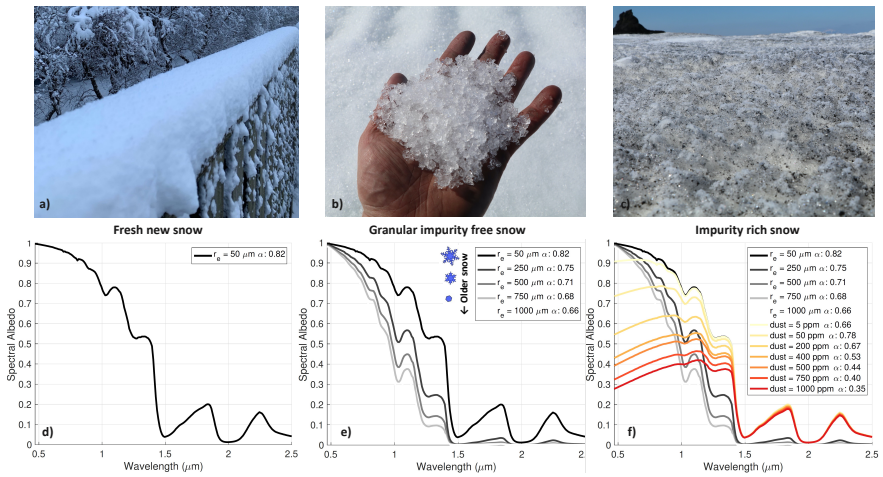

Figure 2.6. Spectral properties of snow and ice. ***Panels a to c*** *show a visual example of clean snow (a), clean granular snow (b) and granular impurity-rich snow (c).* ***Panels d to f****, show the calculated spectral response curves for different states of snow crystals.* ***Panel d)*** *shows the spectral response for fresh clean new snow with broadband albedo of 0. 82 (Panel a) for visual example).* ***Panel e)*** *shows the spectral response of snow ranging from new fresh snow to granular older snow with no light-absorbing particles.* ***Panel f)*** *shows the spectral response of snow at different ages (same as Panel e) but with light-absorbing particles added to the snow for the same snow grain effective radius (r). Calculations of spectral snow albedo (images d to f) done using SNICAR-AD v3 (Flanner et al., 2021). Photos by Andri Gunnarsson.*

previously mentioned MODSCAG also retrieves broadband snow surface albedo of clean snow using subpixel grain size through a relationship fitting a radiative transfer modeling of snow endmembers and albedo. An associate product with MODSCAG is MODDRFS (MODIS Dust Radiative Forcing in Snow), where a spectral unmixing model that retrieves surface radiative forcing by light-absorbing particles in snow cover from MODIS surface reflectance data coupled to estimates of incoming melt energy (Painter et al., 2012). The product quantifies the enhancements of solar radiation forcing of a snow surface leading to accelerated snow- and ice-melt and enhanced glacier melt.

2.2 Modeling of snow and ice

Data on snow and glacier processes can come from field observations and remote sensing, but data from these sources often are limited, offering a partial description of the system. Often these sources of data cannot account for all characteristics of snow and glaciers, and the data record is often relatively short. Satellite observations date back only to the mid-1970s; other observations, such as field observations of hydrologcal and meteorological parameters, may go back as far as the late 19th century, but are quite often sparse.To reconstruct a complete picture of the evolution of this system, both from a historical and future perspective, models are used to simulate these processes, often augmented with field observations and data from remote sensing.

A model can be defined as a mathematical representation of a real-world physical process. These frameworks can be data driven (e.g., linear and multivariate regression, empirical orthogonal functions, machine learning and neural networks), conceptual (e.g., black/grey box, liner bucket) or physically-based (e.g., WRF-Hydro, DHSVM, VIC, UEB, SNTHERM, NOAH LSM) or a combination of more than one configuration, i.e., parts of the framework is data driven while other parts are physically-based. Models are applied over a range of horizontal, vertical, and temporal resolutions depending on the intended output use. Broadly, snow and glacier melt models can be divided into empirical models (temperature index models), correlating melt to air temperature, and physically-based energy-balance models, which use energy balance theory to solve for the energy available to melt snow or ice (Hock, 2005; MacDougall et al., 2011).

Temperature index (TI) models are often relatively simple while retaining a physical basis, describing the statistical relationships between melting and climatic parameters and require few inputs (Jóhannesson et al., 1995; Hock, 2005; Ohmura, 2001). This makes them often favorable in operational aspects, as they are computationally efficient with limited data input requirements which often are only air temperature and precipitation. Air temperature is easily observed in the field, often has decades of data and spatial variations are relatively easily understood in many cases, compared to other parameters influencing the surface energy balance of snow and glaciers such as radiation. Precipitation, especially solid precipitation, is more challenging to observe and interpret due to under-catch in windy conditions at automatic weather stations often leading to severe underestimation of precipitation (Førland et al., 1996; Sigurðsson et al., 2003;

Crochet et al., 2007; Rasmussen et al., 2012).

Recent advances and developments in high-resolution atmospheric models suggest that simulated total annual rain and snowfall in well configured models can outperform in-situ observational networks of precipitation gauges with significantly better estimates than radar or satellite-derived products although many challenge remain, such as representation of individual storms (Rögnvaldsson et al., 2004, 2007; Lundquist et al., 2019).

As an example, a simple but widely used temperature index model is the SNOW-17 snow accumulation and ablation model developed by Anderson (1976), the Stanford Watershed Model by Crawford (1966) and Hydrologiska byråns vattenbalansavdelning (HBV) developed by Bergström and Forsman (1973). These models have been developed and updated since their original development, and might be considered a hybrid versions of TI models, but still operate based on the original temperature index concept (Lisette Klok and Oerlemans, 2002; Hock, 2005).

SNOW 17 by Anderson (1976) is widely used to predict snow melt extent and timing, especially in the US as it was primarily designed for river forecasting. It simulates important physical processes occurring within the snowpack in a simplified form with capabilities of running with hourly time steps. As all processes index to the observed air temperature and precipitation, historical weather data can be used for calibration and validation of the model and real-time observations for operational applications. Calibration procedures include adjustments to parameters discriminating precipitation in rain and snow, adjusting for undercatch of precipitation and accounting for seasonal variations in melt factors. Known underestimations with TI models are when turbulent fluxes are large and when short-wave dominates melt energy. Overestimation are known in warm and calm conditions as well.

Physically-based energy-balance models (EBMs) compute energy balance fluxes between the surface and atmosphere from physically-based calculations. They provide insight into hydrological processes but uncertainties in forcing data, model parameter estimations and model structure may propagate from the model inputs to outputs (Raleigh et al., 2015). EBMs require more complex input data, beyond air temperature and precipitation, which are often unavailable at automatic weather stations especially in complex terrain and instead require empirical estimation (Raleigh et al., 2016). EBMs are often forced with climate and weather models that provide the high-resolution input data as well as a number of required parameters .

EBMs generally have fewer "free" model parameters to adjust as they are physically based. Hybrid model, fusing together TI and EBMs functionality have also been developed and tested gradually transitioning from conventional TI to EBMs type models by increasing the number of meteorological input variables (Hock, 1999; Oerlemans, 2001; Lisette Klok and Oerlemans, 2002). Often, simple calculation schemes in TI models allow for extensive calibration procedures of many parameters using optimization. Here, various configurations of parameter values can be tested and validated against a selected

metric evaluating the model performance (Franz et al., 2008). Energy-balance models often require more computational power, which has become cheaper and available in recent years, allowing for parameter optimization to some extent. In various applications using the WRF-Hydro model, the Dynamically Dimensional Search Algorithm by Tolson and Shoemaker (2007) has successfully been used where the search strategy in model parameter space is scaled to the maximum number of iterations specified. When optimization routines are too expensive or too time-consuming, a parameter sensitivity analysis can reveal the most sensitive parameters to calibrate, which can then be optimized.

Generally, modeled SWE in mountainous regions is associated with high uncertainty due to forcing uncertainties and snow depth spatial variability in complex terrain (Kim et al., 2021). Estimations of precipitation in gridded and regional estimations of precipitations increase at high elevations often with limited observations to validate and high spatial variability (Hughes et al., 2020). To capture the spatio-temporal variability of SWE various snow data assimilation schemes and project have been developed, from adopting in-situ snow-depth observations (SYNOP observations), fusing remotely sensed snow cover to constrain energy balance to high resolution mapping of snow depth for SWE modelling (de Rosnay et al., 2015; Painter et al., 2016; Rittger et al., 2016; Bair et al., 2016; Smyth et al., 2019; Oaida et al., 2019; Largeron et al., 2020).

First utilized by Martinec and Rango (1981), the snow-water equivalent reconstruction method uses space-based remote sensing of snow cover to retrospectively estimate the amount of water stored as snow for each pixel back to the last significant snowfall. The reconstruction technique has been adopted and successfully validated in many studies across various regions with various modifications and improvements and appears to be one of the most reliable way to estimate spatial distribution of SWE (Raleigh and Lundquist, 2012; Lettenmaier et al., 2015; Rittger et al., 2016; Bair et al., 2018a). The method provides a post-peak SWE estimate without the need for total precipitation which can be highly uncertain, especially in topographically complex regions (Adam and Lettenmaier, 2003; Adam et al., 2006). The main limitation is that the reconstructed SWE can only be estimated after snow disappears on the ground, i.e., when snow disappears from a given pixel after total melt out, limiting real-time usage.

Cline et al. (1998) reconstructed SWE in a small, well-studied, mountain basin in the Sierra Nevada using Landsat Thematic Mapper data to estimate fractional snow cover and spatially constant snow surface albedo decaying over time. The reconstructed SWE, compared to in-situ observations, showed a non-significant difference (6%) for maximum SWE estimation. Molotch et al. (2004) used basin-average albedo estimated from remotely-sensed Airborne Visible/Infrared Imaging Spectroradiometer (AVIRIS) to show more accurate estimates of the timing and magnitude of snow melt using remotely sensed albedo over common snow-age-based empirical relations. Rittger et al. (2016) applied the approach to reconstruct the Sierra Nevada maritime snowpack using Moderate Resolution Imaging Spectroradiometer (MODIS) data using the MODSCAG model for fractional snow cover and albedo (Painter et al., 2009). Results showed that the model could accurately estimate SWE in a variety of topographic settings for a

range of wet to dry years in the Sierra Nevada. Work by Schneider and Molotch (2016) applies MODIS based reconstructed SWE to improve real-time estimates of SWE in the Upper Colorado River using linear regression and in-situ SNOTEL data reporting reduced biases and slightly lower RMSE values. Recent work by Bair et al. (2018a) uses machine learning to estimate SWE throughout the snow melt season for watersheds of Afghanistan using physiographic and remotely sensed information as predictors and reconstructed SWE as the target. Results report a 14% mean bias across the study period and RMSE values range from 46 to 48 mm illustrating possibilities to accurately estimate SWE during the snow season in remote mountains.

Machine learning has received increasing attention in recent times to many aspects of climate, weather and hydrological forecasting and monitoring (Brenowitz and Bretherton, 2018; Bair et al., 2018a; Rasp et al., 2018; Broxton et al., 2019; Baraka et al., 2020). These models require less computational power than traditional state-of-the-art physical models for the same output extent in space and time making them attracting for, e.g., rapid data predictions over a range of possible expected outcomes for a weather event (Weyn et al., 2020).

2.3 Field data

The longest available record for any observed hydrological phenomenon is the gauging of the water level in the Nile river describing interannual water level fluctuations for more than five millennia (Jarvis, 1936; Eltahir and Wang, 1999). The Nilometer, a graded marble octagonal column, was used to observe the water level in the river Nile providing estimates of water availability determining the area's prosperity. These observations are like the current concept of water level observations in river gauging and lake elevation measurements today. Indeed technology has certainly evolved and taken over the need for daily manned observations but the Nilometer remains a good example of how simple reliable field data are collected providing the perception of an environmental phenomenon and describing its behavior.

The oldest method of observing and monitoring seasonal snow and glacier mass balance is by in-situ observations, using scientific instrumentation, often simple instruments, to measure, investigate, understand, and predict processes by measuring the physical properties of the system (Kinar and Pomeroy, 2015). Knowledge of the water content in Spring stored in the mountain snowpack is invaluable in the Western US as the availability of water for agriculture, energy production, industry, transportation, and recreation greatly affects economic decisions and information about snow and water supply forecasting go hand in hand. That importance drove the development of systematical snow surveying in the US, pioneered by Dr. James E. Church in early twentieth century which has evolved significantly through time. Systematic snow courses have data extended decades in for the past and the SNOTEL weather station network provides real-time data of snow conditions for large areas in the West Coast today.

In Iceland, generally more focus has been on observing glacier surface mass and energy balance and the associated runoff contribution rather than measuring and monitoring seasonal snow, especially in the highlands. Surface mass balance data of Icelandic glaciers has been systematically collected bi-annually by a network of institutes and stakeholders in Iceland. Data are collected where winter and summer mass balance are observed with conventional glaciological methods, for Vatnajökull, Langjökull and Hofsjökull with intermittent observations for Drangajökull, Mýrdalsjökull and other smaller glaciers (Ágústsson et al., 2013; Þorsteinsson et al., 2017; Pálsson et al., 2020a,b). The longest continuous observations are for Hofsjökull, from 1988, for Vatnajökull from 1992 and for Langjökull since 1998. The procedures for drilling and post processing of data are described in many previous studies and annual reports of mass balance (Ágústsson et al., 2013; Þorsteinsson et al., 2017; Pálsson et al., 2020a,b).

Long-term observations of snow cover in local municipals have been conducted since 1924 at manned observation sites among other weather-related observations (Jónsson, 2002). The network is operated by the Icelandic Meteorological Office (IMO) including daily manned observation of snow cover at 09:00 AM. Data are reported as local snow cover estimate (SNC) and snow cover in mountains (SNCM). For each observation, the local snow cover is reported as snow free (Code 0), patchy snow cover (Code 2) and fully snow covered (Code 4). In accordance with the observational procedure of local snow cover, the area observed is within 1 km of the observer and has no more than a 50 m elevation difference. Although this is the longest continuous record of snow cover in Iceland and provides insights to local snow cover in the lowlands, limited data are available for the highlands of Iceland. The data also only includes snow cover assessment, but fewer SWE estimates have systematically been collected which generally are of more interest for resource assessment and hydrological modeling. Manned observations of snow data are affected by changes in station location, observing practices between observers and land-cover changes among other factors that influencing data quality and comparability over historic timescales and between sites (Lemke et al., 2007). Observations of seasonal snow and peak SWE in Spring are though quite sparse, especially in the highlands (Jónsson and Jónasson, 1997). The single longest continuous record for snow depth, density and other properties of the snowpack were collected at Hvervellir in the central highlands from 1965 until 2004 when the site was upgraded to automatic measurements which previously were manned (Sigurðsson et al., 2003).

In certain hydro power areas in the highlands, seasonal snow programs have been commissioned to improve understanding of snow hydrology (Rist, 1958, 1966, 1981). At these sites, snow courses have been installed with 1–2 observations of snow depth and density each winter although few of these site have fully continuous data (Sigurðsson, 2002; Jóhannesson and Sigurðsson, 2014). The data has been collected by various institutes, the National Energy Authority, the Icelandic Met Office and the National Power Company. Figure 2.7 shows a straightforward yet effective depiction of spring flood water volume forecasting based on snow surveys in the highlands. The forecast is made for one of the major glacier fed river in Iceland, Þjórsá river, an important source of melt water for reservoir storage and energy production. The horizontal axis shows snow survey average observed SWE while the vertical axis shows the associated water

volume in gigaliters (Gl).

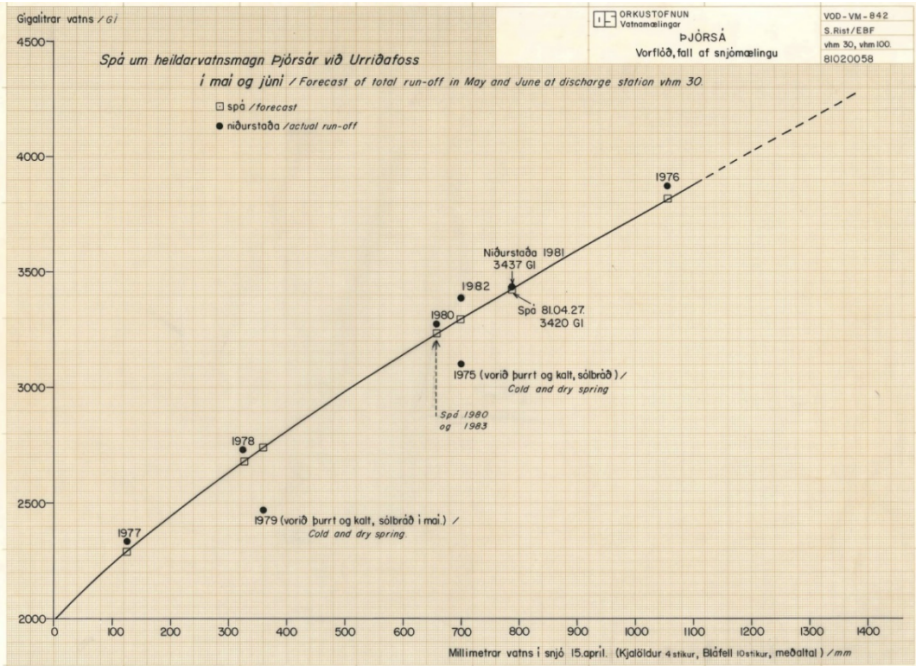

Figure 2.7. Spring flood volume forecast for Þjórsá river at Urriðarfoss based on snow survey observations for a selection of years. The horizontal axis show average observed SWE at selected snow survey locations while the vertical axis shows the estimated spring flood volume in Gl. Figure from Rist (1981).

Observations were done with portable and stationary instruments where portable devices can be moved to multiple locations (i.e., federal snow sampler) and stationary instruments are fixed to a point (i.e., automatic weather station, river gauging station). Snow-depth observations with rods or rulers are an example of old, simple, and robust instrument, used to measure snow depth, down to centimeter accuracy. Along with a snow-density measurement SWE is determined, which is often of interest in hydrological applications (DeBeer and Pomeroy, 2010). As snow depth is more variable within an area than snow density, Sturm and Holmgren (2018) developed an automatic snow depth probe (magnaprobe) capable of increasing snow depth sampling within a field sampling window by automating part of the process.

Point-based snowpack density is estimated by snow pit observations. In its simplest terms, a pit is dug in the snowpack down to the ground level, allowing an observer to record in detail snow stratigraphy, density, temperature and other relevant parameters. Snow pits are frequently used by avalanche forecasters to analyze weak layer formation and mechanical properties to estimate avalanche risk and in snow hydrology where details of the snowpack are required (McClung and Schaerer, 2006). Density cutters are frequently used with various sampling volumes to sample the snow pit face at know

depths to derive a density/SWE profile. Snow pit observations are time-consuming compared to snow tubing method, where less details about the snowpack are observed, but depth and density can quickly be determined. Snow tubes are used to extract gravimetric samples where the volume of the sample and depth is known, allowing for direct SWE estimation. Figure 2.8 shows an example of different snow data types being collected in the Icelandic highlands.

Figure 2.8. ***Left:*** *A typical snow pit where detailed density and temperature have been collected at a range of depths, allowing for SWE determination.* ***Right:*** *Collection of depth and bulk SWE data using the Federal snow sampler. Photos by Andri Gunnarsson.*

Collection of glacier surface mass balance (SMB) data has many similarities to observations of seasonal snow data. In the case of glaciers, mass balance is simply the gain and loss of ice from the glacier system but is collected in the Spring for winter mass balance, and then again in the Fall to collect the summer mass balance (Benn and Evans, 2010). The difference of the two represents the net mass balance of the point or representative glaciers and indicates whether mass is being lost or gained. Surface winter mass balance follows the same principles as peak SWE data for seasonal snow in non-glaciated areas. A measurement is carried out to estimate the accumulated mass of solid precipitation during winter, usually by drilling shallow snow cores at selected locations in the spring to determine the density and depth of the winter snow cover. Stakes, in the accumulation zone, and wires, in the ablation zone, are then left during the summer for a readout in the fall allowing for an estimate of the summer mass balance.

Stationary observations, such as automatic weather stations (AWS), allow for temporally continuous observations of the development of seasonal snow or glacier surfaces.Air

temperature at 2 m height above the surface is often sampled by AWS. To prevent solar radiation from heating the sensors, white naturally aspirated plastic shields cover the sensor in many cases. Precipitation can also be measured, often with heated precipitation gauges where grid electricity is available, but in most snow-dominated catchments this is seldom the case. There, precipitation gauges filled with antifreeze material accumulate the precipitation in a bucket which is continuously weighed, allowing the formation of a time series of mass changes over time. High-quality precipitation observations are challenging, especially in windy snow-dominated areas (Rasmussen et al., 2012).

Incoming solar radiation, a dominating energy flux component, is observed with radiometers equipped with two pyranometers facing upward and downward, respectively, measuring the incident, and reflected short-wave radiation. The ratio of both quantities allows the bi-hemispherical albedo of the surface to be estimated which controls the surface radiative forcing. These instruments are as well sensitive to various factors that affect their accuracy such as, solar zenith angle, tilting of the instruments, riming, snow and liquid precipitation on the sensor domes.

Snow depth can be observed using a sonic ranging device horizontally mounted, observing the distance from the sensor membrane to the surface. As snow builds up, the distance to the sensor is reduced allowing for depth determination. In parallel if the mass of snow is estimated, SWE can be derived. For certain types of snowpack, were bridging does not occur (strong layer of snow lies over a weak layer), a snow pillow can be used, a liquid-filled membrane with an internal pressure observation, able to observe the weight of snow covering the membrane. Other more complex methods such as gamma back scattering passively detect the change in naturally occurring electromagnetic energy from the ground after it passes through the snow cover.

The availability of snow data that spans long historical periods enables interpretation on the impacts of natural and climate variability as well as model calibration and validation. In recent years, technological advancements have extended the possibilities to survey detailed snow information. The advancement and availability of remote sensing and airborne sensors allows for large areas to be mapped in detail for snow depth and other surface properties. The Airborne Snow Observatory (ASO) is an brilliant example of how accurate snow depth, snow water equivalent, and snow albedo observations across large catchments are collected. The data can be used to constraining physically-based, distributed snow models for accurate daily representation of snow mass and energy states, improving daily to seasonal snow melt runoff forecasts. Snow depth and snow albedo data are collected using airborne scanning lidars and imaging spectrometers (Painter et al., 2016). Still, the high-spatial-resolution retrievals of snow depth need to be converted into snow water equivalent by using in-situ data combined with modeling (Painter et al., 2016).

Even though technology evolves fast, from the perspective of remote sensing and modeling, ground-truth data and field observations remain vital to the success of model and sensing technology outputs. Hydrological models are calibrated and validated against observed stream flow, models simulating snow processes are calibrated and

validated against snow course and snow pit data (Painter et al., 2016; Rittger et al., 2016), glacier mass and energy balance models are validated and calibrated against observed surface mass balance measurements and observed energy balance at automatic meteorological stations (Gascoin et al., 2017; Aðalgeirsdóttir et al., 2020; Gunnarsson et al., 2021),radiometric-calibration of remote-sensing sensors and remote sensing products is done against measurements taken from objects on the ground surface (Painter et al., 2009; Bernstein et al., 2012; Schmidt et al., 2017; Wittmann et al., 2017; Gunnarsson et al., 2019, 2021) and so on and so forth, illustrating the importance of high-quality field data.

3 Results and discussion

The original PhD proposal submitted in 2016 was aimed at snow surface energy exchanges and snow melt in Icelandic highlands but evolved into a stronger remote-sensing focus than originally planned. This is partly due to the various knowledge gaps in the field on snow hydrology in Iceland and the associated opportunities in developing understanding though the tools remote-sensing offers. Researchers and academics in the U. S. have been on the forefront in remote sensing of seasonal snow for decades and have a strong connection to the water resources community, supporting operational decisions and improving water resource assessments.The year spent at the University of Washington in 2017–18, strengthened the focus on applied remote-sensing and the collaboration and discussion with many of the leading experts in remote-sensing fueled this interest.

This PhD dissertation started with an exploratory analysis of MODIS data to study snow cover, revealing several limitations in daily usage in Iceland, mainly due to clouds and polar darkness during winter. Figure 3.1 provides a schematic overview of papers produced, how they relate to each other and the main tools and data sources used in each one. Although each paper can be interpreted individually, methods developed, processing pipelines and data sources flow between them, providing the foundation for the PhD dissertation. Sections 5.1–5.4 provide a summary of each paper individually published or submitted in this dissertation work.

The work published in **Paper I** (Icelandic snow cover analysis) aimed at addressing many of these problems by developing a methodology to create near-real-time spatio-temporal continuous snow-cover data set for Iceland which had not been developed before. To ensure the quality of the data set, it was thoroughly validated by alternative higher-resolution remote-sensing products and using available in-situ observations. The daily available MODIS MOD10A1 (Terra) and MYD10A1 (Aqua) snow products were obtained spanning from early 2000–2019, referred to as the MODIS period, but the data have been extended to date. The processing includes daily merging of Aqua and Terra data, temporal aggregation and gap-filling where several classification methods were tested. Further details of these steps are found in the Paper I and II methodology sections. The output from the work includes a daily gap-filled snow cover product that has the potential to be used in operational or historical analytic perspective from February to November since 2000. Paper I further analyses recent changes in snow cover in Iceland spanning the study period, 2000–2017. Various descriptive spatio-temporal dynamics of snow cover in Iceland were derived, such as number of snow-free dates (SFDs), first snow-free date (FSFD) and last snow-free date (LSFD). Variability in the

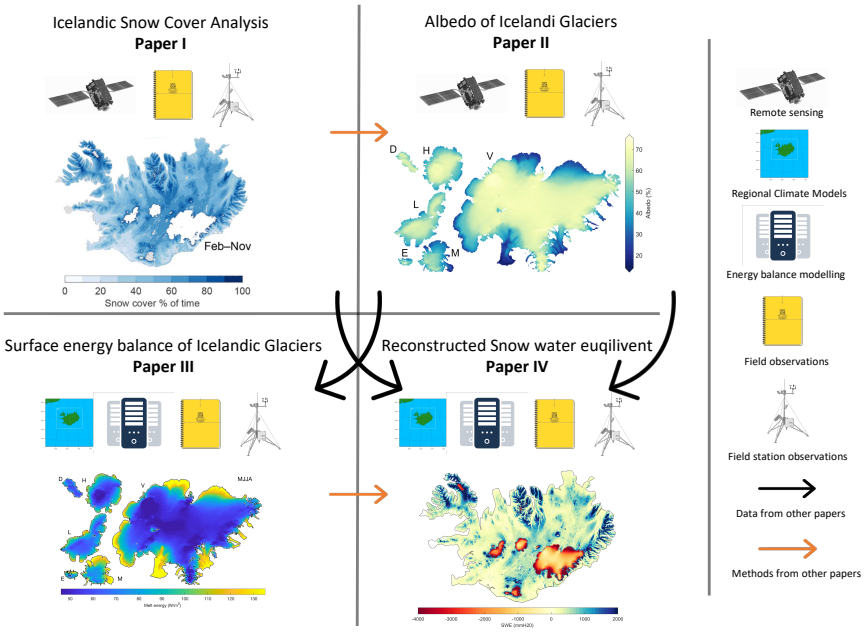

Figure 3.1. Overview of the papers and of their interrelations. Paper I provided methods to Paper II and Paper III provided methods to Paper IV. Data from Paper II was used in Paper III and data from Paper I and II was used in Paper IV.

snow cover was strongly correlated with elevation and indications of a longer snow cover duration in April through September were observed. Since the data only spans 18 years, statistical interpretation such as trends should be treated with care. Recently, ESA published through its Snow Climate Change Initiative Daily Global Snow Cover Fraction from AVHRR spanning the period from 1982–2019 (Naegeli et al., 2021). Since the challenges partially overcome in the methodology developed for MODIS data in Paper I are the same for AVHRR data, the processing pipeline could be adopted to extend the snow cover analysis ranging from 1982 to 2021. This would provide a longer historical time series of snow cover in Iceland illustrating impacts of recent climate change. This illustrates the potential of the method developed and capabilities to extend longer historical perspective and comparable results between satellite sensors.

The work published in **Paper II** (Albedo of Icelandic glaciers) aimed at addressing many of the similar problems faced in Paper I to develop a methodology to create near-real-time spatio-temporal continuous snow and ice albedo data set for Icelandic glaciers. Many of the developments and tools developed on Paper I where adapted and improved in Paper II. It is also notable to mention, that the tools and process pipelines developed have been used in an operational context extending the period investigated in each paper. A spatio-temporal surface albedo product has not previously been developed for glaciers in Iceland. Gascoin et al. (2017) investigated surface albedo for Icelandic glaciers using

the MODIS MCD43A3 albedo product without addressing some of the shortcomings of the MCD43A3 product for glaciers in Iceland, i.e., data availability due to cloud cover. Paper II aimed at deriving an albedo data set suitable for operational use as well as a scientific study of spatial and temporal variations in albedo. The daily MODIS snow products (MOD10A1 and MYD10A1) products were chosen to increase temporal resolution over the strict filtering of the MCD43A3A product. This allowed for more flexibility in post-processing, statistical filtering, and near-real-time data posting. The main objectives in Paper II were, to create a gap-filled MODIS-based surface-albedo product for glaciers in Iceland for the MODIS period, validated with in-situ data suitable for the monitoring and modeling of glaciers in an operational context and monitoring of long-term changes in surface albedo and the associated change in surface radiative forcing. The resulting gap-filled product was then used to analyze and quantify spatio-temporal patterns of albedo for Icelandic glaciers for the time period, with monthly statistics and a detailed interpretation of the variation in albedo with elevation and trends over time. Since the data only spans 20 years, statistical interpretation such as trends should be treated with care. In the future, the data can be used to assess the impact and distribution of volcanic ash depositing in glaciers and seasonal snow, quantifying the impact on runoff and melt enhancement. Figure 3.3 shows the evolution of surface albedo for the major glaciers in Iceland extended through the melt season in 2021. The data provide insight into a dynamic melt season in 2021 where May and June were cold with high cloud cover and little precipitation while July and August where the warmest months in decades. The data extension reveals what previously was demonstrated in Paper II, the high variability of surface albedo for the Icelandic glaciers. The significant positive trends near the equilibrium line in northern Vatnajökull for the period 2000–2019 have become non-significant by adding the melt seasons for 2020 and 2021 to the data set.

The work published in **Paper III** (Energy balance of Icelandic glaciers) uses spatio-temporal albedo data from remote-sensing developed in Paper II to model the surface energy balance of glaciers. Since short-wave radiation is a major melt energy supply for the melting of snow and ice, the correct representation of albedo is crucial. Direct utilization of remotely-sensed albedo has not been done previously for Icelandic glaciers and provides a better understanding of the distribution of radiative forcing, both spatially and with time. A simple energy-balance model for a snow/ice surface was applied with the capability of using any climate forcing at the appropriate resolution in time and space in conjunction with a spatially-distributed albedo. The model solves the surface energy balance of a snow-covered surface by iteratively solving for surface temperature.

The results further support the importance of short-wave radiation as a major melt energy component and shows variability in melt energy between glaciers and years. The impacts of volcanic eruptions in 2010 and 2011 are clearly seen through the radiative forcing by light-absorbing particles (LAPs) in snow and glacier surface from tephra deposits. Similar processes through radiative forcing by light-absorbing particles were also extensive in 2019 with an early melt-out of seasonal snow in the spring and favorable conditions for dust and sand transport from pro-glacial areas (dust hot spots) upon glacier surfaces. The melt enhancement from increased radiative forcing, for

selected eruption years due to LAPs, was estimated by modeling alternative scenarios. The same climatology was assumed but different albedo evolution based on long-term mean values excluding the high LAPs impact years. Estimates showed that melt enhancement due to high LAPs for volcanic eruptions was 20–50% higher than average, depending on glacier investigated.

Since surface energy balance modulates the surface mass balance, analysis of the surface energy balance relationship with large-scale atmospheric circulation anomalies was studied to better understand drivers of variability in surface energy balance. Significant relationships were found between melt energy and the Greenland Blocking Index (GBI), the North Atlantic Oscillation (NAO) and sea-surface temperature illustrating the importance of ocean currents and surface conditions for the climate in Iceland.

The area south of Iceland has been observed to experience sea-surface cooling in the past years, contrary to the global sea-surface temperatures, showing a clear increase. This region of local cooling has been referred to as the North Atlantic warming hole (NAWH), as it shows clear fingerprints of a change in climate. The NAWH showed significant correlation with cloud cover for Icelandic glaciers which modulates available incoming short-wave radiation, impacting the surface energy balance. The links to large-scale circulation patterns also emphasize the influences that changes in these large-scale systems might have for glacier energy balance and might provide insight into the impacts of climate change in the near future. Since the data only spans 20 years, statistical interpretation such as trends should be treated with care.

The work published in **Paper IV** (Reconstructing seasonal snow and glacier melt) utilizes the potential brought forth by Papers I, II and III. It incorporates the availability of spatio-temporal fractional snow cover and albedo from remote sensing, utilized in a surface energy balance model to estimate daily melt energy availability. Incoming short-wave energy contributing to daily estimates of melt energy were constrained by remotely sensed surface albedo for snow covered surfaces, similar to the work in Paper III. Fractional snow cover was used for non-glaciated areas, as it provides estimates of snow cover for each pixel. Therefore, available daily estimates of melt energy in a given area, were the product of the possible melt energy and the fractional snow cover of the area or pixel, for non-glaciated areas. For seasonal snow, available daily estimates of melt energy were summed from the day of snow disappearance until March 15th each year. For glaciers, since snow cover is 100% during all periods, all available melt energy were summed to account for annual summer melt. This provided daily estimates of melt water to estimate seasonal snow and glacier melt in Iceland for the period 2000–2019.

Observations from snow pits on land and glacier summer mass balance were used for validation purposes. The agreement between reconstructed SWE and observations was generally acceptable for Vatnajökull while poorest for Mýrdalsjökull with R^2 values ranging from 0.8–0.94 and RMS errors ranging from 0.35–0.43 mH20. For glaciers melt was systematically overestimated at higher elevations (deeper winter snowpack), mostly visualized for Mýrdalsjökull. Seasonal snow was also partially validated with the limited data set of observed SWE in the Icelandic highlands showing and RMS error

of 0.29 mH2O and R^2 of 0.46.

The results show that the inter-annual SWE variability were generally high both for seasonal snow and glaciers. For seasonal snow the largest SWE (>1000 mm) were found in mountainous and alpine areas close to the coast, notably in the East- and Westfjords, Tröllaskaga, and in the proximity of glaciers. Lower SWE values were observed in the central highlands, flatter inland areas and at lower elevations. For glaciers, generally more SWE (more summer melt) was associated with lower glacier elevations while less melt is observed at higher elevations. For the impurity-rich bare-ice areas exposed annually, observed SWE was larger than 3000 mm.

Figure 3.4 shows annual spatial patterns for melt season (MJJA) SWE anomalies for 2000–2019. Blue colors represent anomalies below the mean, i.e., lower melt season average SWE values, while red areas represent values above the mean, contributing more seasonal SWE. No clear correlation was found for seasonal snow and glacier melt, i.e., positive melt anomalies were not necessarily associated with positive anomalies for glaciers, although certain patterns could be identified.

The largest anomalies for glaciers were observed at all glaciers in 2010 associated with severe LAPs depositions due to the volcanic eruptions in Eyjafjallajökull along a warm and sunny summer. Less melt enhancement was observed associated with the 2011 Grímsvötn eruption at Vatnajökull although the LAPs deposits were quite clear in surface albedo data south and southeast of the Grímsvötn eruption site. One difference between these two events for the southern outlet of Vatnajökull was a later onset of LAPs in 2011 but also a colder cloudier spring. Less incoming short-wave energy was forced by the surface in June and much less in July and August in 2011 than for 2010 explaining most of the difference in melt.

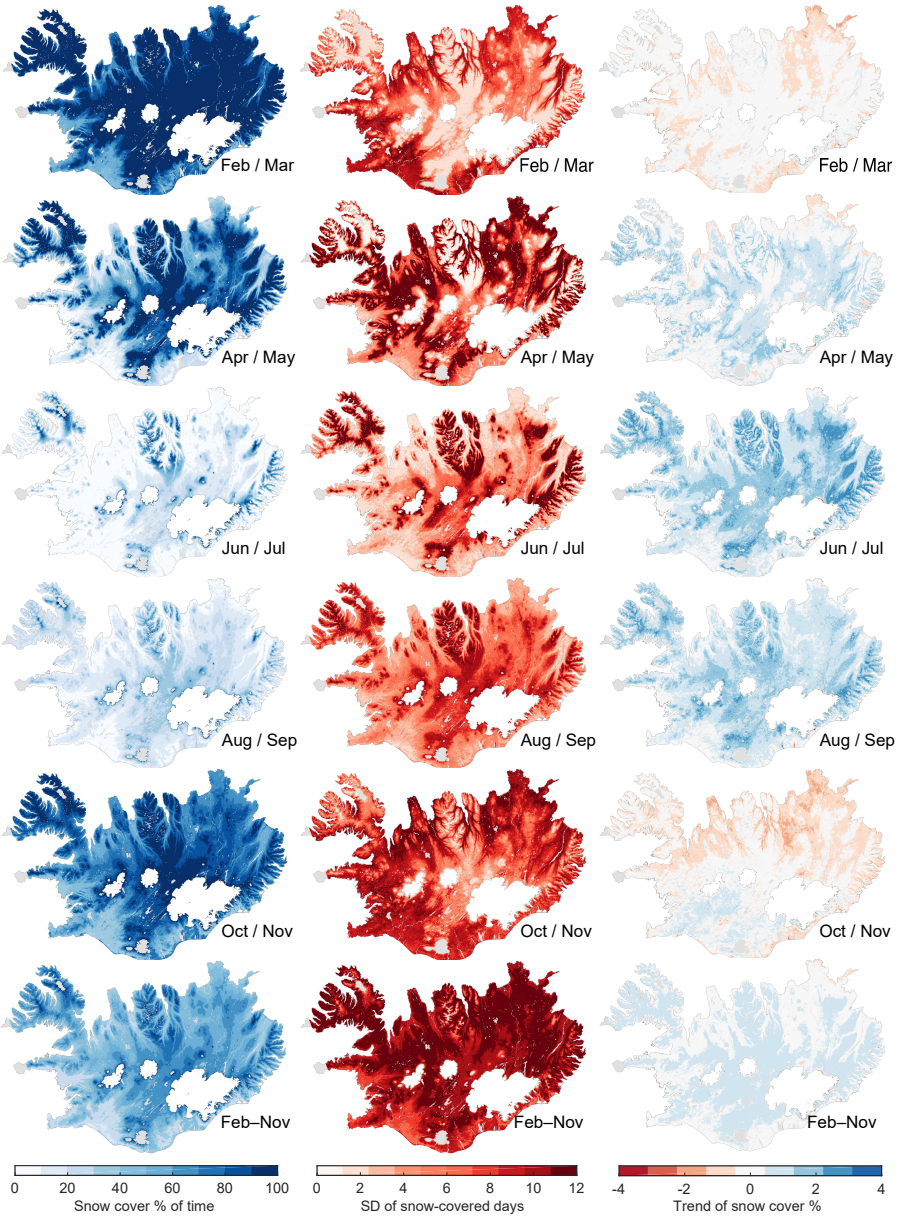

Figure 3.2. First column: mean snow cover duration as percentage of time for each period. Second column: standard deviation of days for each period. Third column: mean trend in snow cover duration as percentage of time for each period. Rows represent different combinations of monthly values and the bottom row is for the whole period from February to November. Figure from Paper I.

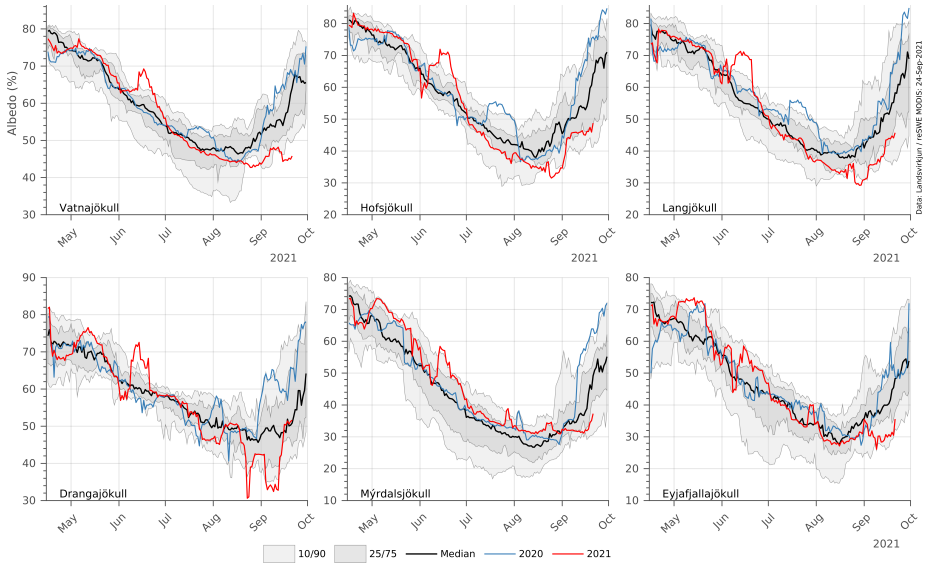

Figure 3.3. Extended time series for surface albedo for the glaciers studied in Paper II adding melt season 2020 and 2021. Comparable to Figure 8 in Paper II.

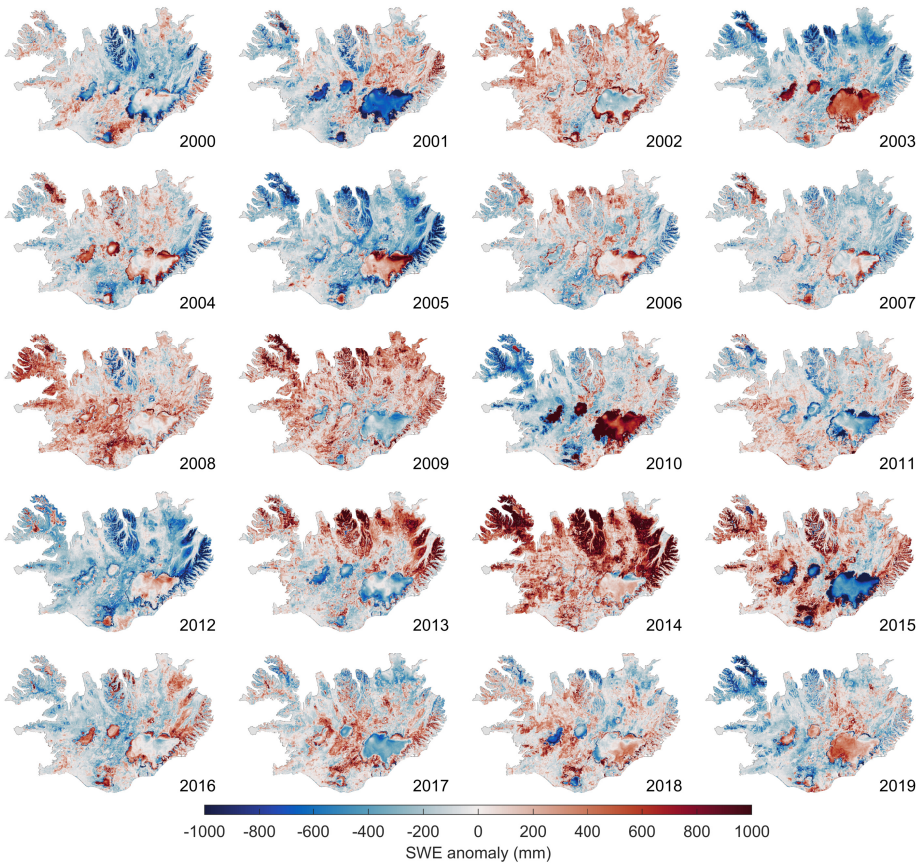

Figure 3.4. Annual spatial patterns for melt season (MJJA) SWE anomalies for 2000–2019. Red colors denote positive values where melt was above the average, i.e., more melt while blue colors show the opposite.

4 Conclusion

The objective of the PhD research was too obtain a better understanding of the spatio-temporal signatures of snow and glacier related properties such as snow cover, snow surface albedo, snow water equilivent, surface energy balance, timing of melting and changes and trends of those properties over time.

Optical remote sensing, with daily overpass at a course resolution, was adopted to develop methods to address some of the shortcomings and challenges posed in Iceland. The main challenge for optical sensors relates to the fact that cloud cover is generally high, limiting usable data on daily timescales. Other challenges included preprocessing steps of variables already undertaken in existing products (e.g., MCD43A3 surface albedo), such as snow- and ice albedo, rejecting large samples of data due to strict general filtering. These issues were addressed by developing a processing framework utilizing daily MODIS data fused in a process that merges daily non-cloud obscured data and then applies further temporal aggregation with outlier removal to enhance data availability. In many areas, these steps were not sufficient to provide gap-filled data in space and time but by applying machine learning methods to classify the remaining cloud obscured pixels, a spatio-temporal product could be derived.

The process described was applied for snow cover of the surface and for snow- and ice albedo yielding a spatio-temporal data set from 2000–2021 with capabilities to run the production of data operationally. The products generated were thoroughly validated using alternative remote-sensing products and in-situ data with overall good visual and statistical results. From the products developed, spatial and temporal variability were analyzed and reported providing insights into recent changes and trends. In general, high annual and inter-annual variability was confirmed for snow cover and albedo. To quantify and describe these physical processes, various descriptive statistics were derived. The products were used to analyze and estimate the impacts on surface albedo from volcanic eruptions and light-absorption particle deposits on snow- and ice-covered surfaces.

The results showed that volcanic eruptions could have significant impact on albedo, even if the eruption location was distant. Light-absorbing particles deposits from non-eruption events were also identified to have a potential for significant lowering of albedo, associated with general melt enhancement. Due to the hydrophobic behavior of LAPs, accumulating in the surface of snow, the earlier onset of deposits yielded a more prolonged effect through the melt season. Snow cover showed a general increase in spring and early summer with a reduction of snow-cover duration in the fall for the

period although individual years with high/low snow cover impacted the trend. As found for albedo, snow cover was highly variable between years. Operational use of the products seems feasible, with opportunities to estimate the impacts in near-real-time of volcanic and LAP deposits on surface albedo and the evolution of snow cover in spring, summer, and fall.

Harnessing further the potential brought forth with the gap-filled snow and albedo products, an energy balance model was developed that had the capabilities to reconstruct the surface energy balance of snow- and ice-covered surfaces by coupling remotely sensed snow cover and albedo and climate forcing data. The reconstruction results in an estimate of the surface energy balance of Icelandic glaciers and seasonal snow for 2000 to 2021 at a 500 m daily resolution. The surface energy balance was used to estimate and quantify various processes and the impacts of volcanic eruptions and LAP events. This methodology provides usage of observed processes to constrain model calculations and improve the estimation of energy and mass fluxes that are constrained by snow cover and albedo. Especially in the case of surface albedo, frequent LAPs deposits and annual evolution of bare-ice exposure can be challenging to represent in physical models. To provide better understanding of the large-scale atmospheric processes driving the variability in surface energy balance, relations between various climate and oceanographic processes were extracted and relationships identified. The analysis shows close relation between seas surface temperature, cloud cover and incoming short-wave radiation and the possible implications changes in these processes could have of the surface energy balance.

The results showed that incoming short-wave radiation forced at the surface, modulated by surface albedo, was the major surface energy balance component contributing melt energy. This reflected the importance as well of accurately estimating surface albedo, especially for LAPs events where melt enhancement was significant. The large-scale atmospheric patterns and sea-surface temperatures also detailed the correlation between these processes and the surface energy balance. Notably, a strong relationship between sea-surface temperatures south of Iceland and cloud cover over glaciers was observed impacting net forced short-wave radiation, illustrating impacts of sea-surface temperatures on low level cloud cover production, which then modulates incoming short-wave radiation.

In a rapidly changing world, it is important to build upon the products developed to continue monitoring and observations of changes. Future work, extending the work done here, might include fusing alternative data to the analysis of snow cover. Successfully applied here, NASA's MODIS sensors are approaching end-of-life after supplying valuable information about Earth's surface since early 2000. New data from more recent and future satellite missions allow for continuity so snow cover and albedo can be monitored into the near future. Since the challenge of cloud obscured surfaces remains and is unlike to change in the near future further fusion of different sensors might be of value to increase the number of non-cloud-obscured pixels. Alternative data sources, such as Synthetic-aperture radar (SAR) which has cloud penetrating capabilities might be promising to address some of the limitations of optical sensors for snow-cover

studies.

The availability of remote sensing products has increased rapidly in the past two decades with exponential growth in the past five years. Mega smallsat constellations are now a reality leading a paradigm shift in how the Earth is observed and monitored for changes. Remote sensing is evolving from a single data source problem to multiple sources, at multiple timescales from multiple sensors, creating big data applications that need innovative methodologies fusing these streams into usable information. Data challenges, method development and analysis remain related to extracting information to be communicated to various audiences and for decision support.

5 Summary of Publications

In this chapter, the papers on which the PhD dissertation is based are summarized individually and the main conclusion set forth for each individual paper. The interrelation of the papers is shown in Figure 3.1 and discussed in Section 3.

5.1 Paper I: Icelandic snow cover characteristics

Gunnarsson, A., Garðarsson, S. M., and Sveinsson, Ó. G. B.: *Icelandic snow cover characteristics derived from a gap-filled MODIS daily snow cover product*, Hydrol. Earth Syst. Sci. , 23, 3021–3036, https://doi. org/10. 5194/hess-23-3021-2019, 2019.

Paper I developed a spatio-temporal continuous data set for snow cover in Iceland based on the Moderate Resolution Imaging Spectroradiometer (MODIS) from 2000–2018. An operational processing pipeline was developed aimed at extending the data period in Paper I with capabilities to provide near-real-time data for hydrological modeling or monitoring of snow cover in Iceland. The main limiting factors for data availability of remotely-sensed optical data at higher latitudes were cloud cover and polar darkness which reduce the usable data significantly. In Iceland, the average cloud cover is about 75% with some spatial variations. Polar darkness reduces data availability from the MODIS sensor from late November until mid-January, limiting observations during that period. By applying daily data merging from NASA Terra and Aqua polar orbiting satellites and a temporal data aggregation of 7 day, pixels classified as clouds were reduced from 75% to 14%. The remaining unclassified pixels after daily merging and temporal aggregation were reclassified with classification learners trained with classified data, pixel location, aspect, and elevation.

Various classification methods, from simple to complex, such as classification trees, *k*-nearest neighbor algorithms (fine, coarse, cubic, weighted, boosted), supportive vector machines (SVMs), and linear and quadratic discriminant classification learners were tested in various configurations. Overall, no one method tested surpassed the others significantly although large variations were found in training time of the different models. Average classification accuracy ranged over 90% for all methods tested. The marginal best classification performance was by a weighted *k*-nearest neighbor (wkNN) classifier witch was selected for further use, both because of its simplicity and computational ease.

MODIS snow cover data were validated over Iceland with comparison to manned in-situ observations and Landsat 7/8 and Sentinel 2 data. Overall, a very good agreement was found between in-situ observed snow cover, with an average agreement of 0.925. Agreement of Landsat 7/8 and Sentinel 2 was found to be acceptable, with R2 values 0.96, 0.92 and 0.95, respectively, and in agreement with other studies.

Various snow cover characteristic metrics were derived for each pixel such as snow cover duration, first and last snow-free dates, deviation and dynamics of snow cover and trends during the study period. The main conclusion was that for the study period a trend of increasing snow cover duration was observed for all months except October and November. However, statistical testing of the trends indicated that there was only a significant trend in June. The slight increase in average snow cover in spring, likely driven by cold springs in 2013, 2014 and 2015 and extended liquid-phase precipitation in the fall for the same years. This aligns with observations of winter mass balance of Icelandic glaciers in recent years with a slight significant positive trend for the past 20 years. No clear signs of melt enhancement in spring for 2010 and 2011 were seen, associated with the volcanic eruptions in Eyjafjallajökull and Grímsvötn, although albedo and summer melt of Icelandic glaciers were greatly influenced as shown in Papers II and III.

The gap-filled snow-cover product provides a useful tool to monitor and analyze inter-annual variability and long-term trends in snow cover in Iceland. The methodology applied can be applied to other satellite sensors such as Sentinel 3 or the Visible Infrared Imaging Radiometer Suite (VIIRS) to extend the temporal range of data beyond the MODIS mission.

5.2 Paper II: Albedo of Icelandic glaciers

Gunnarsson, A., Gardarsson, S. M., Pálsson, F., Jóhannesson, T., and Sveinsson, Ó. G. B.: *Annual and interannual variability and trends of albedo for Icelandic glaciers*, The Cryosphere, 15, 547–570, https://doi. org/10. 5194/tc-15-547-2021, 2021.

During the melt season, absorbed solar energy, modulated at the surface predominantly by albedo, is one of the main governing factors controlling surface-melt variability for glaciers in Iceland. Therefore the correct representation of surface albedo is critical for correct glacier-melt modeling.

Paper II develops a spatio-temporal continuous data set for surface albedo for snow and ice for Icelandic glaciers based on the Moderate Resolution Imaging Spectroradiometer (MODIS) from 2000 to 2019. Similar to the work in Paper I, an operational processing pipeline was developed aimed at extending the data period in Paper II with capabilities to provide near-real-time data for hydrological and glacier modeling or monitoring of glacier albedo in Iceland. Similar challenges arise as in Paper I, to mitigate limited data

availability due to frequent cloud-covered pixels.

Overall, good visual and statistical agreement was found between the surface albedo data produced and in-situ albedo from automatic weather station data observations over a range of elevations and glacier locations. Higher RMSE values were found in the ablation zone, which could be related to higher albedo variability within a MODIS pixel for impurity-rich bare-ice in the ablation zone, indicating that care must be taken when comparing point-based in-situ observations with data with a larger spatial footprint.

The results show that spatio-temporal patterns for the melt season have generally high annual and inter-annual variability for Icelandic glaciers, ranging from high fresh-snow albedo of about 85—90% in spring to 5—10% in the impurity-rich bare-ice area during the peak melt season. The analysis shows that the volcanic eruptions in 2010 and 2011 had significant impact on albedo and had a residual effect in the following years. Furthermore, airborne dust, from unstable sandy surfaces close to the glaciers, is shown to enhance radiative forcing and decrease albedo.

A significant positive albedo trend was observed for northern Vatnajökull while other glaciers have non-significant trends for the study period. The results indicate that the high variability in albedo for Icelandic glaciers is driven by climatology, i.e., snow metamorphosis, tephra fallout during volcanic eruptions and their residual effects in the post-eruption years, and dust loading from widespread unstable sandy surfaces outside the glaciers. This illustrates the challenges in albedo parameterization for glacier surface-melt modelling for Icelandic glaciers, as albedo development is driven by various complex phenomena, which may not be correctly captured in conventional energy-balance models.

5.3 Paper III: Energy balance for Icelandic glaciers

Gunnarsson, A., Gardarsson, S. M. and Pálsson, F.: *Modeling of surface energy balance for Icelandic glaciers using remote sensing albedo*, to be submitted.

During the melt season, absorbed solar energy, modulated at the surface, predominantly by albedo, is one of the main governing factors controlling surface-melt variability for glaciers in Iceland. Therefore the correct representation of surface albedo is critical for correct glacier melt modeling.

Many of the desert areas near glaciers are sources of active dust emission, defined as dust hot spots (e.g., glacio-fluvial plains, beached and sand plains) that are unstable surfaces and are prone to dust aerosol production that can deposit in snow and glacier surfaces influencing the surface albedo, and thus the radiative forcing. Activity in glacier-covered volcanoes can also cause volcanic ash and tephra fall-outs on glaciers during eruptions, enhanced melt or in some cases, glacier surface isolation reducing

melt significantly. Energy balance models generally do not simulate processes effected by atmospheric dust and light absorbing particle depositions, as they are often complex and can originate far from glaciated surfaces unless they are forced with observational data.

An energy balance model was developed with the possibility to utilize the spatio-temporal albedo products developed in Paper II driven by high-resolution climate forcing data reconstructing the surface energy balance (SEB) for all Icelandic glaciers. The surface energy balance was reconstructed from April through September for 2000–2021 at a daily timestep with a 500 m spatial resolution. Validation was performed using observations from various glaciers spanning different locations and elevations with good visual and statistical results.

The results indicate that the inter-annual surface energy balance (SEB) variability for Icelandic glaciers was generally high, mostly driven by variability in forced short-wave radiation. A strong elevation gradient in surface energy balance reduction aligns with increased albedo with elevation.

Large impacts on the surface energy balance were observed for years with high LAPs deposits, such as volcanic eruptions in 2004, 2010, 2011 and the sand and dust rich year of 2019. The impacts of volcanic eruptions and other LAPs events were estimated using historical mean albedo under the same climatology forcing, to provide estimations of melt energy enhancements. The results showed that in many cases, the impacts were significant even though the glaciers were far away from the eruption location. Drangajökull seemed to be the only glacier not impacted by LAPs events in general, consequent with the lowest variability in short-wave radiation forcing.

For the period 2000–2012, cloud cover was overall below average as well as albedo for the MJJA average, increasing short-wave radiation availability.For the period after 2012, cloud cover was on average higher and for albedo, similar changes were observed for all glaciers, an average increase in albedo of 1.5% was observed excluding the impacts of 2010 and 2011.

To understand the role and impacts of large-scale atmospheric circulation anomalies, various patterns such as the Greenland Blocking Index (GBI), North Atlantic Oscillation (NAO), cloud cover and sea-surface temperature data from different regions around Iceland was considered. Analysis of these data shows the strong significant relationship between cloud cover and sea-surface temperatures which impacts cloud cover over Icelandic glaciers, modulating available incoming short-wave radiation. The results highlight the implications further changes in ocean currents and heat transport around Iceland might have on glacier surface-energy balance modulating surface mass balance.

5.4 Paper IV: Spatial estimation of snow water equivalent by for glaciers and seasonal snow in Iceland using remote sensing snow cover and albedo

Gunnarsson, A., Gardarsson, S. M.: *Spatial estimation of snow water equivalent by for glaciers and seasonal snow in Iceland using remote sensing snow cover and albedo*, manuscript in preparation.

Reliable estimations of snow water equivalent (SWE) in alpine and mountainous terrain remain a challenge in the observational, modeling and remote sensing domains. An energy balance model was developed with the possibility to utilize spatio-temporal fractional snow cover and albedo from remote sensing. Fractional snow cover was used for non-glaciated areas, as it provides estimates of snow cover for each pixel and surface albedo provides a constrain on incoming short-wave radiation available as melt energy for snow and ice. The model was forced by high-resolution climate reanalysis data outputting energy balance components and melt energy. For seasonal snow, available daily estimates of melt energy were summed from the day of snow disappearance until March 15th each year. For glaciers, since snow cover is 100% during all periods, all available melt energy were summed to account for annual summer melt. This provided daily estimates of melt water to estimate seasonal snow and glacier melt in Iceland for the period 2000–2021.

The results show that the inter-annual SWE variability were generally high both for seasonal snow and glaciers. For seasonal snow the largest SWE (>1000 mm) were found in mountainous and alpine areas close to the coast, notably in the East- and Westfjords, Tröllaskaga, and in the proximity of glaciers. Lower SWE values were observed in the central highlands, flatter inland areas and at lower elevations. For glaciers, generally more SWE (more summer melt) was associated with lower glacier elevations while less melt is observed at higher elevations. For the impurity-rich bare-ice areas exposed annually, observed SWE was larger than 3000 mm.

In April and May, seasonal snow at lower and mid elevations was mostly depleted with May generally producing more melt than in April. The highest melt volumes were in May and June. In June and July seasonal snow was mostly constrained with high SWE accumulation areas. In September small snowfalls were often observed generally melted but in some higher elevation areas forming the base for the following winters snowpack. For glaciers the onset of melt was observed in April at lower elevations. Especially for the low elevation outlet glacier of southern Vatnajökull large quantities of melt were observed for the all months. With warmer temperatures and increasing short-wave energy in May and June more glacier melt was observed generally peaking in late June to mid-July. As winter snow was melted exposing impurity-rich bare-ice areas with lower albedo values more short-wave energy was forced increasing melt.

Negative significant trends at the terminus of glaciers were expected due to glacier retreat in recent decades, with associated debris deposits on dead ice. For sesaonal snow, significant positive trends were observed for most of Austfirðir and Tröllaskagi but also for smaller mountainous areas in east and north Iceland. These trends align with recent results from the same period from (Gunnarsson et al., 2019) reporting that the snow cover extent was spanning a longer time, i.e., that snow cover was extending further into the spring and summer months.

References

Acevedo, P., Ruiz-Fons, F., Estrada, R., Márquez, A. L., Miranda, M. A., Gortázar, C., and Lucientes, J. (2010). A broad assessment of factors determining culicoides imicola abundance: Modelling the present and forecasting its future in climate change scenarios. *PLOS ONE*, 5(12):1–13.

Ackroyd, C., Skiles, S. M., Rittger, K., and Meyer, J. (2021). Trends in Snow Cover Duration Across River Basins in High Mountain Asia from Daily Gap-Filled MODIS Fractional Snow-Covered Area. *Frontiers in Earth Science*, 9:828.

Adam, J. C., Clark, E. A., Lettenmaier, D. P., and Wood, E. F. (2006). Correction of Global Precipitation Products for Orographic Effects. *Journal of Climate*, 19(1):15–38.

Adam, J. C., Hamlet, A. F., and Lettenmaier, D. P. (2008). Implications of global climate change for snowmelt hydrology in the twenty-first century. *Hydrological Processes*, 23(7):962–972.

Adam, J. C. and Lettenmaier, D. P. (2003). Adjustment of global gridded precipitation for systematic bias. *Journal of Geophysical Research: Atmospheres*, 108(D9).

Adolph, A. C., Albert, M. R., Lazarcik, J., Dibb, J. E., Amante, J. M., and Price, A. (2017). Dominance of grain size impacts on seasonal snow albedo at open sites in New Hampshire. *Journal of Geophysical Research: Atmospheres*, 122(1):121–139.

Alexander, D. (2013). Volcanic ash in the atmosphere and risks for civil aviation: A study in European crisis management. *International Journal of Disaster Risk Science*, 4(1):9–19.

Anderson, E. A. (1976). A point energy and mass balance model of a snow cover. *U.S. Dept. of Commerce, National Oceanic and Atmospheric Administration, National Weather Service, Office of Hydrology,*.

Andreadis, K. M. and Lettenmaier, D. P. (2006). Assimilating remotely sensed snow observations into a macroscale hydrology model. *Advances in Water Resources*, 29(6):872–886.

Aðalgeirsdóttir, G., Magnússon, E., Pálsson, F., Thorsteinsson, T., Belart, J. M. C., Jóhannesson, T., Hannesdóttir, H., Sigurðsson, O., Gunnarsson, A., Einarsson, B., Berthier, E., Schmidt, L. S., Haraldsson, H. H., and Björnsson, H. (2020). Glacier Changes in Iceland from 1890 to 2019. *Frontiers in Earth Science*, 8:520.

Bair, E. H., Abreu Calfa, A., Rittger, K., and Dozier, J. (2018a). Using machine learning for real-time estimates of snow water equivalent in the watersheds of Afghanistan. *The Cryosphere*, 12(5):1579–1594.

Bair, E. H., Davis, R. E., and Dozier, J. (2018b). Hourly mass and snow energy balance measurements from mammoth mountain, ca usa, 2011–2017. *Earth System Science Data*, 10(1):549–563.

Bair, E. H., Rittger, K., Davis, R. E., Painter, T. H., and Dozier, J. (2016). Validating reconstruction of snow water equivalent in California's Sierra Nevada using measurements from the NASA Airborne Snow Observatory. *Water Resources Research*, 52(11):8437–8460.

Bair, E. H., Rittger, K., Skiles, S. M., and Dozier, J. (2019). An Examination of Snow Albedo Estimates from MODIS and Their Impact on Snow Water Equivalent Reconstruction. *Water Resources Research*, 55(9):7826–7842.

Baraka, S., Akera, B., Aryal, B., Sherpa, T., Shresta, F., Ortiz, A., Sankaran, K., Ferres, J. L., Matin, M., and Bengio, Y. (2020). Machine learning for glacier monitoring in the Hindu Kush Himalaya. *Computer Vision and Pattern Recognitio*, abs/2012.05013.

Barnett, T. P., Adam, J. C., and Lettenmaier, D. P. (2005). Potential impacts of a warming climate on water availability in snow-dominated regions. *Nature*, 438:303.

Barrett, A. P. (2003). *National Operational Hydrologic Remote Sensing Center snow data assimilation system (SNODAS) products at NSIDC*. National Snow and Ice Data Center, Cooperative Institute for Research.

Barry, R. G. (2002). The Role of Snow and Ice in the Global Climate System: A Review. *Polar Geography*, 26(3):235–246.

Barsotti, S., Di Rienzo, D. I., Thordarson, T., Björnsson, B. B., and Karlsdóttir, S. (2018). Assessing impact to infrastructures due to tephra fallout from Öræfajökull volcano (Iceland) by using a scenario-based approach and a numerical model. *Frontiers in Earth Science*, 6:196.

Benn, D. and Evans, D. (2010). Glaciers and Glaciation, 2nd edition. *Routledge, London*, page 816.

Bergström, S. and Forsman, A. (1973). Development of a conceptual deterministic rainfall-runoff model. *Nordic Hydrol.*, 4:147–170.

Bernstein, L. S., Jin, X., Gregor, B., and Adler-Golden, S. M. (2012). Quick atmospheric correction code: algorithm description and recent upgrades. *Optical Engineering*, 51(11):1 – 12.

Biemans, H., Siderius, C., Lutz, A. F., Nepal, S., Ahmad, B., Hassan, T., von Bloh, W., Wijngaard, R. R., Wester, P., Shrestha, A. B., and Immerzeel, W. W. (2019). Importance of snow and glacier meltwater for agriculture on the Indo-Gangetic Plain. *Nature Sustainability*, 2(7):594–601.

Björnsson, H. (2003). *The Annual Cycle of Temperature in Iceland.* Reykjavík : Veðurstofa Íslands, Reykjavík.

Björnsson, H., Bjarni Diðrik Sigurðsson, Brynhildur Davíðsdóttir, Jón Sigurður Ólafsson, Ólafur S. Ástþórsson, Snjólaug Ólafsdóttir, Trausti Baldursson, and Trausti Jónsson (2018). Loftslagsbreytingar og áhrif þeirra á Íslandi : Skýrsla vísindanefndar um loftslagsbreytingar 2018. Technical report, Veðurstofa Íslands, Reykjavík.

Björnsson, H. (1975). Subglacial water reservoirs, jökulhlaups and volcanic eruptions. *Jökull*, 25:1–14.

Björnsson, H. (1978). The surface area of glaciers in Iceland. *Jökull*, 28:31.

Björnsson, H. (1992). Jökulhlaups in Iceland: prediction, characteristics and simulation. *Annals of Glaciology*, 16:95–106.

Björnsson, H. (2010). Understanding jökulhlaups: From tale to theory. *Journal of Glaciology*, 56(200):1002–1010.

Björnsson, H. and Pálsson, F. (2008). Icelandic glaciers. *Jökull*, 58:365–386.

Bojinski, S., Verstraete, M., Peterson, T. C., Richter, C., Simmons, A., and Zemp, M. (2014). The Concept of Essential Climate Variables in Support of Climate Research, Applications, and Policy. *Bulletin of the American Meteorological Society*, 95(9):1431–1443.

Bolić, T. and Źarko Sivčev (2011). Eruption of Eyjafjallajökull in Iceland: Experience of European Air Traffic Management. *Transportation Research Record*, 2214(1):136–143.

Box, J. E., Fettweis, X., Stroeve, J. C., Tedesco, M., Hall, D. K., and Steffen, K. (2012). Greenland ice sheet albedo feedback. thermodynamics and atmospheric drivers. *The Cryosphere*, 6(4):821–839.

Brenowitz, N. D. and Bretherton, C. S. (2018). Prognostic validation of a neural network unified physics parameterization. *Geophysical Research Letters*, 45(12):6289–6298.

Broxton, P. D., van Leeuwen, W. J. D., and Biederman, J. A. (2019). Improving snow water equivalent maps with machine learning of snow survey and lidar measurements. *Water Resources Research*, 55(5):3739–3757.

Chen, X., Liang, S., and Cao, Y. (2016). Satellite observed changes in the Northern Hemisphere snow cover phenology and the associated radiative forcing and feedback between 1982 and 2013. *Environmental Research Letters*, 11(8):084002.

Choi, G., Robinson, D. A., and Kang, S. (2010). Changing Northern Hemisphere Snow Seasons. *Journal of Climate*, 23(19):5305–5310.

Claverie, M., Ju, J., Masek, J. G., Dungan, J. L., Vermote, E. F., Roger, J.-C., Skakun, S. V., and Justice, C. (2018). The Harmonized Landsat and Sentinel-2 surface reflectance data set. *Remote Sensing of Environment*, 219:145–161.

Cline, D. W., Bales, R. C., and Dozier, J. (1998). Estimating the spatial distribution of snow in mountain basins using remote sensing and energy balance modeling. *Water Resources Research*, 34(5):1275–1285.

Crawford, N. H. (1966). Digital Simulation in Hydrology : Stanford Watershed Model IV. *Stanford Univ. Tech. Report.*, 39.

Crochet, P., Jóhannesson, T., Jónsson, T., Sigurðsson, O., Björnsson, H., Pálsson, F., and Barstad, I. (2007). Estimating the Spatial Distribution of Precipitation in Iceland Using a Linear Model of Orographic Precipitation. *Journal of Hydrometeorology*, 8(6):1285–1306.

Damby, D. E., Horwell, C. J., Larsen, G., Thordarson, T., Tomatis, M., Fubini, B., and Donaldson, K. (2017). Assessment of the potential respiratory hazard of volcanic ash from future Icelandic eruptions: a study of archived basaltic to rhyolitic ash samples. *Environmental Health*, 16(1):98.

de Rosnay, P., Isaksen, L., and Dahoui, M. (2015). Snow data assimilation at ECMWF. *ECMWF Newsletter*, 143:26–31.

DeBeer, C. M. and Pomeroy, J. W. (2010). Simulation of the snowmelt runoff contributing area in a small alpine basin. *Hydrology and Earth System Sciences*, 14(7):1205–1219.

Dietz, A. J., Wohner, C., and Kuenzer, C. (2012). European Snow Cover Characteristics between 2000 and 2011 Derived from Improved MODIS Daily Snow Cover Products. *Remote Sensing*, 4(8):2432–2454.

Dong, C. (2018). Remote sensing, hydrological modeling and in situ observations in snow cover research: A review. *Journal of Hydrology*, 561:573–583.

Donlon, C., Berruti, B., Buongiorno, A., Ferreira, M.-H., Féménias, P., Frerick, J., Goryl, P., Klein, U., Laur, H., Mavrocordatos, C., Nieke, J., Rebhan, H., Seitz, B., Stroede, J., and Sciarra, R. (2012). The Global Monitoring for Environment and Security (GMES) Sentinel-3 mission. *Remote Sensing of Environment*, 120:37–57.

Donohoe, A. and Battisti, D. S. (2011). Atmospheric and Surface Contributions to Planetary Albedo. *J. Climate*, 24(16):4402–4418.

Dozier, J. (1989). Spectral signature of Alpine snow cover from LANDSAT Thematic Mapper. *Remote Sensing of Environment*, 45:9–22.

Dozier, J., Painter, T. H., Rittger, K., and Frew, J. E. (2008). Time–space continuity of daily maps of fractional snow cover and albedo from MODIS. *Advances in Water Resources*, 31(11):1515–1526.

Drusch, M., Bello], U. D., Carlier, S., Colin, O., Fernandez, V., Gascon, F., Hoersch, B., Isola, C., Laberinti, P., Martimort, P., Meygret, A., Spoto, F., Sy, O., Marchese, F., and Bargellini, P. (2012). Sentinel-2: ESA's Optical High-Resolution Mission for GMES Operational Services. *Remote Sensing of Environment*, 120:25 – 36.

Einarsson, M. A. (1984). Climates of the Oceans, H. Van Loon (ed.). Vol. 15 of World Survey of Climatology, editor-in-chief H. E. Landsberg. *Journal of Climatology*, 5(1):673–697.

Eltahir, E. A. B. and Wang, G. (1999). Nilometers, El Niño, and climate variability. *Geophysical Research Letters*, 26(4):489–492.

Emery, W. and Camps, A. (2017). Chapter 1 - The History of Satellite Remote Sensing. In Emery, W. and Camps, A., editors, *Introduction to Satellite Remote Sensing*, pages 1 – 42. Elsevier.

Fernandes, R., Zhao, H. X., Wang, X. J., Key, J., Qu, X., and Hall, A. (2009). Controls on Northern Hemisphere snow albedo feedback quantified using satellite Earth observations. *Geophysical Research Letters*, 36:L21702.

Fischer, A., Olefs, M., and Abermann, J. (2011). Glaciers, snow and ski tourism in Austria's changing climate. *Annals of Glaciology*, 52(58):89–96.

Flanner, M. G., Arnheim, J., Cook, J. M., Dang, C., He, C., Huang, X., Singh, D., Skiles, S. M., Whicker, C. A., and Zender, C. S. (2021). SNICAR-AD v3: A community tool for modeling spectral snow albedo. *Geoscientific Model Development Discussions*, 2021:1–49.

Flanner, M. G., Shell, K. M., Barlage, M., Perovich, D. K., and Tschudi, M. A. (2011). Radiative forcing and albedo feedback from the Northern Hemisphere cryosphere between 1979 and 2008. *Nature Geoscience*, 4:151–155.

Ford, K. R., Ettinger, A. K., Lundquist, J. D., Raleigh, M. S., and Hille Ris Lambers, J. (2013). Spatial heterogeneity in ecologically important climate variables at coarse and fine scales in a high-snow mountain landscape. *PLOS ONE*, 8(6):1–13.

Franz, K. J., Hogue, T. S., and Sorooshian, S. (2008). Operational snow modeling: Addressing the challenges of an energy balance model for National Weather Service forecasts. *Journal of Hydrology*, 360(1):48 – 66.

Frazier, A. E. and Hemingway, B. L. (2021). A Technical Review of Planet Smallsat Data: Practical Considerations for Processing and Using PlanetScope Imagery. *Remote Sensing*, 13(19).

Førland, E. J., Allerup, P., Dahlström, B., Elomaa, E., Jónsson, T., Madsen, H., Perälä, J., Rissanen, P., Vedin, H., and Vejen, F. (1996). *Manual for operational correction of Nordic precipitation data.* Norske Meteorologiske Institutt., Nordic Working Group on Precipitation (NWGP).

Gardner, A. S. and Sharp, M. J. (2010). A review of snow and ice albedo and the development of a new physically based broadband albedo parameterization. *Journal of Geophysical Research: Earth Surface*, 115(F1).

Gascoin, S., Guðmundsson, S., Aðalgeirsdóttir, G., Pálsson, F., Schmidt, L., Berthier, E., and Björnsson, H. (2017). Evaluation of MODIS Albedo Product over Ice Caps in Iceland and Impact of Volcanic Eruptions on Their Albedo. *Remote Sensing*, 9(5):399.

Gascoin, S., Hagolle, O., Huc, M., Jarlan, L., Dejoux, J.-F., Szczypta, C., Marti, R., and Sánchez, R. (2015). A snow cover climatology for the Pyrenees from MODIS snow products. *Hydrol. Earth Syst. Sci.*, 19(5):2337–2351.

Gomes, V. C. F., Queiroz, G. R., and Ferreira, K. R. (2020). An overview of platforms for big earth observation data management and analysis. *Remote Sensing*, 12(8).

Grenfell, T. C., Warren, S. G., and Mullen, P. C. (1994). Reflection of solar radiation by the Antarctic snow surface at ultraviolet, visible, and near-infrared wavelengths. *Journal of Geophysical Research: Atmospheres*, 99(D9):18669–18684.

Guan, B., Molotch, N. P., Waliser, D. E., Jepsen, S. M., Painter, T. H., and Dozier, J. (2013). Snow water equivalent in the Sierra Nevada: Blending snow sensor observations with snowmelt model simulations. *Water Resources Research*, 49(8):5029–5046.

Gunnarsson, A., Gardarsson, S. M., Pálsson, F., Jóhannesson, T., and Sveinsson, O. G. B. (2021). Annual and inter-annual variability and trends of albedo of Icelandic glaciers. *The Cryosphere*, 15(2):547–570.

Gunnarsson, A., Gardarsson, S. M., and Sveinsson, O. G. B. (2019). Icelandic snow cover characteristics derived from a gap-filled MODIS daily snow cover product. *Hydrology and Earth System Sciences*, 23(7):3021–3036.

Guðmundsson, S., Björnsson, H., Pálsson, F., and Haraldsson, H. H. (2009). Comparison of energy balance and degree–day models of summer ablation on the Langjökull ice cap, SW-Iceland. *Jökull*, 59:1–18.

Hall, D. K. and Riggs, G. A. (2007). Accuracy assessment of the MODIS snow products. *Hydrological Processes*, 21(12):1534–1547.

Hall, D. K., Riggs, G. A., Salomonson, V. V., DiGirolamo, N. E., and Bayr, K. J. (2002). MODIS snow-cover products. *Remote Sensing of Environment*, 83(1–2):181–194.

Hannah, W. M., Jones, C. R., Hillman, B. R., Norman, M. R., Bader, D. C., Taylor, M. A., Leung, L. R., Pritchard, M. S., Branson, M. D., Lin, G., Pressel, K. G., and Lee, J. M. (2020). Initial results from the super-parameterized e3sm. *Journal of Advances in Modeling Earth Systems*, 12(1):e2019MS001863.

Hannesdóttir, H., Sigurðsson, O., Þrastarson, R. H., Guðmundsson, S., Belart, J., Pálsson, F., Magnússon, E., Víkingsson, S., and Jóhannesson, T. (2020). Variations in glacier extent in Iceland since the end of the Little Ice Age. *Jökull*, 70:1–34.

Hao, S., Jiang, L., Shi, J., Wang, G., and Liu, X. (2019). Assessment of MODIS-Based Fractional Snow Cover Products Over the Tibetan Plateau. *IEEE Journal of Selected Topics in Applied Earth Observations and Remote Sensing*, 12(2):533–548.

Helfrich, S. R., McNamara, D., Ramsay, B. H., Baldwin, T., and Kasheta, T. (2007). Enhancements to, and forthcoming developments in the Interactive Multisensor Snow and Ice Mapping System (IMS). *Hydrological Processes*, 21(12):1576–1586.

Henderson, G. R., Peings, Y., Furtado, J. C., and Kushner, P. J. (2018). Snow–atmosphere coupling in the Northern Hemisphere. *Nature Climate Change*, 8(11):954–963.

Henriksen, S. (2003). *Report on the Approximation of the Annual Cycle of Temperature in Iceland.* Reykjavík : Veðurstofa Íslands, Febr. 2003.

Hock, R. (1999). A distributed temperature-index ice- and snowmelt model including potential direct solar radiation. *Journal of Glaciology*, 45(149):101–111.

Hock, R. (2005). Glacier melt: a review of processes and their modelling. *Progress in Physical Geography: Earth and Environment*, 29(3):362–391.

Hudson, S. R. (2011). Estimating the global radiative impact of the sea ice-albedo feedback in the Arctic. *Journal of Geophysical Research-Atmospheres*, 116:D16102.

Hughes, M., Lundquist, J. D., and Henn, B. (2020). Dynamical downscaling improves upon gridded precipitation products in the Sierra Nevada, California. *Climate Dynamics*, 55(1):111–129.

Jarvis, C. (1936). Flood-stage records of the river Nile. *Transactions of the American Society of Civil Engineers*, 101(1):1012–1030.

Jóhannesson, T., Aðalgeirsdóttir, G., Björnsson, H., Crochet, P., Elíasson, E., Guðmundsson, S., Jónsdóttir, J., Ólafsson, H., Pálsson, F., Rögnvaldsson, O., Sigurðsson, O., Snorrason, A., Sveinsson, O., and Þorsteinsson, Þ. (2007). *Effect of Climate Change on Hydrology and Hydro-Resources in Iceland.* Reykjavík : Orkustofnun, 2007, Reykjavík.

Jordan, R. E. (1991). A one-dimensional temperature model for a snow cover : technical documentation for sntherm.89. *CRREL Special Report 91-16*, page 64p.

Jóhannesson, T., Sigurdsson, O., Laumann, T., and Kennett, M. (1995). Degree-day glacier mass-balance modelling with applications to glaciers inIceland, Norway and Greenland. *Journal of Glaciology*, 41(138):345–358.

Jóhannesson, T. and Sigurðsson, O. (2014). Samantekt um snjómælingar á hálendi Íslands.

Jónsson, T. (2002). Langtímasveiflur I, Snjóhula og snjókoma. *Veðurstofa Íslands*, (Greinargerð 02035).

Jónsson, T. and Jónasson, K. (1997). Fimmtíu ára snjódýpt á Íslandi. *Veðurstofa Íslands*, (Greinargerð VÍ-G97025-ÚR20).

Keegan, K. (2021). Snow metamorphism and firn compaction. In *Reference Module in Earth Systems and Environmental Sciences*. Elsevier.

Key, J. R., Wang, X., Stoeve, J. C., and Fowler, C. (2001). Estimating the cloudy-sky albedo of sea ice and snow from space. *Journal of Geophysical Research: Atmospheres*, 106(D12):12489–12497.

Kim, R. S., Kumar, S., Vuyovich, C., Houser, P., Lundquist, J., Mudryk, L., Durand, M., Barros, A., Kim, E. J., Forman, B. A., Gutmann, E. D., Wrzesien, M. L., Garnaud, C., Sandells, M., Marshall, H.-P., Cristea, N., Pflug, J. M., Johnston, J., Cao, Y., Mocko, D., and Wang, S. (2021). Snow Ensemble Uncertainty Project (SEUP): quantification of snow water equivalent uncertainty across North America via ensemble land surface modelin. *The Cryosphere*, 15(2):771–791.

Kinar, N. and Pomeroy, J. (2015). Measurement of the physical properties of the snowpack. *Reviews of Geophysics*, 53:n/a–n/a.

Klein, A. G. and Barnett, A. C. (2003). Validation of daily MODIS snow cover maps of the Upper Rio Grande River Basin for the 2000–2001 snow year. *Remote Sensing of Environment*, 86(2):162–176.

Klein, A. G. and Stroeve, J. (2002). Development and validation of a snow albedo algorithm for the MODIS instrument. *Annals of Glaciology*, 34:45–52.

Knudsen, K. L., Eiríksson, J., and Bartels-Jónsdóttir, H. B. (2012). Oceanographic changes through the last millennium off North Iceland: Temperature and salinity reconstructions based on foraminifera and stable isotopes. *Marine Micropaleontology*, 84-85:54 – 73.

Largeron, C., Dumont, M., Morin, S., Boone, A., Lafaysse, M., Metref, S., Cosme, E., Jonas, T., Winstral, A., and Margulis, S. A. (2020). Toward snow cover estimation in mountainous areas using modern data assimilation methods: A review. *Frontiers in Earth Science*, 8:325.

Lemke, P., Ren, J., Alley, R., Allison, I., Carrasco, J., Flato, G., Fujii, Y., Kaser, G., Mote, P., Thomas, R., and Zhang, T. (2007). Observations: Changes in snow, ice and frozen ground. *Climate Change 2007: The Physical Science Basis. Contribution of Working Group I to the Fourth Assessment Report of the Intergovernmental Panel on Climate Change*.

Lettenmaier, D. P., Alsdorf, D., Dozier, J., Huffman, G. J., Pan, M., and Wood, E. F. (2015). Inroads of remote sensing into hydrologic science during the WRR era. *Water Resources Research*, 51(9):7309–7342.

Liang, S., Stroeve, J., and Box, J. E. (2005). Mapping daily snow/ice shortwave broadband albedo from Moderate Resolution Imaging Spectroradiometer (MODIS): The improved direct retrieval algorithm and validation with Greenland in situ measurement. *Journal of Geophysical Research: Atmospheres*, 110(D10).

Lisette Klok, E. and Oerlemans, J. (2002). Model study of the spatial distribution of the energy and mass balance of Morteratschgletscher, Switzerland. *Journal of Glaciology*, 48(163):505–518.

Lozier, M., Owens, W., and Curry, R. G. (1995). The climatology of the North Atlantic. *Progress in Oceanography*, 36(1):1 – 44.

Lundquist, J., Hughes, M., Gutmann, E., and Kapnick, S. (2019). Our skill in modeling mountain rain and snow is bypassing the skill of our observational networks. *Bulletin of the American Meteorological Society*, 100(12):2473–2490.

Lundquist, J. D., Dettinger, M. D., and Cayan, D. R. (2005). Snow-fed streamflow timing at different basin scales: Case study of the tuolumne river above hetch hetchy, yosemite, california. *Water Resources Research*, 41(7).

Lv, Z., Pomeroy, J. W., and Fang, X. (2019). Evaluation of SNODAS Snow Water Equivalent in Western Canada and Assimilation Into a Cold Region Hydrological Model. *Water Resources Research*, 55(12):11166–11187.

MacDougall, A. H., Wheler, B. A., and Flowers, G. E. (2011). A preliminary assessment of glacier melt-model parameter sensitivity and transferability in a dry subarctic environment. *The Cryosphere*, 5(4):1011–1028.

Male, D. H. and Granger, R. J. (1981). Snow surface energy exchange. *Water Resources Research*, 17(3):609–627.

Marks, D., Kimball, J., Tingey, D., and Link, T. (1998). The sensitivity of snowmelt processes to climate conditions and forest cover during rain-on-snow: a case study of the 1996 Pacific Northwest flood. *Hydrological Processes*, 12(10):1569–1587.

Marshall, G., Rees, W., and Dowdeswell, J. (1993). Limitations imposed by cloud cover on multitemporal visible band satellite data sets from polar regions. *Annals of Glaciology*, 17:113–120.

Martinec, J. and Rango, A. (1981). Areal distribution of snow water equivalent evaluated by snow cover monitoring. *Water Resources Research*, 17(5):1480–1488. John Wiley & Sons, Ltd.

McClung, D. and Schaerer, P. (2006). *The Avalanche Handbook*. Mountaineers Bks. Mountaineers Books.

Micheletty, P. D., Kinoshita, A. M., and Hogue, T. S. (2014). Application of MODIS snow cover products: wildfire impacts on snow and melt in the Sierra Nevada. *Hydrology and Earth System Sciences*, 18(11):4601–4615.

Molotch, N. P., Painter, T. H., Bales, R. C., and Dozier, J. (2004). Incorporating remotely-sensed snow albedo into a spatially-distributed snowmelt model. *Geophysical Research Letters*, 31(3).

Morriss, B. F., Ochs, E., Deeb, E. J., Newman, S. D., Daly, S. F., and Gagnon, J. J. (2016). Persistence-based temporal filtering for MODIS snow products. *Remote Sensing of Environment*, 175:130–137.

Mote, P. W., Hamlet, A. F., Clark, M. P., and Lettenmaier, D. P. (2005). Declining Mountain Snowpack in Western North America. *Bulletin of the American Meteorological Society*, 86(1):39 – 50.

Möller, R., Dagsson-Waldhauserova, P., Möller, M., Kukla, P. A., Schneider, C., and Gudmundsson, M. T. (2019). Persistent albedo reduction on southern Icelandic glaciers due to ashfall from the 2010 Eyjafjallajökull eruption. *Remote Sensing of Environment*, 233:111396.

Möller, R., Möller, M., Björnsson, H., Gudmundsson, S., Pálsson, F., Oddsson, B., Kukla, P., and Schneider, C. (2014). MODIS-derived albedo changes of Vatnajökull (Iceland) due to tephra deposition from the 2004 Grimsvötn eruption. *International Journal of Applied Earth Observation and Geoinformation*, 26:256–269.

Naegeli, K., Damm, A., Huss, M., Wulf, H., Schaepman, M., and Hoelzle, M. (2017). Cross-comparison of albedo products for glacier surfaces derived from airborne and satellite (sentinel-2 and landsat 8) optical data. *Remote Sensing*, 9(2):110.

Naegeli, K., Huss, M., and Hoelzle, M. (2019). Change detection of bare-ice albedo in the Swiss Alps. *The Cryosphere*, 13(1):397–412.

Naegeli, K., Neuhaus, C., Salberg, A.-B., Schwaizer, G., Wiesmann, A., Wunderle, S., and Nagler, T. (2021). ESA Snow Climate Change Initiative (Snow CCI): Daily global snow cover fraction - viewable (SCFV) from AVHRR (1982–2019), version 1.0. *NERC EDS Centre for Environmental Data Analysis*.

Nolin, A. W. (2010). Recent advances in remote sensing of seasonal snow. *Journal of Glaciology*, 56(200):1141–1150.

Nolin, A. W., Sproles, E. A., Rupp, D. E., Crumley, R. L., Webb, M. J., Palomaki, R. T., and Mar, E. (2021). New snow metrics for a warming world. *Hydrological Processes*, 35(6):e14262.

Oaida, C. M., Reager, J. T., Andreadis, K. M., David, C. H., Levoe, S. R., Painter, T. H., Bormann, K. J., Trangsrud, A. R., Girotto, M., and Famiglietti, J. S. (2019). A High-Resolution Data Assimilation Framework for Snow Water Equivalent Estimation across the Western United States and Validation with the Airborne Snow Observatory. *Journal of Hydrometeorology*, 20(3):357–378.

Oerlemans, J. (2001). Glaciers and climate change. *Stanford Univ. Tech. Report.*, ISBN:90–265–1813–7.

Ohmura, A. (2001). Physical basis for the temperature-based melt-index method. *Journal of Applied Meteorology*, 40(4):753–761.

Ólafsson, H., Furger, M., and Brümmer, B. (2007). The weather and climate of Iceland. *Meteorologische Zeitschrift*, 16(1):5–8.

Painter, T. H., Berisford, D. F., Boardman, J. W., Bormann, K. J., Deems, J. S., Gehrke, F., Hedrick, A., Joyce, M., Laidlaw, R., Marks, D., Mattmann, C., McGurk, B., Ramirez, P., Richardson, M., Skiles, S. M., Seidel, F. C., and Winstral, A. (2016). The Airborne Snow Observatory: Fusion of scanning lidar, imaging spectrometer, and physically-based modeling for mapping snow water equivalent and snow albedo. *Remote Sensing of Environment*, 184:139–152.

Painter, T. H., Bryant, A. C., and Skiles, S. M. (2012). Radiative forcing by light absorbing impurities in snow from MODIS surface reflectance data: Radiative forcing by impurities in snow. *Geophysical Research Letters*, 39(17).

Painter, T. H., Rittger, K., McKenzie, C., Slaughter, P., Davis, R. E., and Dozier, J. (2009). Retrieval of subpixel snow covered area, grain size, and albedo from MODIS. *Remote Sensing of Environment*, 113(4):868 – 879.

Parajka, J. and Blöschl, G. (2006). Validation of MODIS snow cover images over Austria. *Hydrol. Earth Syst. Sci.*, 10(5):679–689.

Pomeroy, J., Essery, R., and Toth, B. (2004). Implications of spatial distributions of snow mass and melt rate for snow-cover depletion: observations in a subarctic mountain catchment. *Annals of Glaciology*, 38:195–201.

Pope, A., Rees, W. G., Fox, A. J., and Fleming, A. (2014). Open Access Data in Polar and Cryospheric Remote Sensing. *Remote Sensing*, 6(7):6183–6220.

Pálsson, F., Gunnarsson, A., Jónsson, G., Pálsson, H. S., and Steinþórsson, S. (2020a). Vatnajökull: Mass balance, meltwater drainage and surface velocity of the glacial year 2018–19. *Landsvirkjun, Reykjavík*, RH-01-20 - LV-2020-016:56.

Pálsson, F., Gunnarsson, A., Pálsson, H. S., and Steinþórsson, S. (2020b). Afkomu- og hraðamælingar á Langjökli jökulárið 2018–2019. *Landsvirkjun, Reykjavík*, RH-10-20 / LV-2020-017:27.

Raleigh, M. S., Livneh, B., Lapo, K., and Lundquist, J. D. (2016). How does availability of meteorological forcing data impact physically based snowpack simulations? *Journal of Hydrometeorology*, 17(1):99 – 120.

Raleigh, M. S. and Lundquist, J. D. (2012). Comparing and combining SWE estimates from the SNOW-17 model using PRISM and SWE reconstruction. *Water Resources Research*, 48(1).

Raleigh, M. S., Lundquist, J. D., and Clark, M. P. (2015). Exploring the impact of forcing error characteristics on physically based snow simulations within a global sensitivity analysis framework. *Hydrology and Earth System Sciences*, 19(7):3153–3179.

Ramsay, B. H. (1998). The interactive multisensor snow and ice mapping system. *Hydrological Processes*, 12(10-11):1537–1546.

Rasmussen, R., Baker, B., Kochendorfer, J., Meyers, T., Landolt, S., Fischer, A. P., Black, J., Thériault, J. M., Kucera, P., Gochis, D., Smith, C., Nitu, R., Hall, M., Ikeda, K., and Gutmann, E. (2012). How Well Are We Measuring Snow: The NOAA/FAA/NCAR Winter Precipitation Test Bed. *Bulletin of the American Meteorological Society*, 93(6):811–829.

Rasp, S., Pritchard, M. S., and Gentine, P. (2018). Deep learning to represent subgrid processes in climate models. *Proceedings of the National Academy of Sciences*, 115(39):9684–9689.

Raup, B. H., Andreassen, L. M., Bolch, T., and Bevan, S. (2015). *Remote sensing of glaciers*, chapter 7. John Wiley and Sons, Ltd.

Redpath, T. A. N., Sirguey, P., and Cullen, N. J. (2019). Characterising spatio-temporal variability in seasonal snow cover at a regional scale from MODIS data: the Clutha Catchment, New Zealand. *Hydrology and Earth System Sciences*, 23(8):3189–3217.

Reijmer, C. H., Knap, W. H., and Oerlemans, J. (1999). The Surface Albedo Of The Vatnajökull Ice Cap, Iceland: A Comparison Between Satellite-Derived And Ground-Based Measurements. *Boundary-Layer Meteorology*, 92(1):123–143.

Renner, A. H. H., Sundfjord, A., Janout, M. A., Ingvaldsen, R. B., Beszczynska-Möller, A., Pickart, R. S., and Pérez-Hernández, M. D. (2018). Variability and Redistribution of Heat in the Atlantic Water Boundary Current North of Svalbard. *Journal of Geophysical Research: Oceans*, 123(9):6373–6391.

Rist, S. (1958). Snjómæling inni á hálendinu. Úrkomumælingar. *Vatnamælingar, Raforkumálastjóri*, (Skilagrein 164):9.

Rist, S. (1966). Snjómælingar vetur 1965/1966. *Vatnamælingar, Raforkumálastjóri*, (Skilagrein 292):1.

Rist, S. (1981). Afstæð snjódýptarmæling á hálendinu. *Orkustofnun*, (SR-81/03):4.

Rittger, K., Bair, E. H., Kahl, A., and Dozier, J. (2016). Spatial estimates of snow water equivalent from reconstruction. *Advances in Water Resources*, 94:345–363.

Rittger, K., Painter, T. H., and Dozier, J. (2013). Assessment of methods for mapping snow cover from MODIS. *Advances in Water Resources*, 51:367–380.

Rossby, T. (1996). The North Atlantic Current and surrounding waters: At the crossroads. *Reviews of Geophysics*, 34(4):463–481.

Rögnvaldsson, O., Crochet, P., and Ólafsson, H. (2004). Mapping of precipitation in Iceland using numberical simulations and statistical modeling. *Meteor. Z.*, 13:209–219.

Rögnvaldsson, O., Jónsdóttir, J., and Olafsson, H. (2007). Numerical simulations of precipitation in the complex terrain if Iceland – Comparison with glaciological and hydrological data. *Meteor. Z.*, 16:71–85.

Salomonson, V. and Appel, I. (2004). Estimating fractional snow coverage from MODIS using the Normalized Difference Snow Index (NDSI). *Remote Sensing of Environment*, 89:351–360.

Schaaf, C. B., Gao, F., Strahler, A. H., Lucht, W., Li, X., Tsang, T., Strugnell, N. C., Zhang, X., Jin, Y., Muller, J.-P., Lewis, P., Barnsley, M., Hobson, P., Disney, M., Roberts, G., Dunderdale, M., Doll, C., d'Entremont, R. P., andm Shunlin Liang, B. H., Privette, J. L., and Roy, D. (2002). First operational BRDF, albedo nadir reflectance products from MODIS. *Remote Sensing of Environment*, 83(1):135 – 148.

Schaaf, C. K. and Wang, Z. (2015). MCD43A3/MODIS/Terra+Aqua BRDF/Albedo Daily L3 Global - 500m V006 500m Grid, Version 6. Technical report, NASA EOSDIS Land Processes DAAC, Boulder, Colorado USA.

Schmidt, L. S., Aðalgeirsdóttir, G., Guðmundsson, S., Langen, P. L., Pálsson, F., Mottram, R., Gascoin, S., and Björnsson, H. (2017). The importance of accurate glacier albedo for estimates of surface mass balance on Vatnajökull: evaluating the surface energy budget in a regional climate model with automatic weather station observations. *The Cryosphere*, 11(4):1665–1684.

Schneider, D. and Molotch, N. P. (2016). Real-time estimation of snow water equivalent in the Upper Colorado River Basin using MODIS-based SWE Reconstructions and SNOTEL data. *Water Resources Research*, 52(10):7892–7910.

Sigurðsson, F. H., Pálsdóttir, T., and Antonsson, T. K. (2003). Veðurstöð og veðurfar á Hveravöllum á Kili. *Rit Veðurstofu Íslands 20*.

Sigurðsson, O. (2002). Fyrirkomulag snjómælinga á hálendi Íslands. *Orkustofnun*, (Greinargerð OSig-2002/03):3.

Skaugen, T. (2007). Modelling the spatial variability of snow water equivalent at the catchment scale. *Hydrology and Earth System Sciences*, 11(5):1543–1550.

Skiles, S. M., Flanner, M., Cook, J. M., Dumont, M., and Painter, T. H. (2018a). Radiative Forcing by Light-Absorbing Particles in Snow. *Nature Climate Change*, 8(11):964.

Skiles, S. M., Mallia, D. V., Hallar, A. G., Lin, J. C., Lambert, A., Petersen, R., and Clark, S. (2018b). Implications of a shrinking Great Salt Lake for dust on snow deposition in the Wasatch Mountains, UT, as informed by a source to sink case study from the 13–14 April 2017 dust event. *Environmental Research Letters*, 13(12):124031.

Skiles, S. M. and Painter, T. H. (2018). Assessment of radiative forcing by light-absorbing particles in snow from in situ observations with radiative transfer modeling. *Journal of Hydrometeorology*, 19(8):1397 – 1409.

Skiles, S. M., Painter, T. H., Deems, J. S., Bryant, A. C., and Landry, C. C. (2012). Dust radiative forcing in snow of the Upper Colorado River Basin: 2. Interannual variability in radiative forcing and snowmelt rates. *Water Resources Research*, 48(7).

Smyth, E. J., Raleigh, M. S., and Small, E. E. (2019). Particle Filter Data Assimilation of Monthly Snow Depth Observations Improves Estimation of Snow Density and SWE. *Water Resources Research*, 55(2):1296–1311.

Stroeve, J. (2001). Assessment of Greenland Albedo Variability from the Advanced Very High Resolution Radiometer Polar Pathfinder Data Set. *Journal of Geophysical Research: Atmospheres*, 106(D24):33989–34006.

Stroeve, J., Box, J. E., Gao, F., Liang, S., Nolin, A., and Schaaf, C. (2005). Accuracy Assessment of the MODIS 16-Day Albedo Product for Snow: Comparisons with Greenland in Situ Measurements. *Remote Sensing of Environment*, 94(1):46–60.

Stroeve, J., Box, J. E., Wang, Z., Schaaf, C., and Barrett, A. (2013). Re-evaluation of MODIS MCD43 Greenland albedo accuracy and trends. *Remote Sensing of Environment*, 138:199–214.

Stroeve, J., Nolin, A., and Steffen, K. (1997). Comparison of AVHRR-Derived and in Situ Surface Albedo over the Greenland Ice Sheet. *Remote Sensing of Environment*, 62(3):262–276.

Sturm, M. and Holmgren, J. (2018). An automatic snow depth probe for field validation campaigns. *Water Resources Research*, 54(11):9695–9701.

Sturm, M., Holmgren, J., and Liston, G. E. (1995). A Seasonal Snow Cover Classification System for Local to Global Applications. *Journal of Climate*, 8(5):1261–1283.

Sturm, M., Taras, B., Liston, G. E., Derksen, C., Jonas, T., and Lea, J. (2010). Estimating Snow Water Equivalent Using Snow Depth Data and Climate Classes. *Journal of Hydrometeorology*, 11(6):1380–1394.

Taylor, L. S., Quincey, D. J., Smith, M. W., Baumhoer, C. A., McMillan, M., and Mansell, D. T. (2021). Remote sensing of the mountain cryosphere: Current capabilities and future opportunities for research. *Progress in Physical Geography: Earth and Environment*.

Tedesco, M. (2015). *Remote sensing and the cryosphere*, chapter 1. John Wiley and Sons, Ltd.

Tolson, B. A. and Shoemaker, C. A. (2007). Dynamically dimensioned search algorithm for computationally efficient watershed model calibration. *Water Resources Research*, 43(1).

Torres, R., Snoeij, P., Geudtner, D., Bibby, D., Davidson, M., Attema, E., Potin, P., Rommen, B., Floury, N., Brown, M., Traver, I. N., Deghaye, P., Duesmann, B., Rosich, B., Miranda, N., Bruno, C., L'Abbate, M., Croci, R., Pietropaolo, A., Huchler, M., and Rostan, F. (2012). GMES Sentinel-1 mission. *Remote Sensing of Environment*, 120:9 – 24.

Tran, H., Nguyen, P., Ombadi, M., Hsu, K.-l., Sorooshian, S., and Qing, X. (2019). A cloud-free MODIS snow cover dataset for the contiguous united states from 2000 to 2017. *Scientific Data*, 6(1):180300.

Ustin, S. L. and Middleton, E. M. (2021). Current and near-term advances in earth observation for ecological applications. *Ecological Processes*, 10(1):1.

Warren, S. G. (1982). Optical Properties of Snow. *Reviews of Geophysics*, 20(1):67–89.

Warren, S. G. and Wiscombe, W. J. (1980). A Model for the Spectral Albedo of Snow. II: Snow Containing Atmospheric Aerosols. *Journal of the Atmospheric Sciences*, 37(12):2734–2745.

Weyn, J. A., Durran, D. R., and Caruana, R. (2020). Improving Data-Driven Global Weather Prediction Using Deep Convolutional Neural Networks on a Cubed Sphere. *Journal of Advances in Modeling Earth Systems*, 12(9):e2020MS002109.

Williams, R. S., J., Boedvarsson, A., Fridriksson, S., Palmason, G., Rist, S., Sigtryggsson, H., Thorarinsson, S., and Thorsteinsson, I. (1973). Satellite geological and geophysical remote sensing of Iceland: Preliminary results from analysis of MSS imagery. *NASA. Goddard Space Flight Center Symp. on Significant Results obtained from the ERTS-1, Vol. 1, Sect. A and B*, 1(19730019509).

Williams, J. R. S. (1983). Satellite glaciology in Iceland. *Jökull*, 33:3–12.

Williams, J. R. S. and Þórarinsson, S. (1973). ERTS-1 image of the Vatnajökull area: General comments. *Jökull*, 23:1–6.

Williams, R. S. (1987). Satellite Remote Sensing of Vatnajökull, Iceland. *Annals of Glaciology*, 9:127–135.

Williams, Jr, R. S. (1973a). Satellite geological and geophysical remote sensing of Iceland. Progress report, 1 Sep-31 Oct 1973. [Torfajokull and Reykjanes geothermal areas]. *Geological Survey*, E-74-10385; NASA-CR-137170(5170250).

Williams, Jr, R. S. (1973b). Satellite geological and geophysical remote sensing of Iceland. Progress report, 1 September–31 October 1973. *Geological Survey*, E-74-10385(5026158).

Williams, Jr, R. S. (1974). Satellite geological and geophysical remote sensing of Iceland. Progress report, 1 Sep 1973-28 Feb 1974. *Geological Survey*, E-74-10467; NASA-CR-136868(5140046).

Williams, Jr, R. S. and Pálmason, G. (1973). Satellite geological and geophysical remote sensing of Iceland. Special report No. 1. *Geological Survey*, E-73-10874; NASA-CR-133491(5140054).

Winther, J.-G. (1993). Landsat TM derived and in situ summer reflectance of glaciers in Svalbard. *Polar Research*, 12(1):37–55.

Wittmann, M., Groot Zwaaftink, C. D., Steffensen Schmidt, L., Guðmundsson, S., Pálsson, F., Arnalds, O., Björnsson, H., Thorsteinsson, T., and Stohl, A. (2017). Impact of dust deposition on the albedo of Vatnajökull ice cap, Iceland. *The Cryosphere*, 11(2):741–754.

WMO (2011). Systematic Observation Requirements for Satellite-based Products for Climate Supplemental details to the satellite-based component of the Implementation Plan for the Global Observing System for Climate in Support of the UNFCCC: 2011 update. *GCOS- No. 154*, 154:138.

Wulder, M. A., White, J. C., Loveland, T. R., Woodcock, C. E., Belward, A. S., Cohen, W. B., Fosnight, E. A., Shaw, J., Masek, J. G., and Roy, D. P. (2016a). The global Landsat archive: Status, consolidation, and direction. *Remote Sensing of Environment*, 185:271 – 283. Landsat 8 Science Results.

Wulder, M. A., White, J. C., Loveland, T. R., Woodcock, C. E., Belward, A. S., Cohen, W. B., Fosnight, E. A., Shaw, J., Masek, J. G., and Roy, D. P. (2016b). The global Landsat archive: Status, consolidation, and direction. *Remote Sensing of Environment*, 185:271–283.

Xiong, X., Butler, J., Cao, C., and Wu, X. (2018). Optical Sensors - VIS/NIR/SWIR. In Liang, S., editor, *Comprehensive Remote Sensing*, pages 353 – 375. Elsevier, Oxford.

Yang, J., Gong, P., Fu, R., Zhang, M., Chen, J., Liang, S., Xu, B., Shi, J., and Dickinson, R. (2013). The role of satellite remote sensing in climate change studies. *Nature Climate Change*, 3(10):875–883.

Zhao, J., Yang, J., Semper, S., Pickart, R. S., Våge, K., Valdimarsson, H., and Jónsson, S. (2018). A Numerical Study of Interannual Variability in the North Icelandic Irminger Current. *Journal of Geophysical Research: Oceans*, 123(12):8994–9009.

Zhu, Z., Wulder, M. A., Roy, D. P., Woodcock, C. E., Hansen, M. C., Radeloff, V. C., Healey, S. P., Schaaf, C., Hostert, P., Strobl, P., Pekel, J.-F., Lymburner, L., Pahlevan, N., and Scambos, T. A. (2019). Benefits of the free and open Landsat data policy. *Remote Sensing of Environment*, 224:382–385.

Ágústsson, H., Hannesdóttir, H., Thorsteinsson, T., Pálsson, F., and Oddsson, B. (2013). Mass balance of Mýrdalsjökull ice cap accumulation area and comparison of observed winter balance with simulated precipitation. *Jökull*, 63:91–104.

Ólafsdóttir, S., Jennings, A. E., Áslaug Geirsdóttir, Andrews, J., and Miller, G. H. (2010). Holocene variability of the North Atlantic Irminger current on the south- and northwest shelf of Iceland. *Marine Micropaleontology*, 77(3):101–118.

Úlfarsson, G. F. and Unger, E. A. (2011). Impacts and Responses of Icelandic Aviation to the 2010 Eyjafjallajökull Volcanic Eruption: Case Study. *Transportation Research Record*, 2214(1):144–151.

Þorsteinsson, Þ., Jóhannesson, T., Sigurðsson, O., and Einarsson, B. (2017). Afkomumælingar á Hofsjökli 1988-2017. *Veðurstofa Íslands, Reykjavík*, 2017-016:82.

Þórarinsson, S., Sæmundsson, K., and Williams, J. R. S. (1973). ERTS-1 image of Vatnajökull: Analysis of glaciological, structural and volcanic features. *Jökull*, 23:7–17.

A Appendix

Paper I

Icelandic snow cover characteristics derived from a gap-filled MODIS daily snow cover product

Andri Gunnarsson, Sigurdur M. Gardarsson and Óli G. B. Sveinsson

Hydrol. Earth Syst. Sci, 23,3021–3036

Hydrol. Earth Syst. Sci., 23, 3021–3036, 2019
https://doi.org/10.5194/hess-23-3021-2019

Hydrology and Earth System Sciences
Open Access
EGU

Icelandic snow cover characteristics derived from a gap-filled MODIS daily snow cover product

Andri Gunnarsson[1,2], **Sigurður M. Garðarsson**[1], **and Óli G. B. Sveinsson**[2]

[1]University of Iceland, Civil and Environmental Engineering, Hjardarhagi 2–6, IS-107 Reykjavik, Iceland
[2]Landsvirkjun, Department of Research and Development, IS-107 Reykjavík, Iceland

Correspondence: Andri Gunnarsson (andrigun@lv.is)

Received: 14 February 2019 – Discussion started: 28 February 2019
Revised: 14 June 2019 – Accepted: 17 June 2019 – Published: 17 July 2019

Abstract. This study presents a spatio-temporal continuous data set for snow cover in Iceland based on the Moderate Resolution Imaging Spectroradiometer (MODIS) from 2000 to 2018. Cloud cover and polar darkness are the main limiting factors for data availability of remotely sensed optical data at higher latitudes. In Iceland the average cloud cover is 75 % with some spatial variations, and polar darkness reduces data availability from the MODIS sensor from late November until mid January. In this study MODIS snow cover data were validated over Iceland with comparison to manned in situ observations and Landsat 7/8 and Sentinel 2 data. Overall a good agreement was found between in situ observed snow cover, with an average agreement of 0.925. Agreement of Landsat 7/8 and Sentinel 2 was found to be acceptable, with R^2 values 0.96, 0.92 and 0.95, respectively, and in agreement with other studies. By applying daily data merging from Terra and Aqua and a temporal aggregation of 7 d, unclassified pixels were reduced from 75 % to 14 %. The remaining unclassified pixels after daily merging and temporal aggregation were removed with classification learners trained with classified data, pixel location, aspect and elevation. Various snow cover characteristic metrics were derived for each pixel such as snow cover duration, first and last snow-free dates, deviation and dynamics of snow cover and trends during the study period. On average the first snow-free date in Iceland is 27 June, with a standard deviation of 19.9 d. For the study period a trend of increasing snow cover duration was observed for all months except October and November. However, statistical testing of the trends indicated that there was only a significant trend in June.

1 Introduction

On a global scale snow cover has a strong interaction with the cryosphere and ocean systems and therefore the climate system of the Earth. The two main effects of snow on the cryosphere are its control on the reflection of radiation, reaching the surface of Earth and balancing its radiation budget (Barry, 2002; Warren, 1982) and isolating properties which can influence the length of the growing season (Keller et al., 2005; Barichivich et al., 2013). Snow albedo dominates the control of its irradiance feedback, which depends on various factors such as snow depth, snow cover extent, vegetation and cloud cover (Fernandes et al., 2009; Qu and Hall, 2007).

In the Northern Hemisphere the spring snow cover extent has decreased significantly, influencing the dynamics of spring melt intensity and timing in recent years (Adam et al., 2008; Barnett et al., 2005; Choi et al., 2010; Hori et al., 2017). Various studies using remotely sensed data, observations and climate models unanimously agree that on the Northern Hemisphere scale snow cover extent is receding by 2.5 to 10 days per decade depending on the study period (Eythorsson et al., 2019; Fontrodona Bach et al., 2018; Choi et al., 2010; Hori et al., 2017; Wang et al., 2018; Liston and Hiemstra, 2011). On regional scales snow cover changes can vary depending on local climatology and its variability. Future projections with warming trends predict less precipitation to fall as snow and snowmelt to occur earlier in spring, affecting runoff and water resources downstream (Vaughan et al., 2013; IPCC, 2013).

On regional scales, seasonal snow is a vital part of water budgets in mountain and highland catchments where pre-

Published by Copernicus Publications on behalf of the European Geosciences Union.

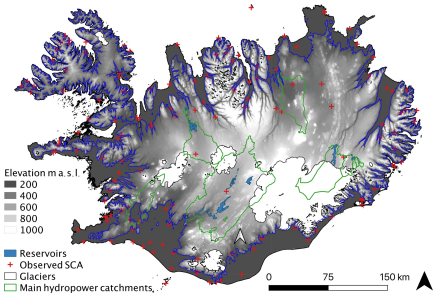

Figure 1. Overview of Iceland. Red outlines show the main catchment boundaries for large hydropower diversions, reservoirs and power plants. Manned sites for observed snow cover are shown in green points. Contours are shown for the 200 m elevation band. A solid blue contour represents 200 m elevation.

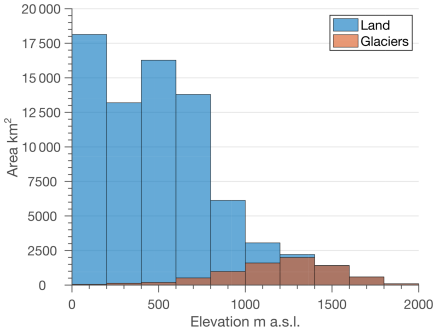

Figure 2. Elevation distribution for Iceland for both land and glaciers. Glaciers cover about 11 % of Iceland.

cipitation falls as snow during winter (Raleigh et al., 2013). Seasonal snow spring melt is also important for many applications such as irrigation for downstream agriculture areas, drinking water supply, and availability of water for hydropower energy production, and in some regions is critical for tourism, in particular ski resorts and winter tourism (Jóhannesson et al., 2007; Fischer et al., 2011; Kiparsky et al., 2014; Wagner et al., 2016).

Iceland is an island with an area of 103 100 km^2 located in the North Atlantic Ocean, close to the Arctic Circle (between 63 and 66° N). The central highlands correspond to 40 % of the island, with an average altitude of ∼550 m a.s.l., and only a quarter of the island lies below 200 m a.s.l. (Figs. 1 and 2). About 50 % of Iceland's land area is classified as open spaces and bare soils with sparse vegetation and 37 % as non-vegetated where vegetation cover is less than 10 %. These two types include most of the central highlands. Less than 1 % is forested and, in general, low shrub, wetland and heathland are the main types of vegetation (Einarsson et al., 2005; Traustason and Snorrason, 2008). Precipitation climatology has been characterized by a precipitation reduction with higher latitudes controlled by the orographic generation of precipitation in mountainous regions corresponding to the dominating SE-to-SW wind direction (Crochet et al., 2007; Björnsson et al., 2018). Area average precipitation is $\sim 1.7\,\mathrm{m}H_2O$ with the highest values at glacier peaks in the south (up to $10\,\mathrm{m}H_2O$). During winter heavy snowfall is frequently induced by cyclones crossing the North Atlantic, where air and water masses of tropical and Arctic origins meet (Einarsson, 1984; Ólafsson et al., 2007). In the highlands this leads to the formation of a seasonal snowpack and the sustainment of glaciers. At present, about 11 % of the country is covered by glaciers (Björnsson and Pálsson, 2008) (Figs. 1 and 2). During summer the average temperature at lower elevations (< 400 m a.s.l.) ranges from 8 to 10 °C, with a country-wide average of 7 °C. In winter the average temperature is 0–3 °C at lower elevations and about −5 °C for the whole island (Björnsson, 2003; Henriksen, 2003). From the seasonal snow cover classification system proposed by Sturm et al. (1995, 2010), Icelandic snowpack is generally classified as a combination of taiga, tundra and maritime types with overall shallow snowpack in depth with high density, frequent melt and wind-blown features (Jóhannesson and Sigurðsson, 2014).

In Iceland runoff from snowmelt is critical for hydropower production and reservoir storage as the energy system is strongly dependent on snowmelt and glacier melt. Over 13 % of the highland area in Iceland is developed for hydropower generation which provides over 72 % of the total average energy produced in Iceland (Hjaltason et al., 2018). A system of reservoirs and diversions stores melt water during the melt season in the spring and summer which generally consists of a seasonal snowmelt period (April–June) followed by a glacier melt period (June–September). As glacier melt recedes in the fall liquid precipitation is a large contributor to inflow (August–October). During winter reservoir storage provides regulation of water resources for energy production. The isolation and high natural climate variability pose a risk to the energy security of the power system as drought conditions and low-flow periods are usually not foreseen. In the longer term inflow to the energy systems is projected to increase due to climate warming and associated increase in glacier melt (Jóhannesson et al., 2007). Flow dynamics, i.e., timing and magnitude for seasonal snow, will also change, posing a challenge for operational control of energy infrastructure and climate change adaptation for both current energy projects as well as future development (Björnsson and Thorsteinsson, 2012; Sveinsson, 2016).

Spaceborne sensors operating in the visible and near-infrared range of electromagnetic spectrum have proven to be useful in effectively mapping snow cover for large areas since the early 1980s (Baumgartner et al., 1987; Dozier and Marks, 1987). Snow cover extent maps at various resolutions have been derived by the National Oceanic and Atmospheric Administration (NOAA) since 1966 (Dewey, 1987; Matson, 1991; Robinson et al., 1993). Since 2000 the MODIS sensor (Moderate Resolution Imaging Spectroradiometer) has provided daily global coverage of snow cover in cloud-free areas at a spatial resolution ranging from 250 to 1000 m. The sensor is carried on two Sun-synchronous, near-polar circular orbit satellites, Terra (descending node at approximately 10:30 local time) and Aqua (ascending node at approximately 13:30 local time). Terra was launched on 18 December 1999 and has had data available since September 2000, while Aqua was launched in May 2002. The sensor has 36 spectral bands that are used for various cryosphere, land, ocean and atmospheric scientific data sets and applications.

A range of snow cover products has been developed from the Aqua and Terra satellites carrying the MODIS sensor dating back to the early 2000s (Hall et al., 2002). The MODIS daily snow cover products (MOD10A1 from Terra and MYD10A1 from Aqua) have been a standard for snow cover monitoring at medium resolution since mid-year 2000 and are commonly used to analyze and monitor snow cover development in snow-dominated catchments, and their near-real-time availability makes them desirable for real-time applications such as for short-term forecasting and validation of runoff. The discrimination of snow and land is based on the Normalized Difference Snow Index (NDSI) which utilizes the spectral signature of snow being highly reflective in the visible spectral range (VIS) and has very low reflectance in the shortwave infrared spectral ranges (IR). In MODIS Terra bands 4 (VIS / 0.545–0.565 µm) and 6 (IR / 1.628–1652 µm) are used for the NDSI calculations, while the MODIS Aqua product relies on bands 4 and 7, as band 6 is non-functional (Salomonson and Appel, 2006).

MODIS snow cover products have been widely tested and validated for various land covers, topographic regions, and climates, with a typical average absolute accuracy of 93 % (Hall and Riggs, 2007; Huang et al., 2011; Klein and Barnett, 2003; Parajka and Blöschl, 2006). One of the main drawbacks of MODIS snow cover products, as well as other products that rely on optical satellite sensors, is the reliance on cloud-free conditions to produce snow cover maps. Various methods have been tested to provide gap-filled products of optical remote-sensing products including snow cover. Gao et al. (2010) used the MODIS high spatial resolution and cloud-penetrating ability of AMSR-E to reduce gaps in snow cover maps, while (Gascoin et al., 2015) applied a classification tree to gaps after merging daily Aqua and Terra snow cover tiles together and applying a temporal aggregating filter. Data from higher spatial resolution satellite platforms are available from high-resolution visible/near-infrared sensors such as from the USGS Landsat program (∼ 30 m) and ESA Sentinel 2 (∼ 20 m) program but at a lower temporal resolution, often making them less attractive for operational observations of snow cover.

The aim of this study was to create a gap-filled snow cover product for Iceland and extract snow cover characteristics for the period from 2000 to 2018. The first objective was a thorough validation of MODIS sensor-derived snow-covered maps over Iceland to validate the quality of the product and assess its limitations. Validation was an important and necessary step due to the annual and seasonal variability in climate, high average cloud cover and polar darkness during winter. The second objective of the study was to reduce the gaps to provide a spatio-temporal continuous product. By merging of data and temporal aggregation methods, data gaps are reduced and finally eliminated by using classification learners trained on topography and location of pixels. Based on the gap-filled data set snow cover characteristics on a regional scale over Iceland were derived showing relations to elevation, aspect and general trends in snow cover extent and duration.

2 Data

2.1 Observational in situ data

In Iceland in situ snow cover and depth observations are sparse, especially in the highlands. Few sites have had automatic observations of properties of snow until recently. The Icelandic Meteorological Office (IMO) operates a network of synoptic meteorological observations including daily manned observation of snow cover at 09:00. Figure 1 shows the location of these sites (green points) and how few of them are in or near the central highland area. Data were obtained from the IMO for the time period from 1 February 2000 to 31 December 2017 spanning a total of 152 sites and 585 880 observations. The data set consists of daily observations with a site number, date and snow cover classifications as well as a metadata file with site number, site name and site location and elevation (Veðurstofa Íslands, 2017).

2.2 MODIS snow cover data

MOD10A1 (Terra) and MYD10A1 (Aqua) Version 6 were obtained from the National Snow and Ice Data Center (NSIDC) (Hall and Riggs, 2016a, b) for the period from 23 February 2000 to 31 June 2018, which corresponds to 6702 dates where 6640 (99 %) MOD10A1 granules were available and 5829 (87 %) MYD10A1 dates were available. For MOD10A1 62 dates were missing and 12 for MYD10A1 from NSIDC excluding data missing due to polar darkness. Polar darkness limits the data availability during winter from MODIS in Iceland from ∼ 20 November until 26 January (63 d) each year, reducing the data set during winter (Dietz et al., 2012). During polar darkness M*D10A1 snow product

pixels are classified as night when the solar zenith angle is larger than or equal to 85°. Every granule from tile h17v02 was used in this project as it covers all the central highlands in Iceland and leaves out only a small portion of the western Snæfellsnes and the Westfjords.

2.3 Landsat 7/8 and Sentinel 2 data

Data acquired by the Landsat 7 Thematic Mapper (TM), Landsat 7 Enhanced Thematic Mapper Plus (ETM+), Landsat 8 Thematic Mapper (TM) and Landsat 8 Thermal Infrared Sensor (TIRS) were used. The data were downloaded from the United States Geological Survey (USGS) (https://earthexplorer.usgs.gov/, last access: 1 September 2018) using bulk download utilities. In total 264 Landsat 7 scenes were available from 12 April 2000 to 1 April 2015 and 124 scenes from Landsat 8 from 26 April 2013 to 22 June 2018 where land cloud cover was equal to or less than 20 % and the solar zenith angle not too large for processing the scene.

Data acquired by a European Space Agency (ESA) Sentinel 2A and B multispectral instrument (MSI) sensor were also used. The data were downloaded from the ESA's data hub (https://scihub.copernicus.eu/dhus, last access: 15 August 2018). In total 1090 Sentinel 2A/B scenes were acquired from 21 tracks covering Iceland. Only images where land cloud cover was equal to or less than 20 % were used. Images acquired in December and January each year have been left out due to polar darkness of MODIS data for all satellite products. Both Landsat and Sentinel products are in UTM/WGS84 projection.

2.4 Geospatial data

Digital elevation models (DEMs) and masking data for water bodies and glaciers were obtained from the National Land Survey of Iceland. The original DEM is a raster with a 10 m spatial resolution which is resampled to match the grid of the MODIS pixels using nearest neighbor sampling. From the resampled 500 m DEM the aspect data are calculated.

3 Methods

3.1 In situ data processing

Manned observations of snow cover from the IMO are reported daily at 09:00. Observations are made both at the local site where the instruments are located as well as in mountains where applicable; these are reported as local snow cover (SNC) and snow cover in mountains (SNCM). For each observation the local snow cover is reported as snow free (Code 0), patchy snow cover (Code 2) and fully snow covered (Code 4) (Veðurstofa Íslands, 2008). In accordance with the observational procedure of local snow cover the area observed was within 1 km of the observer and had no more than a 50 m elevation difference. We only used the local SNC for our analysis and omitted patchy snow cover classification from our comparison, but no further adjustments were made to the data set. In total 213 011 observations matches are found, i.e., where manned observations were available and a cloud-free pixel from MCDAT.

3.2 MODIS snow cover product processing

From the MOD10A1 and MYD10A1 daily data tiles we extracted the MOD Grid Snow 500 m grid and the variable NDSI snow cover was used for further analysis of snow cover. It is based on the MOD10-L2 algorithm which selects the best observation of the day to write to the daily data set. The variable NDSI snow cover ranges from 0 to 100, but in addition various other classifications are provided with the tile. As a preprocessing step data were reclassified to (a) snow, (b) no snow (land) and (c) no data (clouds, missing data, no decision, saturated detector). As the spatial extent of the tile is $\sim 1200\,\text{km} \times 1200\,\text{km}$ (data dimension 2400×2400), values that are beyond the Icelandic coast were masked out, including values only on land. A processing pipeline of MODIS snow data was adopted from Gascoin et al. (2015) and Parajka and Blöschl (2008) with modifications. The main steps are the following.

1. Daily tile merging: daily tiles from Aqua and Terra are merged to a single data set to improve daily coverage with data. Data from Terra have priority over data from Aqua as previous studies have found data from Terra to be of higher accuracy (Gascoin et al., 2015). For the first 2 years only Terra was in orbit, so the period from 23 February 2000 to 4 May 2002 is only based on Terra. The output data set used for further processing is named MCDAT (MODIS Combined Data for Aqua and Terra).

2. Temporal aggregation: for the remaining unclassified pixels in the daily merged data tiles (MCDAT) we apply temporal aggregation to further reduce unclassified pixels due to clouds in the data. Each MCDAT tile from step 1 is given a center date as the date of acquisition ($t = 0$) and a temporal aggregation range selected. The temporal aggregation range is set as the number of days backwards and forwards each center date data is allowed to search for classified pixel data which are missing in the original MCDAT center date data tile. Priority is given to data closest to the center date data (newest data relative to the center date) and from the forward date if both backward and forward dates have data. We select a temporal aggregation range as 3 d backward/forward ($t = \pm 3\,\text{d}$); i.e., in total 7 d can contribute data to the temporal aggregation product. The output data set used for further processing is named MCDAT7D.

3. Gap filling with classifiers: after the first two processing steps the remaining gaps are classified as snow or

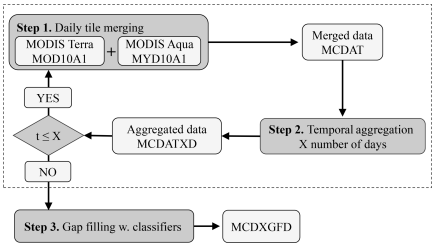

Figure 3. A simple process flow diagram for the daily tile merging, temporal aggregation and gap filling. X denotes the number of days selected for temporal aggregation, which includes t number of aggregation steps.

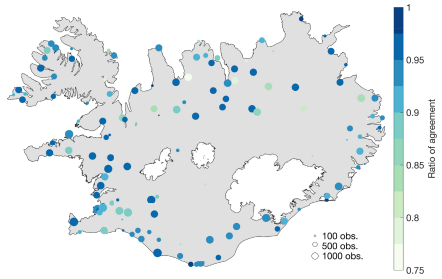

Figure 4. Comparison of observed snow cover and MODIS daily combined snow cover. For the whole data set the overall classification accuracy was 0.925.

no snow with classification learners. For each data set the unclassified pixels are reclassified with four predicting variables, location (easting, northing), elevation (Z) and aspect. The final output data set used for further processing is named MCD7GFD.

Figure 3 shows a flow diagram of the daily Aqua and Terra tile merging (Step 1), temporal aggregation of the daily merged tiles for X number of days (Step 2) and finally the gap-filling step for the remaining unclassified pixels (Step 3).

3.3 Landsat and Sentinel 2A/B processing

Landsat 7 and 8 data were retrieved as L1TP surface reflectance products. These products have a terrain correction and are radiometrically calibrated. The U.S. Geological Survey (USGS) uses the Landsat Ecosystem Disturbance Adaptive Processing System (LEDAPS) for Landsat 7 Surface Reflectance generation, while Landsat 8 is processed with the Landsat Surface Reflectance Code system (LaSRC) (USGS, 2018, 2019). Systems include for each date tile a pixel quality map where classifications of clouds, shadows, land, water and snow are presented.

Sentinel 2 data were retrieved as an L1C ortho-image product. Images are in top-of-atmosphere reflectances in cartographic geometry and have undergone geometric transformation and radiometric interpolation with a constant GSD (ground sampling distance) (Delwart, 2015). Sentinel 2 L1C data were processed using the Sen2Corr application from ESA to produce Level 2A data (Louis et al., 2016; Müller-Wilm et al., 2013). Level 2A Sen2Corr output data were an atmospherically corrected bottom of the atmosphere (BOA) product and have a scene classification map (SCL) on a pixel basis discriminating the surface into 11 categories, including no data, various types of clouds, water and snow or ice, among other categories. Data were processed at 20 and 30 m spatial resolution for Sentinel 2 and Landsat 7 and 8, respectively. Data were then resampled to the MODIS data grid at 500 m spatial resolution using GDAL utilities (GDAL/OGR contributors, 2019) with an average resampling method. Classification from the classification map in the L2A product were used for further analysis. Snow and ice were classified with the NDSI method (Müller-Wilm, 2018; Salomonson and Appel, 2004).

3.4 Classification learners

To classify the data we need to select a classification method. In general terms a model is trained with the training data set and the trained fit applied to the data that need classification. Within the Matlab Classification Toolbox (Matlab, 2017) there are many methods and algorithms available, and no clear selection criteria are evident.

In general snowfall in a region and formation of a snowpack are dependent on several climate and geographic factors such as latitude, longitude, elevation, distance from moist sources (ocean and lakes) and regional air mass circulation (DeWalle and Rango, 2008). To classify the remaining unclassified pixel information about pixel location (latitude, longitude), pixel elevation and pixel aspect are derived to use for the gap-filling algorithm. To test different classification methods a simple workflow was applied where the pre-processed MODIS data set (after temporal aggregation) of 2400 by 2400 pixels for the tile covering (hv017v14) Iceland was masked with the coastline of Iceland, selecting only pixels that fell on land, reducing the data size from 5.75 million pixels to 472 000 pixels. Next all pixels were categorized depending on whether they had data or not (snow/no snow/cloud). All cloud-covered pixels were arranged to classify a data set and pixels with valid snow cover data were arranged to a training data set. Information on location (X, Y), elevation (Z) and aspect (A) data for each pixel was derived to train the classifiers. Finally the classifier was applied to the training data set and the classified data set

Table 1. Confusion matrix for observations of snow compared to the Modis Aqua and Terra daily snow product combined.

		MCDAT	
		No snow	Snow
Obs.	No snow	96.9 %	3.1 %
	Snow	11.4 %	88.6 %

reclassified as snow/no snow with the trained classification data set. To assess the accuracy of the classification method 25 % of the classified data set prior to classification was withheld for cross-correlation. Glaciers were set to a fixed snow cover and water bodies were masked out.

4 Results and discussion

4.1 Validation results

4.1.1 Comparison with observed snow cover

Overall a good agreement was found between in situ observed snow cover and MODIS daily combined snow cover (MCDAT). Figure 4 shows the average agreement for each of the 152 sites investigated compared to the MODIS product for the whole period where the circle size shows the number of observations for each site. Out of the 585 800 observations in the database 213 011 matches were found when data were available from the MCDAT daily product and manned observations. The average agreement between observed snow and MODIS was 0.925. Table 1 shows a confusion matrix for the agreement between manually observed snow and NDSI snow cover from MCDAT. Observations and MCDAT agreed 96.9 % of the time when there was no snow on the ground according to the manual observations and 88.6 % of the time when snow was present. The poorest agreement was for sites located in the bottom of fjords and sounds where snow was observed during the manual observation, but was not present at the 10:30 / 01:30 UTC Terra / Aqua overpass. Possible explanations for a higher agreement for no snow classification over snow classification (Table 1) could be related to many of the in situ snow cover sites being located within or close to cities and small municipalities where buildings, roads and other civil structures could influence the NDSI value from MODIS towards classifying the pixel as not snow covered while the manned observation would classify the site as snow covered.

4.1.2 Comparison to Landsat/Sentinel data

Table 2 shows confusion matrix classification results from pixel-based comparison of snow cover derived from the combined daily Aqua and Terra product from MODIS and snow cover derived from Landsat 7/8 and Sentinel 2. For Landsat 7 8.21 million pixels were compared, 8.6 million for Landsat 8 and 3.77 million for Sentinel 2. For Landsat 7 86.9 % of snow-covered pixels were correctly classified in the MCDAT product, while 93.2 % of snow-free pixels were correctly classified. For Landsat 8 83.8 % of snow-covered pixels were correctly classified in the MCDAT product, while 92.7 % of snow-free pixels were correctly classified. Finally, for Sentinel 2 85.6 % of snow-covered pixels were correctly classified in the MCDAT product, while 91.8 % of snow-free pixels were correctly classified. Validation data from all satellites provide data over all of Iceland for multiple times. Pixel density, i.e., the number of overlappping pixels for the study period, ranges from 110, 30 and 90 for Landsat 7, Landsat 8 and Sentinel 2, respectively. Figure 5 shows the average agreement for snow-covered pixels for Landsat 7/8 and Sentinel 2 compared to the MCDAT product. Visually the agreement is good in all cases, with R^2 values of 96 %, 92 % and 95 % for Landsat 7/8 and Sentinel 2, respectively. No clear trends or correlation can be seen between months within the year and classification accuracy. These results are in agreement with similar studies where a pixel-based comparison was conducted (Huang et al., 2011; Gascoin et al., 2015).

Table 2. Confusion matrix for snow cover derived from Landsat 7, Landsat 8 and Sentinel 2 compared to the Modis Aqua and Terra daily snow product combined.

		MCDAT	
		No snow	Snow
Landsat 7	No snow	93.2 %	6.8 %
	Snow	13.6 %	86.9 %
Landsat 8	No snow	92.7 %	7.3 %
	Snow	16.6 %	83.8 %
Sentinel 2	No snow	91.8 %	8.2 %
	Snow	14.4 %	85.6 %

For each Landsat 7/8 and Sentinel 2 tile a classification map was constructed. The classification maps show the agreement of different satellite sources to the MCDAT product. A selected sample of the maps was manually screened to identify patterns in misclassification. The screening reveals that disagreement was mainly located at snow cover boundaries, i.e., where snow-free land meets snow-covered land as well as boundaries of clouds and land. Previous studies in snow-covered Arctic and alpine areas have revealed a similar effect when comparing MODIS to higher-resolution data (Gascoin et al., 2015; Déry et al., 2005; Rittger et al., 2012). A source of misclassification has been related to effects of forested areas which should be limited in Iceland due to few forested areas and sparse vegetation in general, especially at higher elevations. The effect of the MODIS sensor view angle has also been identified as a source of errors where the M*D10_L2 swath granule (source data for MODIS snow

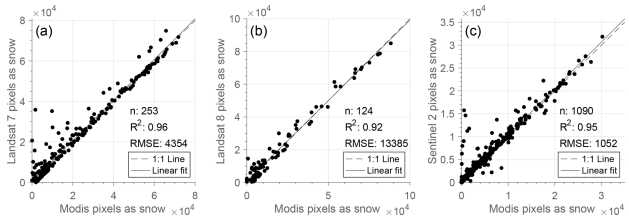

Figure 5. Relationship of classified snow pixels for Landsat 7/8 and Sentinel 2 with the MCDAT product.

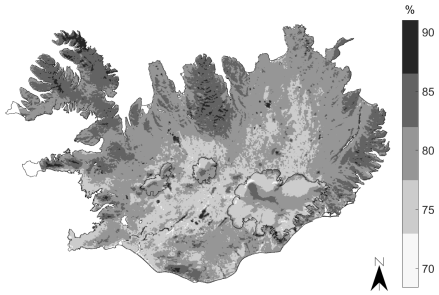

Figure 6. Average cloud cover over Iceland based on the MCDAT product for February to November each year from 2000 to 2018.

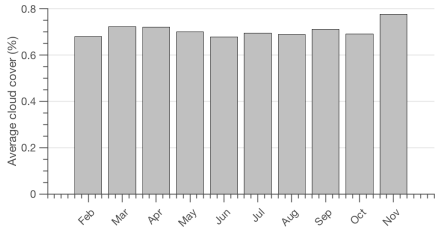

Figure 7. Average cloud cover distribution between months.

products) has different boundaries producing a "bow-tie" effect which can increase misclassification (Gómez-Landesa et al., 2004).

4.2 Gap filling with merging and temporal filtering

Figures 7 and 6 show the average cloud cover frequency in Iceland based on 18 years of MODIS data from 2000 to 2018 (MCDAT). Average cloud cover for Iceland was 79 %, while certain patterns are observed in the central highlands, over glaciers and in mountainous areas near the coast. In general cloud cover was less in the highlands but highest near the coast and in mountainous areas and fjords, such as Tröllaskagi, Austfirðir and Strandir. This illustrates the cloud obscurity problem for optical satellite remote sensing in Iceland. Figure 8 shows the results from daily merging and temporal aggregation of snow cover data. The two daily snow cover tiles from MOD10A1 and MYD10A1 had similar average cloud cover (76 %–78 %). Data from Aqua (afternoon overpass) showed 1.5 % average more cloud-covered pixels than Terra. Merging of the Aqua and Terra daily data sets provided on average a 7 % reduction in cloud-obscured pixels which was mostly related to moving cloud patterns within the day. Temporal aggregation of daily merged tiles had an exponential decaying shape of unclassified pixel reduction with the highest benefit for aggregating 1 day. The disadvantage of aggregating more days to a center date to further reduce unclassified pixels is temporal dampening of events and rapid changes in the snow cover. For our study 3 d were aggregated to the center date, both forward and backward, meaning that for each date of aggregated data in total 7 d contributed data with priority to the most recent observations. On average the unclassified pixels were reduced from $\sim$ 70 % to 14 %.

In general the advantage of temporal aggregation of data is reduced cloud-obscured pixels, which provides a spatio-temporal continuous product. The trade-off of temporal aggregation contrasts with the dampening of the response of the snow cover to rapid melt or snowfall events. This poses a limitation on the use of the data in real-time applications such as short-term flow forecasting for water resources.

4.3 Gap filling with classification learners

After applying a temporal aggregation to the data, unclassified pixels still remained in the data set. To classify the remaining pixels, various classifiers were tested to assess their classification accuracy. Various configurations of classification trees, *k* nearest neighbor algorithms (fine, coarse, cubic, weighted, boosted), supportive vector machines (SVMs), and linear and quadratic discriminant classification learners were tested in various configurations. Overall no one method and configuration provided a significant classification accu-

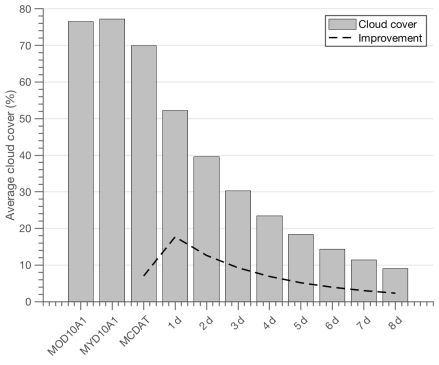

Figure 8. Average gap-filling improvement with merging of daily data and temporal aggregation.

racy improvement. Average classification accuracy ranged over 90 % for all methods tested and in general had lower classification accuracy during the melt season (April, May, June). The marginal best classification performance was by a weighted k nearest neighbor (wkNN) classifier which had 100 number of neighbors. The average classification accuracy for the whole data set was 96.4 % with a standard deviation of 2.7 % and a minimum classification accuracy of 83.4 %. This was based on a 25 % withheld classified population for every date classified in every method tested. The weighted k nearest neighbor was selected for further use.

4.4 Snow cover spatial and temporal characteristics in Iceland

A daily gap-filled snow cover product was derived for Iceland based on MODIS sensor bi-daily overpasses at a temporal resolution from 1 March 2000 to 30 June 2018. All water bodies and glaciers were excluded from the gap-filled snow cover product. Based on the data set, various descriptive spatio-temporal dynamics of snow cover in Iceland can be derived. The main limitation to the data set was polar darkness during December and January that limits the continuous temporal structure of the data set. Snow cover duration within a season is a parameter that is often used to describe characteristics of snow cover. The duration of snow cover is a property that can be linked to many applications such as seasonal snowmelt magnitude for operational water resources and length of vegetation growing season.

Figure 9 shows the distribution of snow cover over the whole country of Iceland from February 2000 to December 2017 as a percentage of land area in Iceland. A value of 100 % indicates that all non-glaciated land is fully covered with snow, while 0 % indicates a snow-free area. During late winter (February, March) most land area (> 90 %) was snow covered, while during April, May and June seasonal snow cover recedes rapidly due to longer daylight hours and increasing average temperatures. Extended snow cover duration was seen in 2013, 2014, 2015 and 2016, with more than 50 % of Iceland snow covered until the end of May. Specific snowfall events can be seen in May, increasing snow cover extent, but generally these events had a short impact. In the fall many events can be observed where snow cover increases in a snowfall event and then melts a few days/weeks later. This shows quite well the temporal structure of Icelandic snow cover where large areas covered with snow can melt out quickly during fall and winter due to storm tracks bringing warm air masses that can precipitate as both liquid or solid precipitation. For hydropower operations in Iceland snowfall in the fall (late August, beginning of September) can be a critical point in time as it can indicate lowering of inflows to reservoirs and diversions and the start of the reservoir regulation season, i.e., more water is flowing out of storage than in. This is related to the influence fresh snow cover with high albedo has on the dark glacier ice in the ablation zone, reducing severely the available energy for melt.

Figure 10 shows descriptive fits for number of snow-free dates (SFDs), first snow-free date (FSFD) and last snow-free date (LSFD) for the gap-filled data set. The criteria were that the representative area had 10 % or less of the area snow covered for more than 5 consecutive days and in the case of the last snow-free date the area needed to have 10 % or higher snow cover for 5 consecutive days. The number of snow-free dates is the number of days between these values (FSFD and LSFD) annually. A commonly used valuable snow cover metric is length of snow season, i.e., the number of days where snow covers the ground. Due to polar darkness this limits the temporal continuity of the data set during winter, so length of snow season can not be described fully here.

In various studies of snow cover where polar darkness applies, a filter assuming that if a pixel has snow at the beginning of polar darkness (late November in Iceland) and the same pixel still has snow when polar darkness recedes (mid January in Iceland), it can be assumed that the snow cover is continuous for that time period (Lindsay et al., 2015; Dietz et al., 2012). In Iceland the assumption of a continuous snow season during polar darkness is feeble as winter floods can influence large areas in a single depression low event (Kundzewicz, 2012; Rist, 1990).

Figure 10a shows the first snow-free date for each year in the data set and can be related to the timing when no snow remains within an area. An expected behavior is observed where lower-elevation areas experience meltout earlier in the year than higher-elevation areas. The average first snow-free date for Iceland is 27 June each year, with a standard deviation of 19.9 d (standard deviation is shown in parentheses from now on). The elevation band from 0 to 200 m a.s.l. (25 % of Iceland) has an earlier first snow-free date (7 May, ±13 d), while as with higher elevations the snow cover ex-

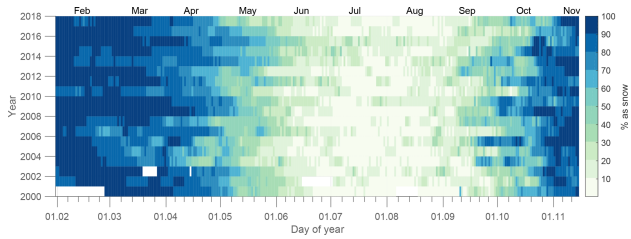

Figure 9. Snow cover duration (SCD) in Iceland from 1 March 2000 to 31 December 2017; 100 % indicates full snow cover, while 0 % represents a snow-free area. Glaciers and water bodies are not included.

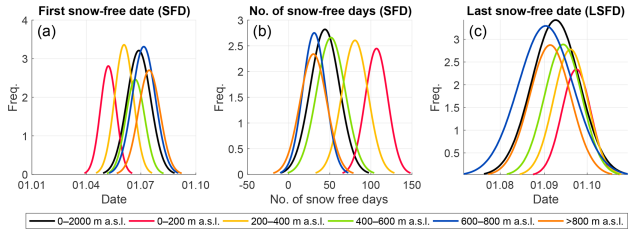

Figure 10. Normal distributions for extracted first snow-free date, number of snow-free days and last snow-free date.

tent is prolonged into the summer months. Figure 10b shows the number of SFDs. For all of Iceland the number of snow-free days is 44.1 d with a standard deviation of 17.8 d. For elevations from 0 to 200 m a.s.l., 106.8 d are snow free with a deviation of 13.7 d. For higher elevations the snow cover is more persistent and snow cover days total 80.6 d (±15.9 d), 51.4 d (±17.5 d) and 31.0 d (±13.8 d) for 200–400, 400–600 and 600–800 m a.s.l., respectively. For the highest-elevation bands (> 800 m a.s.l.) fewer pixels are non-glaciated (see Fig. 1), with 30 (±16.1) snow-free days. Figure 10c shows the LSFD, which is on average for Iceland 8 September (±16 d). This is highly influenced by snowfall events in the late fall in the highlands where snowfall events are frequently observed in late August or early September. These events will frequently melt out again, which can be seen in the variable snow cover duration in Fig. 9. In general higher elevations have snowfall events earlier in the fall, which coincides with a later snow-free date annually and fewer snow-free dates, as expected.

Figure 11 (first column) shows the mean snow cover duration for pairs of months as well as for the whole period the data set covers from February to November. Monthly averages are combined for pairs of months February and March, April and May, June and July, August and September, and October and November. These 2-month period pairs can be related to seasonality of the snow cover where February and March represent late winter where rain on snow events or warm storms are dominant in reducing the snow cover extent. April and May represent the conventional snowmelt season with snowmelt commencing earlier at lower elevations and is mostly driven by gradually warming temperatures, and June and July represent the summer season where most areas are snow free except at higher elevations and glaciers. In general this also is the period when glacier melt becomes the dominating water source in glacier-fed rivers and succeeds seasonal snowmelt. August and September represent late summer and early fall where highlands start to have lower temperatures, freezing during the night can be common and snowfall events are observed. October and November then represent the early winter period. In February and March land above 200 m a.s.l. is on average 100 % covered with snow with a more varying snow cover extent at lower elevations, especially near the coastline and in the southeastern and southwestern parts. In April and May larger areas are snow free from 0 to 400 m a.s.l., while snow cover is persistent in the highlands on higher mountains and at glacier boundaries. Snow cover has more extent in the northern part of Iceland as well in the western and eastern fjords. In June and July snow cover is generally at its minimum, with patchy snow cover in the center highlands and on higher mountain tops and ridges, especially in the northern Westfjords on Tröllaskagi in the north. Generally the first snow is observed

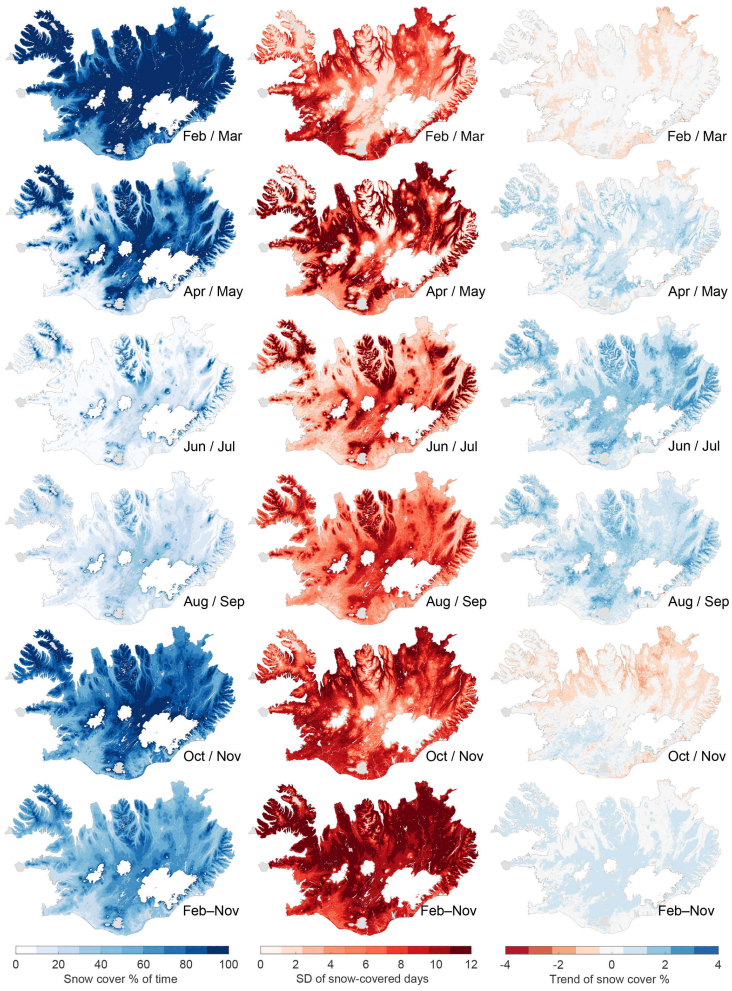

Figure 11. First column: mean snow cover duration as percentage of time for each period. Second column: standard deviation of days for each period. Third column: mean trend in snow cover duration as percentage of time for each period. Rows represent different combinations of monthly values and the bottom row is for the whole period from February to November.

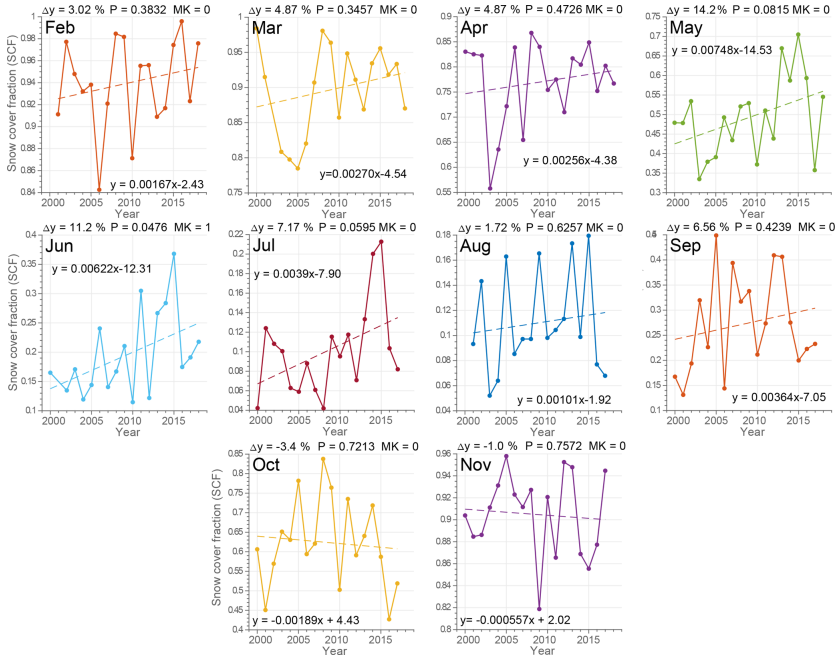

Figure 12. Monthly mean results for snow cover. For each month mean snow cover extent is calculated and a linear fit applied. The results from the Mann–Kendall test are shown as 1 or 0, where 1 indicates a significant change in trend. A linear equation shows the results for a fitted linear model to the data set. Δy is a non-statistical parameter and shows the average linear slope of the trend.

in August and September on glaciers and highlands with less frequent events at lower elevations in August, though often in September. On average the highlands are fully snow covered in October and November.

Figure 11 (second column) shows changes in snow cover within each period, presented with the standard deviations of data. The data are identical to snow cover extent characteristics where there is more deviation in the lower elevations in general during winter and which moves higher in elevation during the melt season. In February and March deviation is highest below 200 m a.s.l. and near the coast. The highest deviation is observed on the southern central lowlands and along the southeastern coast, which relates to the governing storm track alignment during winter (Einarsson, 1984). In April and May the variability moves higher in elevation associated with seasonal snowmelt and is still the highest in areas in the north, while the east and west have less variability. In June and July the highest areas in the north, east and west are melting, extending into August and September. In early winter, October and November, the snow cover in the highlands has stabilized, with more variability at lower elevations.

Figure 11 (third column) shows trends in snow cover within each period. In February and March the average trend is close to zero (insignificant for all areas). For April/May, June/July and August/September the average trend for each period is positive, indicating that the snow cover extent was spanning a longer time, i.e., that snow cover was extending further into the spring and summer months. For early winter, October and November, the average trend was slightly negative, meaning that snow cover was on average less, especially in the east and north, on the order of 0.4 to 3 d. Further details of this are shown in Fig. 11, where monthly mean snow cover extent was calculated for all years and the data were fitted linearly.

As previously mentioned, the data set only spans 18 years, so statistical interpretation such as trends should be treated with care. To evaluate whether these trends are significant, a linear trend test and a Mann–Kendall test were performed

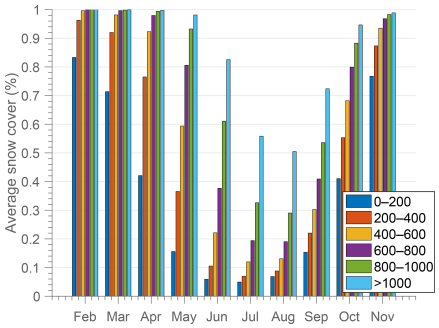

Figure 13. Average elevation distribution of snow cover for 2000–2018. Fractions of area for each elevation band are 23.9 % for 0–200 m a.s.l., 17.5 % for 200–400 m a.s.l., 21.7 % for 400–600 m a.s.l., 18.4 % for 600–800 m a.s.l., 8.2 % for 800–1000 m a.s.l. and 9.9 % for elevations over 1000 m a.s.l.

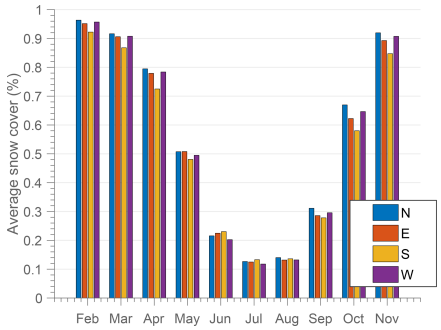

Figure 14. Average aspect distribution of snow cover for 2000–2018. Fractions of area for each aspect are 22.8 % for 0–90°, 23.8 % for 90–180°, 23.4 % for 180–270° and 26.6 % for 270–360°.

on monthly mean snow cover extents for α equal to 0.05. The Mann–Kendall test was a non-parametric test to identify trends in data over time where no assumption of normality was required (Mann, 1945; Helsel and Hirsch, 2002). Results indicate that the observed trends in the data are insignificant for all months except June, tested with both the Mann–Kendall test as well as the linear trend test. As identified visually, of the data in Fig. 12 for May, June and July, the steep trend was governed by snow cover extent in 2013, 2014 and 2015, which were abnormal years compared to previous years, with below-normal spring and summer temperatures which resulted in an extended length of the seasonal snow cover season which was also reflected in a positive mass balance of all Icelandic glaciers for the first time in over 20 years (Pálsson and Gunnarsson, 2016b, a; Þorsteinsson et al., 2017). Similarly, a slightly negative trend for October and November was calculated from a linear fit and was also governed, less though, by extended liquid precipitation events in these months in 2014, 2015 and 2016. A non-statistical parameter, Δy, was calculated to represent the average change over the period. This is merely the average slope of the linear fit but provides insight into the average characteristic of the snow cover trend.

Figure 13 shows average snow cover extent for different elevation bands for Iceland. The influence of elevation on the average snow cover extent is a strong controlling factor where large areas over 800 m a.s.l. retain the snow cover throughout the summer. During spring (April/May) a strong increase in snow cover extent was observed between 0 and 200 m a.s.l. and for the evaluation bands above 200 m a.s.l. This is consistent with results from Björnsson et al. (2018), where the annual average 0 °C isotherm is defined as ranging from 200 to 300 m a.s.l. During winter, elevations over 600 m a.s.l. are mostly fully covered with snow. The snowmelt season occurs in April to July, depending on elevation. In the fall a strong increase was also observed between September and October. Figure 14 shows the distribution of snow cover within the four main aspect classes (N, E, W, S). During February, March, April, October and November it shows that the snow cover tends to persist longer on the north-, west-, and east-facing slopes. During summer (June, July, August) this effect is less dominant. This is consistent with the expected snowpack energy balance, where in general north-facing slopes receive less solar radiation for melt while east- and west-facing slopes are exposed to a similar amount of solar radiation at different times of the day (west facing in the afternoon and east facing in the morning).

5 Conclusions

In this study, a gap-filled satellite-observed snow cover was produced from daily MODIS Aqua / Terra observations with duration from early 2000 until 2018 at a 500 m spatial resolution. Overall a good agreement was found between the daily combined MODIS Terra / Aqua data set and the validation data sets from Landsat 7/8, Sentinel 2 and in situ observations in Iceland. The Landsat and Sentinel data showed that boundary artifacts were present in the MODIS product at cloud–land boundaries, while no seasonal patterns of agreement were found when validating alternative remotely sensed products.

Average cloud cover in Iceland is high (75 % average), providing a significant limitation to the application of MODIS data and all optical remote-sensing instruments. No significant temporal patterns were found in cloud cover, while the central highland in general has lower average cloud cover. This was addressed with temporal aggregation of data

where the tradeoff from temporal aggregation (7 d) could have implications for hydrological applications of the data set where onset of melt and melt events could be retained or smoothed out of the product. This was also a limitation for identifying rain on snow events during winter.

Availability of MODIS data during polar darkness was also a temporal limitation for the data set. From late November to mid January no data were available, which limits the application of the data set to identify rain on snow events that can cause flooding and deplete areas of snowpack. Due to the dynamics of Icelandic snow during winter, especially at lower elevations, this is challenging to solve without combining other data sources such as snow models or other sources of remote sensing, for example synthetic aperture radar such as the ESA's Sentinel 1, which has a frequent overpass over Iceland.

The changes over time (trend) analyzed for the 18 years showed a slight increase in average snow cover in spring, likely driven by cold springs in 2013, 2014 and 2015 and extended liquid-phase precipitation in the fall for the same years. This aligns with observations of winter mass balance of Icelandic glaciers in recent years with a slight significant positive trend for the past 20 years (Pálsson and Gunnarsson, 2016c) as well as an observed precipitation increase (Björnsson et al., 2018). These results are consistent with previous findings that suggest that an slight increase in snow cover extent/area is observed in Iceland (Eythorsson et al., 2019; Wang et al., 2018) even though a general decreasing snow cover extent/area and shortening of the melt season in the Northern Hemisphere is reported in many other studies (Choi et al., 2010; Hori et al., 2017).

Another influencing factor for onset of melt and melt enhancement is radiative forcing by light-absorbing particles (Painter et al., 2018; Skiles et al., 2018). Due to frequent volcanic eruptions in Iceland volcanic ash and tephra can be transported great distances (Gudmundsson et al., 2012; Sólnes et al., 2013). The volcanic eruptions in Eyjafjallajökull in 2010 and Grímsvötn in 2011 took place in April and May, respectively, and are within the MODIS data period (2000–2018). Figures 9 and 12 show no clear sign of melt enhancement for spring 2010 and 2011, although albedo and summer melt of Icelandic glaciers were greatly influenced (Gascoin et al., 2017; Pálsson and Gunnarsson, 2016c).

The gap-filled snow cover product provides a useful tool to monitor and analyze inter-annual variability and long-term trends in snow cover in Iceland. The methodology applied here can be applied to other satellite sensors such as Sentinel 3 or the Visible Infrared Imaging Radiometer Suite (VIIRS) to extend the temporal range of data beyond the MODIS mission.

Code and data availability. Code used in the project to process data is available at https://github.com/andrigunn/isca (Gunnarsson, 2019). MODIS data are available from https://nsidc.org/data/ (Hall and Riggs, 2016b), Sentinel 2 data are available at https://scihub.copernicus.eu/dhus/ (European Space Agency, 2018), and Landsat 7 and 8 data are available at https://earthexplorer.usgs.gov/ (United States Geological Survey, 2018). Data set tiles, paths and version numbers are defined in Sect. 2. Geospatial data for Iceland are available from the National Land Survey of Iceland at https://atlas.lmi.is/LmiData/index.php (National Land Survey of Iceland, 2018). Observations of snow cover from manned IMO sites are available upon request to fyrirspurnir@vedur.is.

Author contributions. AG conceived and designed the study, performed the analyses, and prepared the manuscript. SMG and ÓGBS contributed to the study design, interpretation of the results, and writing of the manuscript.

Competing interests. The authors declare that they have no conflict of interest.

Acknowledgements. We would like to thank Jessica D. Lundquist, University of Washington, for discussion and valuable feedback during the design of the study. Special thanks to Helgi Jóhannesson, project manager at Landsvirkjun, for providing constructive feedback during review of the manuscript. The Valle Scholarship and Scandinavian Exchange Program at the University of Washington is also thanked for financial support during the academic year 2017–2018 at the University of Washington.

Review statement. This paper was edited by Ryan Teuling and reviewed by two anonymous referees.

References

Adam, J. C., Hamlet, A. F., and Lettenmaier, D. P.: Implications of Global Climate Change for Snowmelt Hydrology in the Twenty-First Century, Hydrol. Process., 23, 962–972, https://doi.org/10.1002/hyp.7201, 2008.

Barichivich, J., Briffa, K. R., Myneni, R. B., Osborn, T. J., Melvin, T. M., Ciais, P., Piao, S., and Tucker, C.: Large-scale variations in the vegetation growing season and annual cycle of atmospheric CO_2 at high northern latitudes from 1950 to 2011, Global Change Biol., 19, 3167–3183, https://doi.org/10.1111/gcb.12283, 2013.

Barnett, T. P., Adam, J. C., and Lettenmaier, D. P.: Potential Impacts of a Warming Climate on Water Availability in Snow-Dominated Regions, Nature, 438, 303–309, 2005.

Barry, R. G.: The Role of Snow and Ice in the Global Climate System: A Review, Polar Geography, 26, 235–246, https://doi.org/10.1080/789610195, 2002.

Baumgartner, M. F., Seidel, K., and Martinec, J.: Toward Snowmelt Runoff Forecast Based on Multisensor Remote – Sensing Informnation, IEEE T. Geoscie. Remote, 25, 746–750, https://doi.org/10.1109/TGRS.1987.289744, 1987.

Björnsson, H.: The Annual Cycle of Temperature in Iceland, Reykjavík, Veðurstofa Íslands, Reykjavík, 2003 October, 2003.
Björnsson, H. and Pálsson, F.: Icelandic Glaciers, Jökull, 365–386, 2008.
Björnsson, H. and Thorsteinsson, T.: Climate Change and Energy Systems: Impacts, Risks and Adaptation in the Nordic and Baltic Countries, TemaNord, Nordic Council of Ministers, Copenhagen, https://doi.org/10.6027/TN2011-502, 2012.
Björnsson, H., Sigurðsson, B. D., Davíðsdóttir, B., Ólafsson, J. S., Ástþórsson, O. S., Ólafsdóttir, S., Baldursson, T., and Jónsson, J.: Loftslagsbreytingar Og Áhrif Þeirra á Íslandi: Skýrsla Vísindanefndar Um Loftslagsbreytingar 2018, Tech. Rep., Veðurstofa Íslands, Reykjavík, 238 pp., 2018.
Choi, G., Robinson, D. A., and Kang, S.: Changing Northern Hemisphere Snow Seasons, J. Climate, 23, 5305–5310, https://doi.org/10.1175/2010JCLI3644.1, 2010.
Crochet, P., Jóhannesson, T., Jónsson, T., Sigurðsson, O., Björnsson, H., Pálsson, F., and Barstad, I.: Estimating the Spatial Distribution of Precipitation in Iceland Using a Linear Model of Orographic Precipitation, J. Hydrometeorol., 8, 1285–1306, https://doi.org/10.1175/2007JHM795.1, 2007.
Delwart, S.: ESA Standard Document, Tech. Rep., European Space Agency, 64 pp., 2015.
Déry, S. J., Salomonson, V. V., Stieglitz, M., Hall, D. K., and Appel, I.: An Approach to Using Snow Areal Depletion Curves Inferred from MODIS and Its Application to Land Surface Modelling in Alaska, Hydrol. Process., 19, 2755–2774, https://doi.org/10.1002/hyp.5784, 2005.
DeWalle, D. R. and Rango, A.: Principles of Snow Hydrology, Cambridge University Press, Cambridge, https://doi.org/10.1017/CBO9780511535673, 2008.
Dewey, K. F.: Satellite-Derived Maps of Snow Cover Frequency for the Northern Hemisphere, J. Clim. Appl. Meteorol., 26, 1210–1229, 1987.
Dietz, A. J., Wohner, C., and Kuenzer, C.: European Snow Cover Characteristics between 2000 and 2011 Derived from Improved MODIS Daily Snow Cover Products, Remote Sens., 4, 2432–2454, https://doi.org/10.3390/rs4082432, 2012.
Dozier, J. and Marks, D.: Snow Mapping and Classification from Landsat Thematic Mapper Data, Ann. Glaciol., 9, 97–103, https://doi.org/10.3189/S026030550000046X, 1987.
Einarsson, E., Jóhannesson, H., Sigurðsson, O., Eldjárn, O., Sigurðsson, O., and Hansen, H. H.: Íslandsatlas, Reykjavík, Edda, 2005, Reykjavík, 2005.
Einarsson, M. A.: Climates of the Oceans, Vol. 15 of World Survey of Climatology, edited by: Van Loon, H., J. Climatol., 5, 673–697, https://doi.org/10.1002/joc.3370050110, 1984.
European Space Agency: Copernicus Open Access Hub, available at: https://scihub.copernicus.eu/dhus/, last acces: 1 September 2018.
Eythorsson, D., Gardarsson, S. M., Ahmad, S. K., Hossain, F., and Nijssen, B.: Arctic climate and snow cover trends – Comparing Global Circulation Models with remote sensing observations, Int. J. Appl. Earth Obs., 80, 71–81, https://doi.org/10.1016/j.jag.2019.04.003, 2019.
Fernandes, R., Zhao, H. X., Wang, X. J., Key, J., Qu, X., and Hall, A.: Controls on Northern Hemisphere Snow Albedo Feedback Quantified Using Satellite Earth Observations, Geophys. Res. Lett., 36, L21702, https://doi.org/10.1029/2009gl040057, 2009.
Fischer, A., Olefs, M., and Abermann, J.: Glaciers, Snow and Ski Tourism in Austria's Changing Climate, Ann. Glaciol., 52, 89–96, https://doi.org/10.3189/172756411797252338, 2011.
Fontrodona Bach, A., van der Schrier, G., Melsen, L. A., Klein Tank, A. M. G., and Teuling, A. J.: Widespread and Accelerated Decrease of Observed Mean and Extreme Snow Depth Over Europe, Geophys. Res. Lett., 45, 12312–12319, https://doi.org/10.1029/2018GL079799, 2018.
Gao, Y., Xie, H., Yao, T., and Xue, C.: Integrated Assessment on Multi-Temporal and Multi-Sensor Combinations for Reducing Cloud Obscuration of MODIS Snow Cover Products of the Pacific Northwest USA, Remote Sens. Environ., 114, 1662–1675, https://doi.org/10.1016/j.rse.2010.02.017, 2010.
Gascoin, S., Hagolle, O., Huc, M., Jarlan, L., Dejoux, J.-F., Szczypta, C., Marti, R., and Sánchez, R.: A snow cover climatology for the Pyrenees from MODIS snow products, Hydrol. Earth Syst. Sci., 19, 2337–2351, https://doi.org/10.5194/hess-19-2337-2015, 2015.
Gascoin, S., Guðmundsson, S., Aðalgeirsdóttir, G., Pálsson, F., Schmidt, L., Berthier, E., and Björnsson, H.: Evaluation of MODIS Albedo Product over Ice Caps in Iceland and Impact of Volcanic Eruptions on Their Albedo, Remote Sens., 9, 399, https://doi.org/10.3390/rs9050399, 2017.
GDAL/OGR contributors: GDAL/OGR Geospatial Data Abstraction software Library, Open Source Geospatial Foundation, available at: https://gdal.org (last access: 1 May 2018), 2019.
Gómez-Landesa, E., Rango, A., and Bleiweiss, M.: An Algorithm to Address the MODIS Bowtie Effect, Can. J. Remote Sens., 30, 644–650, https://doi.org/10.5589/m04-028, 2004.
Gray, D. and Male, D.: Handbook of Snow: Principles, Processes, Management & Use, Blackburn Press, 776 pp., 2004.
Gudmundsson, M. T., Thordarson, T., Höskuldsson, Á., Larsen, G., Björnsson, H., Prata, F. J., Oddsson, B., Magnússon, E., Högnadóttir, T., Petersen, G. N., Hayward, C. L., Stevenson, J. A., and Jónsdóttir, I.: Ash generation and distribution from the April–May 2010 eruption of Eyjafjallajökull, Iceland, Sci. Rep., 2, 572, https://doi.org/10.1038/srep00572, 2012.
Gunnarsson, A.: Code Repository for ISCA, available at: https://github.com/andrigunn/isca, last access: 15 January 2019.
Hall, D. K. and Riggs, G. A.: Accuracy Assessment of the MODIS Snow Products, Hydrol. Process., 21, 1534–1547, https://doi.org/10.1002/hyp.6715, 2007.
Hall, D. K. and Riggs, G. A.: MODIS/Aqua Snow Cover Daily L3 Global 500 m Grid, Version 6, Tech. Rep., NASA National Snow and Ice Data Center Distributed Active Archive Center, Boulder, Colorado USA, 2016a.
Hall, D. K. and Riggs, G. A.: MODIS/Terra Snow Cover Daily L3 Global 500 m Grid, Version 6, Tech. Rep., NASA National Snow and Ice Data Center Distributed Active Archive Center, available at: https://nsidc.org/data/, https://doi.org/10.5067/MODIS/MOD10A1.006, Boulder, Colorado USA, 2016b.
Hall, D. K., Riggs, G. A., Salomonson, V. V., DiGirolamo, N. E., and Bayr, K. J.: MODIS Snow-Cover Products, Remote Sens. Environ., 83, 181–194, https://doi.org/10.1016/S0034-4257(02)00095-0, 2002.
Helsel, D. and Hirsch, R.: Statistical Methods in Water Resources Techniques of Water Resources Investigations, Tech. Rep., Book 4, Chapter A3, U.S. Geological Survey, 2002.

Henriksen, S.: Report on the Approximation of the Annual Cycle of Temperature in Iceland, Reykjavík, Veðurstofa Íslands, February 2003, Reykjavík, 2003.

Hjaltason, S., Guðmundsdóttir, M., Haukdal, J. A., and Guðmundsson, J. R.: Energy statistics in Iceland 2017, Energy Statistics in Iceland, Orkustofnun, 2 pp., 2018.

Hori, M., Sugiura, K., Kobayashi, K., Aoki, T., Tanikawa, T., Kuchiki, K., Niwano, M., and Enomoto, H.: A 38-year (1978–2015) Northern Hemisphere daily snow cover extent product derived using consistent objective criteria from satellite-borne optical sensors, Remote Sens. Environ., 191, 402–418, https://doi.org/10.1016/j.rse.2017.01.023, 2017.

Huang, X., Liang, T., Zhang, X., and Guo, Z.: Validation of MODIS Snow Cover Products Using Landsat and Ground Measurements during the 2001–2005 Snow Seasons over Northern Xinjiang, China, Int. J. Remote Sens., 32, 133–152, https://doi.org/10.1080/01431160903439924, 2011.

IPCC: Climate Change 2013: The Physical Science Basis, Contribution of Working Group I to the Fifth Assessment Report of the Intergovernmental Panel on Climate Change, Cambridge University Press, Cambridge, United Kingdom and New York, NY, USA, https://doi.org/10.1017/CBO9781107415324, 2013.

Jóhannesson, T. and Sigurðsson, O.: Samantekt Um Snjómælingar á Hálendi Íslands, Reykjavík, Veðurstofa Íslands, 2014, Reykjavík, 2014.

Jóhannesson, T., Aðalgeirsdóttir, G., Björnsson, H., Crochet, P., Elíasson, E. B., Guðmundsson, S., Jónsdóttir, J. F., Ólafsson, H., Pálsson, F., Rögnvaldsson, Ó, Sigurðsson, O., Snorrason, Á., Blöndal Sveinsson, O. G., and Þorsteinn, Þ.: Effect of Climate Change on Hydrology and Hydro-Resources in Iceland, Reykjavík, Orkustofnun, 2007, Reykjavík, 2007.

Sólnes, J., Sigmundsson, F., and Bessason, B.: Náttúruvá á Íslandi, eldgos og jarðskjálftar, Reykjavík, Viðlagatrygging Íslands, Háskólaútgáfan, 2013.

Keller, F., Goyette, S., and Beniston, M.: Sensitivity Analysis of Snow Cover to Climate Change Scenarios and Their Impact on Plant Habitats in Alpine Terrain, Clim. Change, 72, 299–319, https://doi.org/10.1007/s10584-005-5360-2, 2005.

Kiparsky, M., Joyce, B., Purkey, D., and Young, C.: Potential Impacts of Climate Warming on Water Supply Reliability in the Tuolumne and Merced River Basins, California, PLOS ONE, 9, e84946, https://doi.org/10.1371/journal.pone.0084946, 2014.

Klein, A. G. and Barnett, A. C.: Validation of Daily MODIS Snow Cover Maps of the Upper Rio Grande River Basin for the 2000–2001 Snow Year, Remote Sens. Environ., 86, 162–176, https://doi.org/10.1016/S0034-4257(03)00097-X, 2003.

Kundzewicz, Z.: Changes in Flood Risk in Europe, https://doi.org/10.1201/b12348, 2012.

Lindsay, C., Zhu, J., Miller, E. A., Kirchner, P., and Wilson, L. T.: Deriving Snow Cover Metrics for Alaska from MODIS, Remote Sens., 7, https://doi.org/10.3390/rs71012961, 12961–12985, 2015.

Liston, G. E. and Hiemstra, C. A.: The Changing Cryosphere: Pan-Arctic Snow Trends (1979—2009), J. Climate, 24, 5691–5712, https://doi.org/10.1175/JCLI-D-11-00081.1, 2011.

Louis, J., Debaecker, V., Pflug, B., Main-Knorn, M., Bieniarz, J., Mueller-Wilm, U., Cadau, E., and Gascon, F.: SENTINEL-2 SEN2COR: L2A processor for users, in: Living Planet Symposium, p. 8, 2016.

Mann, H. B.: Nonparametric Tests Against Trend, Econometrica, 13, 245–259, https://doi.org/10.2307/1907187, 1945.

Matlab: R2017a, The Mathworks Inc., Natick, Massachusetts, 2017.

Matson, M.: NOAA Satellite Snow Cover Data, Operational satellites: Sentinels for the monitoring of climate and global change, Global Planet. Change, 4, 213–218, https://doi.org/10.1016/0921-8181(91)90095-E, 1991.

Müller-Wilm, U.: S2 MPC. Sen2Cor – Configuration and User Manual, Tech. Rep., S2-PDGS-MPC-L2A-SUM-V2.5.5, 2018.

Müller-Wilm, U., Louis, J., Richter, R., Gascon, F., and Niezette, M.: Sentinel-2 Level-2A Prototype Processor: Architecture, Algorithms and First Results, in: ESA Living Planet Symposium, Edinburgh, UK, 2013.

National Land Survey of Iceland: IS 50V 24/12 2015 – Elevation data, available at: https://atlas.lmi.is/LmiData/index.php, last access: 1 January 2018.

Ólafsson, H., Furger, M., and Brümmer, B.: The Weather and Climate of Iceland, Vol. 16, Meteorol. Z., https://doi.org/10.1127/0941-2948/2007/0185, 2007.

Painter, T. H., Skiles, S. M., Deems, J. S., Brandt, W. T., and Dozier, J.: Variation in Rising Limb of Colorado River Snowmelt Runoff Hydrograph Controlled by Dust Radiative Forcing in Snow, Geophys. Res. Lett., 45, 797–808, https://doi.org/10.1002/2017GL075826, 2018.

Pálsson, F. and Gunnarsson, A.: Langjökull, Afkomu- Og Hraðamælingar á Langjökli Jökulárið 2015–2016, Tech. Rep., Reykjavík, 2016a.

Pálsson, F. and Gunnarsson, A.: Vatnajökull, Mass Balance, Meltwater Drainage and Surface Velocity of the Glacial Year 2014–2015, Tech. Rep., Reykjavík, 2016b.

Pálsson, F. and Gunnarsson, A.: Vatnajökull, Mass Balance, Meltwater Drainage and Surface Velocity of the Glacial Year 2015–2016., Tech. Rep., Reykjavík, 2016c.

Parajka, J. and Blöschl, G.: Validation of MODIS snow cover images over Austria, Hydrol. Earth Syst. Sci., 10, 679–689, https://doi.org/10.5194/hess-10-679-2006, 2006.

Parajka, J. and Blöschl, G.: Spatio-Temporal Combination of MODIS Images – Potential for Snow Cover Mapping: Spatio-temporal combination of modis images, Water Resour. Res., 44, https://doi.org/10.1029/2007WR006204, 2008.

Qu, X. and Hall, A.: What Controls the Strength of Snow-Albedo Feedback?, J. Climate, 20, 3971–3981, https://doi.org/10.1175/JCLI4186.1, 2007.

Raleigh, M. S., Rittger, K., Moore, C. E., Henn, B., Lutz, J. A., and Lundquist, J. D.: Ground-Based Testing of MODIS Fractional Snow Cover in Subalpine Meadows and Forests of the Sierra Nevada, Remote Sens. Environ., 128, 44–57, https://doi.org/10.1016/j.rse.2012.09.016, 2013.

Rist, S.: Vatns Er Þörf, Reykjavík, Menningarsjóður, 248 pp., 1990.

Rittger, K., Painter, T., and Dozier, J.: Assessment of Methods for Mapping Snow Cover from MODIS, Adv. Water Res., 51 https://doi.org/10.1016/j.advwatres.2012.03.002, 367–380, 2012.

Robinson, D. A., Dewey, K. F., and Heim, R. R.: Global Snow Cover Monitoring – An Update, B. Am. Meteorol. Soc., 74, 1689–1696, 1993.

Salomonson, V. and Appel, I.: Estimating Fractional Snow Cover from MODIS Using the Normalized Differ-

ence Snow Index, Remote Sens. Environ., 89, 351–360, https://doi.org/10.1016/j.rse.2003.10.016, 2004.

Salomonson, V. V. and Appel, I.: Development of the Aqua MODIS NDSI Fractional Snow Cover Algorithm and Validation Results, IEEE T. Geoscie. Remote, 44, 1747–1756, https://doi.org/10.1109/TGRS.2006.876029, 2006.

Skiles, S. M., Flanner, M., Cook, J. M., Dumont, M., and Painter, T. H.: Radiative forcing by light-absorbing particles in snow, Nat. Clim. Change, 8, 964–971, https://doi.org/10.1038/s41558-018-0296-5, 2018.

Sturm, M., Holmgren, J., and Liston, G. E.: A Seasonal Snow Cover Classification System for Local to Global Applications, J. Climate, 8, 1261–1283, https://doi.org/10.1175/1520-0442(1995)008<1261:ASSCCS>2.0.CO;2, 1995.

Sturm, M., Taras, B., Liston, G. E., Derksen, C., Jonas, T., and Lea, J.: Estimating Snow Water Equivalent Using Snow Depth Data and Climate Classes, J. Hydrometeorol., 11, 1380–1394, https://doi.org/10.1175/2010JHM1202.1, 2010.

Sveinsson, O.: Energy in Iceland: Adaptation to Climate Change, UNU-FLORES Policy Briefs, United Nations University Institute for Integrated Management of Material Fluxes and of Resources (UNU-FLORES), Dresden, 4 pp., 2016.

Þorsteinsson, Þ., Jóhannesson, T., Sigurðsson, O., and Einarsson, B.: Afkomumælingar á Hofsjökli 1988–2017, Reykjavik, Veðurstofa Íslands, 2017.

Traustason, B. and Snorrason, A.: Spatial Distribution of Forests and Woodlands in Iceland in Accordance with the CORINE Land Cover Classification, Iceland Agriculutre Science, 21, 39–47, 2008.

United States Geological Survey: Landsat Earth Explorer, available at: https://earthexplorer.usgs.gov/, last access: 1 September 2018.

USGS: Landsat 7 (L7) Data Users Handbook, Tech. Rep., LSDS-1927, USGS, Sioux Falls, South Dakota, 2018.

USGS: Product guide – Landsat 8 surface reflectance code (LASRC) product, Version 4.3, Tech. Rep., Department of the Interior U.S. Geological Survey, 2019.

Vaughan, D., Comiso, J., Allison, I., Carrasco, J., Kaser, G., Kwok, R., Mote, P., Murray, T., Paul, F., Ren, J., Rignot, E., Solomina, O., Steffen, K., and Zhang, T.: Observations: Cryosphere, in: Climate Change 2013: The Physical Science Basis. Contribution of Working Group I to the Fifth Assessment Report of the Intergovernmental Panel on Climate Change, edited by: Stocker, T., Qin, D., Plattner, G.-K., Tignor, M., Allen, S., Boschung, J., Nauels, A., Xia, Y., Bex, V., and Midgley, P., Cambridge University Press, Cambridge, United Kingdom and New York, NY, USA, 317–382, https://doi.org/10.1017/CBO9781107415324.012, 2013.

Veðurstofa Íslands: Reglur Um Veðurathuganir, Skýrslufærslur Og Skeytasendingar á Skeytastöðvum, Tech. Rep., VÍ-ES01, Veðurstofa Íslands, Reykjavík, 2008.

Veðurstofa Íslands: Verkbeiðnakerfi Veðurstofunnar – Útgáfu Númer (ID) 49996, Dataset ID 49996, Veðurstofa Íslands, Reykjavík, 2017.

Wagner, T., Themeßl, M., Schüppel, A., Gobiet, A., Stigler, H., and Birk, S.: Impacts of Climate Change on Stream Flow and Hydro Power Generation in the Alpine Region, Environ. Earth Sci., 76, 4, https://doi.org/10.1007/s12665-016-6318-6, 2016.

Wang, Y., Huang, X., Liang, H., Sun, Y., Feng, Q., and Liang, T.: Tracking Snow Variations in the Northern Hemisphere Using Multi-Source Remote Sensing Data (2000–2015), Remote Sens., 10, https://doi.org/10.3390/rs10010136, 2018.

Warren, S. G.: Optical Properties of Snow, Rev. Geophys., 20, 67–89, https://doi.org/10.1029/RG020i001p00067, 1982.

Paper II

Annual and inter-annual variability and trends of albedo of Icelandic glaciers

Andri Gunnarsson, Sigurdur M. Gardarsson, Finnur Pálsson, Tómas Jóhannesson and Óli G. B. Sveinsson

The Cryosphere, 15, 547-570

The Cryosphere, 15, 547–570, 2021
https://doi.org/10.5194/tc-15-547-2021

The Cryosphere Open Access EGU

Annual and inter-annual variability and trends of albedo of Icelandic glaciers

Andri Gunnarsson[1,4], Sigurdur M. Gardarsson[1], Finnur Pálsson[2], Tómas Jóhannesson[3], and Óli G. B. Sveinsson[4]

[1]University of Iceland, Civil and Environmental Engineering, Hjardarhagi 2-6, 107 Reykjavík, Iceland
[2]Institute of Earth Sciences, University of Iceland, Sturlugata 7, 101 Reykjavík, Iceland
[3]Icelandic Meteorological Office, Bústaðavegi 7–9, 105 Reykjavík, Iceland
[4]Landsvirkjun, Department of Research and Development, 107 Reykjavík, Iceland

Correspondence: Andri Gunnarsson (andrigun@lv.is)

Received: 30 December 2019 – Discussion started: 27 January 2020
Revised: 30 November 2020 – Accepted: 7 December 2020 – Published: 8 February 2021

Abstract. During the melt season, absorbed solar energy, modulated at the surface predominantly by albedo, is one of the main governing factors controlling surface-melt variability for glaciers in Iceland. Using MODIS satellite-derived daily surface albedo, a gap-filled temporally continuous albedo product is derived for the melt season (May to August (MJJA)) for the period 2000–2019. The albedo data are thoroughly validated against available in situ observations from 20 glacier automatic weather stations for the period 2000–2018. The results show that spatio-temporal patterns for the melt season have generally high annual and inter-annual variability for Icelandic glaciers, ranging from high fresh-snow albedo of about 85 %–90 % in spring to 5 %–10 % in the impurity-rich bare-ice area during the peak melt season. The analysis shows that the volcanic eruptions in 2010 and 2011 had significant impact on albedo and also had a residual effect in the following years. Furthermore, airborne dust, from unstable sandy surfaces close to the glaciers, is shown to enhance radiative forcing and decrease albedo. A significant positive albedo trend is observed for northern Vatnajökull while other glaciers have non-significant trends for the study period. The results indicate that the high variability in albedo for Icelandic glaciers is driven by climatology, i.e. snow metamorphosis, tephra fallout during volcanic eruptions and their residual effects in the post-eruption years, and dust loading from widespread unstable sandy surfaces outside the glaciers. This illustrates the challenges in albedo parameterization for glacier surface-melt modelling for Icelandic glaciers as albedo development is driven by various complex phenomena, which may not be correctly captured in conventional energy-balance models.

1 Introduction

Surface albedo is defined as the unitless ratio of radiant flux reflected from the Earth's surface to the incident flux. It is a controlling parameter, which governs the portioning of the shortwave radiative energy between the atmosphere and the surface and, therefore, a control of the surface energy balance modulated by the solar zenith angle, cloud optical thickness, cloud cover, and transmission properties of the atmosphere (Klein and Stroeve, 2002; Gardner and Sharp, 2010; Donohoe and Battisti, 2011). The evolution of albedo for impurity-free snow and ice is controlled by the snow metamorphism process where snow-grain size increases with time and lowers albedo at all wavelengths while fresh new snow increases albedo (Warren, 1982). Light-absorbing particles (LAPs), such as sand, mineral and volcanic dust/tephra, black carbon, soot, and algae, in the near-surface layers of the snow and ice further lower the albedo, enhancing the energy absorbed by the surface (Warren and Wiscombe, 1980; Box et al., 2012; Painter et al., 2012; Meinander et al., 2014; Peltoniemi et al., 2015; Dagsson-Waldhauserova et al., 2015; Stibal et al., 2017; Skiles et al., 2018; Zubko et al., 2019).

Optical satellite remote sensing offers a way to observe surface albedo continuously at large spatio-temporal scales but is limited to times of clear-sky overpasses. Various studies have shown that surface albedo over snow and ice can be

Published by Copernicus Publications on behalf of the European Geosciences Union.

successfully derived from visible and near-infrared satellite sensors (Stroeve et al., 1997; Reijmer et al., 1999; Stroeve, 2001; Klein and Stroeve, 2002; Liang et al., 2005; Stroeve et al., 2005, 2013). Since October 1978, regular polar coverage has been provided by the National Oceanographic and Atmospheric Administration (NOAA) satellites carrying the advanced very-high-resolution (AVHRR) radiometers (Stroeve et al., 1997; Xiong et al., 2018). The AVHRR sensor has visible, near-infrared, and thermal channels that observe the top-of-the-atmosphere (TOA) radiances under clear-sky conditions, which allows for conversions of narrow-band reflectance measurements to broadband albedo by applying an atmospheric correction and using a radiative transfer model with successful results over snow- and ice-covered surfaces (Lindsay and Rothrock, 1994; de Abreu et al., 1994; Stroeve et al., 1997; Reijmer et al., 1999). Spatial resolution is 4 and 1.1 km depending on the collection mode (global or local), allowing for sufficient representation of surface albedo for larger ice caps or sheets that encompass large areas such as Greenland (Steffen et al., 1993; Zhou et al., 2019) and the main ice caps of Iceland. Higher-spatial-resolution optical data have been obtained from the Landsat constellation (30 m spatial resolution) for albedo retrievals with capabilities to further resolve smaller-scale patterns, more detailed variability of albedo, and sub-pixel variability of large-footprint satellite sensors (Winther, 1993; Reijmer et al., 1999; Gascoin et al., 2017; Naegeli et al., 2017, 2019). Higher-spatial-resolution satellite data generally have the disadvantage of lower temporal resolution, which excludes the possibility of daily albedo observations.

Since February 2000, the Moderate Resolution Imaging Spectroradiometer (MODIS) instrument, on board the NASA Terra satellite, has collected daily multi-spectral radiance data (36 spectral bands) viewing the entire Earth's surface every 1 to 2 d at 500 m spatial resolution. Followed by the NASA Aqua satellite launch in July 2002, also carrying the MODIS sensors, MODIS data have significantly improved understanding of global earth and lower-atmosphere processes and dynamics. Various albedo products for snow- and ice-covered surfaces have been developed and analysed to further understand the inter-annual and seasonal variability of albedo for glaciers and ice sheets (Stroeve et al., 2005; Box et al., 2012; Möller et al., 2014; Gascoin et al., 2017).

Glacier research is important in Iceland for several reasons. Seasonal glacier melt is essential for hydropower production and meltwater storage in reservoirs as the energy system is strongly dependent on glacier and snowmelt, which provides over 72 % of the total average energy produced in Iceland (Hjaltason et al., 2018). The system isolation and high natural climate variability can pose a risk to the reliability of the energy system as drought conditions, low-flow periods, and years with low summer melt are difficult to predict. Volcanic activity in glacier-covered volcanoes can cause volcanic ash and tephra fallout on glaciers during explosive eruptions, leading to enhanced melt or in some cases isolation of the glacier surface, reducing melt significantly (Möller et al., 2014; Wittmann et al., 2017; "oller et al., 2019). For Icelandic glaciers, surface albedo is the dominant factor governing the annual variability of surface melt (De Ruyter De Wildt et al., 2002; Guðmundsson et al., 2009), and the correct representation of surface albedo is critical for glacier melt modelling (Schmidt et al., 2017).

Reijmer et al. (1999) found that the temporal and spatial variations in the surface albedo of the Vatnajökull ice cap were reproduced fairly well by using AVHRR data for the 1996 melt season. To confirm this hypothesis, Reijmer et al. (1999) compared in situ data and higher-spatial-resolution remote sensing data from the Landsat 5 Thematic Mapper sensor. The results showed greater variability in surface albedo, implying that the scale of the albedo variations is larger than the AVHRR pixel (1.1 km) could resolve. De Ruyter De Wildt et al. (2002) assessed Vatnajökull glacier albedo using AVHRR images and found a strong correlation (R^2: 0.87–0.94) between the mean albedo of the entire ice cap through the melting season and observed specific mass balance for the period 1991–1999. In the accumulation area, average albedo was found to decrease from 80 % down to 60 %, with a gradual decrease during the melt season, while in the ablation area, values as low as 10 % ranging up to 35 %, with considerable variation, were found. Gascoin et al. (2017) indicate a good ability of the MODIS MCD43A3 multi-look product to characterize seasonal and inter-annual albedo changes, with correlation coefficients ranging from 0.47 to 0.90, but high RMSE values in comparison with in situ data. Sub-pixel variability was also investigated using Landsat 5 and 7 data similar to Reijmer et al. (1999) with generally better results. Möller et al. (2014) investigated the influence of tephra depositions from the 2004 Grímsvötn eruption in Vatnajökull glacier using the MODIS MCD43A3 multi-look product in combination with daily observations from the MOD10A1 product. By developing an empirically based model to describe the albedo decrease across the glacier surface caused by the deposited tephra, they found that the tephra-induced albedo changes were largest and most widely distributed over the glacier surface during the 2005 summer season, when the observed albedo decrease reached 35 % compared with modelled undisturbed conditions. A study by Wittmann et al. (2017) for the 2012 melt season states that the positive radiative forcing of airborne dust on Brúarjökull can add up to an additional 1.1 m w.e. (water equivalent) of snowmelt (42 %) compared with a hypothetical clean glacier surface. This represents the influence of volcanic eruptions and airborne dust deposits on the mass balance of Icelandic glaciers. In most cases, dust, and tephra will amplify surface melt due to additional radiative forcing during the melt season, but in some cases, ash layers exceeding a certain critical thickness can cause insulation of the underlying snow and ice. Results by Dragosics et al. (2016) showed that this critical thickness

ranged from 9 to 15 mm depending on grain size and material type.

Cloud cover is a major challenge for remote sensing in Iceland; even though data from both Aqua and Terra are used, the number of cloud-covered pixels is still high (Gunnarsson et al., 2019). For albedo derived from the MODIS MCD43A3 product, the strict processing criteria of the multi-look product reduce the number of usable pixels even further than collected by Aqua and Terra. This is especially true at higher elevations for Vatnajökull where persistent cloud cover is frequently observed, resulting in fewer valid albedo pixels during the melt season. Melt increase from dust and ash deposit events is observed to extend the active melt area of the glaciers, i.e. LAP deposit in the accumulation area, increasing melting. Therefore data from these areas are very important for monitoring and forecasting runoff from glaciers in Iceland. Lag times of MCD43A3 (14–16 d) make this less feasible for near-real-time monitoring and operational modelling, for example, in the case of a major dust deposit or volcanic eruption. Additionally, MCD43A3 is not gap-filled, requiring some post-processing prior to monitoring or hydrological modelling efforts.

This study aims to address some of the shortcomings of the MCD43A3 product for glaciers in Iceland and derive an albedo data set suitable for operational use as well as a scientific study of spatial and temporal variations in albedo. The daily M∗D10A1 products were chosen to increase temporal resolution, allowing for more flexibility in post-processing, statistical filtering, and near-real-time data posting. There are two main objectives of the study. The first objective is to create a gap-filled MODIS-based surface-albedo product for glaciers in Iceland for this time period from 2000 to 2019 validated with in situ data suitable for the monitoring and modelling of glaciers in an operational context. Second, the resulting gap-filled product was used to analyse and quantify spatio-temporal patterns of albedo for Icelandic glaciers for the time period, with monthly statistics and a detailed interpretation of the variation in albedo with elevation and trends over time.

2 Data and methods

Figure 1 shows a location map of the Icelandic glaciers referred to in the study. These were glaciers that are at least 2 km^2 or eight unmixed MODIS pixels. For the larger glaciers, Vatnajökull, Langjökull, Hofsjökull, Mýrdalsjökull, and Drangajökull, smaller areas were defined to represent the main ice flow basins of the glaciers for more detailed analysis.

2.1 MODIS products

Daily snow cover data products calculated from the MODIS spectroradiometer on the NASA Terra (MOD10A1 V006) and Aqua (MYD10A1 V006) platforms were obtained from the National Snow and Ice Data Center (NSIDC). The products provide daily estimates of snow cover and blue-sky albedo and a quality assessment at 500 m spatial resolution for cloud-free conditions at the satellite platform overpass (Hall and Riggs, 2016a, b). Daily albedo calculations use reflectances of the first seven visible and near-infrared bands of the MODIS spectroradiometer (459–2155 µm) which have been corrected for atmospheric effects. To correct for anisotropic scattering effects of snow and ice, the DIScrete Ordinates Radiative Transfer (DISORT) model is applied. The daily estimated blue-sky albedo corresponds to the broadband albedo for actual direct and diffusive illumination (Klein and Stroeve, 2002) and is therefore directly comparable to field observations with broadband radiometers (Stroeve et al., 2013). For comparison and validation purposes, the multi-look MCD43A3 albedo product V006 was obtained as well from LP DAAC (Schaaf and Wang, 2015). MCD43A3 provides daily albedo using 16 d of Terra and Aqua MODIS data at 500 m resolution. Data are temporally weighted to the ninth day of the 16 d. The MCD43A3 product provides black-sky albedo (directional hemispherical reflectance) and white-sky albedo (bihemispherical reflectance) data at local solar noon for the same bands as used in M∗D10A1 albedo products.

The quality of remotely sensed albedo retrievals decreases during autumn and winter as the incoming solar irradiance and solar incidence angle decreases. With an increase in solar zenith angles (SZAs) and especially beyond 70°, the accuracy of satellite- and ground-based instruments declines for albedo retrievals. This results in cases where unrealistic and unexpected values are observed and often exceed expected maximum clear-sky snow albedo. Due to polar darkness (SZA > 85°), MODIS data are generally not available from mid-November until mid-January each year over Iceland (Dietz et al., 2012). Cloud cover in Iceland also poses a challenge when using optical remote sensing as average cloud cover ranges from 70 % to 90 % with little inter-annual variability (Gunnarsson et al., 2019).

The scope of this study was limited to the melt season of Icelandic glaciers, when SZAs are low and incoming solar irradiance is high (MJJA). Every granule from MODIS tile h17v02 was used in this project as it covered all the central highlands in Iceland and left out only a small portion of the western Snæfellsnes peninsula and the Westfjords.

2.2 Meteorological in situ data

The Icelandic Glacier Automatic Weather Stations network (ICE-GAWS) has provided automatic weather-station observations from Vatnajökull, Langjökull, Hofsjökull, and Mýrdalsjökull since 1994, 2001, 2016, and 2015, respectively. Most stations in the network were operated during the extended melt season (MJJASO) annually, while a few sites were operated all year round. All sensors were tested and

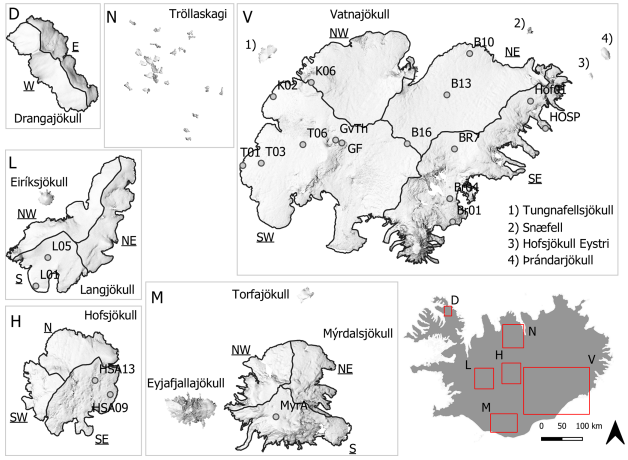

Figure 1. Location map of Icelandic glaciers used in the study. These were glaciers that were at least 2 km^2 or eight unmixed MODIS pixels. For the larger glaciers, Vatnajökull, Langjökull, Hofsjökull, Mýrdalsjökull, and Drangajökull, smaller areas are defined to the main ice flow basins of the glaciers for further analysis. These delineated areas are annotated with underlined text (e.g. NW for northwest). In total, 28 areas are processed, including the sub-areas, but small mountain glaciers in northern Iceland were merged into one processing unit. Available glacier automated weather stations are shown with grey dots. Further details of these stations are given in Table 1. A shaded relief representation of a glacier DEM is from Jóhannesson et al. (2013) and catchment delineation from Magnússon et al. (2016), for Drangajökull, Björnsson (1988) and Björnsson et al. (2000) for Hofsjökull and Mýrdalsjökull, and Pálsson et al. (2015, 2020a) for Langjökull and Vatnajökull.

validated annually before deployment in the field in spring. Locations of the sites are shown in Fig. 1, and location, elevation, observation period, and radiometer instrumentation are shown in Table 1.

Radiation was measured with a net radiometer equipped with two pyranometers facing upward and downward, respectively, used to measure the incident (SW↓) and reflected shortwave radiation (SW↑) as a 10 min average. The ratio of both quantities allowed the bi-hemispherical albedo of the surface to be estimated. For comparison purposes in this study, daily integrated albedo is used instead of selecting the hourly-mean albedo measured closest in time to the satellite overpasses. Daily integrated albedo was calculated as the running 24 h sum of upward shortwave divided by the running 24 h sum of the downward shortwave. This method minimizes the effect of solar zenith angle on the accuracy of the albedo estimation and is less sensitive to radiometer level and cosine response errors since it integrates errors that partly cancel each other (Box et al., 2012). Daily integrated albedo has been shown to represent the daily variability of the glacier surface but only partially represent diurnal variability, such as onset of melt (Stroeve et al., 2005).

Most sites in the GAWS network used Kipp and Zonen CM14, CNR1, and CNR4 radiation sensors which have relatively uniform spectral response ranging from 0.3 to 2.8 µm with uncertainty that has been reported to be 3 to 10 % for daily totals over ice- and snow-covered surfaces (Van den Broeke et al., 2004b, a; Guðmundsson et al., 2009; Kipp and Zonen, 2019). The LI-COR 200 SZ pyranometers were used at a few sites. They have reduced spectral response (0.4 to 1.1 µm) compared with the Kipp and Zonen instruments. Tilting of the instruments with respect to the glacier surface was not monitored and could add to the uncertainty, especially in the ablation zone of the glaciers (Van den Broeke et al., 2004b). The incoming and reflected shortwave measurements from 20 AWSs during the period 2000–2018 were used to validate the MODIS remotely sensed albedo products.

Manual quality control of the data was done by screening shortwave and albedo data and removing obvious errors, periods when stations are buried in snow and calibration periods prior to site instalment in spring. Obvious cases of instrument failure were also rejected. Observations of upward solar irradiance exceeding downward solar irradiance were also removed. Quality control was carried out on the data at

an hourly time step prior to aggregating to daily and monthly time steps. Daily albedo values were calculated from sums of hourly radiation averages if within each day at least 20-hourly values or more were available and monthly averages were calculated from daily values if within each month 24 daily values or more were available.

2.3 Data processing

2.4 MODIS data processing

From the MOD10A1 and MYD10A1 daily data tiles, the *MOD Grid Snow 500 m* grid and the grid variable *Snow Albedo Daily Tile* were used for the albedo analysis. Snow albedo is reported in the range 0–100 where the snow and ice cover mask in the M∗D10A1 product identifies whether a pixel is snow-covered or not. A processing pipeline for MODIS snow-albedo data was partly adopted from Box et al. (2012), with modifications and adoptions for Icelandic glaciers.

Temporal aggregation was applied to the MOD10A1 and MYD10A1 data to reduce the number of unclassified daily pixels due to clouds at the overpass time. The temporal aggregation range was set as the number of days backwards and forwards at each centre date ($t = 0$) to merge to a single stack for further processing. A temporal aggregation range of 5 d backward and forward ($t = \pm 5$ d) was selected; i.e. in total 11 d can contribute data to the temporally aggregated product. A total of 22 values are potentially available for each pixel (i.e. 11 d of MOD10A1 and 11 d of MYD10A1). This reduces by 66 % the number of pixels classified as no data (cloud cover, detector saturation, etc.). Extremely high MODIS albedo values from the original products (MOD10A1 and MYD10A1) ($\alpha > 90\,\%$) are excluded as these are considered unrealistic values under clear skies (Konzelmann and Ohmura, 1995; Box et al., 2012).

Cloud cover is known to be a major challenge in optical remote sensing of the Earth surface, especially for snow- and ice-covered surfaces. Various methods exist to differentiate between clouds and snow- and ice-covered surfaces (Ackerman et al., 1998; Sirguey, 2009), but omission errors are difficult to avoid completely, leading to misclassification of surface albedo and clouds. Manual inspection of the raw MODIS albedo data for Icelandic glaciers revealed misclassified pixels due to various artefacts such as cloud boundaries, cloud shadows, contrails, cirrus clouds, and fog, especially in the glacier terminus area. These artefacts create abrupt changes in the surface-albedo time series, making it possible to reject them based on the temporally aggregated data statistics. On a pixel-by-pixel basis, the method of Box et al. (2012) was applied to reject values exceeding 2 standard deviations from the 11 d temporally aggregated data stack. The method is only applied if 4 or more pixels in the data stack have valid albedo data. To prevent rejection of valid data, values within a certain threshold of the median were not rejected to account for albedo changes. The outlier thresholds were manually adjusted, mostly related to the elevation of the glaciers, ranging from 1 % to 4 %, for higher to lower elevation, respectively. This means that data from the 11 d temporal aggregate were not rejected, even if the difference between the albedo value and the median was greater than 2 standard deviations, if the difference falls within the pixel-defined threshold value. From the 22 potentially available values, the mean is calculated to represent the surface albedo, after median-based statistical rejection of outliers.

An important aspect of M∗D10A1 products is that they only provide albedo of pixels detected as snow covered while MCD43A3 provides albedo over all land masses. This does limit the application of the method presented here during or after an explosive volcanic eruption event with thick tephra depositions. Similarly, tephra plumes discharged into the atmosphere with high tephra concentrations might further induce misclassifications during explosive eruptions. In this study, during periods of volcanic eruptions, the outlier thresholds are not applied, allowing a greater range of expected albedo values, especially lower values at higher elevations where tephra deposits were observed. This applies to the melt seasons 2010 and 2011. Visual inspection of the gap-filled product during these periods was used to validate the performance of MCD11. In most cases, the method presented here was able to reconstruct albedo with acceptable accuracy, as shown in Sect. 3.1.

Figure A3 shows an example for a date after the eruption in Grímsvötn in 2011 (18 June 2020) with the original M∗D10A1 products, MCD43A3 and MCD11 after median-based outlier removal and gap filling. The performance of MCD11 is good while the figure also illustrates the challenge with pixel availability for MCD4A3. The gap-filling method is capable of reconstructing albedo values in areas with thick tephra deposits.

Finally, after temporal aggregation, outlier removal, and statistical filtering, the remaining pixels classified as clouds were classified statistically with four predicting variables, location (easting, northing), elevation (Z), and aspect, with a daily trained random forest model (Matlab, 2017). Topographic and masking data for ice-covered surfaces were obtained from the National Land Survey of Iceland. The original digital elevation model was a raster with a 10 m spatial resolution which is resampled to match the grid of the MODIS pixels using bilinear sampling (GDAL/OGR contributors, 2019). Aspect was then calculated for each pixel. To evaluate the model classification performance, 25 % of the classified data from the temporal aggregation were withheld for comparison purposes. The average RMSE of the classified data was 3.49 %, with a standard deviation of 0.80 %, for the period from May to August. On a monthly basis the lowest RMSE was observed in May (μ: 3.17 %, σ: 0.80 %) and the highest in August (μ: 4.03 %, σ: 0.83 %) while June and July fall in between. For individual years the RMSE values were highest in 2010 (μ: 4.02 %, σ: 1.42 %) and 2011 (μ:

Table 1. Overview of average location, elevation, average operating period, and radiometer instrument of the GAWS network used for validation. All stations have temperature probes while GV (Grímsvötn) and GF (Grímsfjall) only observe temperature and incoming shortwave irradiation. Location and elevation are based on the average location of the site for the observation period, i.e. mean location values for multi-year installations which might not be the exact same location from one year to another.

Site	Glacier outlet	Latitude	Longitude	m a.s.l.	Operation	Radiometer
Kokv	Vatnajökull SW	64.589	−17.860	1096	MJJAS	LiC
BRE	Vatnajökull SE	64.094	−16.325	210	MJJAS	CNR1
B10	Vatnajökull NE	64.728	−16.112	779	All year	CNR1/CNR4
B13	Vatnajökull NE	64.576	−16.328	1216	MJJASO	CM14/CNR4
B16	Vatnajökull NE	64.402	−16.681	1526	MJJASO	CNR1
BRE1	Vatnajökull SE	64.097	−16.329	116	All year	CNR1
BRE4	Vatnajökull SE	64.183	−16.335	529	MJJASO	CNR1
BRE7	Vatnajökull SE	64.369	−16.282	1243	MJJASO	CNR1
T01	Vatnajökull SW	64.326	−18.118	772	All year	CNR4
T03	Vatnajökull SW	64.337	−17.977	1069	MJJASO	CNR1
T06	Vatnajökull SW	64.404	−17.609	1466	MJJASO	CNR1
K06	Vatnajökull SW	64.639	−17.523	1946	MJJASO	CM14
MYRA	Mýrdalsjökull	63.612	−19.158	1346	MJJAS	CM14
HSA09	Hofsjökull SE	64.770	−18.543	840	MJJASO	CNR1
HSA13	Hofsjökull SE	64.814	−18.648	1235	MJJASO	CNR1
L05	Langjökull S	64.595	−20.375	1103	MJJASO	CNR1
SKE02	Vatnajökull SW	64.303	−17.153	1208	MJJASO	CNR1
L01	Langjökull S	64.514	−20.450	589	All year	CNR1
Hof01	Vatnajökull SE	64.539	−15.597	1142	All year	LiC
Hosp	Vatnajökull SE	64.431	−15.478	76	MJJASO	LiC

4.73 %, σ: 1.32 %) for MJJA averages. This was most likely due to the volcanic eruptions in Eyjafjallajökull in 2010 and Grímsvötn in 2011. This resulted in volcanic tephra depositions on Icelandic glaciers that poorly correlate to topographic patterns of albedo as the random forest model was trained on location, elevation, and aspect. The final output, a daily gap-filled albedo grid, which was used for further processing, is hereafter referenced to as MCD11.

For MCD43A3 multi-look data to be comparable with GAWS data, the blue-sky albedo was calculated as the average between the black-sky albedo and the white-sky albedo tiles in the product, assuming a constant fraction of diffuse illumination as done by Möller et al. (2014) and Gascoin et al. (2017) in previous studies of Icelandic glaciers. For cloud cover estimations, daily valid pixels in MOD10A1 (AM overpass) and MYD10A1 (PM overpass) were merged into a single daily product, representing average daily cloud cover.

To quantify the changes in albedo over time, trends were calculated. The calculations are pixel-based from annual MJJA averages for the period 2000–2019. Significance of the estimated trends was calculated using the non-parametric Mann–Kendall test that detects the presence of a monotonic tendency in chronological data and identifies trends in data over time without an assumption of normality (Helsel and Hirsch, 2002). Trends are considered statistically significant when then the p value is lower than 0.05. For this study, glacier boundaries delineated in 2010 and 2012 were used for Vatnajökull, and boundaries in 2007 and 2008 were used for Langjökull and Hofsjökull, respectively. This was selected as a midpoint representing an average glacier area during the period 2000–2019. This needs to be considered when interpreting rapid changes at the glacier terminus, as some areas in 2000 were part of an active glacier but might in 2019 be dead ice or land.

3 Results and discussion

3.1 MODIS albedo validation

Figure 2 shows the comparison results for MJJA for MCD11. Overall good visual and statistical agreement is found between the MODIS MCD11 data and in situ albedo from GAWS observations. For the whole period from May to August, the RMSE is 7.2 % with an R^2 of 0.9. The GAWS observation network captures a wide range of melt season variability of albedo ranging from 6 % to 90 % which is well captured with the MODIS MCD11 product as demonstrated by the overall high correlation coefficients. Based on linear regression (red lines in Fig. 2) for all months, albedo was slightly underestimated for higher values (albedo $>\sim 55$) and slightly overestimated at lower values by the MODIS MCD11 product. Various reasons could contribute to these differences, such as sensor accuracy and instrument installation configuration (i.e. tilting, riming on the sensor dome). In

the ablation zone, where the lowest albedo values were observed, high melt rates (surface lowering of 3–7 m) can contribute to progressive tilting of the instruments over the ablation period. Large sand, dust and tephra-covered areas have been observed in the instrument footprint during field visits, as well as melt channels and small meltwater ponds offsetting the spectral properties of the surface compared with the spectral response of snow and ice, inducing errors in the comparison between in situ and remotely sensed albedo. The temporal aggregation of the remotely sensed data includes a dampening effect on the MCD11 data compared with the GAWS observations, which may partially explain outliers in July and August when the in situ observations are higher than the MCD11. Extensive snowfall events, occurring under cloud cover and limiting accurate data retrievals by the satellites, will lead to albedo that is not correctly represented in the MCD11 reconstruction due to the 11 d temporal aggregation.

Table 2 shows a comparison of MCD11 with other albedo products from MODIS, i.e. MOD10A1, MYD10A1, and MCD43A3. In most cases, the MCD11 product had lower RMSE values and higher correlation coefficients, indicating successful removal of spurious values such as misclassified clouds, image stripes, and other artefacts in the original MODIS products. No correlation was found between RMSE and GAWS location (elevation or glacier/location). No further adjustments or calibrations are applied to the MCD11 product in the rest of this study. Table A1 shows validation results for individual stations for MOD10A1, MYD10A1, MCD43A3, and MCD11.

The comparison presented here is in fact similar to previous work on Icelandic glaciers by Gascoin et al. (2017) where the MCD43A3 was evaluated with RMSE values ranging from 8 % to 21 %, although the results from Gascoin et al. (2017) are based on daily values. Various studies in Greenland using in situ AWS report lower RMSE values, ranging from 2.8 % to 5.4 % on a monthly basis for MOD10A1 using 17 stations for validation by Box et al. (2012) and a total RMSE of 6.7 % in a study by Stroeve et al. (2013) using MCD43A3 high-quality retrievals. It is important to consider how representative point-based in situ observations are (observing $\sim$ 120–180 m^2; Kipp and Zonen, 2019), compared with the spatial footprint of the MODIS data (0.25 km^2), especially in glaciated areas with high spatial albedo variability and MODIS sub-pixel variability as is observed in the bare-ice areas of the Icelandic glaciers.

Sub-pixel variability has been investigated by Reijmer et al. (1999), Pope et al. (2016), and Gascoin et al. (2017) for Icelandic glaciers. The study by Reijmer et al. (1999) using AVHRR and Landsat TM data at Vatnajökull reported large systematic differences for some of the automatic weather stations on the ice, attributed to sub-pixel-scale variations in the albedo. Results implied that the scale of the albedo variations was smaller than the scale of the AVHRR and TM pixels. Pope et al. (2016) studied high-resolution (5 m) airborne multi-spectral data collected over Langjökull in 2007, with comparison to near-contemporaneous Landsat ETM+ and MODIS imagery showing albedo to be highly variable at small spatial scales. Work by Gascoin et al. (2017) suggested that the RMSE of the difference between the in situ automatic weather station data and MODIS data tends to increase when the corresponding Landsat sub-pixel spatial variability is higher. Lower standard deviation values were consistently obtained where the surface was less heterogeneous (accumulation areas).

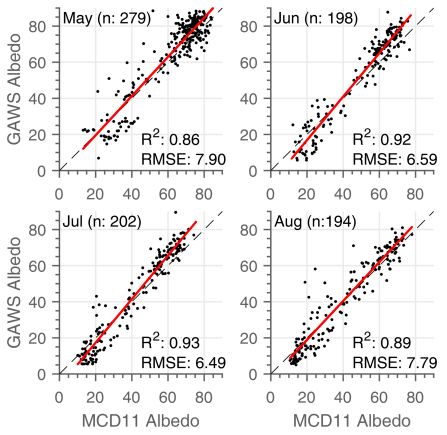

Figure 2. Comparison of monthly-averaged MODIS albedo with in situ GAWS albedo observations for May, June, July, and August for the period 2000–2019 where data were available for the MCD11 data product.

3.2 Gap-filled albedo

Figure 3 shows the average cloud cover for the main Icelandic glaciers from April to September, based on daily MODIS data from Aqua and Terra. This highlights the challenges for optical satellite remote sensing in Iceland due to cloud obscurity problems. The average cloud cover for glaciers was 73.8 % for MJJA and slightly higher for AMJJAS, at 74.4 %. Monthly variability within the melt season was low, with the highest values seen in April, July, and September (78 %, 76 %, and 75 %, respectively) and lower values in May, June, August, and October (73 %, 73.5 %, 72.8 %, and 72.8 %, respectively; individual months are shown in Fig. A1). The highest average cloud cover was observed for Eyjafjallajökull (80.3 %), Drangajökull (79.6 %) and Mýrdalsjökull (77 %) for melt season averages while the other glaciers have lower average cloud cover ranging from 71 % to 74 %.

Table 2. Comparison of MODIS albedo products (MOD10A1, MYD10A1, MCD43A1, and MCD11) with GAWS in situ albedo on a monthly timescale.

	MOD10A1		MYD10A1		MCD43A3		MCD11	
Month	RMSE	R^2	RMSE	R^2	RMSE	R^2	RMSE	R^2
May	8.66	0.82	8.34	0.84	8.28	0.84	7.9	0.86
June	7.07	0.91	7.20	0.91	7.49	0.91	6.59	0.92
July	7.08	0.92	6.30	0.93	7.09	0.91	6.49	0.93
August	8.24	0.88	7.52	0.90	11.0	0.75	7.79	0.89

A figure showing a similar pattern as Fig. 3 was presented by Gascoin et al. (2017). Figure A1 additionally shows average monthly cloud cover from May to September depicting how the cloudiness pattern varies within the melt season, indicating how cloud cover affects incoming short-wave radiation. The figure in Gascoin et al. (2017) also shows the mean annual number of days with missing data during the period 2001–2012 based on data available within a 16 d period in the MCD43A3 product. Their figure also highlights the data availability limitation of the MCD43A3 product, especially for Vatnajökull as previous discussed.

The average daily cloud cover in MOD10A1 data was 79 % and slightly lower for MYD10A1, at 78 %, based on data from April to October each year for the period 2000–2019. By joining these two products on a daily basis, cloud-obscured pixels were reduced to 74 %. Temporal aggregation (11 d) of the products had an exponential decaying shape of unclassified pixel reduction, with the highest benefit for aggregating 1 d. For this study, data were aggregated 5 d forward and backward, allowing 11 d of both Aqua and Terra MODIS albedo data to contribute to a daily average. This resulted in an average unclassified pixel reduction down to 12 %.

The main advantage of the temporal aggregation of the data was the reduction of cloud-obscured pixels, which provides a more spatially continuous product in a simple and computationally efficient way. This comes with the primary disadvantages of response dampening of rapid changes, experienced as a smoothing effect on the albedo time series. This could pose a limitation on daily near-real-time flow forecasting, while for weekly to monthly time scale applications, the product should be representative. Cloud detection in the MODIS products is based on the M∗D35−L2 cloud mask providing four categories for discrimination of clouds, i.e. cloudy, uncertain, probably clear, and confidently clear. Cloud and snow confusion is known to be present in MODIS data for many reasons, such as cold clouds with ice content, very similar spectral responses to snow of some cloud types, and cirrus clouds that are not detected (Sirguey et al., 2009; Box et al., 2012). The approach in this study to reduce cloud artefacts is based on robust statistics with a median-based outlier removal. The drawback of this approach is that with a too strict criterion for rejection, valid data could be rejected, with loss of good quality data, especially in cases where surface albedo changes rapidly.

3.3 Annual and inter-annual variability of albedo

Inter-annual albedo variations for Icelandic glaciers were generally high. Figure 4 shows spatial patterns for melt season mean albedo for the investigated glaciers for the period 2000–2019 (MJJA). The lowest albedo values (< 35 %) were found in bare-ice areas where the winter snow cover is generally completely ablated during summer, revealing dirty and impurity-rich bare ice. Higher albedo values (> 45 %–50 %) were found in the accumulation areas associated with higher elevations and a shorter period of positive surface-energy balance during the melt season.

Figure 5 shows the average albedo distribution and relations to elevation in 100 m bands for the six largest ice caps and their sub-areas defined in Fig. 1. Above 1500 m a.s.l. at Vatnajökull there was limited regional variability while more distinctive patterns were seen between the northern and southern parts, especially in the southeast at lower elevations. In the southeast, the elevation of the glacier ranges all the way down to sea level while the glacier terminus was at a much higher elevation in the north (600–700 m a.s.l.). The average albedo–elevation relationship for Vatnajökull exhibits three elevation gradients. For elevations below 700 m a.s.l. the linear albedo gradient was ∼ 2.3 %/100 m, ∼ 5.1 %/100 m between 700–1300, and ∼ 0.5 %/100 m for elevations above 1300 m. For Hofsjökull, the albedo was generally lower in the southeast than in the northern and southwestern parts; the average albedo elevation gradient below 1400 m a.s.l. was 4 %/100 m and 1.5 %/100 m above 1400 m a.s.l. For Langjökull, the south and northeast areas had overall lower average albedo values compared with the northwestern part of the glacier. At Langjökull, the albedo elevation gradient was 3.5 %/100 m for the whole elevation range, which was similar to elevations below 1400 m a.s.l. at Hofsjökull, but note the start of a change towards a lower gradient at the higher elevations. The northwest part of Mýrdalsjökull had generally higher albedo compared to the southern part. The albedo gradient is 3 %/100 m for the whole elevation range. Distinctive patterns were observed for the east and south parts of Drangajökull, with lower average values

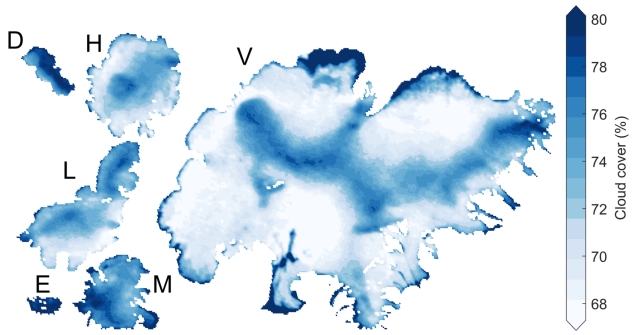

Figure 3. Average cloud cover for the main Icelandic ice caps for the extended melt season from May to September each year from 2000–2019 (average: 73.8 %).

for the south region. A very strong east–south cloud cover gradient also observed at Drangajökull (Fig. 3) could explain these differences, indicating that less SW↓ reaches the surface, accelerating the snow metamorphism and resulting in lower albedo. The average albedo elevation gradient was 3.0 %/100 m for Drangajökull and 2.7 %/100 m for Eyjafjallajökull. In general for Eyjafjallajökull, the southern parts of the main ice caps had a lower albedo. This was most likely controlled or strongly influenced by orographic generation of precipitation in the dominating SW–SE wind, providing more energy from rain and warmer temperatures at the surface, accelerating the snow metamorphism (Einarsson, 1984; Crochet et al., 2007; Björnsson et al., 2018). Local lower albedo gradients at Hofsjökull (SE), Langjökull (S), and Mýrdalsjökull (S) coincide with documented locations of severe or extremely severe dust source areas described in Arnalds et al. (2016).

Figure 6 shows the average distribution of albedo as a function of elevation bands (100 m intervals) and time for the period 2000–2019. The annual maximum albedo value for all elevation bands was generally observed in early April, associated with the last major winter snowfall. The lowest average albedo values were observed from mid-July to mid-August. For higher elevations (accumulation areas), the minimum values were associated with the first snowfall which increases albedo. For bare-ice areas with impurity-rich ice, these impurities can be washed away from the glacier surface by rain which leads to higher albedo without fresh snow, i.e. cleaner ice, with fewer impurities, in late summer.

Figure 7 shows average melt season mean albedo for the glaciers and sub-areas defined in Fig. 1. Glaciers were sorted from the highest to the lowest melt season mean albedo for the whole analysis period (highest at the top of the figure), revealing certain spatial, temporal, and feature position patterns. The lowest albedo values were observed for Mýrdalsjökull, Eyjafjallajökull, and Torfajökull, which cluster together at the south coast of Iceland (Fig. 1, box M). They were also all close to widespread unstable sandy surfaces subject to frequent high-velocity winds, driving numerous wind erosion events and dust production. These unstable erosive surfaces do not sustain seasonal snow cover far into the spring and summer, making them accessible for erosion earlier in the spring than similar areas in the north and east highlands close to Langjökull, Hofsjökull, and Vatnajökull. Dagsson-Waldhauserova et al. (2014, 2015, 2019) have also shown that dust events can occur frequently in southern parts of Iceland during winter given the right surface and meteorological conditions for dust transport. The Mýrdalsjökull, Eyjafjallajökull, and Torfajökull glaciers are also relatively small, indicating that dust-producing events can influence larger areas of the glaciers with dust deposits. Slightly higher annual average albedo was seen for small alpine and valley glaciers with smaller elevation range and surface area compared with the large ice caps.

The main ice caps in Iceland, Vatnajökull, Hofsjökull, and Langjökull, had relatively high average albedo compared with the other glaciers, with the exception of the northwestern part of Langjökull which was close to the Flosaskarð area known for extremely severe erosion (Arnalds et al., 2016). Drangajökull had the highest observed albedo; its location is far from unstable surfaces that produce airborne dust, and volcanic eruptions (2010, 2011) seem to have a minimal effect compared with other Icelandic glaciers. Albedo development at Drangajökull is likely mostly driven by snow metamorphism where snow grain size increases with time and energy input, resulting in lowering of albedo.

On the temporal scale, various events influencing the melt season mean albedo are observed in Fig. 7. For the south coast glaciers (Fig. 1, box M), the influence of the 2010 volcanic eruption in Eyjafjallajökull and the post-eruption influ-

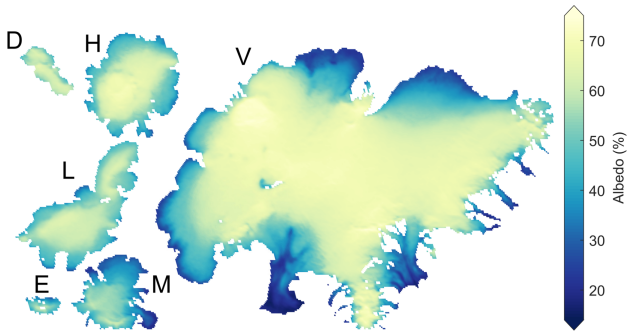

Figure 4. Spatial patterns of mean albedo for the period 2000–2019 (MJJA). D: Drangajökull; H: Hofsjökull; V: Vatnajökull; L: Langjökull; E: Eyjafjallajökull; M: Mýrdalsjökull.

ence in 2011 and 2012 were obvious, and there were also influences on other Icelandic glaciers, with the possible exception of Drangajökull, Hofsjökull Eystri, Snæfell, and Norðurlandsjöklar in the north. The influence on albedo due to the 2011 volcanic eruption in Grímsvötn was seen in south-west Vatnajökull isolating the glacier surface, constricting surface melt in about 420 km^2. Generally albedo was lower for most glaciers in that year, excluding Drangajökull. In 2015, a cold spring and summer, with prolonged snow cover in the highlands, delayed the onset of melt, as well as limiting the capabilities for airborne dust and tephra to be transported to the glacier surface. The highest melt season mean albedo observed during the study period was in 2015 for all glaciers, while the lowest albedo was seen in 2010. The 2019 melt season was furthermore seen to be quite unique. Due to an early winter snow cover melt in the highlands in late April, the earliest and most extensive snow cover depletion for 20 years (MODIS period) (Gunnarsson et al., 2019), followed by a prolonged period with limited precipitation, great amounts of dust and sand from unstable sandy surfaces were transported to the glaciers, providing LAPs that further enhance surface melt. Although similar singular events had been observed historically during the MODIS period, this development was observed at all Icelandic glaciers. Note must be taken when melt season average values are interpreted that they are influenced by the areal elevation distribution of each glacier or sub-area.

Seasonal variability of albedo for Icelandic glaciers was generally high. Figure 8 shows glacier average seasonal albedo distribution for 2000–2019 plotted together with selected years for Vatnajökull, Hofsjökull, Langjökull, Mýrdalsjökull, Eyjafjallajökull, and Drangajökull. The average albedo generally declines from the maximum observed in the first 2 weeks of April each year (70 %–80 %) to an annual minimum in August. The average minimum observed value is 40 %–45 % for Vatnajökull, Hofsjökull, Langjökull, and Drangajökull but reaches lower values at Mýrdalsjökull and Eyjafjallajökull (<30 %). Glacier runoff generally peaks in late June and July (midsummer) (Schmidt et al., 2018), with low albedo and maximum incoming shortwave irradiance near the summer solstice. The variability similarly gradually increased in June, July, and August and was generally highest in August. In the autumn, seasonal weather patterns in Iceland shift with lowering temperatures and an increase in precipitation following shorter days due to a gradual increase in solar zenith angles (Einarsson, 1984; Hanna et al., 2004; Björnsson et al., 2007, 2018). Frequently in the latter half of August and beginning of September, the first snowfall is observed to increase albedo with fresh highly reflective snow. It was not uncommon to see the albedo lower again after the first snowfall due to liquid precipitation or other events that melt the fresh snow cover over the bare glacier ice. This affects the variation in albedo in August and September.

Figure 8 also shows how albedo develops through the melt season for selected abnormal years. The influence of explosive volcanic eruptions in Grímsvötn in Vatnajökull is shown in 2005 (the eruption took place in November 2004) and 2011 and the Eyjafjallajökull eruption in 2010. These events generally influence the albedo of Icelandic glaciers as tephra is discharged into the atmosphere and transported by wind over wide areas. In 2015, seasonal mass balance programmes for Vatnajökull, Langjökull, and Hofsjökull reported unusually thick winter snow cover followed by a cold and cloudy spring and summer which resulted in a positive net surface mass balance, for the first time in 20 years (Pálsson et al., 2020a, b; Þorsteinsson et al., 2017). Figure 8 shows the development of albedo in 2015 to the highest average values for the study period.

Figure 9 shows the spatial distribution of seasonal average albedo as anomalies from the mean. Blue colours rep-

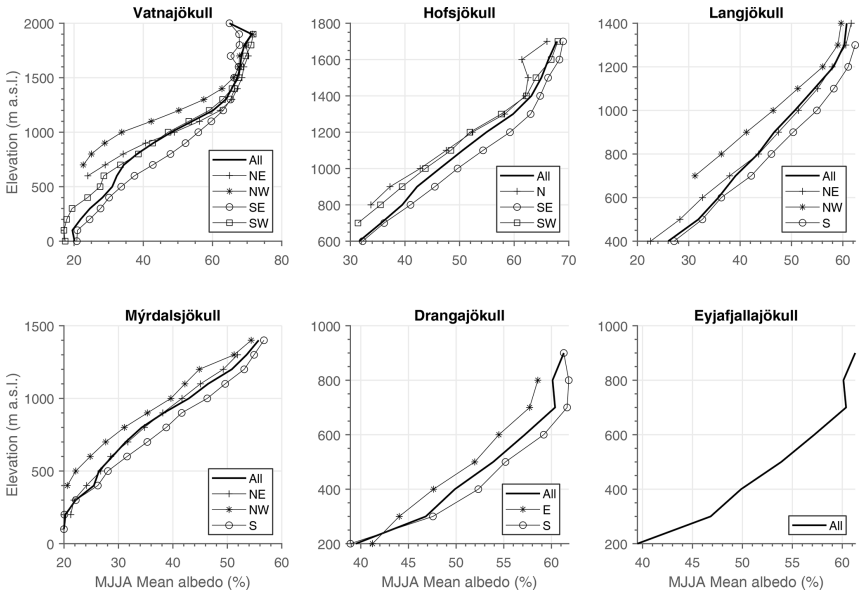

Figure 5. Average albedo for the period as a function of elevation for the period 2000–2019. Data are shown for the six largest ice caps for the whole glaciers (All) as well as for the sub-areas defined in Fig. 1. Note the elevation range varies between figure axes (*y* axis).

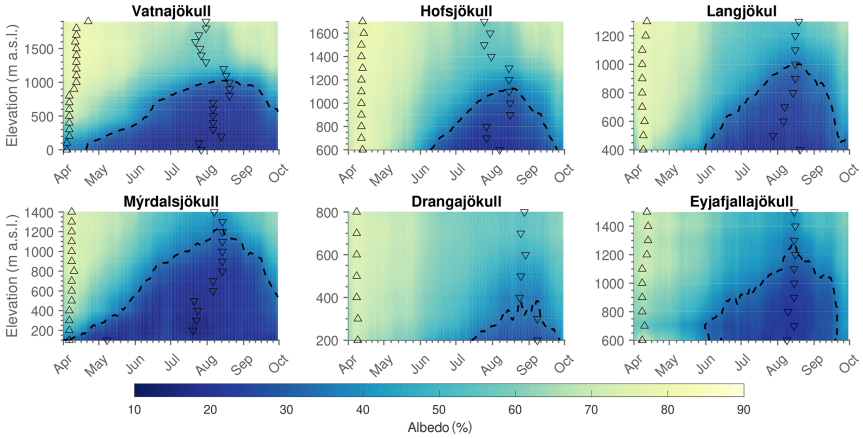

Figure 6. Albedo as a function of elevation and time for the period 2000–2019. Triangles show the max–min values associated with each elevation band, and the dotted black line shows the isoline for 34 % albedo, as defined by Cuffey and Paterson (2010) for bare glacier ice.

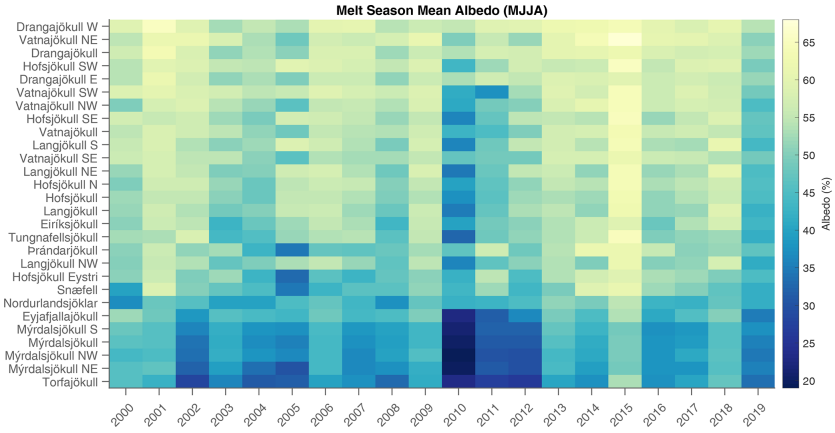

Figure 7. Average melt season albedo for the studied glaciers. The glaciers are sorted from the lowest 2000–2019 melt season average albedo to the highest. For the larger glaciers, data are provided for individual ice flow basins; see Fig. 1.

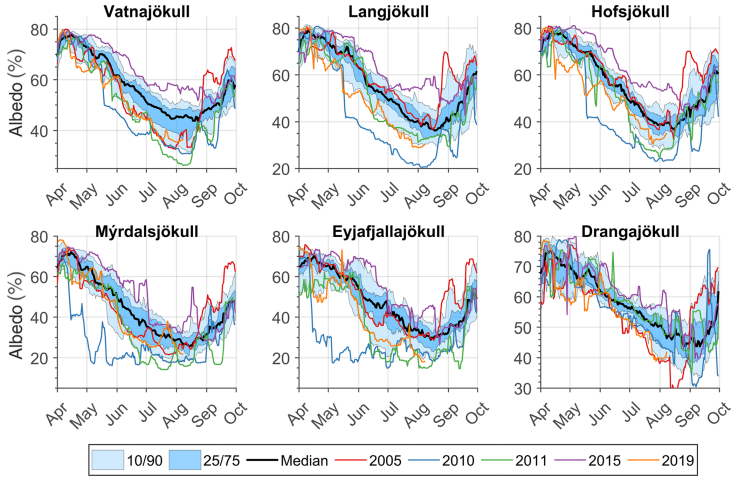

Figure 8. Seasonal variations in average albedo for selected Icelandic glaciers from the MCD11 product for April to October 2000–2019.

resent anomalies above the mean, i.e. higher albedo values, while red areas represent values below the mean. Decisive negative patterns were observed in 2010 and 2011. These are related to the volcanic eruptions in Eyjafjallajökull (2010) and Grímsvötn (2011) as tephra dispersal from explosive eruptions produces high volumes of airborne tephra (Gudmundsson et al., 1997; Guðmundsson et al., 2012; Tesche et al., 2012). Airborne tephra and dust can be transported by high plumes that can extend several kilometres into the atmosphere and be transported great distances, up to several hundred kilometres (Guðmundsson et al., 2012; Watson et al., 2016; Đorđević et al., 2019; Dagsson-Waldhauserova et al.,

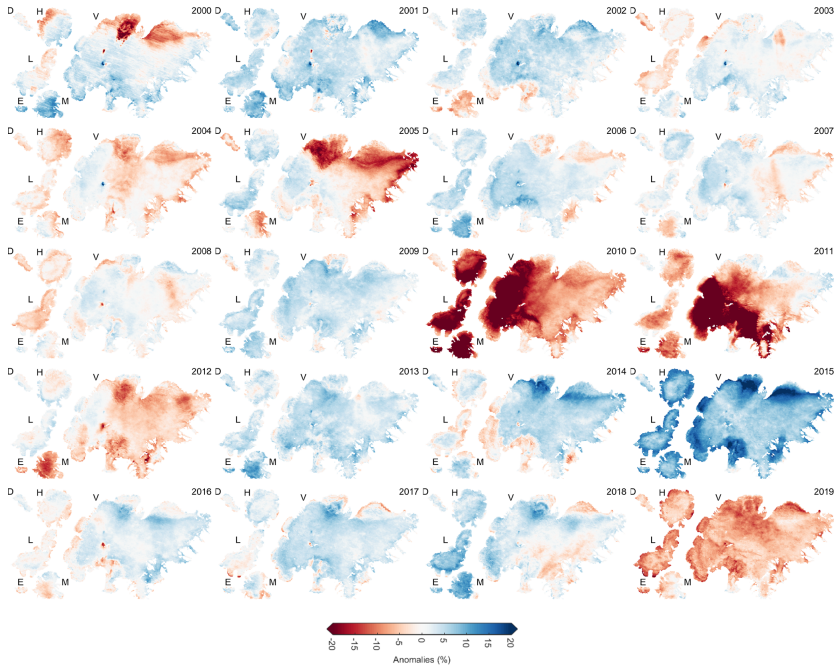

Figure 9. Annual spatial patterns for melt season (MJJA) albedo anomalies for 2000–2019.

2019). Tephra dispersal and fallout patterns from explosive eruptions depend on many factors, including plume height, particle size distribution, and wind direction and velocity. No eruption occurred in 2012, but residual effects were observed as ash deposits from previous eruptions were carried with the prevailing wind directions and high dust storm activity reported in the area, enhancing melt due to the lowering of albedo ("oller et al., 2019; Butwin et al., 2019). These effects were most clear for Eyjafjallajökull and Mýrdalsjökull but also contribute to negative anomalies for Vatnajökull. The impact of dust deposition on albedo in 2012 for Vatnajökull was investigated by Wittmann et al. (2017) using dust-mobilization models to calculate dust emission and a dispersion model to simulate atmospheric dust dispersion and deposition on the glacier surface. The main conclusion was that the influence of dust on albedo could lead to an increase in melt of up to 40 %, which confirms the influence of these events on seasonal glacier melt.

Another influencing factor for negative albedo anomalies was dust, sand, and other LAPs transported from the proglacial areas and sandy deserts which cover more than 22 % of Iceland (Arnalds et al., 2016; Wittmann et al., 2017). Plume-shaped patterns could be identified in particular for the northern part of Vatnajökull, indicating airborne LAP deposits on the glacier surface. For example, in 2001, 2003, 2007, 2008, and 2013, such patterns were observed in the northern part of Vatnajökull (Brúarjökull glacier outlet) extending from the Kverkfjöll mountain range high in the accumulation area as local negative albedo anomalies. These were unlikely to be linked to local climatology, resulting in such distinctive anomalies, as such events or dominating patterns would influence larger areas. In 2014–2015, the lava flow field of the Holuhraun non-explosive eruption covered about 84 km^2 of volcaniclastic sandy desert and proglacial areas north of Vatnajökull. Since then, similar plume-shaped albedo anomalies have not been observed in the data. It is probable that the extent of the lava flow field reduces the dust production of this area significantly, although this cannot be quantified at this point in time; more data over a range of climatologies are needed to fully understand the impact of the

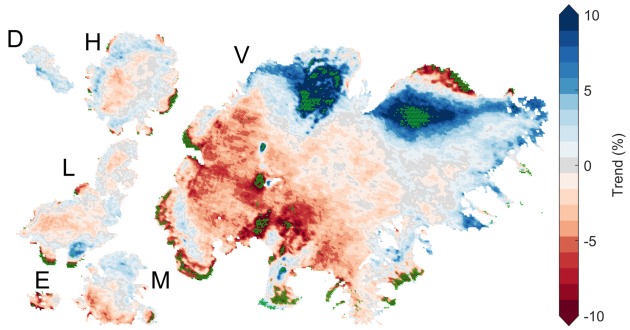

Figure 10. Spatial patterns for albedo trends during the melt season (MJJA) for the period 2000–2019 in terms of the total change of a least-square fit to the albedo over the period. Green stipples indicate areas where significant changes were found.

Holuhraun eruption on dust production. Figure 9 also shows an interesting anomaly pattern for 2019. All the major ice caps had largely negative anomalies driven by dust and mineral deposits with an early onset in the spring. The events leading up to these anomalies have already been discussed above. In 2000, large negative anomalies were seen in Dyngjujökull and Brúarjökull (northern Vatnajökull). These are unlikely to be linked to the 2000 Hekla eruption and are presumed to be a combination of residual effects from the Gjálp eruption in 1996 and dust transported from the proglacial areas near the glacier terminus. Landsat images from summer 2000 show the tephra-covered surroundings of Gjálp to be a possible dust source in combination with proglacial areas.

3.4 Trends of albedo

Figure 10 shows the spatial pattern of melt season (MJJA) trends in terms of the total change of a least-square fit to the albedo during 2000–2019. For Vatnajökull, negative albedo melt season trends were found in the lowest areas of the glacier with the exception of the northwestern part (Dyngjujökull). Negative trends at the terminus of glaciers were expected due to glacier retreat in recent decades, with associated debris deposits on dead ice (Einarsson, 2018; Hannesdóttir et al., 2020). In general, negative trends extend farther into the accumulation area in the southwest while a growing positive trend was observed in the upper part of the ablation area in the northern part with the exception of the terminus area of Brúarjökull. Positive trends in the upper part of the ablation area in the northern part (Brúarjökull and Dyngjujökull) of the ice cap are significant over most of the area. Positive melt season trends were also seen near the equilibrium line elevation at Hofsjökull, for most of Drangajökull, in the northern part of Mýrdalsjökull and distributed parts of Langjökull, suggesting a trend towards either increased snowfall or decreased snowmelt at these glacier outlets. As a melt season average trend (Fig. 10) these positive trends are only significant in the ablation area in the northern part of Vatnajökull. Negative trends were identified at many glacier termini due to the steady glacier retreat in recent decades, with reduction in the duration of snow cover over low-albedo bare ice, while for the accumulation area in southwest Vatnajökull the trend is strongly controlled by volcanic ash fallout in 2010 and 2011.

Figure 11 shows average monthly-mean albedo for the main ice caps for the study period, the associated linear trends, and the average linear slope of the trend. For all the glaciers with the exception of Drangajökull in June, the average linear slope for May and June was negative, i.e. lower average albedo earlier in the spring. For Vatnajökull, Hofsjökull, and Langjökull, the trend was strongly influenced by low May and June albedo in 2017 and 2019. These trends indicate that more incoming shortwave energy is absorbed at the surface during these months with lower albedo. In July and August, the trend was in general positive, trending towards higher mean albedo. The trends in July and August were only statistically significant for Drangajökull and in July for Hofsjökull. Positive trends could indicate more extensive or earlier snowfall in July and August, with fresh highly reflecting snow. Extensive dust transport to the glacier surface, as seen in the 2019 melt season, had a similar overall albedo-lowering effect to that in the eruption years 2010 and 2011 for Vatnajökull, Langjökull, Eyjafjallajökull, and Drangajökull specifically. It is, however, noted that following volcanic eruptions albedo lowering is generally more localized while extensive dust transport tends to affect larger areas.

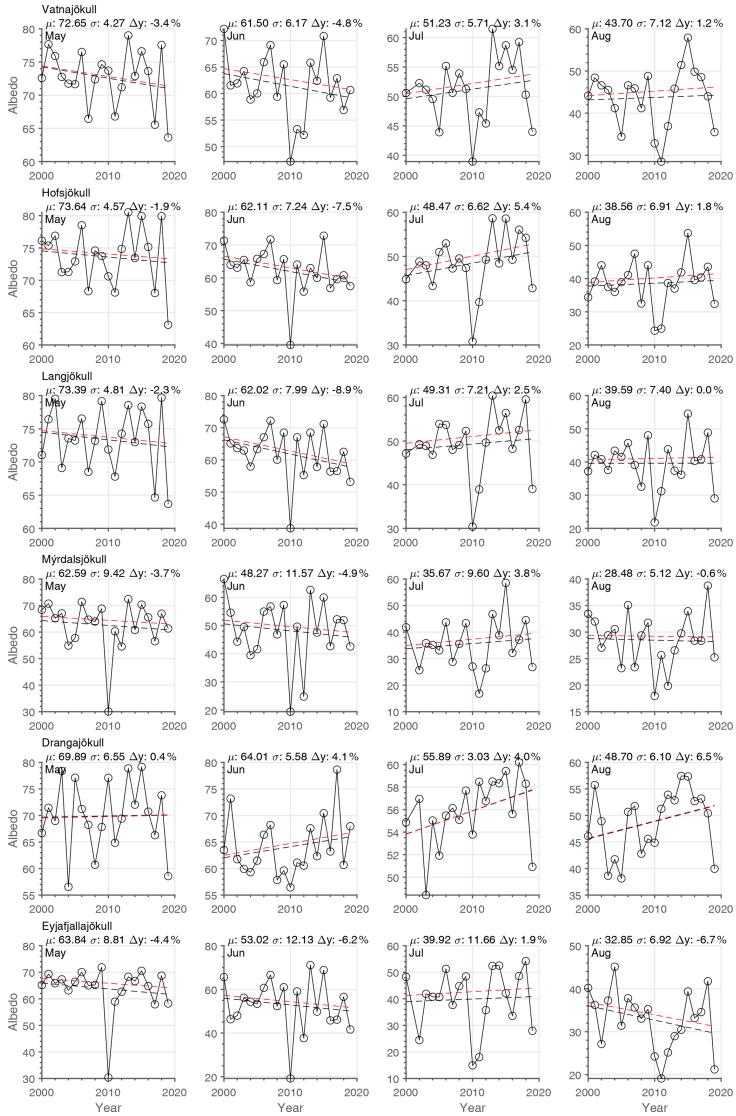

Figure 11. Average monthly mean albedo for the main ice caps in Fig. 8. The mean, standard deviation, and trend (Δy) are shown. Linear trend determined from all years is shown with black lines while red lines exclude the 2010 and 2011 data to omit the influence of volcanic tephra and ash.

4 Conclusions

In this study, a gap-filled satellite-observed albedo data set for Icelandic glaciers (MCD11) was produced from daily MODIS Aqua and Terra observations from early 2000 until 2019 at a 500 m spatial resolution. Overall, good visual and statistical agreement was found between the MCD11 data and in situ albedo from GAWS observations over a range of elevations and glacier locations. Overall, higher RMSE values were found in the ablation zone, which could be related to higher albedo variability within a MODIS pixel for impurity-rich bare ice in the ablation zone, indicating that care must be taken when comparing point-based in situ observations with data with a larger spatial footprint.

The main results show that the large seasonal and inter-annual variability in surface albedo for Icelandic glaciers was captured by the MCD11 data, although limited in situ data were available for the smaller glaciers. Icelandic glacier albedo was observed to be influenced by variability in climate, tephra deposits from volcanic eruptions, and airborne dust from widespread unstable sandy surfaces which are subject to frequent wind erosion and dust production. Details are provided regarding spatial patterns and temporal trends, relations to elevation, and monthly statistics adding to previous work by Gascoin et al. (2017) for 2000 to 2012.

The good visual and statistical agreement that was found between the MCD11 data and in situ albedo from GAWS observations indicates that the gap-filling method applied in this study is able to provide good quality daily albedo estimates both spatially and temporally. This illustrates the main strength of the spatio-temporal MCD11 data set, which is obtained without sacrificing quality compared with other data sources.

Significant positive albedo trends over the study period were found in northern Vatnajökull while other areas and glaciers have a glacier-wide non-significant trend. Average linear trends for monthly data indicate that albedo generally decreased over the study period in May and June whereas a general albedo increase was observed in July and August, although, statistically non-significant in all cases with the exception of Hofsjökull in July and Drangajökull in July and August.

The incorporation of the MCD11 albedo product provides capabilities to improve surface mass balance and runoff forecasting from glaciers. In the case of future volcanic eruptions, the presented methodology allows for rapid assessment of glacier albedo changes in near-real time and the associated influence on melt, which has a direct impact on hydropower production in Iceland and possibly civil infrastructure in some cases. A limitation related to estimating the impact of tephra fallout on a glacier surface from optical data is the assessment of tephra thickness, as very low observed albedo could indicate melt increase due to more surface energy absorbed by the surface but could also indicate an isolating layer limiting melt due to a thick tephra layer.

The methodology allows for predictive and retrospective modes (Dozier et al., 2008), depending on the application. To use the albedo data for runoff forecasting for example, surface albedo estimations using only data until the present (newest MODIS data) can be provided by applying the statistical filtering and gap-filling routines from today and backwards. Alternatively, in retrospective mode, the best estimations can be provided for every day in a period.

Finally, it is noted that the methodology applied in the study, based on MODIS data, can be applied to other satellite albedo products, such as VIIRS and Sentinel-3 as well as future missions, to extend the temporal range beyond the MODIS mission, allowing for short-term as well as long-term monitoring of albedo variations for glaciers in Iceland.

Appendix A

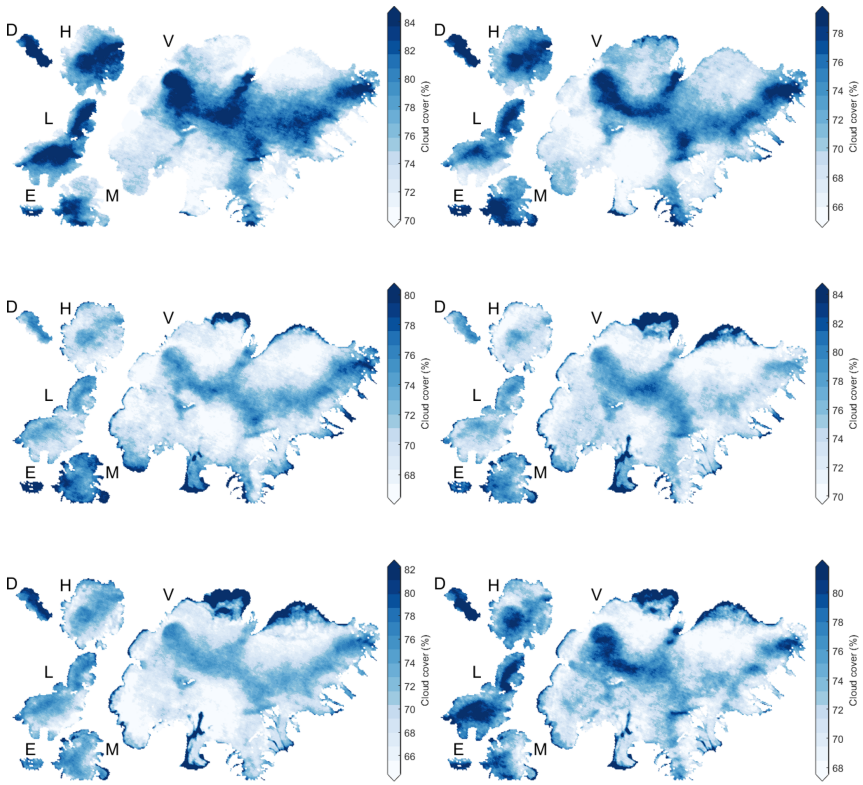

Figure A1. Monthly average cloud cover for selected glaciers in Iceland in April (top left), May (top right), June (middle left), July (middle right), August (bottom left), and September (bottom right).

Table A1. RMSE, R^2 values, and number of months of overlapping data (n) for individual station comparison on a monthly time scale for MOD10A1, MYD10A1, MCD43A, and MCD11.

	MOD10A1			MYD10A1			MCD43A3			MCD11		
Station	RMSE	R^2	n	RMSE	R^2	n	RMSE	R^2	n	RMSE	R^2	n
Kokv	9.78	0.74	5	0	–	0	9.25	0.77	5	9.42	0.77	6
BRE	10.02	0.31	101	9.84	0.37	93	10.95	0.31	80	10.54	0.40	109
B10	10.67	0.21	102	11.30	0.17	93	11.56	0.12	84	11.69	0.26	109
B13	13.24	0.37	107	11.59	0.48	93	9.83	0.61	76	13.69	0.36	108
B16	8.02	0.39	102	5.14	0.62	94	5.46	0.59	26	10.63	0.13	105
BRE1	9.16	0.42	102	9.39	0.43	93	10.49	0.34	97	9.90	0.47	109
BRE4	7.68	0.85	33	9.87	0.76	34	10.90	0.75	34	8.50	0.85	36
BRE7	7.58	0.20	17	6.63	0.39	17	7.23	0.23	11	6.16	0.47	17
T01	16.76	0.45	18	13.92	0.59	12	12.60	0.76	20	9.53	0.86	20
T03	11.84	0.67	99	10.54	0.73	86	13.55	0.59	98	12.67	0.64	102
T06	10.27	0.53	98	14.69	0.26	87	7.11	0.73	69	13.91	0.26	100
L01	12.41	0.73	95	13.26	0.69	87	10.24	0.84	99	11.43	0.80	103
L05	8.35	0.71	100	8.58	0.69	92	7.93	0.75	106	9.83	0.65	114
K06	18.06	0.003	35	17.85	0.02	35	21.57	0.03	11	19.37	0.08	36
MYRA	9.08	0.55	20	9.56	0.51	20	18.68	0.02	16	18.53	0.019	21
HSA09	5.75	0.93	11	9.27	0.83	11	5.67	0.94	12	5.18	0.96	13
HSA13	5.81	0.74	11	4.05	0.87	11	5.59	0.78	11	5.47	0.79	13
SKE02	6.00	0.0004	3	0.25	0.99	3	2.07	0.90	3	0.12	0.99	3
Hof01	14.99	0.14	63	15.31	0.12	61	5.21	0.82	24	19.18	0.2	66
Hosp	10.56	0.27	53	10.59	0.26	53	10.96	0.27	56	11.39	0.22	58

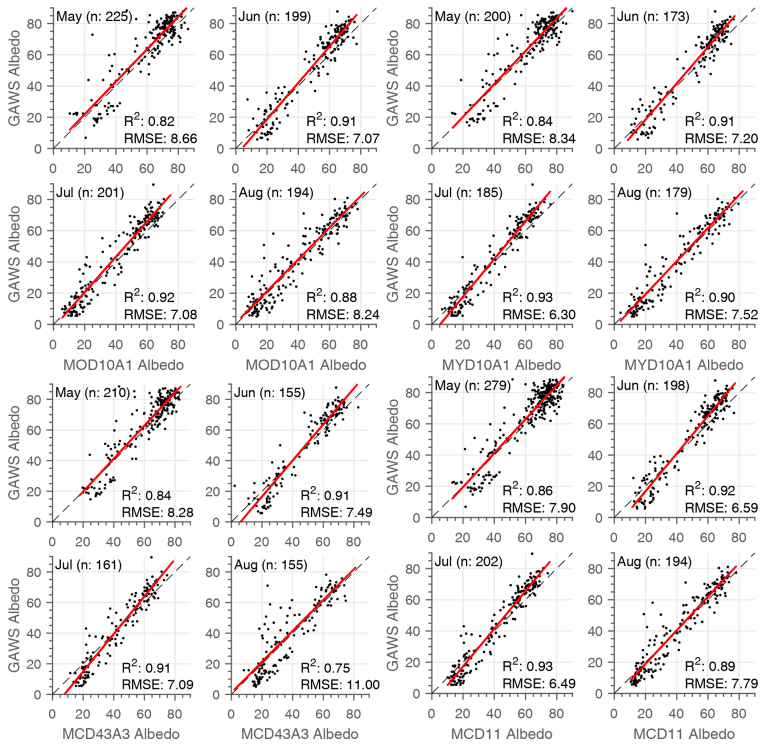

Figure A2. Albedo comparison results from monthly averaged MODIS data for May, June, July, and August for the period from 2000–2019 where data were available for MOD10A1, MYD10A1, MCD43, and MCD11 data products.

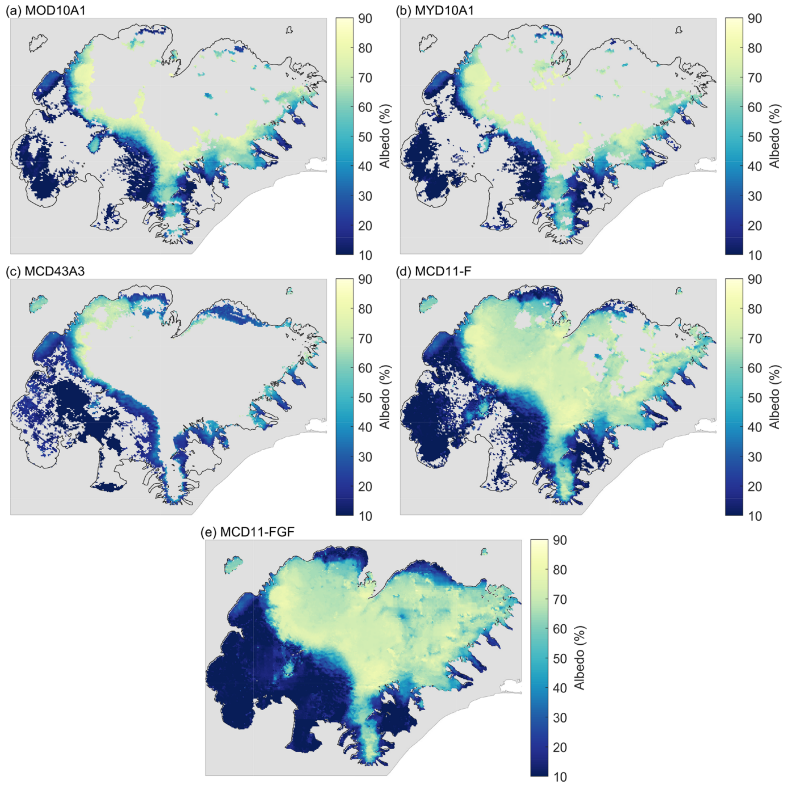

Figure A3. Albedo maps for different processing and products post-eruption at Grímsvötn. Data are shown for 18 June 2011. Panels **(a)** and **(b)** show the original albedo tiles (*Snow Albedo Daily Tile*) for the original MODIS products (M∗D10A1). Panel **(c)** shows albedo data for MCD43A3 (Albedo BSA shortwave). Panel **(d)** shows the MCD11 product (MCD11-F) after median-based outlier removal, and **(e)** shows the final MCD11 (MCD11-FGF) product after median-based outlier removal and gap filling as described in Sect. 2.

Code and data availability. Code used in the project to process data is available at https://github.com/andrigunn/aig2 (last access: 30 December 2019) and https://doi.org/10.5281/zenodo.4445245 (Gunnarsson, 2021). MODIS data are available from https://nsidc.org/data (Hall and Riggs, 2016a, b). Geospatial data for Iceland are available from the National Land Survey of Iceland at https://atlas.lmi.is (NLSI, 2019). Glacier automatic weather station data are available upon request.

Author contributions. AG conceived and designed the study, performed the analyses, and prepared the manuscript. SMG contributed to the study design, interpretation of the results, and writing of the manuscript. FP, TJ, and ÓGBS contributed to the interpretation of the results and writing and reviewing of the manuscript.

Competing interests. The authors declare that they have no conflict of interest.

Acknowledgements. The authors would like to thank the editor Marie Dumont, and two reviewers, Simon Gascoin and Pavla Dagsson-Waldhauserova, for their review, and comments, improving the manuscript.

Review statement. This paper was edited by Marie Dumont and reviewed by Simon Gascoin and Pavla Dagsson Waldhauserova.

References

Ackerman, S. A., Strabala, K. I., Menzel, W. P., Frey, R. A., Moeller, C. C., and Gumley, L. E.: Discriminating clear sky from clouds with MODIS, J. Geophys. Res.-Atmos., 103, 32141–32157, https://doi.org/10.1029/1998JD200032, 1998.

Arnalds, O., Dagsson-Waldhauserova, P., and Ólafsson, H.: The Icelandic volcanic aeolian environment: Processes and impacts – A review, Aeolian Res., 20, 176–195, https://doi.org/10.1016/j.aeolia.2016.01.004, 2016.

Björnsson, H.: Hydrology of ice caps in volcanic regions, Reykjavik Societas Scientarium Islandica, University of Iceland, Polar Record, 26, 132–132, https://doi.org/10.1017/S0032247400011293, 1988.

Björnsson, H., Pálsson, F., and Guðmundsson, M. T.: Surface and bedrock topography of the Mýrdalsjökull ice cap, Iceland: The Katla caldera, eruption sites and routes of jökulhlaups, Jökull, 49, 29–46, 2000.

Björnsson, H., Jónsson, T., Gylfadóttir, S. S., and Ólason, E. Ö.: Mapping the annual cycle of temperature in Iceland, Meteorol. Z., 16, 45–56, https://doi.org/10.1127/0941-2948/2007/0175, 2007.

Björnsson, H., Sigurðsson, B. D., Davíðsdóttir, B., Ólafsson, Ástþórsson, J., Ólafsdóttir, S., Baldursson, T., and Jónsson, T.: Loftslagsbreytingar og áhrif þeirra á Íslandi: skýrsla vísindanefndar um loftslagsbreytingar 2018. (Climate Change and it's impact on Iceland – Report of the scientific committee on Climate), available at: https://www.vedur.is/media/loftslag/Skyrsla-loftslagsbreytingar-2018-Vefur-NY.pdf (last access: 30 December 2019), 2018.

Box, J. E., Fettweis, X., Stroeve, J. C., Tedesco, M., Hall, D. K., and Steffen, K.: Greenland ice sheet albedo feedback: thermodynamics and atmospheric drivers, The Cryosphere, 6, 821–839, https://doi.org/10.5194/tc-6-821-2012, 2012.

Butwin, M. K., Löwis, S. V., Pfeffer, M. A., and Thorsteinsson, T.: The effects of volcanic eruptions on the frequency of particulate matter suspension events in Iceland, J. Aerosol Sci., 128, 99–113, https://doi.org/10.1016/j.jaerosci.2018.12.004, 2019.

Crochet, P., Jóhannesson, T., Jónsson, T., Sigurðsson, O., Björnsson, H., Pálsson, F., and Barstad, I.: Estimating the Spatial Distribution of Precipitation in Iceland Using a Linear Model of Orographic Precipitation, J. Hydrometeorol., 8, 1285–1306, https://doi.org/10.1175/2007JHM795.1, 2007.

Cuffey, K. and Paterson, W.: The Physics of Glaciers, Elsevier Science, 2010.

Dagsson-Waldhauserova, P., Arnalds, O., and Olafsson, H.: Long-term variability of dust events in Iceland (1949–2011), Atmos. Chem. Phys., 14, 13411–13422, https://doi.org/10.5194/acp-14-13411-2014, 2014.

Dagsson-Waldhauserova, P., Arnalds, O., Olafsson, H., Hladil, J., Skala, R., Navratil, T., Chadimova, L., and Meinander, O.: Snow–Dust Storm: Unique case study from Iceland, March 6–7, 2013, Aeolian Res., 16, 69–74, https://doi.org/10.1016/j.aeolia.2014.11.001, 2015.

Dagsson-Waldhauserova, P., Renard, J.-B., Olafsson, H., Vignelles, D., Berthet, G., Verdier, N., and Duverger, V.: Vertical distribution of aerosols in dust storms during the Arctic winter, Sci. Rep., 9, 16122, https://doi.org/10.1038/s41598-019-51764-y, 2019.

de Abreu, R. A., Key, J., Maslanik, J. A., Serreze, M. C., and Ledrew, E. F.: Comparison of in Situ and AVHRR-Derived Broadband Albedo over Arctic Sea Ice, Arctic, 47, 288–297, 1994.

De Ruyter De Wildt, M. S., Oerlemans, J., and Björnsson, H.: A method for monitoring glacier mass balance using satellite albedo measurements: application to Vatnajökull, Iceland, J. Glaciol., 48, 267–278, https://doi.org/10.3189/172756502781831458, 2002.

Dietz, A. J., Wohner, C., and Kuenzer, C.: European Snow Cover Characteristics between 2000 and 2011 Derived from Improved MODIS Daily Snow Cover Products, Remote Sensing, 4, 2432–2454, https://doi.org/10.3390/rs4082432, 2012.

Donohoe, A. and Battisti, D. S.: Atmospheric and Surface Contributions to Planetary Albedo, J. Climate, 24, 4402–4418, https://doi.org/10.1175/2011JCLI3946.1, 2011.

Đorđević, D., Tošić, I., Sakan, S., Petrović, S., Đuričić-Milanković, J., Finger, D. C., and Dagsson-Waldhauserová, P.: Can Volcanic Dust Suspended From Surface Soil and Deserts of Iceland Be Transferred to Central Balkan Similarly to African Dust (Sahara)?, Front. Earth Sci., 7, 142, https://doi.org/10.3389/feart.2019.00142, 2019.

Dozier, J., Painter, T. H., Rittger, K., and Frew, J. E.: Time–space continuity of daily maps of fractional snow cover and albedo from MODIS, Adv. Water Res., 31, 1515–1526, https://doi.org/10.1016/j.advwatres.2008.08.011, 2008.

Dragosics, M., Meinander, O., Jónsdóttír, T., Dürig, T., De Leeuw, G., Pálsson, F., Dagsson-Waldhauserová, P., and Thorsteins-

son, T.: Insulation Effects of Icelandic Dust and Volcanic Ash on Snow and Ice, Arab. J. Geosci., 9, 126, https://doi.org/10.1007/s12517-015-2224-6, 2016.

Þorsteinsson, Þ., Jóhannesson, T., Sigurðsson, O., and Einarsson, B.: Afkomumælingar á Hofsjökli 1988–2017, Veðurstofa Íslands, Reykjavík, 2017-016, 82, 2017.

Einarsson, B.: Jöklabreytingar (glacier variations) 1930–1970, 1970–1995, 1995–2016 og 2016–2017, Jökull, 68, 95–99, 2018.

Einarsson, M. Á.: Climates of the oceans, edited by: Van Loon, H., Vol. 15 of World Survey of Climatology, Elsevier, J. Climatol., 5, 673–697, https://doi.org/10.1002/joc.3370050110, 1984.

Gardner, A. S. and Sharp, M. J.: A review of snow and ice albedo and the development of a new physically based broadband albedo parameterization, J. Geophys. Res.-Earth, 115, F01009, https://doi.org/10.1029/2009JF001444, 2010.

Gascoin, S., Guðmundsson, S., Aðalgeirsdóttir, G., Pálsson, F., Schmidt, L., Berthier, E., and Björnsson, H.: Evaluation of MODIS Albedo Product over Ice Caps in Iceland and Impact of Volcanic Eruptions on Their Albedo, Remote Sensing, 9, 399, https://doi.org/10.3390/rs9050399, 2017.

GDAL/OGR contributors: GDAL/OGR Geospatial Data Abstraction software Library, Open Source Geospatial Foundation, available at: https://gdal.org (last access: 30 December 2019), 2019.

Gudmundsson, M. T., Sigmundsson, F., and Björnsson, H.: Ice–volcano interaction of the 1996 Gjálp subglacial eruption, Vatnajökull, Iceland, Nature, 389, 954–957, https://doi.org/10.1038/40122, 1997.

Guðmundsson, M. T., Þórðarson, Þ., Höskuldsson, Á., Larsen, G., Björnsson, H., Prata, F. J., Oddsson, B., Magnússon, E., Högnadóttir, Þ., Petersen, G. N., Hayward, C. L., Stevenson, J. A., and Jónsdóttir, I.: Ash generation and distribution from the April–May 2010 eruption of Eyjafjallajökull, Iceland, Sci. Rep., 2, 572, https://doi.org/10.1038/srep00572, 2012.

Guðmundsson, S., Björnsson, H., Pálsson, F., and Haraldsson, H. H.: Comparison of energy balance and degree–day models of summer ablation on the Langjökull ice cap, SW-Iceland, Jökull, 59, 1–18, 2009.

Gunnarsson, A.: andrigunn/aig2: open (Version 1), Zenodo, https://doi.org/10.5281/zenodo.4445245, 2021.

Gunnarsson, A., Garðarsson, S. M., and Sveinsson, Ó. G. B.: Icelandic snow cover characteristics derived from a gap-filled MODIS daily snow cover product, Hydrol. Earth Syst. Sci., 23, 3021–3036, https://doi.org/10.5194/hess-23-3021-2019, 2019.

Hall, D. K. and Riggs, G. A.: MODIS/Aqua Snow Cover Daily L3 Global 500m Grid, Version 6, Tech. rep., NASA National Snow and Ice Data Center Distributed Active Archive Center, Boulder, Colorado USA, https://doi.org/10.5067/MODIS/MYD10A1.006, 2016a.

Hall, D. K. and Riggs, G. A.: MODIS/Terra Snow Cover Daily L3 Global 500m Grid, Version 6, Tech. rep., NASA National Snow and Ice Data Center Distributed Active Archive Center, Boulder, Colorado USA, https://doi.org/10.5067/MODIS/MOD10A1.006, 2016b.

Hanna, E., Jónsson, T., and Box, J. E.: An analysis of Icelandic climate since the nineteenth century, International Journal of Climatology, 24, 1193–1210, https://doi.org/10.1002/joc.1051, 2004.

Hannesdóttir, H., Sigurðsson, O., Þrastarson, R., Guðmundasson, S., Belart, J., Pálsson, F., Magnússon, E., Víkingsson, S., and Jóhannesson, T.: Variations in glacier extent in Iceland since the end of the Little Ice Age, Jökull, 1–34, 2020.

Helsel, D. and Hirsch, R.: Statistical Methods in Water Resources Techniques of Water Resources Investigations, Tech. Rep. Book 4, Chapter A3, U.S. Geological Survey, 2002.

Hjaltason, S., Guðmundsdóttir, M., Haukdal, J. Á., and Guðmundsson, J. R.: Energy Statistics in Iceland 2017, Energy Statistics in Iceland, Orkustofnun, available at: https://orkustofnun.is/gogn/Talnaefni/OS-2019-T009-01.pdf (last access: 30 December 2019), 2018.

Jóhannesson, T., Björnsson, H., Magnússon, E., Guðmundsson, S., Pálsson, F., Sigurðsson, O., Thorsteinsson, T., and Berthier, E.: Ice-volume changes, bias estimation of mass-balance measurements and changes in subglacial lakes derived by lidar mapping of the surface of Icelandic glaciers, Ann. Glaciol., 54, 63–74, https://doi.org/10.3189/2013AoG63A422, 2013.

Kipp and Zonen: Instruction Manuel CNR1 Net Radiometer, available at: https://s.campbellsci.com/documents/cn/manuals/cnr4.pdf, last access: 11 September 2019.

Klein, A. G. and Stroeve, J.: Development and Validation of a Snow Albedo Algorithm for the MODIS Instrument, Ann. Glaciol., 34, 45–52, https://doi.org/10.3189/172756402781817662, 2002.

Konzelmann, T. and Ohmura, A.: Radiative Fluxes and Their Impact on the Energy Balance of the Greenland Ice Sheet, J. Glaciol., 41, 490–502, https://doi.org/10.3189/S0022143000034833, 1995.

Liang, S., Stroeve, J., and Box, J. E.: Mapping Daily Snow/Ice Shortwave Broadband Albedo from Moderate Resolution Imaging Spectroradiometer (MODIS): The Improved Direct Retrieval Algorithm and Validation with Greenland in Situ Measurement, J. Geophys. Res.-Atmos., 110, D10109, https://doi.org/10.1029/2004JD005493, 2005.

Lindsay, R. W. and Rothrock, D. A.: Arctic Sea Ice Albedo from AVHRR, J. Climate, 7, 1737–1749, https://doi.org/10.1175/1520-0442(1994)007<1737:ASIAFA>2.0.CO;2, 1994.

Magnússon, E., Belart, J. M. C., Pálsson, F., Anderson, L. S., Gunnlaugsson, A., Berthier, E., Ágústsson, H., and Geirsdóttir, A.: The subglacial topography of Drangajökull ice cap, NW-Iceland, deduced from dense RES-profiling, Jökull, 66, 1–26, 2016.

Matlab: R2017a, The Mathworks Inc., Natick, Massachusetts, 2017.

Meinander, O., Kontu, A., Virkkula, A., Arola, A., Backman, L., Dagsson-Waldhauserová, P., Järvinen, O., Manninen, T., Svensson, J., de Leeuw, G., and Leppäranta, M.: Brief communication: Light-absorbing impurities can reduce the density of melting snow, The Cryosphere, 8, 991–995, https://doi.org/10.5194/tc-8-991-2014, 2014.

Möller, R., Möller, M., Björnsson, H., Gudmundsson, S., Pálsson, F., Oddsson, B., Kukla, P., and Schneider, C.: MODIS-derived albedo changes of Vatnajökull (Iceland) due to tephra deposition from the 2004 Grimsvötn eruption, Int. J. Appl. Earth Obs., 26, 256–269, https://doi.org/10.1016/j.jag.2013.08.005, 2014.

Möller, R., Dagsson-Waldhauserova, P., Möller, M., Kukla, P. A., Schneider, C., and Gudmundsson, M. T.: Persistent albedo reduction on southern Icelandic glaciers due to ashfall from the 2010 Eyjafjallajökull eruption, Remote Sens. Environ., 233, 111396, https://doi.org/10.1016/j.rse.2019.111396, 2019.

Naegeli, K., Damm, A., Huss, M., Wulf, H., Schaepman, M., and Hoelzle, M.: Cross-Comparison of Albedo Products for Glacier Surfaces Derived from Airborne and Satellite (Sentinel-2 and Landsat 8) Optical Data, Remote Sensing, 9, 110, https://doi.org/10.3390/rs9020110, 2017.

Naegeli, K., Huss, M., and Hoelzle, M.: Change detection of bare-ice albedo in the Swiss Alps , The Cryosphere, 13, 397–412, https://doi.org/10.5194/tc-13-397-2019, 2019.

National Land Survey of Iceland (NLSI): IS 50V geospatial data, available at: https://atlas.lmi.is, last access: 30 December 2019.

Painter, T. H., Bryant, A. C., and Skiles, S. M.: Radiative forcing by light absorbing impurities in snow from MODIS surface reflectance data, Geophys. Res. Lett., 39, L17502, https://doi.org/10.1029/2012GL052457, 2012.

Pálsson, F., Gunnarsson, A., Pálsson, H. S., and Steinþórsson, S.: Afkomu- og hraðamælingar á Langjökli jökulárið 2012–2013, Landsvirkjun, Reykjavík, LV-2015-076, 37, 2015.

Pálsson, F., Gunnarsson, A., Jónsson, G., Pálsson, H. S., and Steinþórsson, S.: Vatnajökull: Mass balance, meltwater drainage and surface velocity of the glacial year 2018–19, Landsvirkjun, Reykjavík, RH-01-20/LV-2020-016, 56, 2020a.

Pálsson, F., Gunnarsson, A., Pálsson, H. S., and Steinþórsson, S.: Afkomu-og hraðamælingar á Langjökli jökulárið 2018–2019, Landsvirkjun, Reykjavík, RH-10-20/LV-2020-017, 27, 2020b.

Peltoniemi, J. I., Gritsevich, M., Hakala, T., Dagsson-Waldhauserová, P., Arnalds, Ó., Anttila, K., Hannula, H.-R., Kivekäs, N., Lihavainen, H., Meinander, O., Svensson, J., Virkkula, A., and de Leeuw, G.: Soot on Snow experiment: bidirectional reflectance factor measurements of contaminated snow, The Cryosphere, 9, 2323–2337, https://doi.org/10.5194/tc-9-2323-2015, 2015.

Pope, E. L., Willis, I. C., Pope, A., Miles, E. S., Arnold, N. S., and Rees, W. G.: Contrasting snow and ice albedos derived from MODIS, Landsat ETM+ and airborne data from Langjökull, Iceland, Remote Sens. Environ., 175, 183–195, https://doi.org/10.1016/j.rse.2015.12.051, 2016.

Reijmer, C. H., Knap, W. H., and Oerlemans, J.: The Surface Albedo Of The Vatnajökull Ice Cap, Iceland: A Comparison Between Satellite-Derived And Ground-Based Measurements, Bound.-Lay. Meteorol., 92, 123–143, https://doi.org/10.1023/A:1001816014650, 1999.

Schaaf, C. K. and Wang, Z.: MCD43A3/MODIS/Terra+Aqua BRDF/Albedo Daily L3 Global – 500m V006 500m Grid, Version 6, Tech. rep., NASA EOSDIS Land Processes DAAC, Boulder, Colorado USA, https://doi.org/10.5067/MODIS/MCD43A3.006, 2015.

Schmidt, L., Langen, P., Aðalgeirsdóttir, G., Pálsson, F., Guðmundsson, S., and Gunnarsson, A.: Sensitivity of Glacier Runoff to Winter Snow Thickness Investigated for Vatnajökull Ice Cap, Iceland, Using Numerical Models and Observations, Atmosphere, 9, 11, https://doi.org/10.3390/atmos9110450, 2018.

Schmidt, L. S., Aðalgeirsdóttir, G., Guðmundsson, S., Langen, P. L., Pálsson, F., Mottram, R., Gascoin, S., and Björnsson, H.: The importance of accurate glacier albedo for estimates of surface mass balance on Vatnajökull: evaluating the surface energy budget in a regional climate model with automatic weather station observations, The Cryosphere, 11, 1665–1684, https://doi.org/10.5194/tc-11-1665-2017, 2017.

Sirguey, P.: Simple correction of multiple reflection effects in rugged terrain, Int. J. Remote Sens., 30, 1075–1081, https://doi.org/10.1080/01431160802348101, 2009.

Sirguey, P., Mathieu, R., and Arnaud, Y.: Subpixel monitoring of the seasonal snow cover with MODIS at 250 m spatial resolution in the Southern Alps of New Zealand: Methodology and accuracy assessment, Remote Sens. Environ., 113, 160–181, https://doi.org/10.1016/j.rse.2008.09.008, 2009.

Skiles, S. M., Flanner, M., Cook, J. M., Dumont, M., and Painter, T. H.: Radiative Forcing by Light-Absorbing Particles in Snow, Nature Climate Change, 8, 964, https://doi.org/10.1038/s41558-018-0296-5, 2018.

Steffen, K., Abdalati, W., and Stroeve, J.: Climate sensitivity studies of the Greenland ice sheet using satellite AVHRR, SMMR, SSM/I and in situ data, Meteorol. Atmos. Phys., 51, 239–258, https://doi.org/10.1007/BF01030497, 1993.

Stibal, M., Box, J. E., Cameron, K. A., Langen, P. L., Yallop, M. L., Mottram, R. H., Khan, A. L., Molotch, N. P., Chrismas, N. A. M., Calì Quaglia, F., Remias, D., Smeets, C. J. P. P., van den Broeke, M. R., Ryan, J. C., Hubbard, A., Tranter, M., van As, D., and Ahlstrøm, A. P.: Algae Drive Enhanced Darkening of Bare Ice on the Greenland Ice Sheet, Geophys. Res. Lett., 44, 11463–11471, https://doi.org/10.1002/2017GL075958, 2017.

Stroeve, J.: Assessment of Greenland Albedo Variability from the Advanced Very High Resolution Radiometer Polar Pathfinder Data Set, J. Geophys. Res.-Atmos., 106, 33989–34006, https://doi.org/10.1029/2001JD900072, 2001.

Stroeve, J., Nolin, A., and Steffen, K.: Comparison of AVHRR-Derived and in Situ Surface Albedo over the Greenland Ice Sheet, Remote Sens. Environ., 62, 262–276, https://doi.org/10.1016/S0034-4257(97)00107-7, 1997.

Stroeve, J., Box, J. E., Gao, F., Liang, S., Nolin, A., and Schaaf, C.: Accuracy Assessment of the MODIS 16-Day Albedo Product for Snow: Comparisons with Greenland in Situ Measurements, Remote Sens. Environ., 94, 46–60, https://doi.org/10.1016/j.rse.2004.09.001, 2005.

Stroeve, J., Box, J. E., Wang, Z., Schaaf, C., and Barrett, A.: Re-Evaluation of MODIS MCD43 Greenland Albedo Accuracy and Trends, Remote Sens. Environ., 138, 199–214, https://doi.org/10.1016/j.rse.2013.07.023, 2013.

Tesche, M., Glantz, P., Johansson, C., Norman, M., Hiebsch, A., Ansmann, A., Althausen, D., Engelmann, R., and Seifert, P.: Volcanic ash over Scandinavia originating from the Grímsvötn eruptions in May 2011, J. Geophys. Res.-Atmos., 117, D09201, https://doi.org/10.1029/2011JD017090, 2012.

Van den Broeke, M., Reijmer, C. H., and Van De Wal, R. S.: A study of the surface mass balance in Dronning Maud Land, Antarctica, using automatic weather stations, J. Glaciol., 50, 565–582, https://doi.org/10.3189/172756504781829756, 2004a.

Van den Broeke, M., van As, D., Reijmer, C., and Wal, R.: Assessing and Improving the Quality of Unattended Radiation Observations in Antarctica, J. Atmos. Ocean. Tech., 21, 1417–1431, https://doi.org/10.1175/1520-0426(2004)021<1417:AAITQO>2.0.CO;2, 2004b.

Warren, S. G.: Optical Properties of Snow, Rev. Geophys., 20, 67–89, https://doi.org/10.1029/RG020i001p00067, 1982.

Warren, S. G. and Wiscombe, W. J.: A Model for the Spectral Albedo of Snow. II: Snow Containing Atmospheric Aerosols,

J. Atmos. Sci., 37, 2734–2745, https://doi.org/10.1175/1520-0469(1980)037<2734:AMFTSA>2.0.CO;2, 1980.

Watson, E., Swindles, G., Stevenson, J., Savov, I., and Lawson, I.: The transport of Icelandic volcanic ash: insights from northern European cryptotephra records: Cryptotephra records of volcanic ash, J. Geophys. Res.-Sol. Ea., 121, 7177–7192, https://doi.org/10.1002/2016JB013350, 2016.

Winther, J.-G.: Landsat TM derived and in situ summer reflectance of glaciers in Svalbard, Polar Res., 12, 37–55, https://doi.org/10.3402/polar.v12i1.6702, 1993.

Wittmann, M., Groot Zwaaftink, C. D., Steffensen Schmidt, L., Guðmundsson, S., Pálsson, F., Arnalds, O., Björnsson, H., Thorsteinsson, T., and Stohl, A.: Impact of dust deposition on the albedo of Vatnajökull ice cap, Iceland, The Cryosphere, 11, 741–754, https://doi.org/10.5194/tc-11-741-2017, 2017.

Xiong, X., Butler, J., Cao, C., and Wu, X.: 1.13 – Optical Sensors–VIS/NIR/SWIR, in: Comprehensive Remote Sensing, edited by: Liang, S., Elsevier, Oxford, 353–375, https://doi.org/10.1016/B978-0-12-409548-9.10325-2, 2018.

Zhou, C., Zhang, T., and Zheng, L.: The Characteristics of Surface Albedo Change Trends over the Antarctic Sea Ice Region during Recent Decades, Remote Sensing, 11, 821, https://doi.org/10.3390/rs11070821, 2019.

Zubko, N., Muñoz, O., Zubko, E., Gritsevich, M., Escobar-Cerezo, J., Berg, M. J., and Peltoniemi, J.: Light scattering from volcanic-sand particles in deposited and aerosol form, Atmos. Environ., 215, 116813, https://doi.org/10.1016/j.atmosenv.2019.06.051, 2019.

Paper III

Modeling of surface energy balance for Icelandic glaciers using remote sensing albedo

Andri Gunnarsson, Sigurdur M. Gardarsson, Finnur Pálsson.

To be submitted

Modeling of surface energy balance for Icelandic glaciers using remote sensing albedo

Andri Gunnarsson[1,3], Sigurdur M. Gardarsson[1], and Finnur Pálsson[2]

[1]University of Iceland, Civil and Environmental Engineering, Hjardarhagi 2-6, IS-107 Reykjavik, Iceland
[2]Institute of Earth Sciences, University of Iceland, Sturlugata 7, 101 Reykjavík, Iceland
[3]Landsvirkjun, Department of Research and Development, Reykjavík, IS-107, Iceland

Correspondence: Andri Gunnarsson (andrigun@lv.is)

Abstract.

During the melt season, absorbed solar energy, modulated at the surface by albedo, is one of the main governing factors controlling surface-melt variability for glaciers in Iceland. An energy balance model was developed with the possibility to utilize spatio-temporal MODIS satellite-derived daily surface albedo driven by high-resolution climate forcing data to reconstruct the surface energy balance (SEB) for all Icelandic glaciers for the period 2000–2021. The surface energy balance was reconstructed from April through September for 2000 to 2021 at a daily timestep with a 500 m spatial resolution. Validation was performed using observations from various glaciers spanning distinct locations and elevations with good visual and statistical agreement. The results show that spatio-temporal patterns for the melt season have high annual and inter-annual variability for Icelandic glaciers. The variability was influenced by high climate variability, light absorbing particle depositions (LAPs) from volcanic eruptions and dust hotspots in pro-glacial areas close to the glaciers. Impacts of LAPs can lead to significant melt enhancement due to lowering of albedo and increased short-wave radiative energy forced at the surface. Large impacts on the surface energy balance were observed for years with high LAPs deposits, such as volcanic eruptions in 2004, 2010, 2011 and the sand and dust rich year of 2019. The impacts of volcanic eruptions and other LAPs events were estimated using historical mean albedo under the same climatology forcing to provide estimations of melt energy enhancements. The impact was often significant even though the glaciers were far away from the eruption location.

1 Introduction

Mass and energy balance changes of glaciers are useful indicators of changes in the cryosphere and climate (Jóhannesson, 1986; Jóhannesson et al., 1989; Slater et al., 2021). Projected changes of future climate in the Northern Hemisphere would force reduction in the area and volume of existing glaciers and ice sheets, with significant contribution to global sea level rise (Gregory and Oerlemans, 1998; Zemp et al., 2019; Schmidt et al., 2020; Hofer et al., 2020; Goelzer et al., 2020). In the Northern Hemisphere absorbed short-wave energy during melt season is the primary energy source for surface melting of snow

and glaciers (Male and Granger, 1981; Björnsson and Pálsson, 2008; Fernandes et al., 2009; Hudson, 2011; Box et al., 2012; Chen et al., 2016). Albedo of snow- and ice-covered surfaces is the unitless ratio of the radiant flux reflected from Earth's surface to the incident flux and thus accurate representation of albedo is critical to understand and model surface melt (Schmidt et al., 2017). Changes in snow- and ice-cover duration and extent, can magnify the effect on climate for warming and cooling due to the complex and self-enhancing ice-albedo feedback with temperature (Barnett et al., 2005; Adam et al., 2008; Choi et al., 2010; Hudson, 2011; Flanner et al., 2011; Box et al., 2012). Due to the importance of snow- and ice-albedo as an amplifier of climate change, surface albedo has been defined as an Essential Climate Variable and a requirement for climate monitoring (WMO, 2011; Bojinski et al., 2014).

Iceland is an island (103.000 km^2) located at major climatic boundaries in the North Atlantic Ocean, where changes in atmospheric circulation and ocean currents influence the climate. Iceland has a maritime climate with mild winters, cool summers and high precipitation sustaining a seasonal snow pack and glaciers (Einarsson, 1984; Perkins et al., 1998). The North Atlantic Current, a branch of the Gulf Stream towards north–east, transports warm ocean water to the North Atlantic Subpolar Gyre, explaining milder climates at higher latitudes (Lozier et al., 1995; Rossby, 1996; Ólafsdóttir et al., 2010; Knudsen et al., 2012). Flowing along the southern and western Icelandic coast the Irminger Current brings relatively warm Atlantic water towards Iceland, moderating the climate. In the north and east, the cold East Greenland Current, originated in cold Polar waters, and the cold East Icelandic Current, a branch of the East Greenland Current, bring cold water masses towards the Icelandic coast in the north and east, respectively (Renner et al., 2018; Zhao et al., 2018). Associated with anthropogenic warming, global sea surface temperatures have been observed to increase in the past century. Future projections indicate further warming although increased melting of the Greenland ice sheet and Arctic sea ice has been linked with local SST cooling south of Greenland, a region referred to as the North Atlantic warming hole (NAWH), with possible impacts on surface mass balance of Icelandic glaciers (Rahmstorf et al., 2015; Alexander et al., 2018; Gervais et al., 2019; Keil et al., 2020; Noël et al., 2022).

The total area of glaciers in Iceland in 2019 was approximately 10.400 km^2 ($\sim$10 % of Iceland), containing about 3.400 km^3 of ice (in 2019), corresponding to $\sim$9 mm of potential global sea level rise (Björnsson and Pálsson, 2020; Aðalgeirsdóttir et al., 2020; Hannesdóttir et al., 2020). The mass balance of Icelandic glaciers has changed significantly over the last three decades and all studies and projections indicate that the mass loss of Icelandic glaciers will continue and increase with accelerated warming in the Northern Hemisphere in the future (Jóhannesson and Aðalgeirsdóttir; Schmidt et al., 2020; Noël et al., 2022).

Iceland has about 22.000 km^2 of sandy deserts that are a major source of atmospheric dust and light absorbing particles (LAPs) (Arnalds et al., 2016). Many of those areas are near glaciers and are sources of active dust emission areas, defined as dust hotspots (e.g. glacio-fluvial plains, beached and sand plains), with unstable surfaces and are prone to dust aerosol production that can deposit in snow and glacier surfaces, influencing the surface albedo, thus the radiative forcing (Björnsson and Pálsson, 2008; Wittmann et al., 2017; Dagsson-Waldhauserova et al., 2017; Gunnarsson et al., 2021).

Glacier mass and energy balance models generally do not simulate albedo changes due to atmospheric dust and light absorbing particles deposition, with a few exceptions as the processes involved are complex to model and dust sources can be far away from the glacier surfaces. In volcanic regions, eruption can produce vast amounts of volcanic ash of various grain size where even extremely thin tephra deposits on snow- and ice surfaces can lead to significantly enhanced melt potential; but in cases

of a thick tephra layer deposits (> ∼2 cm) prevent surface melt processes (Warren and Wiscombe, 1980; Möller et al., 2014; Wittmann et al., 2017; Möller et al., 2019; Gunnarsson et al., 2021). The majority of mass loss from glaciers in Iceland is due to surface mass balance processes. However, non-surface mass balance is non-negligible (through the processes of geothermal activity, volcanic eruptions, geothermal heat flux, calving, internal friction and water flow) although these processes amount to only a fraction of the surface ablation (Björnsson et al., 2001; Aðalgeirsdóttir et al., 2020; Jóhannesson et al., 2020).

Research and monitoring of Icelandic glaciers is important for a range of reasons, e.g. civil security due to jökulhlaups, subglacial volcanic activity, stability of river paths, runoff variability, long and short-term changes due to climate change, natural variability, and water resource forecasting for efficient hydro power production. Efficient water resource utilization requires forecasting on a sub-daily, daily and seasonal timescales for operational planning. Longer timescales (years and decades) are also important for refurbishment of older hydro power infrastructure due to climate change adaption and development of new hydro power plants (Jóhannesson and Aðalgeirsdóttir; Sveinsson, 2016). Hydro power production in Iceland corresponds to about 70 % of the total energy production in the country. About 50 % of inflow to reservoirs and diversions for hydro power energy production originates from annual glacier melt in an average hydrological year (Hjaltason et al., 2020). Additionally, because the current Icelandic energy system is a closed loop system, no import nor export of energy (except fossil fuel), high quality forecasting capabilities are of importance.

The surface energy balance of Icelandic glaciers has been investigated over recent decades. Ahlmann (1940) did one of the first meteorological observations during the Swedish-Icelandic expedition crossing Vatnajökull, providing insights to the surface energy balance by observing temperature, humidity, air pressure and other relevant meteorological parameters. Lister (1953, 1959) studied micro meteorological conditions at the snout of Breiðamerkurjökull, making observations on the transfer of heat to the surface of the glacier assessing and comparing energy transfer for clean glacier ice and dirt covered ice surfaces. Results from this work detailed the importance of short-wave radiation as a major contributing component to glacier ablation and its significant increase over dirtier surfaces (bare-ice areas) due to lower albedo. Observations were also done assessing the dirt thickness to provide insulation protection of the ice surface, indicating that 2 to 4 cm were sufficient to provide complete isolation of the glacier surface from the incoming short-wave radiation. Björnsson (1971, 1972) observed and estimated the energy balance components for Bægisárjökull in northern Iceland during the summers 1967 and 1968 by observing daily meteorological conditions and surface mass balance. The results indicated net radiation as the major energy source for melting of the glacier (51 %), sensible heat secondary (33 %), and latent heat (16 %) with the least contribution.

The first modern Automatic Weather Stations (AWS) were installed during the melt season on Vatnajökull ice-cap in 1994 and 1995, one and three units, respectively (Björnsson and Aðalgeirsdóttir, 1995; Björnsson et al., 1996). In 1996 the multi-national European Union supported project TEMBA supported the extension of AWS operated at Vatnajökull to 12 units (Björnsson and Pálsson, 1998; Oerlemans et al., 1999). These were the first systematically operated AWS that observed key meteorological variables allowing extensive estimations of the surface energy balance.

This pioneering work scoped the current AWS operations at Vatnajökull where since, 5–12 units have been operated during the melt season. AWS operation efforts expanded to Langjökull in 2001 with observations of surface mass- and energy balance (Pálsson et al., 2020b) and AWS sites have been operated at Hofsjökull and Mýrdalsjökull as well. These operations are a joint

effort by Landsvirkjun (National Power Company in Iceland) and the Science Institute University of Iceland (now Institute of Earth Sciences, IES) which are fully operational to date (Pálsson et al., 2020a). Since the onset of surface energy balance observations, the program has developed, expanded to new glaciers and alternative glacier outlets of the initial program. A few locations offer over 25 years of observations during the melting period (May through October) annually while a few stations were operated during winter as well (Gunnarsson et al., 2019). The full extent of these observations and operations are referred to as the Icelandic Glacier Automatic Weather Stations network (ICE-GAWS). The meteorological observations from the network and energy balance calculated from these sites have served as key data in providing understanding of the surface energy balance for Icelandic glaciers in many research projects investigating historic, recent and future developments of glaciers (Guðmundsson et al., 2005, 2009; Matthews and Hogdkins, 2016; Wittmann et al., 2017; Schmidt et al., 2017, 2020; Gunnarsson et al., 2021).

The primary objectives of this study were to understand and quantify melt season surface energy balance for Icelandic glaciers using high resolution meteorological climate forcing and remotely sensed glacier surface albedo from the Moderate Resolution Imaging Spectroradiometer (MODIS) sensor. This adds to the previous understanding of spatial and temporal distributions of melt energy, main melt energy sources, variability within and between glaciers in Iceland and provides insight into the melt enhancement due to volcanic eruptions and years with extensive LAP deposits. It also provides a comprehensive overview of the surface energy balance since it is not limited to one glacier or a glacier outlet as many previous studies. Analysis of large-scale atmospheric circulation anomalies permits attribution of surface energy balance variability and identification of mechanisms driving surface energy balance through physical processes.

2 Study area

The analysis in this study extends to the six largest Icelandic glaciers: Vatnajökull, Langjökull, Hofsjökull, Drangajökull, Mýrdalsjökull and Eyjafjallajökull (about 97 % of glaciated areas in Iceland) although the model described in the study was applied to all glaciers in Iceland. Figure 1 shows the outlines (black) of the six glaciers, and their divides into main ice flow basins for detailed analysis. The ice flow basins are named with first letter of respective ice cap and their location (e.g. VNW for the northwest outlet of Vatnajökull). Catchment delineation was from Magnússon et al. (2016a) for Drangajökull, hb and Björnsson et al. (2000) for Hofsjökull and Mýrdalsjökull, and Pálsson and Gunnarsson (2015); Pálsson et al. (2013); Pálsson et al. (2016) for Langjökull and Vatnajökull. The sub-areas are chosen as in Gunnarsson et al. (2021). For the six glaciers and the defined ice flow basins topographic properties were extracted: area, mean, maximum and minimum elevation, and are shown in Table 1. Figure 1 also show the locations of ICE-GAWS sites used for validation purposes in this study with grey dots. Glaciers outlines were kept fixed through the study period (2000-2021) using the available delineation spanning 2007–2013 from Hannesdóttir et al. (2020).

3 Data and methods

3.1 Meteorological in situ data

The Icelandic Glacier Automatic Weather Stations network (ICE-GAWS) stores meteorological observations from AWSs located at sites on Vatnajökull, Langjökull, Mýrdalsjökull and Hofsjökull since 1994, 2001, 2015 and 20156 respectively. Most of the stations were operated during the ablation season, from May through September annually but a few are in all year around operation. In total 20 sites provided data for the study period, all sites measure air temperature and incoming short-wave radiation while 13 sites also measure incoming long-wave radiation. Details on data processing is described in Gunnarsson et al. (2021). Table A1 provides details for the location, elevation and number of observations for each site in the Appendix and Figure 1 shows their location. In the current study observations of air temperature, short- and long-wave incoming radiation were used for validation purposes.

3.2 Surface albedo and cloud cover data

For the surface energy balance model applied in this study, snow- and ice-surface albedo (α) were derived from Moderate Resolution Imaging Spectroradiometer (MODIS) data using processing models developed for Iceland by Gunnarsson et al. (2021). The products rely on the MOD10A1 (Terra satellite) and MYD10A1 (Aqua satellite) snow albedo (Scientific Data set: Snow Albedo Daily Tile) for the grid tile h17v02, covering most of Iceland, excluding a small portion of the Snæfellsnes peninsula. Data were collected from the National Snow and Ice Data Center (NSIDC) (Hall and Riggs, 2016a, b) for further processing. From 2000 until 2002 only Terra was in orbit, so for the period from 23 February 2000 to 4 May 2002 albedo data was only based on Terra. For MOD10A1 62 dates were missing and 12 for MYD10A1 for the study period (April through September each year) excluding data missing due to polar darkness from late November until late January each year.

For snow- and ice-surface albedo, daily merging was applied to the Terra MOD10A1 and Aqua MYD10A1 albedo data to reduce the number of cloud obscured daily pixels, i.e. all non-cloud obscured pixels were merged into a single tile from both products daily. Then, temporal aggregation was applied to further reduce cloud obscured pixels. The temporal aggregation range was set as the number of days backwards and forwards, at each center date to merge to a single stack for further processing. A temporal aggregation range as 5 days backward/forward was selected; allowing 11 days from both MOD10A1 and MYD10A1 to contribute data to the temporally aggregated product. This results in a total of 22 values that are potentially available for each pixel (i.e. 11 days of MOD10A1 and 11 days of MYD10A1). For each data stack, containing the potential 22 values contributing albedo data, the mean was calculated to represent the surface-albedo, after median-based statistical rejection of outliers. The remaining pixels classified as clouds were classified statistically with four predicting variables, location (easting, northing), elevation (Z), and aspect, with a daily trained random forest model. Further information and details are in Gunnarsson et al. (2021).

Cloud cover data was based on the classifications of clouds in the M*D10A1 products (M*D35_L2 cloud mask). For each day the two tiles were merged together creating a daily cloud cover estimate at the time of satellite overpass (10:30 AM and 1:30 PM local time), i.e. cloud or no cloud. Data were then aggregated to monthly and melt season mean values accordingly.

3.3 Sea surface temperature (SST)

Sea surface temperature (SST) observations were from the NOAA OI SST V2 High Resolution Dataset. It is a blend of in situ ship and buoy SSTs with satellite SST derived from the Advanced Very High Resolution Radiometer (AVHRR) (Reynolds et al., 2007; Huang et al., 2021; NOAA, 2021). Data were available from September 1981 at a daily time-step out through the study period. The spatial resolution was a 1/4 deg global grid (∼28 km). Data was processed into daily time series for further analysis by masking certain spatial areas around Iceland. Five areas were selected and processed, Iceland SST south (65° – 60°N and 20° – 30°W), north (70° – 65°N and 10° – 20°W) , east (65° – 60°N and 10° – 20°W), west (70° – 65°N and 20° – 30°W) representing the main cardinal quadrants around Iceland. Despite global temperature warming in the past decades and a well established increase in mean global SST by about 1 °C since 1900 a small region in the North Atlantic ocean has been observed to cool, a occurrence known as the North Atlantic Warming Hole (NAWH) (Rahmstorf et al., 2015; Keil et al., 2020). Allan and Allan (2019) defined the local epicenter of the NAWH around 54°N 36°W confirmed by quantitative measurements of SST slope. In addition to the areas processed around Iceland, data for a NAWH was processed spanning 56° to 50°N and 33° to 39°W referred to as NAWH in the results.

3.4 GBI and NAO

Greenland Blocking Index (GBI) is the mean 500 hPa geopotential height for the 60–80°N, 20–80°W region in the Northern Hemisphere. It represents blocking over Greenland, clearly depicting changes in both climate and weather in the Northern Hemisphere (Hanna et al., 2016). The North Atlantic Oscillation (NAO) is defined as the normalized pressure difference between a station on the Azores and one on Iceland (Jones et al., 1997). NAO generally represents the principal mode of annual variability across much of the Atlantic sector of the Northern Hemisphere.

3.5 Model Forcing

Meteorological forcing based on the Weather Research and Forecast model (WRF version 3.6.1) coupled to the NOAH land surface model was used to provide climatological surface variables at a 2 km spatial resolution and 1 hour temporal resolution spanning the study period from 1.1.2000 to 30.9.2021. For the bulk of the period, data from the WRF-RAV2 configuration were used, developed for the climatological reanalysis RAV2 project (RAV2). Since RAV2 was forced with boundary conditions from the European Centre for Medium Range Weather Forecasts (ECMWF) ERA-Interim reanalysis (Berrisford et al., 2011) data availability, overlapping the current study, spans from 1.1.2000 out through August 2019 due to the end-of-life of ERA-Interim.

To extend the range of data availability, past August 2019, the climatological reanalysis was extended with near the identical model configuration as RAV2, but outer domain boundary conditions forcing were from the Global Forecast System (GFS) from the National Centers for Environmental Prediction (NCEP) weather forecast model (National Centers for Environmental Prediction, 2015). This product was referred to as the IceBox model configuration (IceB) and provides data from 01.09.2018 to 01.09.2020. The IceBox model configuration was also run operationally, as a forecasting system, providing data four times per

day, refereed to as FCST. To extend the analysis range even further, allowing the energy balance model presented here to cover the extraordinary summer weather in 2021, the forecast data from the IceBox domain starting at 01.04.2020 was aggregated to a hourly time series using the shortest forecasting step in each case. Further description of the RAV2 and IceBox model setup and output configuration is found in Rögnvaldsson (2016, 2020). Relevant surface data were extracted for use in the energy balance model, including air temperature at 2 m, surface temperature, incoming long- and short-wave radiation, barometric pressure at surface level and specific humidity; all were resampled to daily average values.

To downscale the meteorological forcing data from the 2 km WRF grid to the 463 m MODIS grid the model uses the IslandsDEM digital elevation model from the National Land Survey of Iceland (Accessed 01.06.2020). A 20 m version of the elevation model was resampled to the native MODIS grid for further processing using bi-cubic interpolation using the *griddata* function in Matlab (Matlab, 2020). Elevation dependent variables (air temperature and long-wave radiation) were also adjusted for the difference between the coarse-resolution WRF DEM and high-resolution IslandsDEM at 463 m using lapse rates.

Statistical downscaling of temperature requires an temperature lapse rate, often taken to be the free-air moist adiabatic lapse rate ranging from 6–7° K km^{-1} (Stone and Carlson, 1979). Hodgkins et al. (2013) investigated temperature lapse rates for outlet glaciers at Langjökull and south-east Vatnajökull during 2003–2007. They report mean monthly lapse rates ranging from -8 ° K km^{-1} to -4.5 ° K km^{-1} with a clear monthly variations from April to October. Generally the lowest lapse rate (-6.5 to -8.0 ° K km^{-1} (mean for April, May, September as -7.0 ° K km^{-1})) was seen in Spring and Fall with higher rates in summer (mean for June, July, August and September as -5.7° K km^{-1}). This coincides well with results from Gardner et al. (2009) over Arctic Glaciers with a ablation season mean of -4.9 ° K km^{-1}. Crochet and Jóhannesson (2011) developed a one-parameter terrain model with a constant vertical lapse rate of -6.5 ° K km^{-1} with validated to ground base temperature observations for Iceland, excluding glaciers. Their results suggested that the assumption of an -6.5 ° K km^{-1} lapse rate was applicable in Iceland. Further work by Nawri et al. (2012) also supports this. Here for glaciated areas an environmental lapse rate of –7.0° K km^{-1} was applied for JFMA and SOND while –5.5 ° K km^{-1} was applied for the active melt season, MJJA, following the results from Hodgkins et al. (2013).

Downward long wave radiation is primarily determined by humidity and temperature vertical atmospheric profiles and thus are a function of elevation (Plüss and Ohmura, 1997; Ohmura, 2001). Hinkelman et al. (2015) used an constant long wave radiation gradient of -29 W m^{-2} km^{-1} to correct for varying elevation (Marty et al., 2002). Enhancement of long wave radiation by surrounding terrain emission is important when sky radiation is low, e.g. in cold and dry atmospheres, generally at high elevations with steep topography (Sicart et al., 2006). In this study no adjustments were made to account for enhancement of long wave radiation due to terrain emission as the effect is small on the large concave ice caps investigated. A lapse rate of -29 W m^{-2} km^{-1} was used for elevation difference adjustment between the WRF and MODIS grids.

In many studies, incoming short-wave radiance are separated into beam and diffuse components and corrections for done terrain elevation, slope and tree-cover fractions (Bair et al., 2016; Rittger et al., 2016). Here, since the WRF data only provides total incoming short-wave radiation, no adjustments were made in this regard.

3.6 Surface Energy balance

The physical processes driving surface melt over snow- and ice-covered surfaces are isolated using estimations of the surface energy balance. The surface energy balance model used in this study was adopted from As et al. (2005), Van As (2011) and Vandecrux et al. (2018), where used with observational data. The model was modified for the input model forcings, described in the previous sections. The surface energy balance was closed by iteratively solving for surface temperature (T_s) where:

$$SW\downarrow(1-\alpha)+(LW\downarrow+LW\uparrow)+SHF+LHF+G+M=0 \tag{1}$$

where $SW\downarrow$ was the incoming short-wave radiation, α was broadband albedo, $LW\downarrow$ and $LW\uparrow$ was the incoming and outgoing long-wave radiation, respectively, SHF was the sensible heat flux, LHF the latent heat flux, G the sub-surface heat flux, with the fluxes defined positive when adding energy to the surface. M was the energy surplus used for surface melt (M = 0 when surface temperature < 273.15 K).

The model solves the energy balance at each time step iteratively with respect to snow surface temperature (T_s) expressed in terms of

$$LW\uparrow(T_s)+SHF(T_s)+LHF(T_s)=0 \tag{2}$$

where solutions for T_s > 273.15 K indicate availability of melt energy. If T_s was > 273.15 K, T_s was set as 273.15 K and melt M was computed, otherwise, if T_s was $\leq$ 273.15 K, T_s was set to zero.

Outgoing long-wave radiation (LW↑), defines the energy emitted to space by Earth's surface and depends on surface temperature. Here, outgoing long-wave radiation was calculated based on the Stefan-Boltzman law:

$$LW\uparrow=\varepsilon\sigma T_s^4 \tag{3}$$

where ε is the broadband emissivity of snow and ice (0.98) (Salisbury et al., 1994), and σ is the Stefan-Boltzman constant.

Turbulent fluxes of sensible heat SHF and latent heat LHF were estimated using the bulk aerodynamic approach with stability corrections based on Monin–Obukhov similarity theory (As et al., 2005; Smeets and van den Broeke, 2008a) using the stability functions of Holtslag and Bruin (1988) for stable stratification and Paulson (1970) for unstable stratification. The sensible heat flux is expressed as:

$$SHF=\rho c_p u_* \emptyset_* = \rho c_p C_H u(\emptyset-\emptyset_s) \tag{4}$$

and latent heat flux as:

$$LHF=\rho\lambda u_* q_* = \rho\lambda C_E u(q-q_s) \tag{5}$$

8

where ρ denotes air density, c_p is the specific heat of dry air at constant pressure, u_* is the friction velocity, λ is the latent heat of sublimation and $\emptyset_*$ and q_* are turbulent scales of temperature and humidity. C_H and C_E are bulk exchange coefficients for heat and moisture, respectively.

Surface roughness lengths for heat and moisture were calculated for snow- and ice separately as in Van As (2011). The surface roughness length for momentum (z_0) varies strongly in time and space and generally is set to different constant values for snow- and ice surfaces (Brock et al., 2006; Smeets and van den Broeke, 2008b). Values for surface roughness lengths of momentum have been reported ranging from 1 - 10 mm while lower values generally apply for snow (0.1 mm) (Brock et al., 2006). Values up to 60 mm have been reported at Breiðamerkurjökull where ice hummocks up to almost 2 m in height can be formed during the melt season but are not representative for the majority of bare-ice areas of glaciers in Iceland (Smeets et al., 1999; Wildt et al., 2004)

Guðmundsson et al. (2009) applied z_0 as 0.1, 2 and 10 mm for new snow, melting snow and ice in the ablation zone respectively, in an surface energy balance model for Langjökull and Wildt et al. (2004) used similar values for Vatnajökull. Schmidt et al. (2017) applied a constant value of 1 mm for both snow and ice modeling the energy balance for Vatnajökull. Since no data exist of spatio-temporal variability of z_0 for glaciers in Iceland, a simple classification scheme discriminating between snow and bare-ice was applied based on surface albedo. For pixel with albedo values lower or equal to 0.45 (bare-ice), z_0 was assigned as 3 mm and for pixels with albedo higher than 0.45 z_0 was assigned as 1 mm (snow). Various studies have estimated the sensitivity of z_0 and impacts on the estimated turbulent fluxes, as underestimated z_0 values will result in underestimation of turbulent fluxes and vice versa (Denby and Greuell, 2000; Schmidt et al., 2017).

All fluxes were evaluated at the surface, and fluxes towards the surface were defined positive. Potential melt water was defined as the direct conversion of melt energy into water equivalent using latent heat of fusion (0.26 mm day^{-1} per W m^{-2}).

4 Validation

4.1 Energy balance components

The down-scaled energy balance components used for calculations, daily incoming solar radiation (SW↓), incoming longwave radiation (LW↓) and air temperature from WRF were validated with in situ data. Figure 2 shows comparison of observed and simulated daily air temperature at 2 m height, SW↓ and LW↓ for the different WRF model configurations, RAV2, ICEB and FCST. Generally, for the whole validation period, from 1. April to 30. October each year, the results show a good agreement, both visually and statistically for all configurations and are within ranges reported by (Schmidt et al., 2017). Table 2 shows the validation results for the whole validation period, similar to Figure 2 but also for each month within the full period.

For air temperature R^2 range from 0.83, 0.93 and 0.94 for the RAV2, ICEB and FCST configurations, respectively, for the whole period from April through October. For all configurations, both for the full period but as well monthly intervals, the temperature bias was slightly negative in the range of -0.27 to -1.15 ° K. The smallest bias values were observed in July and August with slightly higher values closer to spring. The consistent negative bias indicates that the model slightly overestimates air temperature.

SW↓ RMSE ranged from 24 to 62 W m^{-2} with the highest values during summer consistent with the summer solstice. For RAV2 the bias was mostly positive ranging from 9 to 25 W m^{-2} with the exception September and October with slightly negative bias values. The lower and negative values might be related to larger solar zenith angles as less incoming short-wave energy was available. During these months the contribution to melt from short-wave radiation was generally limited. For both ICEB and FCST RMSE values were similar to results for RAV2 but bias values were more consistently negative. In this comparison, much fewer sites were available for validation since the limited temporal range of the ICEB and FCST configurations.

LW↓ agreement was good, with RMSE from 9 to 16 W m^{-2}, R^2 ranging from 0.44 to 0.86 and a general negative bias from -2 to -18 W m^{-2}, with the exception of a mean bias of -16 W m^{-2} in April for RAV2. These outlying values might be related to the fact that spring maintenance to the ICE-GAWS stations generally happens late April or early May. The mean bias was consistently the highest in April for all WRF configurations and generally lowers into the summer months. The instrument reported uncertainty in daily totals was less than 5 % ($\sim$15 W m^{-2}) for short-wave radiation and less than 10 % ($\sim$30 W m^{-2}) for long-wave radiation which could partly explain some of the discrepancies.

Overall the performance of the different WRF configurations were similar although note must be taken as the data period for RAV2 data spans 19 years while much less data was available for validation of ICEB (2 years) and FCST (2 years) configurations. Individual station comparison reveals no prominent patterns related to station elevation or location. Recent work by Schmidt et al. (2017) reported similar results when validating HIRHAM5 for surface mass balance calculations for Vatnajökull while recent work by Huai et al. (2020) validating ERA-Interim and ERA5 against the PROMICE weather station network on the Greenland ice sheet reports overall better comparison for the same statistical parameters. One explanation of the difference might relate to the lower overall cloud cover over the Greenland ice sheet compared to glaciers in Iceland impacting weather simulations. Another explanation might relate to the fact that PROMICE short-wave radiation data are post-processed to adjust for station tilting as inaccurate measurements in clear-sky conditions are expected, providing better comparison (Van As, 2011; Fausto et al., 2021). Validation of MODIS albedo was done in Gunnarsson et al. (2021) and Gascoin et al. (2017) for glaciers in Iceland.

5 Results

5.1 Surface energy balance seasonal and inter-annual variability

Inter-annual surface energy balance (SEB) variability for Icelandic glaciers were generally high. Figure 3 shows the spatial patterns for melt energy for the investigated glaciers over the period 2000–2021 for individual months in the extended melt season (AMJJA) and the extended melt season mean (AMJJA). Spatially, the highest melt energy was observed where the winter snow cover is generally completely ablated during summer, revealing dirty and impurity-rich ice. Lower melt energy values were found in the accumulation areas associated with higher elevations and a shorter period of positive surface-energy balance during the melt season. In April, limited melt occurs, although in areas near the terminus at north and south Vatnajökull outlets and low lying outlets of Mýrdalsjökull, between 10 and 15 % of the total melt energy was observed. At the northern

outlets of Vatnajökull, winter snow thickness is generally shallower than for other outlets, exposing impurity-rich ice with low albedo sooner, enabling greater amounts of the incoming short-wave radiation to be forced at the surface. At the lower elevations of Vatnajökull southern outlets, some extending down to sea level, average winter and spring temperatures are higher, inducing earlier melt out of winter snow, exposing impurity-rich ice and portions of the ablation area in April. In spring and early summer, the positive SEB contributes to the warming and ripening phase of the winter snow before the melt output phase contributing to melt can commence. The highest daily amounts of incoming short-wave energy occur in June and July providing the largest quantities of melt energy associated with small solar zenith angles. As more impurity-rich ice was exposed in the ablation area, with lower surface albedo as the melt season progresses, more incoming short-wave energy was available at the surface, even in August with increasing solar zenith angles. Gunnarsson et al. (2021) revealed that lowest observed albedo values in the accumulation area generally occur early to mid-August prior to precipitation falling as snow, and thus higher albedo, reducing short-wave net radiation (SW_{net}).

Figure 4 shows the average SEB (MJJA) and its main components as function of elevation in 100 m bands for the six largest ice caps and their sub-areas defined in Figure 1. For all the glaciers, SW_{net} was the major SEB component for melt energy while LW_{net} was generally an energy sink. The sensible heat flux (SHF) was an energy source in the lower ablation area, generally decreasing with elevation as air temperatures decreases. Latent heat flux (LHF) was quite small in all cases with much less variability with elevation than other melt energy components. For Vatnajökull, SW_{net} diminishes on average -6.45 W m^{-2} per 100 m with lower gradients for the north-east and north-western outlets (-8.95 and -11.1 W m^{-2} per 100 m), respectively. For Hofsjökull lower values were observed for the south-west outlets (-9.0 W m^{-2} per 100 m) while -6.8 to 8.0 W m^{-2} per 100 m for the south-east and northern outlets, respectively. At Langjökull the north-east and north-west outlets have lower gradients (-9.2 and -10.1 W m^{-2} per 100 m) than the southern outlet (-8.7 W m^{-2} per 100 m). The smaller glaciers had similar average values,-8.2, -5.9, and -6.0 W m^{-2} per 100 m for Eyjafjallajökull, Mýrdalsjökull and Drangajökull, respectively.

Variation of SW_{net} with elevation, depends strongly on albedo, generally increasing with elevation, as impurity-rich ice was exposed later in the melt season or not at all, in the accumulation area. Albedo evolution in the accumulation area, throughout the melt season, was mainly driven by climatology, i.e. snow metamorphosis, not light-absorbing particles although events of sand- and dust deposits could be observed in the albedo data for individual years, impacting SW_{net}. Albedo gradients from Gunnarsson et al. (2021), follow similar patterns with elevation as SW_{net}, for all the glaciers. Cloud cover also influenced SW_{in}, generally increasing slightly with elevation, although persistent cloud cover was observed at the terminus at Vatnajökull northern outlets. Spatial distribution of cloud cover has been reported in Gascoin et al. (2017) and Gunnarsson et al. (2021). LW_{net} was negative (energy sink) for all the glaciers, generally decreasing with elevation. The variability was much less than for SW_{net}, ranging from -1.8 to -0.2 W m^{-2} per 100 m. SHF has similar changes with elevation as LW_{net}, reduction of -1.62 to 0 W m^{-2} per 100 m, with limited elevation variability for Mýrdalsjökull and especially Drangajökull. LHF fluxes were small in all cases, with non-significant elevation dependency.

Figure 5 shows the variation of average monthly melt energy anomaly and albedo anomalies in 100 m elevation bins for Vatnajökull, spanning individual months from April through September for the study period. The anomalies show deviations from the period mean for each month and elevation bin. In years with high summer ablation, a certain pattern was observed relating

to high elevation melt anomalies, i.e. increased melt energy in the accumulation area, with more melt energy contribution. The bare-ice areas generally reach a certain lower limit of albedo (0.1 to 0.25) limiting further radiative forcing, although the timing of bare-ice exposure was important. Figures B1 to B5 in the Appendix show similar patterns for other glaciers studied.

The figure shows that in 2010 and 2011, tephra deposits in the upper elevations, from the eruptions in Eyjafjallajökull (2010) and Grímsvötn (2011), greatly enhanced radiative forcing. In 2012, below average cloud cover, extensively enhanced SW_{in} radiation forcing, while some residual effects from tephra fallout in 2010 and 2011 were possible., increasing SW_{net}. Positive melt energy anomalies at lower elevations in 2015, 2016 and 2017 were related to rapid lowering of albedo associated with warm southerly winds and precipitation in the first months of the melt season. Much colder temperatures and cloudy periods followed, constraining melt energy during the rest of the melt season. The high surface energy balance in 2019 was modulated by negative albedo anomalies, resulting from extensive LAPs deposits from the near pro-glacial areas. This extended the actively melting areas, higher into the usual accumulation zone, contributing more to the summer ablation by increasing melt at higher elevations. The year 2021 was unusual, as May and the first three weeks of June where highly influenced by clear skies but cold temperatures which reversed completely late June, with warm western and southerly winds and clear skies through August.

Figure 6 shows the surface energy balance for the study period and the decomposition into different surface energy balance components, with melt season mean cloud cover and albedo anomalies. The SEB variability between melt seasons is mostly explained with SW_{net} variability while LW_{net} and SHF partially explain the variance. As shown in Figure 4 the latent heat flux had limited contribution to melt energy. SW_{net} was the dominant melt energy source for all locations studied contributing the majority of melt energy. LW_{net} acts as an energy sink, ranging from -20 to -30 W m^{-2} with variability between the glaciers investigated around 4 W m^{-2}.

The figure shows that for Vatnajökull the melt season average SEB components were 97 (σ: 14.5), -30 (σ: 4.2), 16.6 (σ: 2.1) and 2.7 (σ: 1.1) W m^{-2} for SW_{net}, LW_{net} , SHF and LHF for the period, respectively. If 2010 and 2011 were excluded, the SW_{net} was 92 (σ: 10.5) due to the enhancement effects of the volcanic eruptions for those years and the average energy available for melt was 85 W m^{-2} for Vatnajökull. Smaller values were observed for Drangajökull and the north-east outlet of Vatnajökull. Higher SW_{net} were observed at the south-coast glaciers (Mýrdalsjökull, Eyjafjallajökull), which tend to have very low albedo values and earlier onset of melt in spring. The south-coast glaciers were also close to unstable dust hotspot areas where seasonal snow melts out earlier than in the highlands, exposing erosive surfaces. Vice versa, cloud cover was generally higher for the south-coast glaciers, as well as at the coastal Drangajökull in the northwest, with cloud cover ranging from 75–82 %, while less cloud cover, ranging from 70–74 %, was observed for the inland glaciers and their outlets, Vatnajökull (except SE outlets), Langjökull and Hofsjökull. SW_{net} was highly affected by both cloud cover and surface albedo; lower albedo and cloud cover values were observed for areas of high annual melt energy. SW_{net} correlates strongly with the average surface albedo, (Pearson Correlation Coefficient, PCC: -0.85), where a general increase in albedo and therefore lowering SW_{net} was reduced with longitude. (Gunnarsson et al., 2021). However, a non-significant relationship was found between cloud cover and LW_{net} (PCC: 0.72 for Vatnajökull).

Figure 7 shows the monthly average distribution of surface energy balance components and melt energy for the glaciers studied. Generally for all glaciers the SW_{net} and the melt energy was highest in July with Drangajökull as the exception, with similar SW_{net} values in June and July. This can be associated with less impurities in the exposed bare ice, compared to the other main glaciers, closer to volcanic activity and dust hotspots.

SW_{net} had the highest variability in June and July associated with the extent of bare-ice areas, driven by melt intensity in the following spring, and previous winter snow depth. In April, both the cold content of winter snow limits available melt energy to produce melt water and winter snow still covers the impurity-rich ice in the ablation areas. LW_{net} was negative for all months at all locations with a slight decrease (less negative) for the latter half of the melt season (JAS). Turbulent fluxes had small variability between months for the averages presented, while SHF however often had peaks associated with events or prolonged periods transporting warm air enhancing melt.

5.2 Impacts of volcanic eruptions and other LAPs events

Over the study period, three volcanic eruptions were observed in glaciated areas with extensive LAP deposits, affecting the surface energy balance. In November 2004, an eruption in the sub-glacial volcano Grímsvötn, lasting 7 days, produced an estimated 0.06 km^3 bulk volume of tephra. The tephra deposits from the eruption were mainly distributed north-east of Grímsvötn in a narrow plume (Oddsson et al., 2012). In 2010, an eruption in Eyjafjallajökull started on April 14th and lasted 23 days. The tephra plume, carrying an estimated volume of 0.27 km^3 of tephra, was mostly directed towards south and south-east (Gudmundsson et al., 2012). During the last days of the eruption, a short period of diverse wind directions brought notable LAP deposits to all the major glaciers. A second eruption occurred in Grímsvötn May 21st 2011, lasting 7 days and releasing an estimated 0.8 km^3 of basaltic tephra. The tephra deposits were mostly distributed south and south-west during the eruption but a thin layer was noticeable on all of western Vatnajökull, and regions in the south-east (Hreinsdóttir et al., 2014). The onset of the 2010 and 2011 eruptions in early spring, maximized their impact on melt, as the LAPs could enhance radiative forcing for almost the whole melt season while the tephra deposits in the fall 2004 were quickly buried in the winter snow.

Figure 8 shows surface energy balance anomalies as deviations from the period mean. The 2004 eruption in Grímsvötn and the associated LAP deposits had some, though very limited impact on ablation, since it took place in the fall, prior to the build up of the winter snow-pack. In the following melt season (2005), impacts of the tephra deposits were observed at Vatnajökull. For Vatnajökull, the increase in SW_{net} was 15 % above the mean SW_{net} energy over the period. The impacts were notable in the northern and south-east outlets with 20-27 % SW_{net} above the mean of the study period. In the south-west Vatnajökull, SW_{net} was very close to the period mean, with an 1 % increase, indicating limited impacts of the 2004 LAP deposits. The discrimination between tephra deposits from the eruption and loading of LAPs from other sources during the summer of 2005 is complex and perhaps the extensive SW_{net} in the south-east Vatnajökull was a combination of both, i.e. added LAPs from dust hotspots in the northern highlands during the melt season and LAPs from the eruption. For Langjökull, Hofsjökull and Eyjafjallajökull SW_{net} was below average, indicating that influences of the LAPs deposits from the eruption was negligible. The north-east outlet at Mýrdalsjökull had an increase in SW_{net} , more likely due to dust from surroundings hotspots rather than residual effects from the eruption in 2004.

The figure shows for the period from 2000 to 2021, with the exception of Drangajökull, the highest MJJA melt energy was observed in 2010, associated with a warm cloud free summer and SW_{net} amplification due to LAP depositions from the Eyjafjallajökull eruption, generally lowering albedo. For Vatnajökull, the increase in SW_{net} was 25 % above the mean SW_{net} over the study period. For the south-western Vatnajökull, the SW_{net} was 33 % above the period mean, while 20, 29 and 16 % for north-east, north west and south-east outlets of Vatnajökull, respectively. At Hofsjökull, increase in SW_{net} was about 35 % for the whole glacier with the highest anomaly 44 % for the south-east outlet. Lower SW_{net} enhancements were observed at the northern parts of Hofsjökull, 29 % and the south-west outlet had an increase of 36 %. The impacts for Langjökull were similar as for Hofsjökull, with increase in radiative forcing higher for the southern outlets and the north-east (42 % and 43 %) but less for the north-facing outlet (29 %). The spatial variations in radiative forcings were mostly explained by the distribution of the volcanic ash plumes transported from Eyjafjallajökull in mid-May 2010 (Gunnarsson et al., 2021). For Mýrdalsjökull and Eyjafjallajökull, the impacts on SW_{net} had generally less spatial variability, explained by the proximity to the LAP origin and the relative size of these glaciers. For Mýrdalsjökull, the average short-wave radiative forcing increase was 45 %, and 55 % for Eyjafjallajökull. On extensive areas of these glaciers, the tephra layer was thick enough to isolate the surface (larger than 2 cm) and limit the use of melt energy to produce melt water.

In 2011, LAP from the May sub-glacial eruption in Grímvötn enhanced short-wave radiative forcing, mostly influencing the south-west and south-east outlets of Vatnajökull. The melt energy anomaly (compared to the average melt season) at south-west Vatnajökull was 47 %. At the north-east outlet, SW_{net} was slightly below average (99 % of mean) but the south-east and north-west observed some melt enhancement, 10 and 7 %, respectively. For Hofsjökull and Langjökull, similar SW_{net} increase was observed, ranging between 14-22 % with less spatial variability than for the previous year. For Mýrdalsjökull and Eyjafjallajökull, smaller average melt enhancements were seen, 16 and 25 %, respectively. A major climatological difference between 2010 and 2011 relates to the much higher average cloud cover in 2011 influencing SW_{in} and generally lower air temperatures, reducing the melt enhancement potential from LAPs in 2011, compared to 2010. For both 2010 and 2011 limited impacts on SW_{net} forcing were observed for Drangajökull, indicating limited impacts of LAPs from the 2010 and 2011 eruptions.

In late April 2019, rapid melt-out of seasonal snow in the highlands was observed. This was followed by favorable conditions for airborne LAPs, from dust hotspots and pro-glacial areas, enabling wast LAP deposits on glacier surfaces, with the associated lowering of albedo and potential for enhancing radiative forcing. For Vatnajökull SW_{net} was 12 % above average with 3, 8 and 7 % SW_{net} above mean for north-east, north-west and south-east, respectively , but 18 % for the south-west outlet. For Hofsjökull SW_{net} was 16 % above average with 10, 20 and 14 % SW_{net} above the mean for north, south-east and north-west outlets, respectively. At Langjökull the values were somewhat higher, where SW_{net} was 23 % above average with 21, 20 and 25 % SW_{net} above the mean for north-east, north-west and south outlets, respectively. For Mýrdalsjökull, SW_{net} was 12 % over the average, 26 % for Eyjafjallajökull and 10 % for Drangajökull. In 2019 cloud cover was generally slightly above average (more clouds) with a colder than average spring, but a dry warm spell in midsummer.

5.3 Melt enhancement due to volcanic eruptions and other LAPs events

The impacts of the high LAP deposits in 2004, 2010, 2011 and 2019, was assessed to better understand impacts on melt energy. The affect on SW_{net} forcing, was estimated by comparing the surface energy balance, assuming mean albedo for the study period (2000 – 2021), to the energy balance estimated using the observed albedo in 2010, 2011 and 2019, utilizing the same climatology forcings for both albedo scenarios. The estimated difference in SW_{net} forcing, from the observed albedo scenario and the study period mean albedo scenario, were denoted as the SW radiative forcing from LAPs (SW^{f}_{LAP}) and refers to the forcing difference in W m^{-2} above the study period mean values. The difference in melt potential, due to the additional radiative forcing from LAPs, was defined as the direct conversion of SW^{f}_{LAP} into water equivalent using latent heat of fusion (0.26 mm day^{-1} per Wm^{-2}) and was refereed to as SW^{mm}_{LAP}. This approach does not fully consider all physical processes, e. g. as it did not take into account the effect on albedo of different snow metamorphosis processes between years, timing of melt out of impurity-rich ice but in this comparison, these processes were secondary to the overwhelming impact LAPs had on the albedo, especially in 2010 and 2011. Additionally the impacts to turbulent fluxes were ignored as they are considered negligible.

Figure 9 shows the evolution on monthly timescales how the SW^{f}_{LAP} (converted to mm) evolved for these selected years from April to September. In 2005 the SW^{f}_{LAP} was 4.3 W m^{-2}, here associated with the November 2004 eruption in Grímsvötn, yielding a 211 mm SW^{mm}_{LAP} for the AMJJAS period. The sharp increase in SW^{mm}_{LAP} in July was associated with tephra layers melting out of the winter snow in the lower accumulation areas. Other glaciers did not experience a SW^{f}_{LAP} increase with the exception of Drangajökull, unlikely caused by LAPs from the 2004 Grímsvötn eruption. Figure 8 shows the distribution of melt energy indicating that the south-west outlets of Vatnajökull experienced limited impact. In a similar manner the melt potential increase for Mýrdalsjökull, mainly focused on the north-east outlet, was unlikely linked to LAPs from Vatnajökull.

For Vatnajökull the SW^{f}_{LAP} was 18.4 W m^{-2} in 2010, i.e. the estimated additional radiative forcing due to LAPs compared to the long term average for AMJJAS. This corresponds to 892 mm of SW^{mm}_{LAP} for the AMJJAS period. Extensive SW^{f}_{LAP} increase was seen for all the major glaciers in 2010 with the exception of Drangajökull. SW^{f}_{LAP} from LAPs was 27.3, 27.7, 44.6 and 53.2 W m^{-2} for Hofsjökull, Langjökull, Mýrdalsjökull and Eyjafjallajökull, respectively. As expected, the impacts were most extensive at Eyjafjallajökull and Mýrdalsjökull due to the proximity of the eruption and LAPs source. Drangajökull was the exception to these extremes with a slight increase in SW^{f}_{LAP}, 2.5 W m^{-2}, making the impacts of LAPs deposits limited associated with the 2010 eruption. Further increasing the LAPs potential impact on melt energy, 2010 had cloud cover well below average.

The Grímsvötn eruption in 2011, had the most impact on Vatnajökull, notably the south-western outlets. The impact was similar as in 2010 with SW^{f}_{LAP} as 19.1 W m^{-2} (925 mm of SW^{mm}_{LAP}). For other glaciers the impact was much less than in 2010. For Eyjafjalljökull and Mýrdalsjökull the impact was more likely related to the huge quantities of tephra deposits from the 2010 eruption than additional LAPs from the 2011 Grímsvötn eruption. For Langjökull and Hofsjökull the SW^{f}_{LAP} was 8.6 and 8.8 W m^{-2} (415 and 425 mm of SW^{mm}_{LAP}), respectively. As previously mentioned, the melt season in 2011 had a alternative climatology than the previous year with cloud cover above average and lower air temperatures, not fully utilizing the

melt enhancement potential from the LAPs deposited. The wast quantities of tephra transported in 2010, to glaciated surfaces as well as deposited outside glacier covered areas, likely had a residual effect in 2011. SW^f_{LAP} was negative for Drangajökull in 2011.

The large observed LAPs in 2019 yielded a significant SW^f_{LAP} for all glaciers. For Vatnajökull the SW^f_{LAP} was 7.0 Wm^{-2} (341 mm of SW^{mm}_{LAP}), 12.9 Wm^{-2} (624 mm SW^{mm}_{LAP}) at Langjökull and 8.4 Wm^{-2} (407 mm of SW^{mm}_{LAP}) at Hofsjökull. At these glaciers the SW^f_{LAP} was higher in the early melt season with less impact in July and August, partially linked to frequent snow fall events in mid- and late-August increasing albedo and reducing SW_{net}. At Drangajökull the SW^f_{LAP} was the highest for the years studied, resulting a SW^f_{LAP} of 5.6 Wm^{-2}, yielding 245 mm of SW^{mm}_{LAP}.

Care must be taken when interpreting results from areas where the thickness of volcanic tephra deposits was thick enough to isolate the surface. This was the case for Eyjafjallajökull and Mýrdalsjökull in 2010 and very probably in the following years providing partial isolation of the surface. In 2011 parts of the glacier surface around Grímsvötn in Vatnajökull were isolated, but as this occurred mostly in the accumulation area the post-years effect was likely limited. Limited data were available to fully estimate where isolation might have occurred and to fully represent the problem, more complex modeling is needed.

5.4 Melt energy relationships with large-scale circulation variability

To understand the processes driving melt season and inter-annual SEB variability for Icelandic glaciers the SEB was combined with various large-scale circulation patterns, sea surface temperature and cloud cover. Statistical relationships were calculated as Pearson's Correlation Coefficient (PCC) and significance was tested at p = 0.05.

Figure 10 shows MJJA averages for the data compared for Vatnajökull while Figure C1 in the Appendix show similar data for the other glaciers analyzed. Figure 10a show the relations between forced short-wave radiation to the surface, SW_{net}, incoming short-wave radiation, SW_{in}, albedo, α and cloud cover, CC for the six glaciers studied. The series were extracted for each glacier and are shown as anomalies from the mean. over the study period 2000-2021.

For the period 2000–2012 cloud cover was overall below the period average (V: 68.5 %, H: 70.2 %, L: 71.3 %, E: 77.6 %, M: 73.8 % and D: 74.6 %) as well as albedo for the MJJA average (V: 52.8 %, H: 52.1 %, L: 50.4 %, E: 41.0 %, M: 37.4 % and D: 55.9 %). The eruption years in 2010 and 2011 had a big impact on the MJJA averages of albedo but no influence on cloud cover. By excluding 2010 and 2011 in the averages for albedo, albedo at Vatnajökull, Hofsjökull and Langjökull were 1.6 – 2 % higher and 3.5 and -4 % higher for Eyjafjallajökull and Mýrdalsjökull, respectively. At Drangajökull the impact of excluding 2010 and 2011 resulted in 0.3 % lower average albedo and considered unimportant. These changes in albedo were also reflected in higher SW_{net} values for potential melt.

For the period after 2012, cloud cover was on average higher (V: 3.7 %, H: 3.3 %, L: 3.1 %, E: 2.1 %, M: 3.1 % and D: 5.2 %, percent shown as increase between 2000–2012 and 2013–2021). For albedo, similar changes were observed for all glaciers, an average observed increase in albedo of 1.5 % excluding the years of 2010 and 2011, shown as a increase between 2000–2012 and 2013–2021 periods (V: 2.5 %, H: 1.4 %, L: 1.1 %, E: -0.3 %, M: 2.1 % and D: 2.2 %, percent). The difference increased further 1.5–3.5 % by including eruption years. The post-effects on albedo, of the 2004 eruption in Grímsvötn in melt season 2005 was not considered, since the impact was mostly observed locally in northern Vatnajökull. No significant trends for MJJA

averages were found for in the data due to the high variability in the data. High cloud cover in 2015 and 2018 coincides with the only years with positive observed surface balance (Pálsson et al., 2020a).

For Vatnajökull, Hofsjökull, Langjökull and Mýrdalsjökull a strong causal relationship with significant correlation was found between cloud cover and incoming short-wave radiation (PCC: -0.58, -0.43, -0.57 and -0.51, respectively). Although non-significant, a similar but less correlation was observed for Drangajökull and Eyjafjallajökull. Since clouds primarily reflect solar radiation, especially low thick clouds, this relationship was anticipated. Between SW_{net} and SW_{in} there was also significance relationship for all glaciers, anticipated as well, since these values are not independent and correlated through albedo. Relations for all glaciers to albedo and SW_{net} was also highly significant (p>0.0001) since albedo modulates the net energy constrained at the surface.

Figure 10b show the Geenland Base Index (GBI), North Atlantic Oscillation (NAO) and Figure 10c shows the sea surface temperature (SST) areas used in the comparison. represented as anomalies from the study period mean. From the time series of GBI and NAO, a large and significant anti-correlation emerges (PCC: -0.94), since the two indices are not independent (Davini et al., 2012). GBI has been associated with less zonal oriented large-scale flow over the North Atlantic. GBI and NAO revealed a correlation to SW_{in}, where GBI had significance to all glacier except Drangajökull. NAO had significance to SW_{in} for all glaciers with the exception of Vatnajökull and Mýdalsjökull. For SW_{net}, GBI and NAO significance was observed for all glaciers. The SST for the selected areas had internal correlation, i.e. correlate to a degree to one and another. SST_S had significant relation to SST_W, SST_E and NAWH (PCC: 0.43, 0.76 and 0.52, respectively). SST_W correlates significantly with SST_N and SST_E and additionally SST_N correlated significantly with SST_E. Correlation between these areas were expected as they describe the same interrelated system of ocean currents. SST at the NAWH was of special interest as the local changes in SST there have been described as a fingerprint of climate change (Rahmstorf et al., 2015) and has been linked to the future evolution of surface mass balance of Icelandic glaciers (Noël et al., 2022). NAWH has significant correlation (PCC: 0.52) to SST_S but not other SST areas for MJJA averages. For other variables studied the NAWH had significant relations to cloud cover for all glaciers, over the MJJA period. For Hofsjökull and Langjökull SST_S also had a significant relationship to cloud cover while other SST areas had no significance to cloud cover. Sea surface temperatures at SST_E, SST_S and NAO showed a significant relationships with the NAWH (PCC: -0.46, -0.78 and -0.65, respectively). GBI holds a significant relationship with SST_S, NAWH, SW_{net} and SW_{in} (PCC: 0.71, 0.52, 0.52 and 0.45, respectively) Prior to 2010 sea surface temperatures at NAWH has an anticorrelation with the other SST areas investigated but after 2010 all SST areas follow more similar patterns. These periods align to some extent with higher albedo and cloud cover average values after 2012 resulting in less short-wave energy forced for melting. The correlation relationship between sea surface temperatures and cloud cover (significant at NAWH and SST_S) instigates the modulating control sea surface temperatures has on cloud cover, impacting incoming short-wave radiation.

The extent of natural variability and anthropogenic forcing effects of the formation and sustaining of the NAWH anomaly has been studied by many (Rahmstorf et al., 2015; Alexander et al., 2018; Gervais et al., 2019; Keil et al., 2020). It has been linked to the declining Atlantic Meridional Overturning Circulation (AMOC), a part of a global ocean circulation network that transports heat all around the world and has significant effect on climate in Iceland (Caesar et al., 2018; Björnsson et al.,

2018). Keil et al. (2020) have suggested that more low-level clouds are being produced due to cooler sea surface temperatures at NAWH, leading to reductions in incoming solar radiation and further surface cooling. With more Arctic sea ice melting and melting of the Greenland ice-sheet more fresh water flows into the Labrador Sea leading to a reduction in the deep ocean convection, amplifying the atmospheric and oceanographic processes creating the NAWH (Rahmstorf et al., 2015; Alexander et al., 2018; Gervais et al., 2019; Keil et al., 2020). Noël et al. (2022) simulated surface mass balance of Icelandic glaciers under a future high-end warming scenario where mass loss of Icelandic glaciers is mitigated by North Atlantic cooling until the mid-2050s.

6 Conclusions

In this study, melt season surface energy balance for Icelandic glaciers was estimated using high resolution meteorological climate forcing and remotely sensed glacier surface albedo from the MODIS sensor for the melt season from 2000-2021 at a 500 m spatial resolution. The calculation framework was applied to all glaciers in Iceland larger than 8 km^2 but results are presented for the largest glaciers, Vatnajökull, Langjökull, Hofsjökull, Mýrdalsjökull, Eyjafjallajökull and Drangajökull.

The main results show the large melt season and inter-annual variability in surface energy balance for Icelandic glaciers. The variability was influenced by high climate variability, LAPs from tephra deposits from volcanic eruptions and dust hotspots from sources and pro-glacial areas close to the glaciers. Dust hotspots are subject to wind erosion and production of LAPs that can be transported over long distances.

Due to the high variability no significant trends were found, neither in data driving the model nor in the model output data. Details of spatio-temporal patterns were provided as well as relations to elevation and distribution of melt energy with elevation between years. The main energy melt source was from short-wave radiation modulated by surface albedo and cloud cover, which is in good agreement with previous studies.

The impacts of volcanic eruptions during the period (2004, 2010 and 2011) by effect of dust and tephra deposits on radiative forcing were estimated by modelling the short-wave radiative forcing under observed albedo scenarios during the periods influenced and comparing them to alternative evolution of albedo. The impacts were assessed in terms estimation of additional energy forced for surface melting showing that up to 55 % additional melt energy forcing compared to study period average. Radiative forcing due to LAPs in 2019 due to extensive airborne dust and sand deposits were also estimated yielding a significant impact on the energy balance increasing melt energy significantly compared to the study period average albedo development under the same 2019 climate.

To provide insights into the highly variable surface energy balance, large-scale atmospheric circulation anomalies and patterns were compared to surface energy balance variability. Identification of processes driving surface energy balance through physical atmospheric and oceanographic processes were suggested, mainly the impact cloud cover had on incoming short-wave radiation and the links between sea surface temperatures and cloud cover. Significant relationships were found between the North Atlantic Warming Hole (NAWH), sea surface temperatures south of Iceland and cloud cover over the glaciers studied. This suggest that the amplification of negative sea surface temperature anomalies since 2014 impacts the generation of

low-level clouds that reduce the incoming short-wave radiation. Cloud cover was higher for the period from 2013 – 2021 than 2000 – 2012, on average a 4 % increase was observed between the periods from MJJA averages. The highest increase was for Drangajökull (5.5 %) while 3.8, 4.1, 4.3, 2.3 and 3.6 % for Vatnajökull, Hofsjökull, Langjökull, Eyjafjallajökull and Mýrdalsjökull, respectively.

The methodology applied in the study, based on MODIS products and climate forcing data, can be utilized in near-real time to assess the impacts of LAPs associated with volcanic eruptions and dust storms deposits in ice and snow surfaces, providing insights into melt enhancements. It also allows for short-term as well as long-term monitoring of surface energy balance variations for glaciers in Iceland.

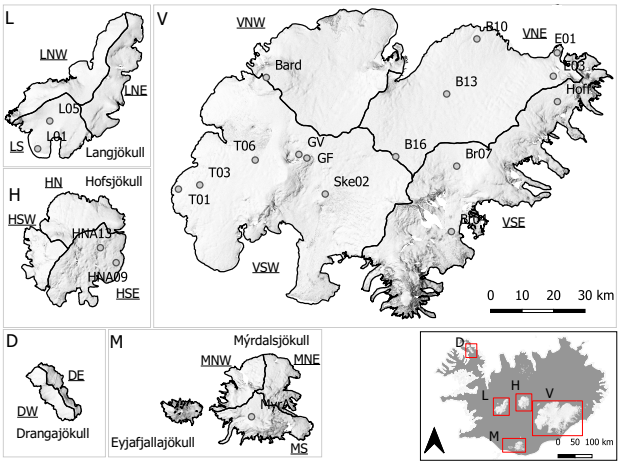

Figure 1. Location map of Icelandic glaciers studied in the study. Vatnajökull, Langjökull, Hofsjökull, Mýrdalsjökull, and Drangajökull are divided into a few main ice flow basins for further detailed analysis. These delineated areas are annotated with underlined text (e.g. NW for northwest). Locations of automatic weather stations (AWSs) are shown with grey dots. Details for the AWSs are given in Table A1. Topographical properties of the ice caps and their sub areas are tabulated in Table 1. The background is shaded relief of Lidar surveyed glacier DEMs (Jóhannesson et al. (2013)) and the catchment delineation are from Magnússon et al. (2016b), for Drangajökull, Björnsson (1988) for Hofsjökull, Björnsson et al. (2000) for Mýrdalsjökull, and Pálsson and Gunnarsson (2015); Pálsson et al. (2020a) for Langjökull and Vatnajökull, respectivly.

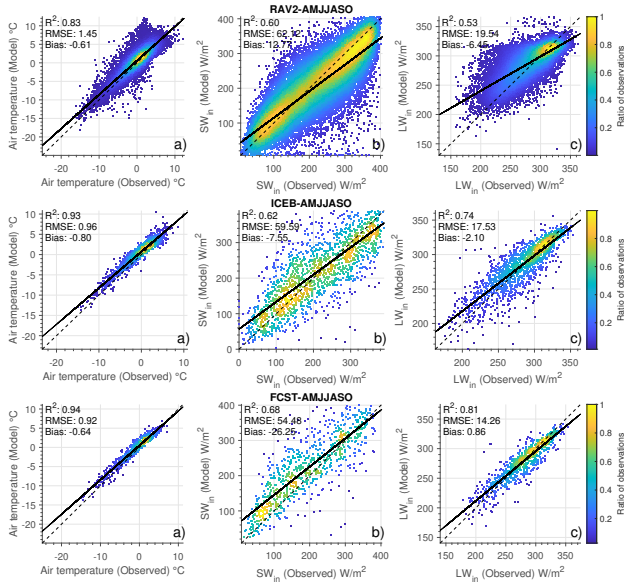

Figure 2. Comparison of the downscaled daily model forcings, 2 m air temperature (a), incoming solar radiation (b) and incoming longwave radiation (c) with ground observations from the GAWS network. Color shows the normalized (0-1) density distribution of data. Dotted black line shows 1:1 and black line the calculated linear fit to the data

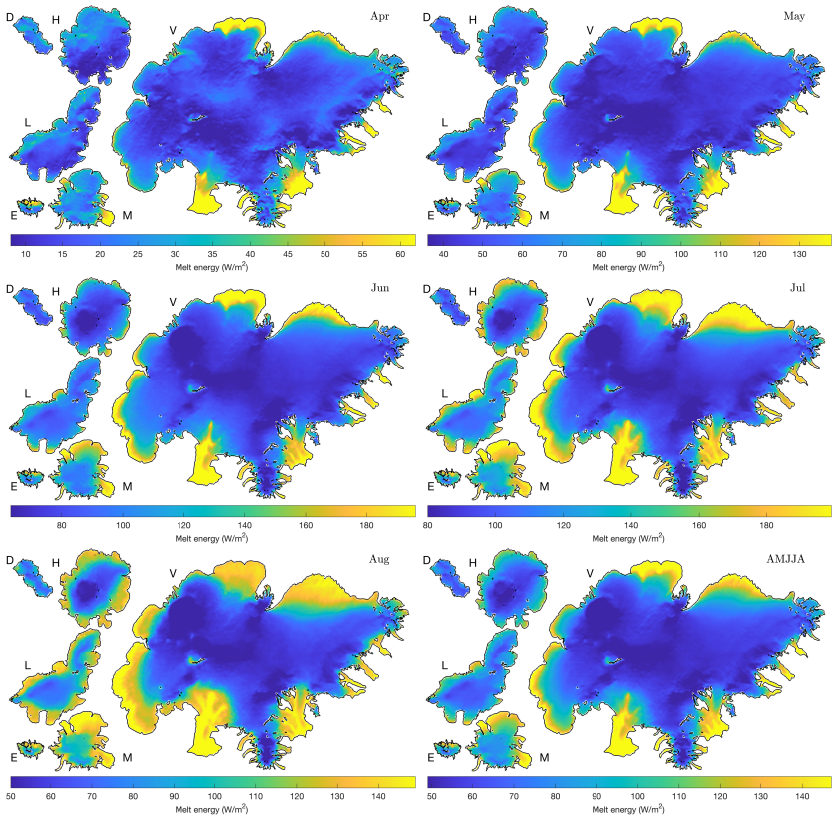

Figure 3. Spatial patterns of mean melt energy for the period 2000–2019 (AMJJA). D: Drangajökull; H: Hofsjökull; V: Vatnajökull; L: Langjökull; E: Eyjafjallajökull; M: Mýrdalsjökull. Note that the color scale varies between months.

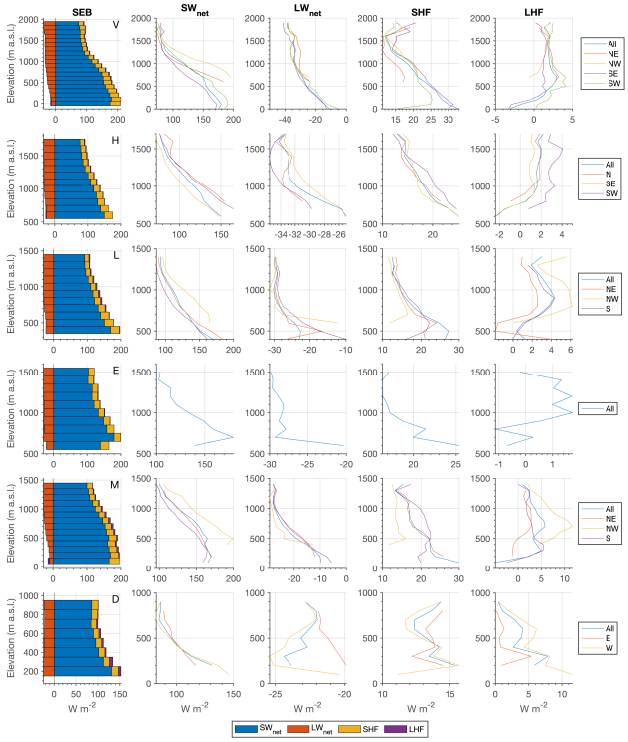

Figure 4. Variation of surface energy balance components with elevation (100 m elevation bins). The first column of images shows the average MJJA energy balance by elevation for the whole glaciers. The other columns show individual SEB components for the glaciers and their main sub-areas as a function of elevation. (Sub-areas are defined in Fig.1). V: Vatnajökull; H: Hofsjökull; L: Langjökull; E: Eyjafjallajökull; M: Mýrdalsjökull; D: Drangajökull;

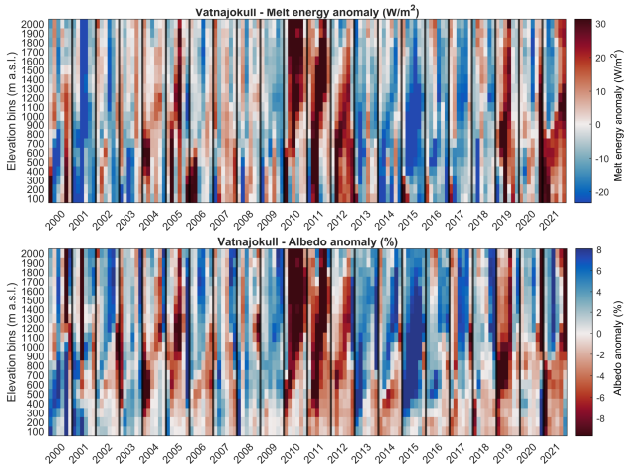

Figure 5. Variation of monthly average melt energy (W m^{-2}, upper panel) and monthly albedo anomalies (lower panel) for Vatnajökull. Elevation (vertical axis) is in bins of 100 m and the horizontal axis shows monthly data for each year from April to September. Black vertical lines separate the years. Figures B1 to B5 in the Appendix show similar figures for other glaciers.

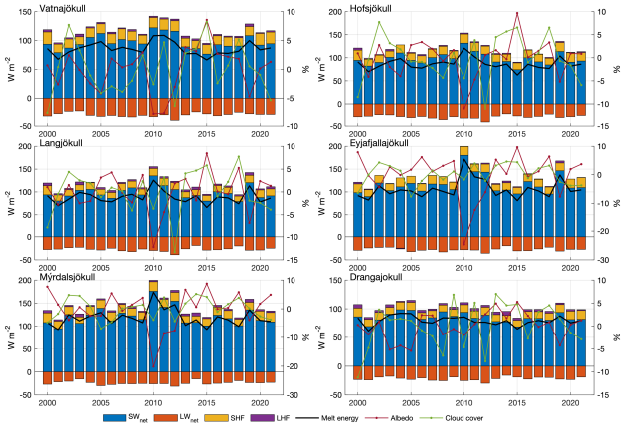

Figure 6. Surface energy balance sources (colored bars) and the available melt energy (solid black line) for the period MJJA 2000 –2021 (left vertical axis). The melt season mean albedo (purple) and cloud cover (green) for each glacier is shown as deviations from the period mean (right vertical axis).

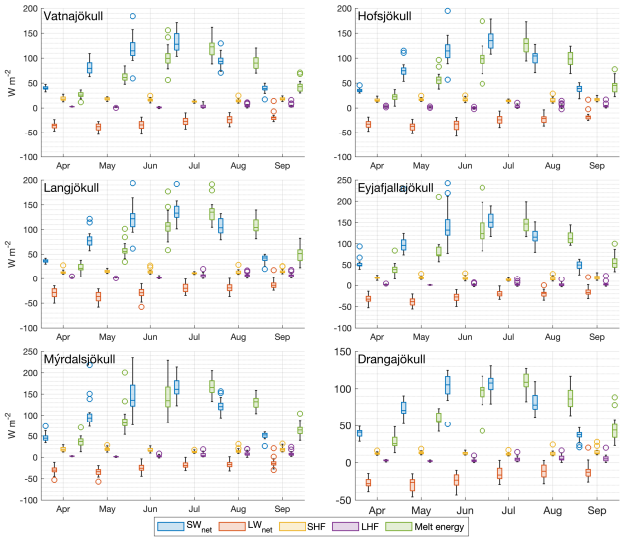

Figure 7. The monthly average distribution of surface net energy balance components and melt energy for the glaciers studied. Circles represent outliers.

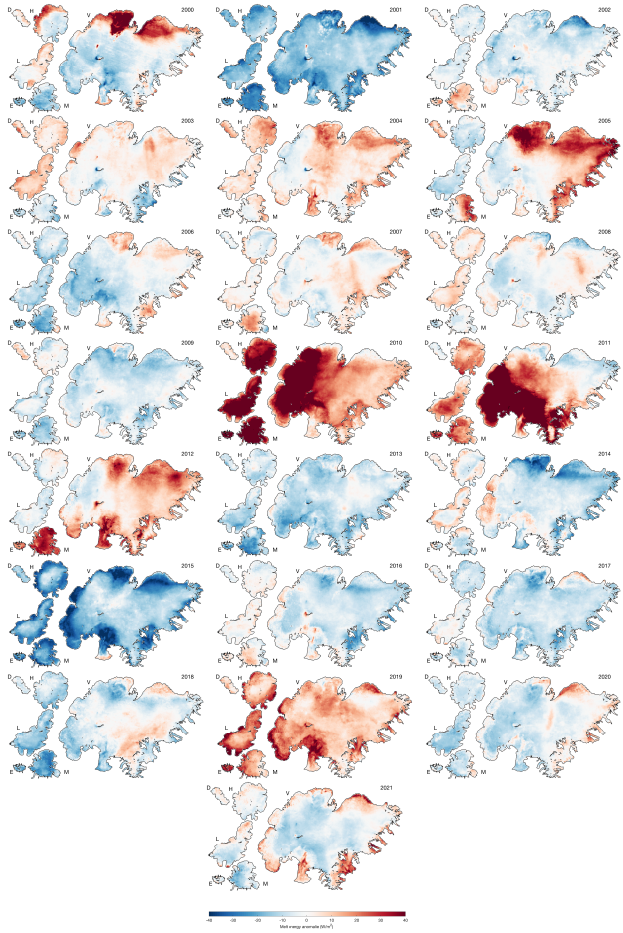

Figure 8. Surface energy balance anomalies from the mean for MJJA 2000–2021. Red colors indicate average melt energy above average (more potential melt energy) while blue colors denote surface energy balance below average.

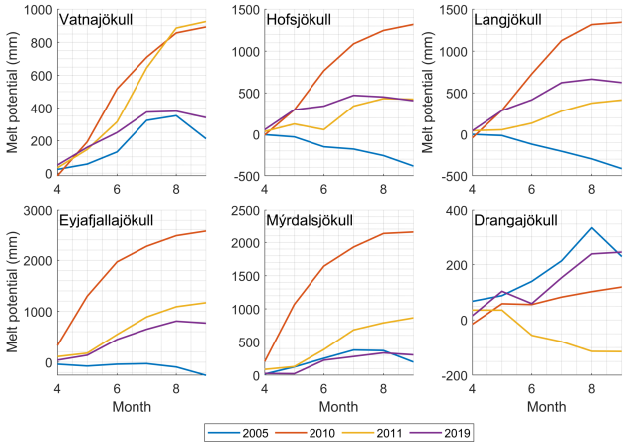

Figure 9. Estimated increase in melt potential (mm of water) due to the effect LAPs had on the surface energy balance in 2005, 2010, 2011 and 2019. Data are shown as the increase in cumulative monthly melt potential due to LAPs, i.e. the difference in melt using historical average albedo (2000-2021 mean excluding 2010, 2011 and 2019 in the mean) and observed albedo for the selected years using the same climatological forcings.

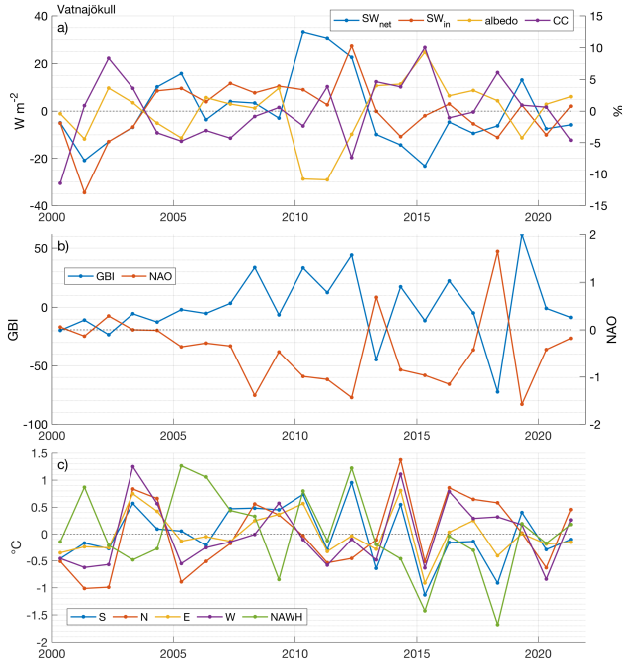

Figure 10. a) Melt season anomalies from the mean (MJJA) for SW_{net}, incoming short-wave radiation, SW_{in}, albedo, α and cloud cover, CC. b) melt season average values (MJJA) for GBI and NAO. c) Sea surface temperatures anomalies from the mean for the selected areas defined in Section 3.4. Data shown for Vatnajökull over the study period 2000-2021.

Table 1. Topographic properties of the 6 main glaciers catchments and their 15 sub-areas. Id column refers to the sub-glacier areas shown in Figure 1. Ratio defines the area percentage of each sub-area with respect to the relevant glacier total area. Elevation data is from Jóhannesson et al. (2013) and glacier area from Hannesdóttir et al. (2020).

Id	Glacier	Area	z_{mean}	z_{max}	z_{min}	Ratio
		km^2	m a.s.l.	m a.s.l.	m a.s.l.	-
	Vatnajökull	7881	1223	2030	0	-
VNE	NE	1669	1229	1888	629	21 %
VNW	NW	1239	1406	1988	729	15 %
VSE	SE	1952	1066	2030	0	25 %
VSW	SW	3051	1225	1994	61	39 %
	Hofsjökull	852	1252	1789	624	-
HN	N	287	1289	1789	830	34 %
HSE	SE	402	1200	1789	637	47 %
HSW	SW	162	1346	1789	735	19 %
	Langjökull	896	1102	1435	419	-
LNE	NE	304	1090	1435	419	34 %
LNW	NW	307	1137	1435	620	35 %
LS	S	284	1020	1400	444	31 %
	Mýrdalsjökull	562	1000	1485	118	-
MNE	NE	151	893	1377	223	27 %
MNW	NW	149	1051	1455	414	26 %
MS	S	271	997	1485	118	47 %
	Drangajökull	144	658	914	213	-
DE	E	52	653	872	297	37 %
DW	W	92	655	914	186	62 %
Eyj	Eyjafjallajökull	79	1156	1564	294	-

Table 2. Summary statistics for daily incoming solar radiation (SW↓), incoming longwave radiation (LW↓), and air temperature from different WRF configurations validated with ground observations. No. sites refers to the number of stations that where available for comparison purposed for each period.

RAV2 data	T (°C)			SW↓ (W m^{-2})			LW↓(W m^{-2})			Period
No. sites	RMSE	R^2	Bias	RMSE	R^2	Bias	RMSE	R^2	Bias	Month
20	1.09	0.83	-0.65	55.61	0.63	14.36	13.44	0.63	-6.50	AMJJASO
4	1.73	0.84	-1.07	82.21	0.26	14.98	9.68	0.44	-16.33	Apr
18	1.10	0.88	-0.86	55.13	0.42	18.58	13.83	0.61	-13.31	May
20	0.90	0.75	-0.66	61.32	0.45	23.42	12.79	0.63	-6.74	Jun
20	0.99	0.56	-0.50	57.92	0.49	25.50	12.57	0.61	-2.86	Jul
19	1.06	0.59	-0.60	47.19	0.55	9.76	12.48	0.60	-3.20	Aug
17	1.11	0.82	-0.53	34.42	0.50	-4.91	13.33	0.55	-4.60	Sep
12	0.77	0.94	-0.43	27.81	0.41	-6.52	11.31	0.55	-4.99	Oct
ICEB data	T (°C)			SW↓ (W m^{-2})			LW↓(W m^{-2})			Period
No. sites	RMSE	R^2	Bias	RMSE	R^2	Bias	RMSE	R^2	Bias	Month
8	0.83	0.94	-0.84	48.28	0.67	-4.78	14.92	0.78	-3.29	AMJJASO
2	0.95	0.94	-0.97	39.70	0.46	2.33	14.90	0.80	-13.84	Apr
8	0.88	0.93	-1.15	51.75	0.39	-6.26	15.64	0.70	-5.09	May
8	0.74	0.92	-0.97	47.38	0.64	-4.06	12.03	0.81	-3.48	Jun
8	0.66	0.75	-0.45	45.04	0.68	10.46	12.49	0.78	-2.11	Jul
7	0.63	0.80	-0.60	44.22	0.55	-16.47	16.18	0.58	3.69	Aug
5	0.84	0.88	-0.96	30.00	0.49	-14.09	15.62	0.73	-3.43	Sep
FCST data	T (°C)			SW↓ (W m^{-2})			LW↓(W m^{-2})			Period
No. sites	RMSE	R^2	Bias	RMSE	R^2	Bias	RMSE	R^2	Bias	Month
7	0.90	0.92	-0.85	47.38	0.62	-16.28	12.26	0.78	-3.95	AMJJASO
1	0.97	0.95	-1.13	25.05	0.80	-0.36	7.50	0.92	-11.63	Apr
7	0.86	0.92	-0.97	45.62	0.46	-27.75	12.58	0.77	-4.38	May
5	0.70	0.89	-0.79	41.55	0.62	-16.14	9.42	0.86	-0.07	Jun
5	0.66	0.60	-0.58	37.63	0.72	-22.63	9.80	0.86	3.05	Jul
5	0.63	0.68	-0.27	37.03	0.61	-36.67	11.47	0.81	6.05	Aug
5	0.70	0.92	-0.43	24.78	0.65	-24.11	11.78	0.84	1.54	Sep

Appendix A: Glacier weather stations location

Table A1. Summary statistics and location information of meteorological stations. Figure 1 shows the location on a map. The three last columns show the number (N) of daily observations available for validation purposes for each variable used.

Lat.	Lon.	Ele.	Site name	N. T_2 obs.	N. SW_{in} obs.	N. LW_{in} obs.
64.538	15.597	1141	Hoff	1688	1774	
64.514	20.450	588	L01	2246	2254	2254
64.302	17.153	1207	Ske02	37	39	39
64.728	16.111	779	B10	3224	3296	3215
64.575	16.328	1216	B13	2043	2725	2338
64.402	16.681	1526	B16	2575	2730	2569
64.417	17.319	1405	Grímsvötn	2687	791	
64.182	16.335	528	Br04	597	600	
64.368	16.282	1242	Br07	395	397	
64.325	18.117	771	T01	483	567	567
64.336	17.976	1068	T03	1943	2586	2094
64.404	17.608	1466	T06	2538	2632	1691
64.639	17.522	1945	Bard	1509	898	
64.406	17.267	1724	Grímsfjall	2495	1324	
63.611	19.158	1345	MyrA	385	413	
64.594	20.374	1095	L05	2536	2544	2544
64.770	18.543	840	HNA09	292	307	307
64.813	18.648	1235	HNA13	294	307	307
64.677	15.581	766	E01	106	121	121
64.611	15.615	1190	E03	115	122	122

Appendix B: Melt energy and albedo variability with elevation

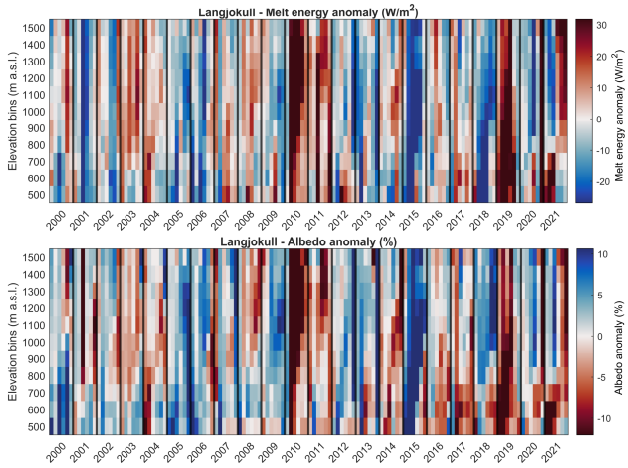

Figure B1. Distribution of melt energy and albedo anomalies (W m^{-2}) with elevation for Langjökull. Vertical show elevation bins in 100 m intervals and horizontal axis shows monthly data for each year from April to September. Black vertical lines separate

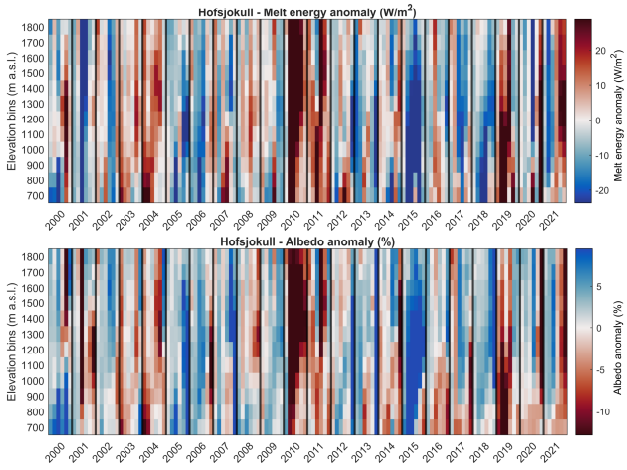

Figure B2. Distribution of melt energy and albedo anomalies (W m^{-2}) with elevation for Hofsjökull. Vertical show elevation bins in 100 m intervals and horizontal axis shows monthly data for each year from April to September. Black vertical lines separate

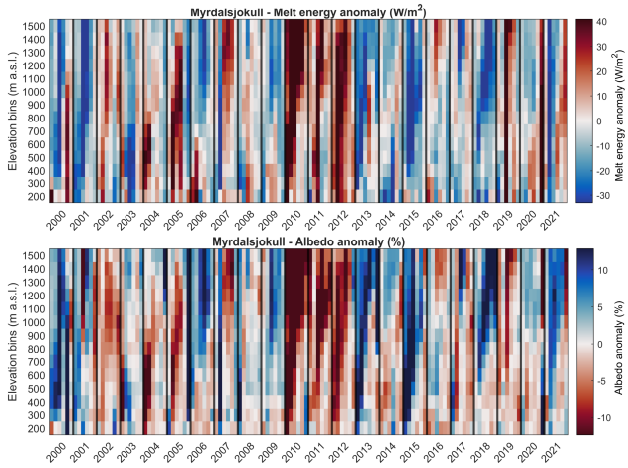

Figure B3. Distribution of melt energy and albedo anomalies (W m^{-2}) with elevation for Mýrdalsjökull. Vertical show elevation bins in 100 m intervals and horizontal axis shows monthly data for each year from April to September. Black vertical lines separate

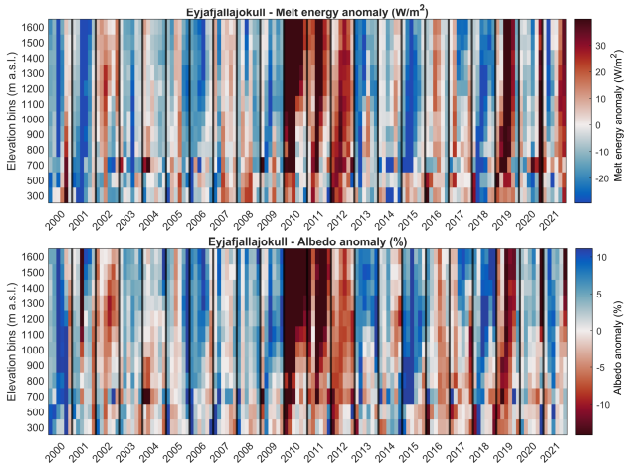

Figure B4. Distribution of melt energy and albedo anomalies (W m^{-2}) with elevation for Eyjafjallajökull. Vertical show elevation bins in 100 m intervals and horizontal axis shows monthly data for each year from April to September. Black vertical lines separate

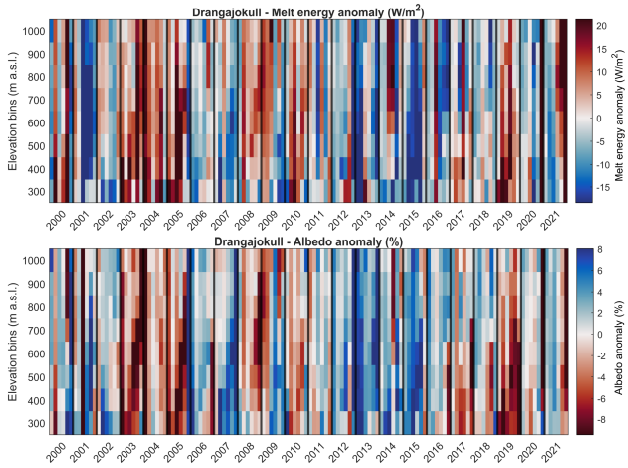

Figure B5. Distribution of melt energy and albedo anomalies (W m^{-2}) with elevation for Langjökull. Vertical show elevation bins in 100 m intervals and horizontal axis shows monthly data for each year from April to September. Black vertical lines separate

Appendix C: Melt energy relationships with large-scale circulation variability

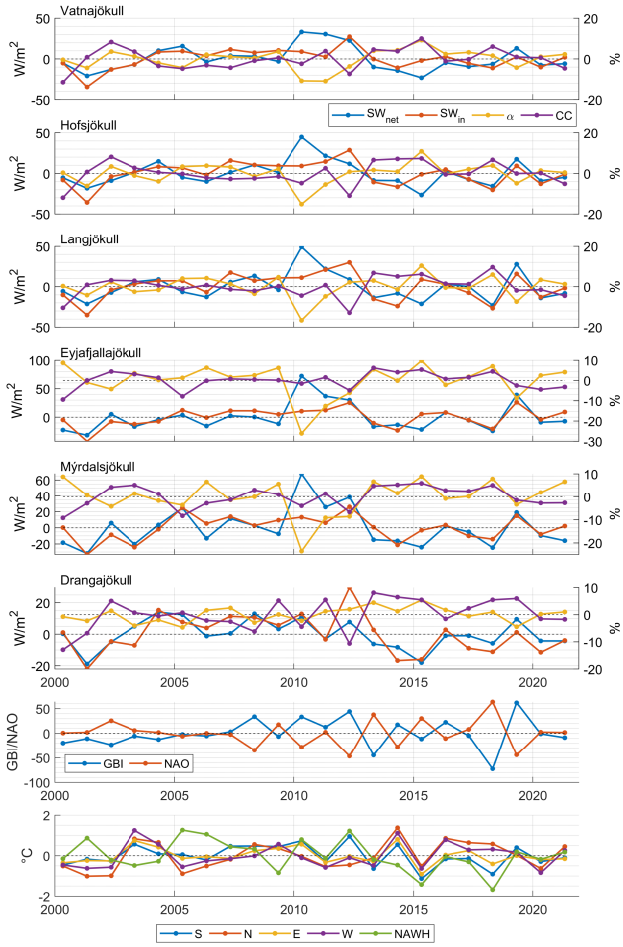

Figure C1. First 6 panels show melt season anomalies from the mean (MJJA) for SW_{net}, incoming short-wave radiation, SW_{in}, albedo, α and cloud cover, CC for the six glacier studied. Panel seven shows melt season average values (MJJA) for GBI and NAO and the bottom panel shows sea surface temperatures anomalies from the mean for the selected areas defined in Section 3.4 Data shown for the study period 2000-2021.

References

Adam, J. C., Hamlet, A. F., and Lettenmaier, D. P.: Implications of Global Climate Change for Snowmelt Hydrology in the Twenty-First Century, Hydrological Processes, 23, 962–972, https://doi.org/10.1002/hyp.7201, 2008.

Ahlmann, H.: Vatnajökull, Scientific Results of The Swedish-Icelandic Investigations 1936-37-38, Geografiska Annaler, 22, 188–205, https://doi.org/10.1080/20014422.1940.11880689, 1940.

Alexander, M. A., Scott, J. D., Friedland, K. D., Mills, K. E., Nye, J. A., Pershing, A. J., and Thomas, A. C.: Projected sea surface temperatures over the 21st century: Changes in the mean, variability and extremes for large marine ecosystem regions of Northern Oceans, Elementa: Science of the Anthropocene, 6, https://doi.org/10.1525/elementa.191, 2018.

Allan, D. and Allan, R. P.: Seasonal Changes in the North Atlantic Cold Anomaly: The Influence of Cold Surface Waters From Coastal Greenland and Warming Trends Associated With Variations in Subarctic Sea Ice Cover, Journal of Geophysical Research: Oceans, 124, 9040–9052, https://doi.org/https://doi.org/10.1029/2019JC015379, 2019.

Arnalds, O., Dagsson-Waldhauserova, P., and Ólafsson, H.: The Icelandic volcanic aeolian environment: Processes and impacts — A review, Aeolian Research, 20, 176–195, https://doi.org/https://doi.org/10.1016/j.aeolia.2016.01.004, 2016.

As, D. v., Broeke, M. v. d., Reijmer, C., and Wal, R. v. d.: The Summer Surface Energy Balance of the High Antarctic Plateau, Boundary-Layer Meteorology, 115, 289–317, https://doi.org/10.1007/s10546-004-4631-1, 2005.

Aðalgeirsdóttir, G., Magnússon, E., Pálsson, F., Thorsteinsson, T., Belart, J. M. C., Jóhannesson, T., Hannesdóttir, H., Sigurðsson, O., Gunnarsson, A., Einarsson, B., Berthier, E., Schmidt, L. S., Haraldsson, H. H., and Björnsson, H.: Glacier Changes in Iceland from 1890 to 2019, Frontiers in Earth Science, 8, 520, https://doi.org/10.3389/feart.2020.523646, 2020.

Bair, E. H., Rittger, K., Davis, R. E., Painter, T. H., and Dozier, J.: Validating reconstruction of snow water equivalent in California's Sierra Nevada using measurements from the NASA Airborne Snow Observatory, Water Resources Research, 52, 8437–8460, https://doi.org/10.1002/2016WR018704, 2016.

Barnett, T. P., Adam, J. C., and Lettenmaier, D. P.: Potential Impacts of a Warming Climate on Water Availability in Snow-Dominated Regions, Nature, 438, 303, 2005.

Berrisford, P., Dee, D., Poli, P., Brugge, R., Fielding, M., Fuentes, M., Kållberg, P., Kobayashi, S., Uppala, S., and Simmons, A.: The ERA-Interim archive Version 2.0, ECMWF, p. 23, 2011.

Björnsson, H., Sigurðsson, B.D., Davíðsdóttir, B., Ólafsson, J. S., Ástþórsson, Ó. S., Ólafsdóttir, S., Baldursson, T., and Jónsson, T.: Loftslagsbreytingar og áhrif þeirra á Íslandi : Skýrsla Vísindanefndar um loftslagsbreytingar 2018., Tech. rep., Veðurstofa Íslands, Reykjavík, 2018.

Björnsson, H.: Bægisárjökull, North-Iceland. Result of glaciological investigations 1967-1968. Part I. Mass balance and general meteorology., Jökull, 21, 1–23, 1971.

Björnsson, H.: Bægisárjökull, North-Iceland. Result of glaciological investigations 1967-1968. Part II. The energy balance., Jökull, 22, 44–61, 1972.

Björnsson, H.: Hydrology of ice caps in volcanic regions., Reykjavík : Vísindafélag Íslendinga, 1988.

Björnsson, H. and Aðalgeirsdóttir, G.: Veður á Brúarjökli sumarið 1994 og samanburður þess við leysingu á jökli og veður utan jökuls, Raunvísindastofnun Háskólans, 1, 1–36, 1995.

Björnsson, H. and Pálsson, F.: Climate sensitivity of glacier mass balance: the effect of topographic barriers (TEMBA), SIUI-Final Report, 1, 1–73, 1998.

Björnsson, H. and Pálsson, F.: Icelandic glaciers, Jökull, 58, 365–386, 2008.

Björnsson, H. and Pálsson, F.: Radio-echo soundings on Icelandic temperate glaciers: history of techniques and findings, Annals of Glaciology, 61, 25–34, https://doi.org/10.1017/aog.2020.10, 2020.

Björnsson, H., Guðmundsson, S., Haraldsson, H., and Pálsson, F.: Veðurathuganir og jökulleysing á Vatnajökli sumarið 1995 og samanburður við veðurstöðvar utan jökuls, Raunvísindastofnun Háskólans, 1, 1–73, 1996.

Björnsson, H., Pálsson, F., and Guðmundsson, M. T.: Surface and bedrock topography of the Mýrdalsjökull ice cap, Iceland: The Katla caldera, eruption sites and routes of jökulhlaups, Jökull, 49, 29–46, 2000.

Björnsson, H., Pálsson, F., and Guðmundsson, S.: Jökulsárlón at Breiðamerkursandur, Vatnajökull, Iceland: 20th century changes and future outlook, Jökull, 50, 1–18, 2001.

Bojinski, S., Verstraete, M., Peterson, T. C., Richter, C., Simmons, A., and Zemp, M.: The Concept of Essential Climate Variables in Support of Climate Research, Applications, and Policy, Bulletin of the American Meteorological Society, 95, 1431–1443, https://doi.org/10.1175/BAMS-D-13-00047.1, 2014.

Box, J. E., Fettweis, X., Stroeve, J. C., Tedesco, M., Hall, D. K., and Steffen, K.: Greenland Ice Sheet Albedo Feedback. Thermodynamics and Atmospheric Drivers, The Cryosphere, 6, 821–839, https://doi.org/10.5194/tc-6-821-2012, 2012.

Brock, B. W., Willis, I. C., and Sharp, M. J.: Measurement and parameterization of aerodynamic roughness length variations at Haut Glacier d'Arolla, Switzerland, Journal of Glaciology, 52, 281–297, https://doi.org/10.3189/172756506781828746, 2006.

Caesar, L., Rahmstorf, S., Robinson, A., Feulner, G., and Saba, V.: Observed fingerprint of a weakening Atlantic Ocean overturning circulation, Nature, 556, 191–196, https://doi.org/10.1038/s41586-018-0006-5, 2018.

Chen, X., Liang, S., and Cao, Y.: Satellite Observed Changes in the Northern Hemisphere Snow Cover Phenology and the Associated Radiative Forcing and Feedback between 1982 and 2013, Environmental Research Letters, 11, 084 002, https://doi.org/10.1088/1748-9326/11/8/084002, 2016.

Choi, G., Robinson, D. A., and Kang, S.: Changing Northern Hemisphere Snow Seasons, Journal of Climate, 23, 5305–5310, https://doi.org/10.1175/2010jcli3644.1, 2010.

Crochet, P. and Jóhannesson, T.: A data set of gridded daily temperature in Iceland, 1949–2010, Jökull, 61, 1–17, 2011.

Dagsson-Waldhauserova, P., Arnalds, O., and Olafsson, H.: Long-term dust aerosol production from natural sources in Iceland, Journal of the Air & Waste Management Association, 67, 173–181, https://doi.org/10.1080/10962247.2013.805703, 2017.

Davini, P., Cagnazzo, C., Neale, R., and Tribbia, J.: Coupling between Greenland blocking and the North Atlantic Oscillation pattern, Geophysical Research Letters, 39, https://doi.org/https://doi.org/10.1029/2012GL052315, 2012.

Denby, B. and Greuell, W.: The use of bulk and profile methods for determining surface heat fluxes in the presence of glacier winds, Journal of Glaciology, 46, 445–452, https://doi.org/10.3189/172756500781833124, 2000.

Einarsson, M. A.: Climates of the Oceans, H. Van Loon (Ed.). Vol. 15 of World Survey of Climatology, Editor-in-Chief H. E. Landsberg, Journal of Climatology, 5, 673–697, https://doi.org/10.1002/joc.3370050110, 1984.

Fausto, R. S., van As, D., Mankoff, K. D., Vandecrux, B., Citterio, M., Ahlstrøm, A. P., Andersen, S. B., Colgan, W., Karlsson, N. B., Kjeldsen, K. K., Korsgaard, N. J., Larsen, S. H., Nielsen, S., Pedersen, A. O., Shields, C. L., Solgaard, A. M., and Box, J. E.: Programme for Monitoring of the Greenland Ice Sheet (PROMICE) automatic weather station data, Earth System Science Data, 13, 3819–3845, https://doi.org/10.5194/essd-13-3819-2021, 2021.

Fernandes, R., Zhao, H. X., Wang, X. J., Key, J., Qu, X., and Hall, A.: Controls on Northern Hemisphere Snow Albedo Feedback Quantified Using Satellite Earth Observations, Geophysical Research Letters, 36, L21 702, https://doi.org/10.1029/2009gl040057, 2009.

Flanner, M. G., Shell, K. M., Barlage, M., Perovich, D. K., and Tschudi, M. A.: Radiative Forcing and Albedo Feedback from the Northern Hemisphere Cryosphere between 1979 and 2008, Nature Geoscience, 4, 151–155, https://doi.org/10.1038/ngeo1062, 2011.

Gardner, A. S., Sharp, M. J., Koerner, R. M., Labine, C., Boon, S., Marshall, S. J., Burgess, D. O., and Lewis, D.: Near-Surface Temperature Lapse Rates over Arctic Glaciers and Their Implications for Temperature Downscaling, Journal of Climate, 22, 4281–4298, https://doi.org/10.1175/2009JCLI2845.1, 2009.

Gascoin, S., Guðmundsson, S., Aðalgeirsdóttir, G., Pálsson, F., Schmidt, L., Berthier, E., and Björnsson, H.: Evaluation of MODIS Albedo Product over Ice Caps in Iceland and Impact of Volcanic Eruptions on Their Albedo, Remote Sensing, 9, 399, https://doi.org/10.3390/rs9050399, 2017.

Gervais, M., Shaman, J., and Kushnir, Y.: Impacts of the North Atlantic Warming Hole in Future Climate Projections: Mean Atmospheric Circulation and the North Atlantic Jet, Journal of Climate, 32, 2673 – 2689, https://doi.org/10.1175/JCLI-D-18-0647.1, 2019.

Goelzer, H., Nowicki, S., Payne, A., Larour, E., Seroussi, H., Lipscomb, W. H., Gregory, J., Abe-Ouchi, A., Shepherd, A., Simon, E., Agosta, C., Alexander, P., Aschwanden, A., Barthel, A., Calov, R., Chambers, C., Choi, Y., Cuzzone, J., Dumas, C., Edwards, T., Felikson, D., Fettweis, X., Golledge, N. R., Greve, R., Humbert, A., Huybrechts, P., Le clec'h, S., Lee, V., Leguy, G., Little, C., Lowry, D. P., Morlighem, M., Nias, I., Quiquet, A., Rückamp, M., Schlegel, N.-J., Slater, D. A., Smith, R. S., Straneo, F., Tarasov, L., van de Wal, R., and van den Broeke, M.: The future sea-level contribution of the Greenland ice sheet: a multi-model ensemble study of ISMIP6, The Cryosphere, 14, 3071–3096, https://doi.org/10.5194/tc-14-3071-2020, 2020.

Gregory, J. M. and Oerlemans, J.: Simulated future sea-level rise due to glacier melt based on regionally and seasonally resolved temperature changes, Nature, 391, 474–476, https://doi.org/10.1038/35119, 1998.

Gudmundsson, M. T., Thordarson, T., Höskuldsson, A., Larsen, G., Björnsson, H., Prata, F. J., Oddsson, B., Magnússon, E., Högnadóttir, T., Petersen, G. N., Hayward, C. L., Stevenson, J. A., and Jónsdóttir, I.: Ash generation and distribution from the April-May 2010 eruption of Eyjafjallajökull, Iceland, Scientific Reports, 2, 572, 2012.

Gunnarsson, A., Pálsson, F., Aðalgeirsdóttir, G., Björnsson, H., and Guðmundsson, S.: Monitoring Energy Balance of Icelandic Glaciers for 25 years, Proc. 27th IUGG General Assembly ,Montréal, Québec, Canada., IUGG19-3435, 2019.

Gunnarsson, A., Gardarsson, S. M., Pálsson, F., Jóhannesson, T., and Sveinsson, O. G. B.: Annual and inter-annual variability and trends of albedo of Icelandic glaciers, The Cryosphere, 15, 547–570, https://doi.org/10.5194/tc-15-547-2021, 2021.

Guðmundsson, S., Björnsson, H., Pálsson, F., and Haraldsson, H. H.: Energy balance of Brúarjökull and circumstances leading to the August 2004 floods in the river Jökla, N-Vatnajökull, Jökull, 55, 121–138, 2005.

Guðmundsson, S., Björnsson, H., Pálsson, F., and Haraldsson, H. H.: Comparison of energy balance and degree–day models of summer ablation on the Langjökull ice cap, SW-Iceland, Jökull, 59, 1–18, 2009.

Hall, D. K. and Riggs, G. A.: MODIS/Terra Snow Cover Daily L3 Global 500m Grid, Version 6, Tech. rep., NASA National Snow and Ice Data Center Distributed Active Archive Center, Boulder, Colorado USA., 2016a.

Hall, D. K. and Riggs, G. A.: MODIS/Aqua Snow Cover Daily L3 Global 500m Grid, Version 6, Tech. rep., NASA National Snow and Ice Data Center Distributed Active Archive Center, Boulder, Colorado USA., 2016b.

Hanna, E., Cropper, T. E., Hall, R. J., and Cappelen, J.: Greenland Blocking Index 1851–2015: a regional climate change signal, International Journal of Climatology, 36, 4847–4861, https://doi.org/https://doi.org/10.1002/joc.4673, 2016.

Hannesdóttir, H., Sigurðsson, O., Þrastarson, R. H., Guðmundsson, S., Belart, J. M., Pálsson, F., Magnússon, E., Víkingsson, S., Kaldal, I., and Jóhannesson, T.: A national glacier inventory and variations in glacier extent in Iceland from the Little Ice Age maximum to 2019, Jökull, 12, 1–34, 2020.

Hinkelman, L. M., Lapo, K. E., Cristea, N. C., and Lundquist, J. D.: Using CERES SYN Surface Irradiance Data as Forcing for Snowmelt Simulation in Complex Terrain*, Journal of Hydrometeorology, 16, 2133–2152, https://doi.org/10.1175/JHM-D-14-0179.1, 2015.

Hjaltason, S., Guðmundsdóttir, M., Haukdal, J. Á., and Guðmundsson, J. R.: Energy Statistics in Iceland 2019, Energy statistics in Iceland, Orkustofnun, 2020.

Hodgkins, R., Carr, S., Pálsson, F., Guðmundsson, S., and Björnsson, H.: Modelling variable glacier lapse rates using ERA-Interim reanalysis climatology: an evaluation at Vestari- Hagafellsjökull, Langjökull, Iceland, International Journal of Climatology, 33, 410–421, https://doi.org/10.1002/joc.3440, 2013.

Hofer, S., Lang, C., Amory, C., Kittel, C., Delhasse, A., Tedstone, A., and Fettweis, X.: Greater Greenland Ice Sheet contribution to global sea level rise in CMIP6, Nature Communications, 11, 6289, https://doi.org/10.1038/s41467-020-20011-8, 2020.

Holtslag, A. A. M. and Bruin, H. A. R. D.: Applied Modeling of the Nighttime Surface Energy Balance over Land, Journal of Applied Meteorology and Climatology, 27, 689 – 704, https://doi.org/10.1175/1520-0450(1988)027<0689:AMOTNS>2.0.CO;2, 1988.

Hreinsdóttir, S., Sigmundsson, F., Roberts, M. J., Björnsson, H., Grapenthin, R., Arason, P., Árnadóttir, T., Hólmjárn, J., Geirsson, H., Bennett, R. A., Gudmundsson, M. T., Oddsson, B., Ófeigsson, B. G., Villemin, T., Jónsson, T., Sturkell, E., Höskuldsson, A., Larsen, G., Thordarson, T., and Óladóttir, B. A.: Volcanic plume height correlated with magma-pressure change at Grímsvötn Volcano, Iceland, Nature Geoscience, 7, 214–218, https://doi.org/10.1038/ngeo2044, 2014.

Huai, B., van den Broeke, M. R., and Reijmer, C. H.: Long-term surface energy balance of the western Greenland Ice Sheet and the role of large-scale circulation variability, The Cryosphere, 14, 4181–4199, https://doi.org/10.5194/tc-14-4181-2020, 2020.

Huang, B., Liu, C., Banzon, V., Freeman, E., Graham, G., Hankins, B., Smith, T., and Zhang, H.-M.: Improvements of the Daily Optimum Interpolation Sea Surface Temperature (DOISST) Version 2.1, Journal of Climate, 34, 2923 – 2939, https://doi.org/10.1175/JCLI-D-20-0166.1, 2021.

Hudson, S. R.: Estimating the Global Radiative Impact of the Sea Ice-Albedo Feedback in the Arctic, Journal of Geophysical Research-Atmospheres, 116, D16 102, https://doi.org/10.1029/2011jd015804, 2011.

Jóhannesson, T. and Aðalgeirsdóttir: Effect of Climate Change on Hydrology and Hydro-Resources in Iceland., Reykjavík : Orkustofnun, 2007, Reykjavík.

Jones, P. D., Jonsson, T., and Wheeler, D.: Extension to the North Atlantic oscillation using early instrumental pressure observations from Gibraltar and south-west Iceland, International Journal of Climatology, 17, 1433–1450, https://doi.org/https://doi.org/10.1002/(SICI)1097-0088(19971115)17:13<1433::AID-JOC203>3.0.CO;2-P, 1997.

Jóhannesson, T.: The Response Time of Glaciers in Iceland to Changes in climate, Annals of Glaciology, 8, 100–101, https://doi.org/10.3189/S0260305500001233, 1986.

Jóhannesson, T., Raymond, C., and Waddington, E.: Time–Scale for Adjustment of Glaciers to Changes in Mass Balance, Journal of Glaciology, 35, 355–369, https://doi.org/10.3189/S002214300000928X, 1989.

Jóhannesson, T., Björnsson, H., Magnússon, E., Guðmundsson, S., Pálsson, F., Sigurðsson, O., Thorsteinsson, T., and Berthier, E.: Ice-volume changes, bias estimation of mass-balance measurements and changes in subglacial lakes derived by lidar mapping of the surface of Icelandic glaciers, Annals of Glaciology, 54, 63–74, https://doi.org/10.3189/2013AoG63A422, 2013.

Jóhannesson, T., Pálmason, B.and Hjartarson, A., Jarosch, A. H., Magnússon, E., Belart, J. M. C., and Gudmundsson, M. T.: Non-surface mass balance of glaciers in Iceland, Journal of Glaciology, 66, 685–697, https://doi.org/10.1017/jog.2020.37, 2020.

Keil, P., Mauritsen, T., Jungclaus, J., Hedemann, C., Olonscheck, D., and Ghosh, R.: Multiple drivers of the North Atlantic warming hole, Nature Climate Change, 10, 667–671, https://doi.org/10.1038/s41558-020-0819-8, 2020.

Knudsen, K. L., Eiríksson, J., and Bartels-Jónsdóttir, H. B.: Oceanographic changes through the last millennium off North Iceland: Temperature and salinity reconstructions based on foraminifera and stable isotopes, Marine Micropaleontology, 84-85, 54 – 73, https://doi.org/https://doi.org/10.1016/j.marmicro.2011.11.002, 2012.

Lister, H.: Report on glaciology at Breiðamerkurjökull 1951, Jökull, 3, 23–31, 1953.

Lister, H.: Micro meteorology over dirt coned ice, Jökull, 9, 1–6, 1959.

Lozier, M., Owens, W., and Curry, R. G.: The climatology of the North Atlantic, Progress in Oceanography, 36, 1 – 44, https://doi.org/https://doi.org/10.1016/0079-6611(95)00013-5, 1995.

Magnússon, E., Belart, J. M., Pálsson, F., Anderson, L. S., Ágúst Þ. Gunnlaugsson, Berthier, E., Ágústsson, H., and Áslaug Geirsdóttir: The subglacial topography of Drangajökull ice cap, NW-Iceland, deduced from dense RES-profiling, Jökull, 66, 1–26, 2016a.

Magnússon, E., Belart, J. M. C., Pálsson, F., Anderson, L. S., Gunnlaugsson, A., Berthier, E., Ágústsson, H., and Geirsdóttir, A.: The subglacial topography of Drangajökull ice cap, NW-Iceland, deduced from dense RES-profiling, Jökull, 66, 1–26, 2016b.

Male, D. H. and Granger, R. J.: Snow surface energy exchange, Water Resources Research, 17, 609–627, https://doi.org/10.1029/WR017i003p00609, 1981.

Marty, C., Philipona, R., Fröhlich, C., and Ohmura, A.: Altitude dependence of surface radiation fluxes and cloud forcing in the alps: results from the alpine surface radiation budget network, Theoretical and Applied Climatology, 72, 137–155, https://doi.org/10.1007/s007040200019, 2002.

Matlab: R2020b, The Mathworks Inc., Natick, Massachusetts, 2020.

Matthews, T. and Hogdkins, R.: Interdecadal variability of degree-day factors on Vestari Hagafellsjökull (Langjökull, Iceland) and the importance of threshold air temperatures, Journal of Glaciology, 62, 310–322, https://doi.org/10.1017/jog.2016.21, 2016.

Möller, R., Möller, M., Björnsson, H., Gudmundsson, S., Pálsson, F., Oddsson, B., Kukla, P., and Schneider, C.: MODIS-derived albedo changes of Vatnajökull (Iceland) due to tephra deposition from the 2004 Grimsvötn eruption, International Journal of Applied Earth Observation and Geoinformation, 26, 256–269, https://doi.org/10.1016/j.jag.2013.08.005, 2014.

Möller, R., Dagsson-Waldhauserova, P., Möller, M., Kukla, P. A., Schneider, C., and Gudmundsson, M. T.: Persistent albedo reduction on southern Icelandic glaciers due to ashfall from the 2010 Eyjafjallajökull eruption, Remote Sensing of Environment, 233, 111 396, https://doi.org/https://doi.org/10.1016/j.rse.2019.111396, 2019.

National Centers for Environmental Prediction: NCEP GFS 0.25 Degree Global Forecast Grids Historical Archive, https://doi.org/10.5065/D65D8PWK, 2015.

Nawri, N., Björnsson, H., Petersen, G. N., and Jónasson, K.: Empirical Terrain Models for Surface Wind and Air Temperature over Iceland, VÍ, 2012-009, Reykjavík : Veðurstofa Íslands, 2012, 2012.

NOAA: NOAA High Resolution SST data, Tech. rep., NOAA/OAR/ESRL PSL, Boulder, Colorado, USA, 2021.

Noël, B., Aðalgeirsdóttir, G., Pálsson, F., Wouters, B., Lhermitte, S., Haacker, J. M., and van den Broeke, M. R.: North Atlantic Cooling is Slowing Down Mass Loss of Icelandic Glaciers, Geophysical Research Letters, 49, e2021GL095 697, https://doi.org/https://doi.org/10.1029/2021GL095697, 2022.

Oddsson, B., Gudmundsson, M., Larsen, G., and Karlsdóttir, S.: Monitoring of the plume from the basaltic phreatomagmatic 2004 Grímsvötn eruption—application of weather radar and comparison with plume models, Bulletin of Volcanology, 74, https://doi.org/10.1007/s00445-012-0598-9, 2012.

Oerlemans, J., Björnsson, H., Kuhn, M., Obleitner, F., Palsson, F., Smeets, C., Vugts, H. F., and Wolde, J. D.: Glacio-Meteorological Investigations On Vatnajökull, Iceland, Summer 1996: An Overview, Boundary-Layer Meteorology, 92, 3–24, https://doi.org/10.1023/A:1001856114941, 1999.

Ohmura, A.: Physical Basis for the Temperature-Based Melt-Index Method, Journal of Applied Meteorology, 40, 753–761, https://doi.org/10.1175/1520-0450(2001)040<0753:PBFTTB>2.0.CO;2, 2001.

Pálsson, F., Guðmundsson, S., and Björnsson, H.: Afkomu- og hraðamælingar á Langjökli jökulárið 2011–2012., Tech. Rep. LV-2014-076, Institute Earth Science, University Iceland and Landsvirkjun, 2013.

Paulson, C. A.: The Mathematical Representation of Wind Speed and Temperature Profiles in the Unstable Atmospheric Surface Layer, Journal of Applied Meteorology and Climatology, 9, 857 – 861, https://doi.org/10.1175/1520-0450(1970)009<0857:TMROWS>2.0.CO;2, 1970.

Perkins, H., Hopkins, T. S., Malmberg, S.-A., Poulain, P.-M., and Warn-Varnas, A.: Oceanographic conditions east of Iceland, Journal of Geophysical Research: Oceans, 103, 21 531–21 542, https://doi.org/doi.org/10.1029/98JC00890, 1998.

Plüss, C. and Ohmura, A.: Longwave Radiation on Snow-Covered Mountainous Surfaces, Journal of Applied Meteorology, 36, 818–824, https://doi.org/10.1175/1520-0450-36.6.818, 1997.

Pálsson, F. and Gunnarsson, A.: Afkomu- og hraðamælingar á Langjökli : jökulárið 2012–2013., Tech. Rep. LV-2015-076, Institute Earth Science, University Iceland and Landsvirkjun, 2015.

Pálsson, F., Gunnarsson, A., Jónsson, G., Pálsson, H. S., and Steinþórsson, S.: Vatnajökull: Mass balance, meltwater drainage and surface velocity of the glacial year 2014–15, Tech. Rep. LV-2016-031, Institute Earth Science, Univeristy Iceland and Landsvirkjun, 2016.

Pálsson, F., Gunnarsson, A., Jónsson, G., Pálsson, H. S., and Steinþórsson, S.: Vatnajökull: Mass balance, meltwater drainage and surface velocity of the glacial year 2018–19, Landsvirkjun, Reykjavík, RH-01-20 – LV-2020-016, 56, 2020a.

Pálsson, F., Gunnarsson, A., Pálsson, H. S., and Steinþórsson, S.: Afkomu- og hraðamælingar á Langjökli jökulárið 2018–2019, Landsvirkjun, Reykjavík, RH-10-20 / LV-2020-017, 27, 2020b.

Rahmstorf, S., Box, J. E., Feulner, G., Mann, M. E., Robinson, A., Rutherford, S., and Schaffernicht, E. J.: Exceptional twentieth-century slowdown in Atlantic Ocean overturning circulation, Nature Climate Change, 5, 475–480, https://doi.org/10.1038/nclimate2554, 2015.

Renner, A. H. H., Sundfjord, A., Janout, M. A., Ingvaldsen, R. B., Beszczynska-Möller, A., Pickart, R. S., and Pérez-Hernández, M. D.: Variability and Redistribution of Heat in the Atlantic Water Boundary Current North of Svalbard, Journal of Geophysical Research: Oceans, 123, 6373–6391, https://doi.org/10.1029/2018JC013814, 2018.

Reynolds, R. W., Smith, T. M., Liu, C., Chelton, D. B., Casey, K. S., and Schlax, M. G.: Daily High-Resolution-Blended Analyses for Sea Surface Temperature, Journal of Climate, 20, 5473 – 5496, https://doi.org/10.1175/2007JCLI1824.1, 2007.

Rittger, K., Bair, E. H., Kahl, A., and Dozier, J.: Spatial estimates of snow water equivalent from reconstruction, Advances in Water Resources, 94, 345–363, https://doi.org/https://doi.org/10.1016/j.advwatres.2016.05.015, 2016.

Rossby, T.: The North Atlantic Current and surrounding waters: At the crossroads, Reviews of Geophysics, 34, 463–481, https://doi.org/10.1029/96RG02214, 1996.

Rögnvaldsson, Ólafur, A.: RÁVII: Tæknileg útfærsla á niðurkvörðun á Íslandsveðri, Tech. rep., Belgingur - Reiknistofa í Veðurfræði, Reykjavik, 2016.

Rögnvaldsson, Ólafur, A.: Technical description of two different dynamical downscaling time series for Icelandi, Tech. rep., Belgingur - Reiknistofa í Veðurfræði, Reykjavik, 2020.

Salisbury, J. W., D'Aria, D. M., and Wald, A.: Measurements of thermal infrared spectral reflectance of frost, snow, and ice, Journal of Geophysical Research: Solid Earth, 99, 24 235–24 240, https://doi.org/https://doi.org/10.1029/94JB00579, 1994.

Schmidt, L. S., Aðalgeirsdóttir, G., Guðmundsson, S., Langen, P. L., Pálsson, F., Mottram, R., Gascoin, S., and Björnsson, H.: The importance of accurate glacier albedo for estimates of surface mass balance on Vatnajökull: evaluating the surface energy budget in a regional climate model with automatic weather station observations, The Cryosphere, 11, 1665–1684, https://doi.org/10.5194/tc-11-1665-2017, 2017.

Schmidt, L. S., Aðalgeirsdóttir, G., Pálsson, F., Langen, P. L., Guðmundsson, S., and Björnsson, H.: Dynamic simulations of Vatnajökull ice cap from 1980 to 2300, Journal of Glaciology, 66, 97–112, https://doi.org/10.1017/jog.2019.90, 2020.

Sicart, J. E., Pomeroy, J. W., Essery, R. L. H., and Bewley, D.: Incoming longwave radiation to melting snow: observations, sensitivity and estimation in Northern environments, Hydrological Processes, 20, 3697–3708, https://doi.org/10.1002/hyp.6383, 2006.

Slater, T., Lawrence, I. R., Otosaka, I. N., Shepherd, A., Gourmelen, N., Jakob, L., Tepes, P., Gilbert, L., and Nienow, P.: Review article: Earth's ice imbalance, The Cryosphere, 15, 233–246, https://doi.org/10.5194/tc-15-233-2021, 2021.

Smeets, C. J. P. P. and van den Broeke, M. R.: The Parameterisation of Scalar Transfer over Rough Ice, Boundary-Layer Meteorology, 128, 339, https://doi.org/10.1007/s10546-008-9292-z, 2008a.

Smeets, C. J. P. P. and van den Broeke, M. R.: Temporal and Spatial Variations of the Aerodynamic Roughness Length in the Ablation Zone of the Greenland Ice Sheet, Boundary-Layer Meteorology, 128, 315–338, https://doi.org/10.1007/s10546-008-9291-0, 2008b.

Smeets, C. J. P. P., Duynkerke, P. G., and Vugts, H. F.: Observed Wind Profiles and Turbulence Fluxes over an ice Surface with Changing Surface Roughness, Boundary-Layer Meteorology, 92, 99–121, https://doi.org/10.1023/A:1001899015849, 1999.

Stone, P. H. and Carlson, J. H.: Atmospheric Lapse Rate Regimes and Their Parameterization, Journal of the Atmospheric Sciences, 36, 415–423, https://doi.org/10.1175/1520-0469(1979)036<0415:ALRRAT>2.0.CO;2, 1979.

Sveinsson, Ó.: Energy in Iceland: Adaptation to Climate Change, UNU-FLORES Policy Briefs, United Nations University Institute for Integrated Management of Material Fluxes and of Resources (UNU-FLORES), Dresden, 2016.

Van As, D.: Warming, glacier melt and surface energy budget from weather station observations in the Melville Bay region of northwest Greenland, Journal of Glaciology, 57, 208–220, https://doi.org/10.3189/002214311796405898, 2011.

Vandecrux, B., Fausto, R. S., Langen, P. L., van As, D., MacFerrin, M., Colgan, W. T., Ingeman-Nielsen, T., Steffen, K., Jensen, N. S., Møller, M. T., and Box, J. E.: Drivers of Firn Density on the Greenland Ice Sheet Revealed by Weather Station Observations and Modeling, Journal of Geophysical Research: Earth Surface, 123, 2563–2576, https://doi.org/https://doi.org/10.1029/2017JF004597, 2018.

Warren, S. G. and Wiscombe, W. J.: A Model for the Spectral Albedo of Snow. II: Snow Containing Atmospheric Aerosols, Journal of the Atmospheric Sciences, 37, 2734–2745, https://doi.org/10.1175/1520-0469(1980)037<2734:AMFTSA>2.0.CO;2, 1980.

Wildt, M., Oerlemans, J., and Björnsson, H.: A calibrated mass balance model for Vatnajökull, Iceland, Jökull, 52, 2004.

Wittmann, M., Groot Zwaaftink, C. D., Steffensen Schmidt, L., Guðmundsson, S., Pálsson, F., Arnalds, O., Björnsson, H., Thorsteinsson, T., and Stohl, A.: Impact of dust deposition on the albedo of Vatnajökull ice cap, Iceland, The Cryosphere, 11, 741–754, https://doi.org/10.5194/tc-11-741-2017, 2017.

WMO: Systematic Observation Requirements for Satellite-based Products for Climate Supplemental details to the satellite-based component of the Implementation Plan for the Global Observing System for Climate in Support of the UNFCCC: 2011 update, GCOS- No. 154, p. 138, 2011.

Zemp, M., Huss, M., Thibert, E., Eckert, N., McNabb, R., Huber, J., Barandun, M., Machguth, H., Nussbaumer, S. U., Gärtner-Roer, I., Thomson, L., Paul, F., Maussion, F., Kutuzov, S., and Cogley, J. G.: Global glacier mass changes and their contributions to sea-level rise from 1961 to 2016, Nature, 568, 382–386, https://doi.org/10.1038/s41586-019-1071-0, 2019.

Zhao, J., Yang, J., Semper, S., Pickart, R. S., Våge, K., Valdimarsson, H., and Jónsson, S.: A Numerical Study of Interannual Variability in the North Icelandic Irminger Current, Journal of Geophysical Research: Oceans, 123, 8994–9009, https://doi.org/10.1029/2018JC013800, 2018.

Ólafsdóttir, S., Jennings, A. E., Áslaug Geirsdóttir, Andrews, J., and Miller, G. H.: Holocene variability of the North Atlantic Irminger current on the south- and northwest shelf of Iceland, Marine Micropaleontology, 77, 101 – 118, https://doi.org/https://doi.org/10.1016/j.marmicro.2010.08.002, 2010.

Paper IV

Spatial estimation of snow water equivalent by for glaciers and seasonal snow in Iceland using remote sensing snow cover and albedo

Andri Gunnarsson, Sigurdur M. Gardarsson.

To be submitted, manuscript in preparation.

Spatial estimation of snow water equivalent for glaciers and seasonal snow in Iceland using remote sensing snow cover and albedo

Andri Gunnarsson[1,2] and Sigurdur M. Gardarsson[1]

[1]University of Iceland, Civil and Environmental Engineering, Hjardarhagi 2-6, IS-107 Reykjavik, Iceland
[2]Landsvirkjun, Department of Research and Development, Reykjavík, IS-107, Iceland

Correspondence: Andri Gunnarsson (andrigun@lv.is)

Abstract. Efficient water resource management in glacier- and snow-dominated basins require accurate estimates of snow water equivalent (SWE) in late winter and spring, timing of melt onset and intensity. To understand the high spatio-temporal variability of snow and glacier ablation, a spatially distributed energy balance model combined satellite-based retrievals of albedo and snow cover was applied. Incoming short-wave energy, contributing to daily estimates of melt energy, were constrained by remotely sensed surface albedo for snow covered surfaces. Fractional snow cover was used for non-glaciated areas, as it provides estimates of snow cover for each pixel to better constrain snow melt. Therefore, available daily estimates of melt energy in a given area, were the product of the possible melt energy and the fractional snow cover of the area or pixel, for non-glaciated areas. This provided daily estimates of melt water to estimate seasonal snow and glacier ablation in Iceland for the period 2000–2019. Observations from snow pits on land and glacier summer mass balance were used for validation and observations from land and glacier-based automatic met stations used to validate model inputs for the energy balance model. The results show that the inter-annual SWE variability was generally high both for seasonal snow and glaciers. For seasonal snow the largest SWE (>1000 mm) was found in mountainous and alpine areas close to the coast, notably in the East- and Westfjords, Tröllaskaga, and in the proximity of glacier margins. Lower SWE values were observed in the central highlands, flatter inland areas and at lower elevations. For glaciers, more SWE (glacier ablation) was associated with lower glacier elevations while less melt was observed at higher elevations. For the impurity-rich bare-ice areas exposed annually, observed SWE was more than 3000 mm.

1 Introduction

Efficient water resource management in glacier- and snow-dominated basins require accurate estimates of snow water equivalent (SWE) in winter and spring, timing of melt onset and intensity among other ice-, snow-, and hydrological catchment properties (Rittger et al., 2016; Sandoval-Solis, 2020).

Snowpack properties (e.g. depth, density, temperature) vary in space and time where point data might not correctly describe the spatial and temporal variability in complex environments (Elder et al., 1991, 1998). Knowledge of the spatio-temporal distribution of snow and glacier ablation is important to accurately estimate partitioning of melt, calibrate and update hydrological models, organize operational planning (flood protection, onset of spring melt, seasonal resource assessment) and real time assessments of water resources.

In Iceland, a system of reservoirs and diversions in the highlands collect and store water for hydro-power production, corresponding to about 70 % of total energy production in the country (Hjaltason et al., 2020). About 60 % of flows for hydro power energy production originate from seasonal snow (10 to 15 %) and glacier ablation (50 %) in an average hydrological year. Due to the high share of hydro power energy production in the total energy production mix, reliable understanding and good forecasting capabilities of water resources development, both in short- and long-term aspects, is key to efficiently utilize water resources. The fact that the current Icelandic energy system is a closed loop system, i.e., no means to import nor export electricity, also emphasis the importance of high quality forecasting capabilities.

Climate in Iceland is modulated by heat transfer by ocean and atmospheric circulations from lower latitudes to higher (Einarsson, 1984; Perkins et al., 1998). Storm tracks, dominating from the southwest and southeast direction, play an important role for the hydrological cycle, as they bring precipitation sustaining the formation of seasonal snow and glaciers in the highlands, decreasing with latitude (Einarsson, 1984; Crochet et al., 2007a). About 10 % of land area in Iceland is covered with glaciers (Hannesdóttir et al., 2020), while the central highlands, accumulating snow in winter, correspond to about 40 % of the island (> 550 m a.s.l.).

Historically in Iceland, more focus has been on observing glacier surface mass and energy balance and the associated runoff contribution rather than measuring and monitoring seasonal snow, especially in the highlands. Surface mass balance data of Icelandic glaciers has been systematically collected bi-annually by a network of collaborators of institutes and stakeholders in Iceland. Data are collected where winter and summer mass balance are observed with conventional glaciological methods, for Vatnajökull, Langjökull and Hofsjökull with intermittent observations for Drangajökull, Mýrdalsjökull and other smaller glaciers (Ágústsson et al., 2013a; Þorsteinsson et al., 2017; Pálsson et al., 2022, 2020b).

Long term observations of snow cover (binary snow cover) in local municipals have been conducted since 1924 at manned observation sites among other weather related observations, operated by the Icelandic Meteorological Office (IMO (Jónsson, 2002). Although this is the longest continuous record of snow cover in Iceland and provides insights to local snow cover in the lowlands limited data is available for the highlands of Iceland.

SWE estimates are of more interest for resource assessment and hydrological modeling but in situ observations of SWE from snow pillows or transects from snow courses are few, sparse and discontinuous providing limited capabilities to analyze and intrepid annual distribution and evolution of snow through time (Jónsson and Jónasson, 1997; Jóhannesson and Sigurðsson, 2014). The single longest continuous record for snow depth, density and other properties of the snowpack were collected at Hvervellir, in the central highlands, from 1965 until 2004 when the site was upgraded to automatic measurements and snow observations decommissioned (Sigurðsson et al., 2003).

In certain areas in the highlands under development or operation for hydro power, seasonal snow monitoring programs have been commissioned to improve understanding of snow hydrology although many have been short lived (Rist, 1958, 1966, 1981). At these sites, snow courses have been installed with 1-2 observations of snow depth and density each winter, although few of these site have fully continuous data (Sigurðsson, 2002; Jóhannesson and Sigurðsson, 2014). The data has been collected by various institutes through time, the National Energy Authority (Orkustofnun), the Icelandic Met Office (Veðurstofa Íslands) and the National Power Company (Landsvirkjun).

Projected future changes in climate indicate that various hydrological changes will be observed in Iceland (Björnsson et al., 2018; Schmidt et al., 2020). Various flow dynamics, such as melt onset, seasonal snow mass, changes in the rain-snow transition elevation and distribution of solid precipitation both in the highlands and at glaciers are foreseen (Jóhannesson et al., 2007; Björnsson et al., 2018). These projected changes will pose a challenge for operational control of water resources as forecasting in an non-stationary statistical environment is demanding (Milly et al., 2008). These changes will as well influence climate change adaptation for both current energy projects, future developments as well as refurbishments of older infrastructure (Björnsson and Thorsteinsson, 2012; Sveinsson, 2016)).

First utilized by Martinec and Rango (1981), the snow water equivalent reconstruction method uses space-based remote sensing of snow cover to retrospectively estimate the amount of water stored as snow for each pixel back to the last significant snowfall. The reconstruction technique has been adopted and successfully validated in many studies across various regions with various modifications and improvements and appears to be a reliable way to estimate spatial distribution of SWE (Raleigh and Lundquist, 2012; Lettenmaier et al., 2015; Rittger et al., 2016; Bair et al., 2018). The method provides a post-peak SWE estimate without the need for total precipitation which can be highly uncertain, especially in topographically complex regions (Adam and Lettenmaier, 2003; Adam et al., 2006)). The main limitation, is that the reconstructed SWE can only be estimated after snow disappears on the ground, i.e., when snow disappears from a given pixel after total melt out, limiting real time usage.

Cline et al. (1998) reconstructed SWE in a small, well studied, mountain basin in the Sierra Nevada using Landsat Thematic Mapper data to estimate fractional snow cover and spatially constant snow surface albedo decaying over time. The reconstructed SWE, compared to in-situ observations, showed a non-significant difference (6 %) for maximum SWE estimation. Molotch et al. (2004) used basin-average albedo estimated from remotely-sensed Airborne Visible/Infrared Imaging Spectroradiometer (AVIRIS) to show more accurate estimates of the timing and magnitude of snow melt using remotely sensed albedo over common snow–age–based empirical relations. Rittger et al. (2016) applied the approach to reconstruct the Sierra Nevada maritime snowpack using Moderate Resolution Imaging Spectroradiometer (MODIS) data using the MODSCAG model for fractional snow cover and albedo (Painter et al., 2009). Results showed that the model could accurately estimate SWE in a variety of topographic settings for a range of wet to dry years in the Sierra Nevada. Work by Schneider and Molotch (2016) applies MODIS based reconstructed SWE to improve real–time estimates of SWE in the Upper Colorado River using linear regression and in situ SNOTEL data reporting reduced biases and slightly lower RMSE values. Bair et al. (2018) applied machine learning models to estimate SWE throughout the snowmelt season for watersheds of Afghanistan using physiographic and remotely sensed information as predictors and reconstructed SWE as the target. Results report a 14 % mean bias across

the study period and RMSE values range from 46 to 48 mm illustrating possibilities to estimate SWE during the snow season in remote mountains.

The primary objective of this study was to understand and quantify spatio-temporal patterns of snow water equivalent and glacier ablation in Iceland using high resolution meteorological climate forcing coupled with remotely sensed snow- and ice surface albedo and fractional snow cover from the Moderate Resolution Imaging Spectroradiometer (MODIS) sensor.

2 Study area

The analysis of this study extends to the whole Iceland although the main emphasis was on catchments with glacier fed rivers or areas that sustain a seasonal snowpack (highlands). Figure 1 show the extent of the 17 main catchments analyzed (black), the six main glaciers investigated and their sub-cardinal areas (red). Table 1 shows the topographic properties of the main catchments. For each catchment topographic properties for the land covered areas (seasonal snowpack) and glaciated area were extracted, showing area, mean, maximum and minimum elevation within each catchment and the glacier ratio for each catchment, i.e., ratio of the glacier covered area to total catchment area.

Table 2 show similar information as in Table 1 for the main catchments but for the main glaciers studied. For the larger glaciers, Vatnajökull, Langjökull, Hofsjökull, Mýrdalsjökull and Drangajökull, smaller areas were defined to the main ice flow basins of the glaciers for detailed analysis. These delineated areas are shown with red boundary lines within each main glacier annotated with red text (e.g. NW for northwest). Glacier catchment delineation was from Magnússon et al. (2016) for Drangajökull, Björnsson (1988) and Björnsson et al. (2000) for Hofsjökull and Mýrdalsjökull, and Pálsson et al. (2013); Pálsson et al. (2016) for Langjökull and Vatnajökull. The sub-areas were chosen as in Gunnarsson et al. (2021).

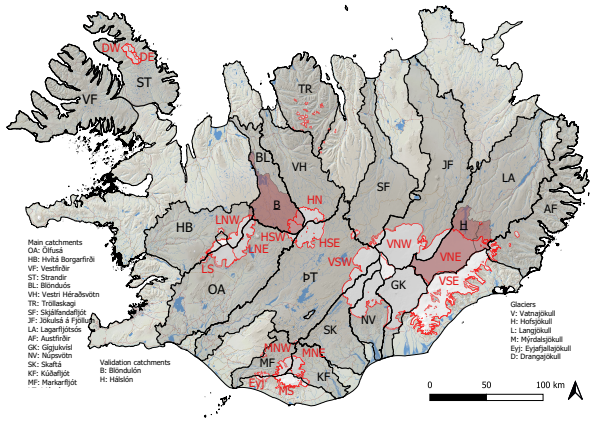

Figure 1. Overview of study area. Main catchments are outlined with black while glacier boundaries used in this study are red. The letters by each area refers to the catchment identification (Id). Topographic properties for each area are shown in Tables 1 and 2.

.

Table 1. Topographic properties of the 17 main catchments. Id. refers to Figure 1. Elevations are in meters above sea level (z). The Land and Glacier columns refer to topographic properties of the catchment divided into non-glaciated and glaciated portions. The last column, Ratio, show the portion of catchment that is glaciated.

			Land				Glacier				
Region	Id	Name	Area	z_{mean}	z_{max}	z_{min}	Area	z_{mean}	z_{max}	z_{min}	Ratio
			km^2		m a.s.l.		km^2		m a.s.l.		-
NE	AF	Austfirðir	4115	438	1180	0	20	1073	1208	925	<1%
NE	LA	Lagarfljótsós	6569	532	1532	0	1658	1236	1791	629	25%
NE	JF	Jökulsá á Fjöllum	6690	571	1822	0	1626	1366	1988	674	24%
NE	SF	Skjálfandafljót	4422	668	1690	0	106	1472	1969	1041	2%
N	TR	Tröllaskagi	3404	560	1432	0	83	1070	1394	812	2%
N	VH	Vestari Héraðsvötn	3793	651	1321	0	250	1280	1789	830	6%
N	BL	Blanda	2533	570	1136	0	237	1353	1789	837	9%
W	ST	Strandir	3541	328	827	0	161	658	914	213	4%
W	VF	Vestfirðir	5029	365	957	0	-	-	-	-	-
SW	HB	Hvítá í Borgarfirði	3844	399	1431	0	325	1169	1664	701	8%
SW	OA	Ölfusá	6357	397	1375	0	691	1081	1715	419	10%
SW	ÞT	Þjórsá	7830	591	1518	0	1041	1261	1994	624	13%
SW	MF	Markarfljót	1228	524	1474	0	209	1078	1551	294	17%
SE	KF	Kúðafljót	1279	244	1169	0	218	898	1387	223	17%
SE	SK	Skaftá	2323	401	1084	0	490	1222	1758	636	21%
SE	NV	Núpsvötn	1150	424	1384	0	680	1123	1724	93	60%
SE	GK	Gígjukvísl	1854	121	1072	0	1502	1196	1724	61	81%

Table 2. Topographic properties of the 6 main glaciers catchments and their 15 sub-areas. Id. refers to Figure 1. Elevations are in meters above sea level (z). The Ratio column show the ratio of sub-glacier area to the main glacier.

Id	Name	Area	z_{mean}	z_{max}	z_{min}	Ratio
		km^2		m a.s.l.		-
	Vatnajökull	8995	1223	2030	0	-
VNE	NE	1949	1229	1888	629	21%
VNW	NW	1457	1406	1988	729	16%
VSE	SE	2273	1066	2030	0	24%
VSW	SW	3528	1225	1994	61	39%
	Hofsjökull	970	1252	1789	624	-
HN	N	322	1289	1789	830	34%
HSE	SE	453	1200	1789	637	47%
HSW	SW	180	1346	1789	735	19%
	Langjökull	1003	1102	1435	419	-
LNE	NE	364	1090	1435	419	33%
LNW	NW	368	1137	1435	620	35%
	S	342	1020	1400	444	32%
	Mýrdalsjökull	622	1000	1485	118	-
MNE	NE	179	893	1377	223	28%
MNW	NW	177	1051	1455	414	27%
MS	S	300	997	1485	118	45%
	Drangajökull	162	658	914	213	-
DE	E	62	653	872	297	37%
DW	W	104	655	914	186	63%
Eyj	Eyjafjallajökull	79	1156	1564	294	-

3 Data and methods

3.1 Meteorological in situ data

Automatic weather station data were used to validate the models performance. For glaciers, the Icelandic Glacier Automatic Weather Stations network (ICE-GAWS) has observations from Vatnajökull, Langjökull, Hofsjökull and Mýrdalsjökull since 1994, 2001, 2016 and 2015, respectively. Most of these stations were operated for summer ablation season, from May out through September annually while few sites had data from all year around operation. Observations of air temperature, short- and long-wave incoming radiation were used for validation purposes. In total 21 sites provided data for the study period, all sites had observations of air temperature and incoming short-wave radiation while 13 sites had data for incoming long-wave radiation. Details on data processing is described in Gunnarsson et al. (2021).

For non-glaciated areas, automatic weather stations (AWS), above 250 m a.s.l. were used in the validation. Data was provided by the Icelandic Met Office (IMO) (Veðurstofa Íslands, 2020) and observations of air temperature, short- and long-wave incoming radiation were used for validation purposes. In total 69 sites were used with air temperature observations, 7 sites where incoming short-wave radiation was available and 6 sites where incoming long-wave radiation was available.

Air temperature was measured inside a fan-aspirated radiation shield and in most cases was a PT100 probe located at 2 m height above ground. At glaciers, the height above ground can vary due to snowfall and melting of the station quad-pod. Most sites in the automatic weather station networks used Kipp and Zonen CM14, CNR1, and CNR4 radiation sensors which have relatively uniform spectral response ranging from 0.3 to 2.8 μm with reported uncertainty ranging from 3 to 10 % for daily totals over ice- and snow-covered surfaces (Van den Broeke et al., 2004a, b).

For both networks (AWS and GAWS), daily averages were calculated if 20 hourly values or more were available within the day, else the observations were omitted for validation. Table A1 in the Appendix provide details for the location, elevation, type of site and number of observations for each site.

3.2 Glacier surface mass balance data

Surface mass balance data of Icelandic glaciers were systematically collected bi-annually by a network of collaborators of institutes and stakeholders in Iceland. Data were collected where winter and summer mass balance were observed with conventional glaciological methods. Shallow snow cores were drilled at selected locations in the spring to determine the density and depth of the winter snow cover. Stakes, in the accumulation zone, and wires or stakes, in the ablation zone, were left during the summer for a readout in the fall allowing for summer mass balance estimates. For Vatnajökull and Langjökull spatially continuous maps were derived based on dense point data (Pálsson et al., 2020a, b) while for Hofsjökull and Mýrdalsjökul point data were available representing the main glacier outlets. These procedures for drilling and post processing of data are described in many previous studies and annual reports of mass balance (Ágústsson et al., 2013b; Þorsteinsson et al., 2017; Pálsson et al., 2020a, b). Data was available for Vatnajökull (glaciological years 1991/92 to 2018/19), Hofsjökull (1987/88 to 2018/19) and Langjökull (1996/97 to 2018/19). Data spanning the study period includes 1227, 389, 383 and 68 surface mass balance observations for Vatnajökull, Hofsjökull, Langjökull and Mýrdalsjökull, respectively.

3.3 Snow cover and albedo data

For the SWE reconstruction model applied in this study, fractional snow covered area (fSCA) and snow- and ice surface albedo (α) were derived from Moderate Resolution Imaging Spectroradiometer (MODIS) data using processing models developed for Iceland by Gunnarsson et al. (2019, 2021). Both products rely on the MOD10A1 (Terra satellite) and MYD10A1 (Aqua satellite) fractional snow cover (Scientific Data Set: NDSI Snow Cover) and snow albedo (Scientific Data Set: Snow Albedo Daily Tile) for the grid tile h17v02 covering most of Iceland, excluding a small portion of the Snæfellsnes peninsula.

For fractional snow cover, three main processing steps were applied. First, daily tiles from MOD10A1 and MYD10A1 were merged to a single daily tile with priority to Terra data due to failure in band 6 in Aqua (Lingli Wang et al., 2006). Second, to reduce the remaining cloud obscured pixels a temporal aggregation was applied. The temporal aggregation range is set as the number of days backwards and forwards each center date data were allowed to search for classified pixel data. Priority was given to data closest to the center date data and from the forward date if both backward and forward dates have data. The aggregation window was 7 days. Finally, the remaining cloud obscured pixels after daily merging and temporal aggregation, were classified using a classification trees trained daily on four predicting variables, location (easting, northing), elevation (Z) and aspect. Further information and details are in Gunnarsson et al. (2019).

For snow- and ice surface albedo, the first processing step were the same as for fSCA while the aggregation window was 11 days for temporal aggregation. The remaining cloud obscured pixels after daily merging and temporal aggregation, were classified with a daily trained random forest model using the same predicting variables as for fSCA. Further information and details are in Gunnarsson et al. (2021).

3.4 Seasonal snow data

Few sites had snow field survey data available for the study period. The most extensive data was from the Setur AWS in the south-central highlands where from 2004 to 2015 ground-based estimates of SWE was available from snow transect surveys conducted in March or April each year. Concurrently, spatial variability of SWE has been estimated on two 1 km long transects with a north-south and east-west orientation where snow depth was collected at 100 m intervals. The main snow pit for SWE location was located at the mid of these two transects. Since 2015 a Campbell Scientific passive CS725 snow-water equivalent sensors has been operated at the site. The sensor detects the attenuation of the electromagnetic energy from the ground, and SWE can be estimated. The CS725 estimates SWE over an area of 50 to 100 square meters and provides a timeseries of SWE estimation.

Snow pit data were also available from other sites spanning the study period. In total 70 estimates of SWE collected from mid-March to mid-April were used. For the majority of the observations snow density was measured in 10 cm increments from the snow surface to the ground using a 1000 cc Snowmetric RIP1 density cutter (Kelly cutter). Combination of depth and density provides point-based SWE estimates at the site. At some sites collections were done with Federal or SnowHydro samplers (coring tubes). In those cases, 3-5 cores were taken at each site and the average of all collections used as the mean SWE estimate.

3.5 Model Forcing

Meteorological forcing were from the RAV2 project. RAV2 is based on the Weather Research and Forecast model (WRF) version 3.6.1 coupled to the NOAH land surface model to provide climatological surface variables at a 2 km spatial resolution and 1 hour temporal resolution spanning the period from 1.9.1957 to 31.8.2019. From 1979 to 2019 the model was forced with boundary conditions from the the European Centre for Medium Range Weather Forecasts (ECMWF) ERA-Interim reanalysis (Berrisford et al., 2011). The model domain spans Iceland in a nested domain at a 2 km spatial resolution at the surface (326 x 256 pixel) whereas the outer domain of the model has a spatial resolution of 10 km (121 x 111 pixels). Vertical resolution is 65 levels up to the 25 hPa level. Relevant surface data for melt calculations were extracted for use in the reconstruction model: air temperature at 2 m, surface temperature, incoming long- and short-wave radiation, surface pressure, specific humidity and re-sampled to daily average values. Further description of the RAV2 model setup and output configuration is found in Rögnvaldsson (2016).

Downscaling of the meteorological forcing from the 2 km RAV2 WRF grid to the 500 m MODIS grid was based on the IslandsDEM digital elevation model (DEM) from the National Land Survey of Iceland at a 20m spatial resolution (Accessed 01.06.2021). Bi-cubic interpolation was applied to regrid the DEM to the MODIS grid. Variables dependent on elevation (air temperature and long-wave radiation) were adjusted for the difference between the coarse-resolution RAV2 DEM and high-resolution IslandsDEM at 500 m using a lapse rate. Air temperature, T_A, was downscaled from 2 km RAV2 reanalysis data to 500 m grid cells using an environmental lapse rate of –6.5°K/km assuming a linear dependence on elevation above mean sea level uniformly across the domain outside of glaciated areas (Crochet and Jóhannesson, 2011; Nawri et al., 2012). For glaciers, an environmental lapse rate of –7.0°K/km was used for JFMA and SOND while –5.5°K/km was applied for the active melt season, MJJA, following results from (Gardner et al., 2009; Hodgkins et al., 2013).

Downward long-wave radiation is primarily determined by humidity and temperature vertical atmospheric profiles, which correlate strongly with elevation (Plüss and Ohmura, 1997; Ohmura, 2001). In this study no adjustments were made to account for enhancement of long-wave radiation due to terrain emission as the conditions were not general in Iceland while a lapse rate of -29 W m^{-2} km^{-1} was used for elevation difference adjustment. Further details on downscaling of temperature and long-wave are in Gunnarsson et al. (2022)

3.6 SWE reconstruction model

The reconstruction model adopted in the present study was based on formulation proposed by Brubaker et al. (1996) and used by Rittger et al. (2016). The formulation uses an explicit calculation for short-wave and long-wave radiation terms and a pseudo-physically based formulation for turbulent fluxes relying on an degree day factor and temperature. The potential melt energy, $(M_{p,j})$, in W m^{-2} at time *j*, was defined as:

$$M_{p,j} = m_f R + \beta T_d \tag{1}$$

where m_f is a conversion factor from energy to melt, 0.26 mm day^{-1} per W m^{-2}, R was the net radiation, β was a degree day factor and T_d was the mean daily temperature above 273.15 K. $M_{p,j}$ was set to zero (no melt) when the temperature was less or equal to 273.15 K or when fSCA was less than 10 % for a given pixel.

The net radiation flux, *R* was defined as:

$$R = SW\downarrow(1-\alpha) + (LW\downarrow + LW\uparrow) \tag{2}$$

where SW↓ is incoming solar radiation, α was broadband albedo from MODIS and LW↓ and LW↑ were incoming and outgoing long-wave radiation, respectively. Outgoing long-wave radiation (LW↑) defines the radiation emitted to space by Earth's surface and depends on surface temperature. Here, outgoing long-wave radiation was calculated based on the Stefan-Boltzman law:

$$LW\uparrow = \varepsilon\sigma T_s^4 \tag{3}$$

where ε was the emissivity of snow (0.99) (Dozier and Warren, 1982), σ was the Stefan-Boltzman constant and T_s was surface temperature in Kelvin. Simple approximations have been adapted assuming surface temperature to be equal to daily average 2 m air temperature but constrained to a maximum of 0°C and to lag 2 m air temperature in time to present surface temperature (Cline et al., 1998; Jepsen et al., 2012; Guan et al., 2013). More complex methods have also been adapted, solving for the snow surface temperature as the equilibrium temperature that balances the energy exchanges (Bair et al., 2016, 2018; Huai et al., 2020). Raleigh et al. (2013) suggested using dew point temperature as an snow surface temperature proxy, which was adopted for further calculations in this study. Solutions for T_s > 273.15 K indicate availability of melt energy and T_s was set as 273.15 K and melt $(M_{p,j})$ was computed, otherwise, melt was set to zero.

At any time *j*, available melt energy $(M_{a,j})$ to melt snow and ice in a given area, was the product of the potential energy $(M_{p,j})$ and the fractional snow cover $(fSCA_j)$ (0-1) of the area or pixel:

$$M_{a,j} = M_{p,j} \times fSCA_j \tag{4}$$

Fractional snow cover and albedo was based on MODIS processed products described in Section 3.3. For glaciated areas a constant fSCA mask at 100 % snow cover was applied and glacier boundaries were kept fixed through the study period (2000–2019) using the available delineation spanning 2007—2013 from Hannesdóttir et al. (2020).

For seasonal snow, $M_{a,j}$ was summed from the day of snow disappearance in the MODIS fSCA data until March 15th each year. In theory, the peak SWE date can be estimated from the earliest date when melt energy was zero for an extended time in Spring. In many studies ancillary information (snow pillows or other SWE sources) was used to estimate the date of peak SWE such as station data or other field data (Rittger et al., 2016; Bair et al., 2016) while in many cases no such data were

available. For glaciers, snow cover was 100 % during all periods and all available melt energy was summed to account for annual summer melt. For seasonal snow maximum SWE was determined as the maximum accumulated value for each pixel. In the case of glaciers all calculated melt was accumulated from March 15th out through September except for 2019 where no climate forcings were available for the month of September due to end-of-life of ERA-Iterim.

In reality, glaciers melt both accumulated winter snow, firn and ice during the melt season. In literature, daily glacier summer melt is referred to as summer ablation and the accumulated summer ablation over the melt period as summer mass balance (b_s) (Cogley et al., 2010). Here, for simplification, snow water equivalent (SWE) was refereed to both reconstructed seasonal snowpack and glacier ablation. For calculated daily melt, the calculation process was the same for glaciers and seasonal snow with the exception of a constant full areal snow cover for glaciers.

3.7 Cold content

Cold content is a component of the snowpack energy balance representing the internal snowpack energy deficit. This deficit must be overcome before runoff from a snowpack can occur. Cold content is a linear function of snow water equivalent (mass) and snowpack temperature where colder and greater SWE snowpacks have higher energy deficits (Jennings et al., 2018). Many previous reconstruction studies estimated cold content by using a proxy. Jepsen et al. (2012) initialized cold content as zero at midnight each day and kept a running total of the net energy flux to the snowpack. This sum, when negative, was set to equal the magnitude of cold content. By applying this method melt spikes during winter where reduced. Bair et al. (2018) used a similar approach while resetting cold content not daily at midnight but daily after sunset.

Cold content was not modeled in this study since the density and depth of the snowpack were not known. A similar method was applied for cold content as in (Jepsen et al., 2012). For seasonal snow daily melt energy was calculated and if negative applied as the pixels cold content for next days calculation. This value was updated each day if the melt energy was negative. For glaciers, generally the winter snowpack was much deeper and holds more cold content, especially at higher elevations and in the accumulation areas compared to seasonal snow. A simple scheme based on elevation was applied where the cold content was based on a running sum over a set number of days and applied daily as the cold content to overcome. The number of days summed over, was based on elevation of the pixel, thus from 250 m a.s.l., in 250 m steps one day was added to the sum. This means that a pixel located on a glacier at or lower than 250 m a.s.l. has the same cold content criteria as seasonal snow while a pixel above 250 m a.s.l. and below 500 m a.s.l. sums negative energy over two days and etc. The thresholds were based on preliminary model testing but seem to have limited influence on melt magnitude on seasonal scales.

4 Validation

4.1 Energy balance components

Figure 2 shows the comparison of observed and modeled air temperature, LW↓ and SW↓ for the different met station locations, on glaciers (GAWS) and on non-glaciated areas (AWS). Validation of RAV2 data has been reported in more detail for glaciers in Gunnarsson et al. (2022). For the full validation period, April through October, each year the results show a good agreement, both visually and statistically and were within ranges reported in other studies (Schmidt et al., 2017). Table 3 shows the validation results for the whole validation period (AMJJASO), similar to Figure 2 but also for individual months within the full validation period.

Coefficient of determination (R^2) for air temperature ranges from 0.92 to 0.56 for glaciers with the lowest values in July and August. For stations on land the R^2 values were higher, ranging from 0.94 to 0.83 with less systematic bias during July and August as for sites on glaciers. Lower R^2 values on glaciers during the the mid- and late summer might relate to underestimation of LW↓ consequent with negative temperature biases. The consistent negative bias indicates that the model slightly overestimates air temperature. A similar bias was observed for the whole period for stations on land. The Root mean square errors (RMSE) were similar, 1.38°C and 1.35°C for glaciers and land. For individual months, air temperature generally had somewhat better results for sites on land than glaciers. For all sites air temperature RMSE ranges from 0.76 to 1.25°C with no systematic pattern for different months. The lowest values were observed in October both for land and glaciers.

For radiation, much fewer sites on land had observations of incoming short- and long-wave radiation. For short-wave RMSE ranged from 9 to 61 W m^{-2} with the highest values during summer consistent with the summer solstice. R^2 values range consistently from 0.41 to 0.64 and overall the bias is positive ranging from -3.6 to 25 W m^{-2}. For long-wave radiation agreement was good, with RMSE from 8 to 26 W m^{-2}, R^2 ranging from 0.55 to 0.79 and a general negative bias from -2 to -18 W m^{-2}. The instrument reported uncertainty in daily total less than 5 % (∼15 W) for short-wave radiation and less than 10 % (∼30 W) for long-wave radiation. Recent work by Schmidt et al. (2017) reported similar results when validating HIRHAM5 for surface mass balance calculations for Vatnajökull.

4.2 Summer mass balance for glaciers

Figure 3, shows the validation results for point summer mass balance data for Vatnajökull, Hofsjökull, Langjökull and Mýrdalsjökull, respectively. The agreement between reconstructed SWE and observations was acceptable for Vatnajökull while poorest for Mýrdalsjökull. For Vatnajökull 1227 observations were available within the study period resulting in an average RMS error of 0.43 m, R^2 as 0.94 with very low bias, only 0.02 m. Recent work by Schmidt et al. (2017) using the hydrostatic RCM HIRHAM5 model with a new albedo parametrization, dependent both on snow age and surface temperature, simulated the mass balance of Vatnajökull. Surface mass balance validation for summer mass balance showed a bias of 0.5 m, and an average RMSE values of 0.8 - 0.94 m. In this study, for Hofsjökull, Langjökull and Mýrdalsjökull higher bias values were observed than at Vatnajökull, 0.38, 0.11 and 0.47 m respectively, with similar RMSE values as seen for Vatnajökull, 0.43, 0.37 and 0.35 m for Hofsjökull, Langjökull and Mýrdalsjökull, respectively. For these glaciers ablation was systematically overestimated

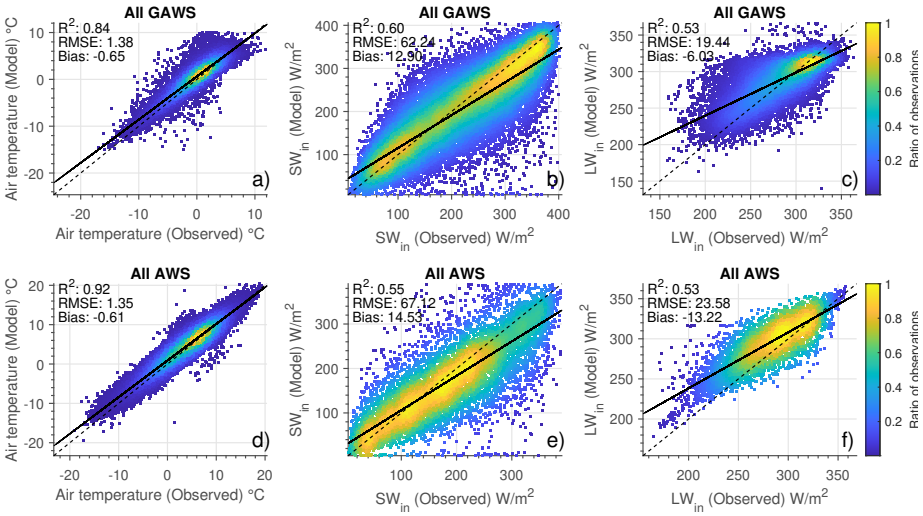

Figure 2. Validation of the downscaled daily RAV2 modeled incoming solar radiation, incoming long-wave radiation, and air temperature with ground observations. **a) to c)** shows results from weather stations operated on glaciers (GAWS) while **d) to f)** shows results from stations outside of glaciers (AWS). Color shows the normalized (0-1) density distribution of data. Doted black line shows 1:1 and black line the calculated linear fit to the data.

at higher elevations (deeper winter snowpack), most visualized for Mýrdalsjökull where winter snow thickness ranges from 10–18 m (Ágústsson et al., 2013a).

Table 3. Summary statistics for observed and simulated air temperature at 2 m height, incoming short-wave radiation and incoming long-wave radiation. Monthly and inter seasonal variations statistics were compiled for the whole period, April through October, as well as for individual months. id refers to type of station (L for land and G for glaciers). No. sites accounts for the number of sites used in the validation. Note that number of sites shows the number of sites used for air temperature calculations. In almost all cases the availability of radiation observations was much lower. Refer to Table A1for individual sites and instruments available.

		T_2 (°C)			SW_{in} (W m^{-2})			LW_{in} (W m^{-2})			
Period	id	No. sites	RMSE	R^2	Bias	RMSE	R^2	Bias	RMSE	R^2	Bias
AMJJASO	L	70	1.07	0.94	-0.55	49.23	0.64	11.35	16.12	0.67	-14.55
AMJJASO	G	20	1.10	0.84	-0.65	55.74	0.63	14.80	13.40	0.63	-6.30
Apr	L	69	1.11	0.91	-1.06	33.73	0.56	-3.61	9.45	0.76	-16.89
Apr	G	1	1.19	0.92	-0.57	45.08	0.39	6.58	18.19	0.39	-31.94
May	L	69	1.14	0.88	-0.99	45.77	0.56	12.26	9.19	0.79	-14.75
May	G	18	1.25	0.83	-1.04	56.81	0.41	19.68	13.88	0.61	-13.53
Jun	L	69	1.12	0.83	-0.42	55.93	0.57	26.09	9.49	0.69	-14.46
Jun	G	20	0.90	0.74	-0.71	61.32	0.45	23.42	12.80	0.63	-6.74
Jul	L	69	0.96	0.85	-0.13	54.42	0.53	23.13	8.79	0.70	-12.82
Jul	G	20	0.94	0.56	-0.53	57.92	0.50	25.50	12.57	0.61	-2.85
Aug	L	70	0.84	0.86	-0.33	55.96	0.49	9.44	26.39	0.56	-17.83
Aug	G	19	1.03	0.60	-0.65	47.18	0.55	9.74	12.48	0.61	-3.17
Sep	L	70	0.78	0.93	-0.50	25.64	0.61	1.30	9.89	0.71	-11.02
Sep	G	17	1.11	0.82	-0.58	34.44	0.50	-4.88	13.32	0.55	-4.57
Oct	L	63	0.76	0.94	-0.70	9.63	0.78	-8.77	8.64	0.68	-11.92
Oct	G	12	0.77	0.94	-0.45	27.81	0.41	-6.52	11.31	0.55	-4.99

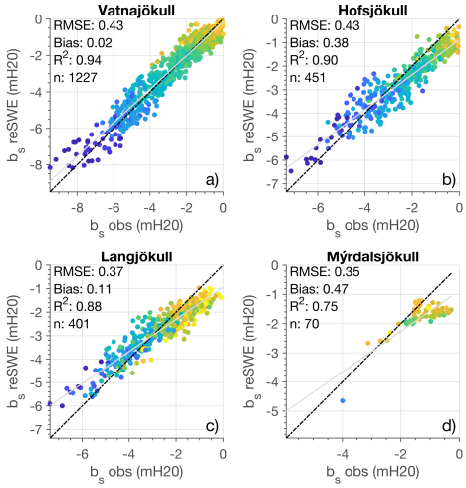

Figure 3. Comparison of calculated and observed summer mass balance (b_s) for selected glaciers. Doted black line shows 1:1 and grey line the calculated linear fit to the data. The colorbar refers to the elevation of each observation point in the comparison with respect to the elevation range of each glacier.

4.3 Seasonal snow

Figure 4a shows comparison of timeseries from SWE calculated with the model and observations from a CS725 Snow Water Equivalent Sensor from April 1st each year (2015-2019) and until mid-July at Setur AWS. The general evolution of the SWE was represented by the model, especially during the active melt period, although discrepancies were observed with overestimations of peak SWE in 2017 and 2018 and underestimation in 2015. In 2019 and 2016 the model reconstructs maximum SWE well. In 2016 to 2018 the timing and temporal evolution melt period was reconstructed well. In 2015 and 2019 the reconstructed SWE plateaus (120 DOY in 2019 and 185 DOY in 2015) and disconnects from the observed melt progress. The AWS at Setur is in a small flat area surrounded by small trenches, hills and gullies where snow can accumulate providing intermittent snow cover during the melt season. This difference could be explained by pixel classification as snow from MODIS data while snow has already melted at the AWS site. A time lapse camera located at Setur partially confirms this behavior and high-resolution imagery from Sentinel 2 and Landsat also show the area with distributed snow patches in late spring. At Setur spatial variability of SWE has also been estimated on two 1 km long transects with a north-south and east-west orientation collected at 100 m intervals. The main snow pit and AWS observations was located at the mid of these two transects. For available observations at Setur the standard deviation of snow depth was 0.3 m with snow depths often observed being more than twice as deep or shallow as at the snow pit location due to wind redistribution.

Figure 4b shows reconstructed maximum SWE from the model compared to all available snow pit observations. Comparison shows RMSE as 0.29 m with a negative bias of 0.18 m. The comparison indicates that in some cases modeled data were overestimated although fewer cases were underestimated. Observed SWE measurements represent well snow depth and density at the location of the observation while in many locations have limited representation of the near surroundings. Glacier mass balance components at Icelandic glaciers have better spatial representation from a point to their near surroundings as the observations were done in relatively flat areas.

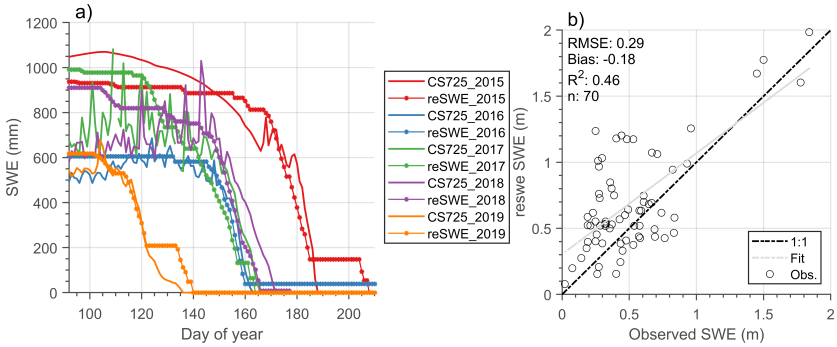

Figure 4. a) Comparison of SWE from April 1st 2015 to 2019 for observed SWE using a CS725 and estimation from the reconstructed SWE. **b)** Comparison of observed maximum SWE in Spring (mid-March to mid-April) against reconstructed SWE for selected years.

5 Results

5.1 General spatio-temporal characteristics of SWE

Annual SWE variability were generally high both for seasonal snow and glaciers. Figure 5 shows the spatial patterns for average reconstructed SWE for seasonal snow and glacier ablation for the period 2000-2019. Two color maps were used to distinguish between glacier ablation (negative) and seasonal snow (positive). For seasonal snow, the largest SWE (>1000 mm) were found in mountainous and alpine areas close to the coast, notably in the East- and Westfjords, Tröllaskaga, and in the proximity of glaciers. Smaller SWE was observed in the central highlands, flatter inland areas and at lower elevations. This agrees with simulated precipitation climatologies by Crochet et al. (2007b) where less precipitation and dryer areas were found north of Vatnajökull and Hofsjökull and in the area in between the two. It must be noted that in lower elevation non-glaciated areas, the reconstruction might not represent accurately the total winter snowpack, as the buildup of a snowpack and complete melt out in the period from October to March every year were frequent due to the high winter weather variability and melt-out events.

For glaciers, generally more SWE (more ablation in ablation area) was associated with lower glacier elevations while less ablation was observed at higher elevations (accumulation areas). For the dirty impurity-rich bare-ice areas exposed annually observed SWE was the highest, averaging more than 3000 mm in agreement with surface mass balance observations (Pálsson, 2020; Þorsteinsson et al., 2017; Pálsson et al., 2020b). Years with high summer ablation reveal certain patterns where more ablation was observed in the accumulation areas associated with cloud free warm summer periods, but also a strong link to below average albedo due to LAPs melt enhancements, reported in (Gunnarsson et al., 2021, 2022). The lower limit of albedo

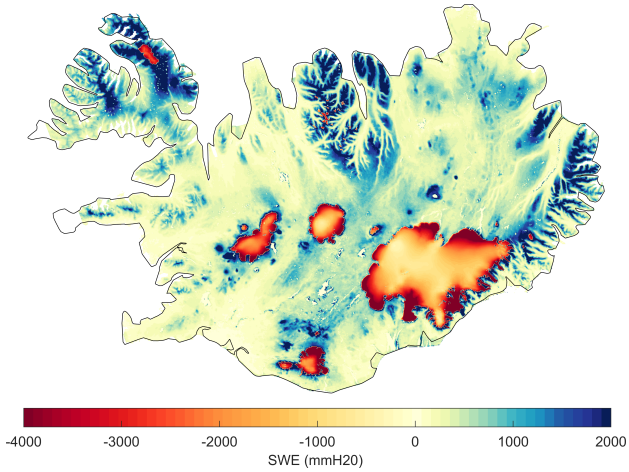

Figure 5. Spatial pattern mean of reconstructed SWE and glacier ablation for the period 2000–2019. Glacier ablation is shown as negative values (white to red) and seasonal snow (white to blue) to distinguish better between seasonal snow and glacier ablation as their total magnitude was generally had diferent ranges.

(0.1 to 0.25) in the bare-ice areas limit further radiative forcing and reduce the annual melt variability in these areas, although melt-out timing of winter snow modulates melt variability and intensity Gunnarsson et al. (2022).

Figure 6 shows spatial distribution of mean SWE for individual months, from April to September for the period, i.e., mean accumulated average melt for each month. Grey areas indicate either snow free areas or snow-covered areas where no melt is produced. In April and May, seasonal snow at lower and mid elevations were mostly depleted with May generally producing more melt than in April. The highest melt volumes were in May and June. In June and July seasonal snow was mostly constrained with high SWE accumulation areas. In September, and even August on a few occasions, small snowfalls were often observed, generally melted out but in some higher elevation areas forming the base for the following winters snowpack.

For glaciers the onset of melt was observed in April at lower elevations, especially for the low elevation outlet glacier of southern Vatnajökull melt was observed for the all months. With warmer temperatures and increasing short-wave energy in May and June more glacier ablation was observed generally peaking in late June to mid-July. As winter snow melted out impurity-rich bare-ice areas were exposed, with low albedo values forcing more short-wave energy, increasing melt.

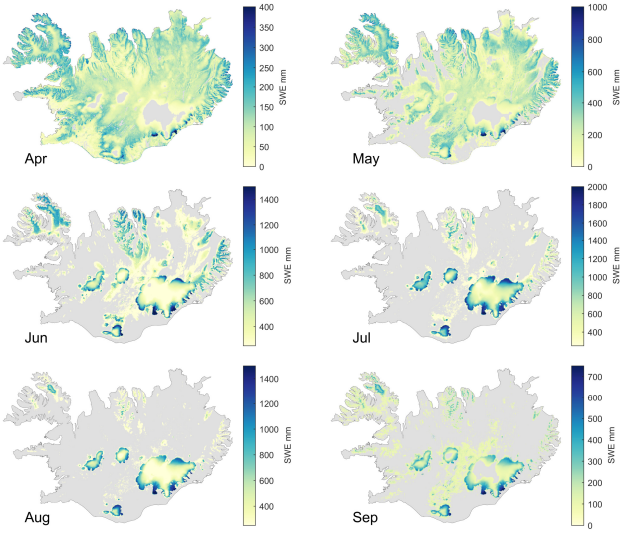

Figure 6. Spatial patterns of mean reconstructed SWE for the period 2000–2019 for individual months from April to September.

5.2 Inter-annual variability of SWE

Figure 7 shows annual spatial patterns for melt season (AMJJAS) SWE anomalies for 2000–2019. Blue colors represent anomalies below the mean, i.e., lower melt season average SWE values, while red areas represent values above the mean, contributing more seasonal SWE. No clear correlation was found for seasonal snow and glacier ablation, i.e., melt anomalies were not associated with same-sign anomalies for glaciers, although certain patterns could be identified.

In 2000 a large negative anomaly was observed for seasonal snow in the north and in Austfirðir at higher elevations in the fjords. In the mountains and fjord closer to the sea in Austfirðir higher values of SWE were observed. In the area north of Mýrdalsjökull and at Strandir a positive SWE anomaly was observed. For all glaciers, except for the northern outlets of Vatnajökull, neutral or negative anomalies were observed. At northwest Vatnajökull (Dyngjujökull) an isolated area of melt enhancement was observed unlikely linked to the 2000 Hekla eruption but presumed to be a combination of residual effects from the Gjálp eruption in 1996 and dust transported from the pro-glacial areas near the terminus (Gunnarsson et al., 2021).

In 2001, 2009, 2011, 2013, 2015 and partially 2017 all main glaciated areas had negative glacier ablation anomalies while high melt years were seen in 2003–2008, 2010, 2012. 2014 and 2019. For glaciers, melt enhancing events can be defined as dust deposits from pro-glacial areas or other unstable erosive surfaces where the production of LAPs were often observed.

Volcanic eruptions can also produce large amounts of ash and tephra than can deposit in glacier surfaces influencing energy balance. The largest anomalies for glaciers were observed at all glaciers in 2010 associated with severe LAP deposition due to the volcanic eruption in Eyjafjallajökull along a warm and sunny summer. Less melt enhancement was observed associated with the 2011 Grímsvötn eruption at Vatnajökull although the LAP depostits were quite clear in surface albedo data south and southeast of the Grímsvötn eruption site (Gunnarsson et al., 2021). One difference between these two events for the southern outlet of Vatnajökull was a later onset of LAPs in 2011 but also a colder cloudier spring and summer. Less incoming short-wave radiation was forced by the surface in June and much less in July and August in 2011 than for 2010 explaining most of the difference in melt. With similar climate in 2011 as 2010 much more melt could have been observed (Gunnarsson et al., 2022). A positive melt anomaly in 2019 at all major glacier except for Drangajökull has been linked with extensive LAP deposits with early melt-out of seasonal snow in the highlands exposing unstable dust hotspots, a rich source of LAPs transported by air.

Care must be taken when interpreting melt in areas were volcanic ash and tephra deposits were influencing melt as the thickness of the deposit layer can have great impact on the melt energy for actual melt. Generally, results show that a thin ash layer increases the snow and ice melt but an ash layer exceeding a certain critical thickness causes insulation. Dragosics et al. (2016) reported that insulation effects of Icelandic dust and volcanic ash on snow and ice were observed at only 9–15 mm thickness depending on the type of material.

Schmidt et al. (2018) did simulations of the surface climate and energy balance of Vatnajökull ice cap to estimate the glacier runoff sensitivity to the spring conditions, e.g., snow thickness. The simulations showed for the whole ice cap runoff variability was on average 31 % as a function of varying spring conditions, while for certain outlets higher (Brúarjökull, 50 % of the variability). Snow thickness in the ablation area had major control on the timing of the exposure of the underlying impurity-rich bare-ice. From figure 7, some years with high seasonal snow (red colors) and low glacier ablation (blue colors) can be identified. Years such as 2001, 2009, 2011, 2013, 2015, 2017 exhibit a pattern where seasonal snow was above average in the highlands and glacier ablation was overall below average. Other years, such as 2003, 2005, 2010, 2012, and 2019 show the opposite, less seasonal snow and above average glacier ablation. This supports the control and relationship between the impact of thick winter snow in the ablation area modulating melt due to delayed timing of impurity-rich bare-ice exposure and vice versa. Since the accumulation of seasonal snow is driven by winter precipitation and temperature climatology and dominant storm tracks during the winter season while glacier summer ablation is driven by spring and summer temperatures, cloud cover extent and persistence and surface albedo, often impacted by LAPs, no consistent annual relations between seasonal snow and glacier ablation patterns were observed, other than the suggested impact of winter snow thickness.

Figure 8 shows in two panels the accumulated maximum SWE in mm for the selected catchments and glaciers in Figure 1. The upper panels show basin wide SWE for non-glaciated areas while the lower panel shows basin wide SWE for the glaciated part of the catchment. Coherently to Fig. 5 high seasonal snow areas where the largest average SWE (>1000 mm) was observed was in Austfirðir, Tröllaskagi, Strandir and Vestfirðir. Medium seasonal snow areas where SWE ranges from 600–1000 mm was observed for Lagarfljótsós, Skjálfandafljót, Markarfljót, Núpsvötn and Gýgjukvísl. Other areas on average had small SWE (<500 mm).

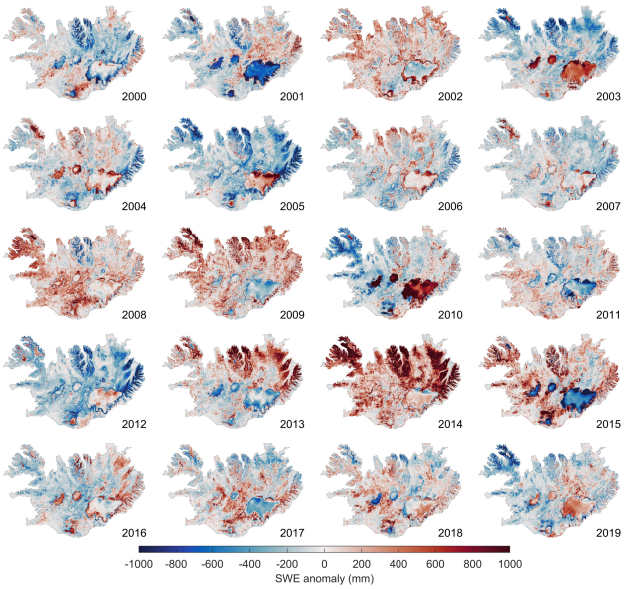

Figure 7. Annual spatial patterns for SWE anomalies for 2000–2019. Red colors denote positive values where melt was above the average, i.e., more melt, while blue colors show less melt.

All areas show high variability with certain grouping of years with similar conditions. Generally, below average conditions were seen in 2001, 2003–2007, 2010, 2012, 2016 and 2019 for all the main catchments. 2005 and 2012 have the largest negative deviations with SWE 130 % below average values. Conditions above average were seen in 2002, 2008–2009, 2014–2015 and 2017–2018. The highest SWE deviations were seen in 2014 and 2015 for all main catchments with SWE 180 % and 135 % on average above average SWE, respectively. Other years have less decisive patterns.

For the glaciated part of the main catchments, the highest SWE values (>3000 mm) were seen for glaciers in Austfirðir, Strandir, Markarfljót and Kúðafljót with average values above 4000 mm for Kúðafljót. Glacier ablation contributing to Markarfljót and Kúðafljót originates from the northern part of Mýrdalsjökull which has large areas of the glacier at relative low elevations (220-300 m a.s.l.) and large unstable erosive surfaces that provide a constant source of light absorbing particles (LAPs) (Gunnarsson et al., 2021). Lowest SWE values (<2000 mm) were seen for Jökulsá á Fjöllum and Skjálfandafljót as could be expected as the glaciated part of the catchment were distributed over quite high elevations, especially in the case for Skjálfandafljót (z_{min} 1040 m a.s.l.). Other glaciated main catchments show average SWE values between 2000 and 3000 mm.

Similar as for seasonal snow melt, glacier ablation variability was quite high between years with below average conditions in 2000, 2001, 2009, 2011–2013 and 2015 where 2001 and 2015 had the largest deviation, 166 % and 173 % below period wide averages, respectively. Above average conditions were seen in 2003 - 2008, 2010, 2014 and 2016 for close to all catchments. In 2019 all glaciers had above average conditions with the exception of glaciers in Vestfirðir and Tröllaskagi. These glaciers were less influenced by conditions providing extensive amounts of LAPs deposited in the glacier surface enhancing melt (Gunnarsson et al., 2021). Other years have less decisive patterns.

No significant correlation was observed between low SWE years for seasonal snow and above average years for glacier ablation. For the period 2003-2007 generally below average SWE values were observed for seasonal snow and above ablation for glaciers. Similar conditions in 2019 were seen where the early country-wide melt out of seasonal snow exposed erosive unstable pro-glacial surfaces and favorable weather conditions allowed for severe dust depositing events.

Figure 9 shows the distribution of melt volume contribution for the main catchments divided between SWE from seasonal snow and glacier ablation. The variability was smaller for areas with very high or low ratios of the glaciers in the catchment. For Austfirðir less than 5 % of annual melt water was a contribution from glacier ablation, less than 10-15 % for Skjálfandi, Standir and Töllaskagi while more than 90 % of the melt water contribution was glacier based for Gýgja although 20 % of the catchment area is non-glaciated. For Blanda and Hvíta í Borgarfirði only about 8-9 % of the catchment was glaciated but provides roughly 20-60 % of the melt water volume. Jökulsá á Fjöllum, Kúðafljót, Lagarfljót, Markarfljót og Skaftá have 15-20 % of their catchment glaciated but receive glaciated ablation water volume ranging from 30 up to 75 %.

Figure 10 shows melt in mm (upper panel) and melt volume anomalies in percent (lower figure) for the main Icelandic glaciers and their sub-areas. A melt anomaly of 100 % represents the mean for the period form 2000 - 2019 year while values below 100 % represent below average melt and vice versa. Glaciers and their sub-outlets are listed from the lowest average ablation (top) to the highest (bottom).

The highest ablation was observed for the northeastern Mýrdalsjökull while closely followed by the other main outlets for Mýrdalsjökull. The northeastern outlet of Mýrdalsjökull is relatively flat with the lowest elevations spans at Mýrdalsjökull. The glacier has close proximity to dust producing erosive pro-glacial areas and warmer temperatures in proximity to the south coast of Iceland. Due to his close proximity to the south coast it receives large amounts of precipitation from frequently passing lows from the south and southwest storm tracks with large orographic uplift and precipitation compared to most other glaciers in Iceland (Ágústsson et al., 2013a; Crochet et al., 2007a). Therefore the high summer ablation is counterbalanced by high winter accumulation. Langjökull and Hofsjökull often had similar summer ablation magnitudes while in most cases more ablation was observed at Langjökull, especially at the southern outlets. The largest glacier, Vatnajökull, had the lowest average summer ablation values. In similar manner as the southern outlets at Mýrdalsjökull, the southern outlets of Vatnajökull had higher ablation values than other outlets, especially in the north. This was driven by similar processes as at Mýrdalsjökull, general warmer temperatures, proximity to the coast and frequently passing lows from the south and southwest storm tracks.

High annual variability was observed for all glaciers. Figure 10 lower panel shows the melt volume anomalies from total annual melt volumes. As previously discussed, high positive 2010 anomaly was driven by melt enhancing LAPs from the eruption at Eyjafjallajökull and a persistent cloud free summer with warm temperature, maximizing the impact of LAPs in the

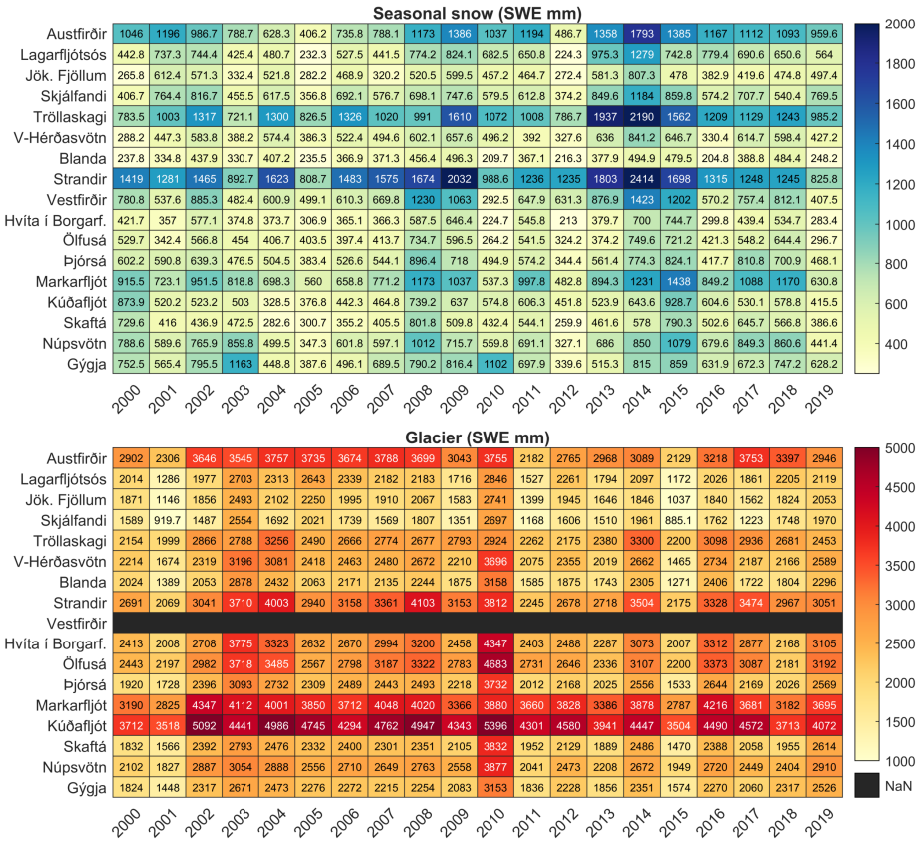

Figure 8. Reconstructed SWE for the main catchments and individual years.

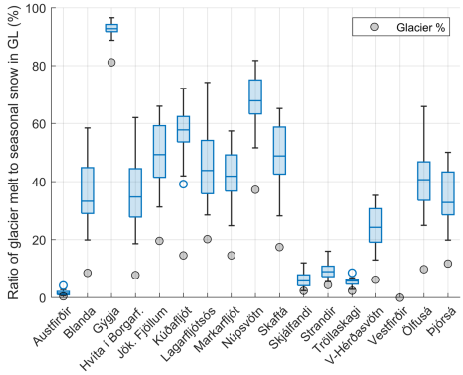

Figure 9. Variability of ratio between melt contribution from seasonal snow and glacier ablation. Grey circles show the catchment area ratio between land and glacier. On each box, the central mark indicates the median, and the bottom and top edges of the box indicate the 25th and 75th percentiles, respectively. The whiskers extend to the most extreme data points not considered outliers.

glacier surfaces. Generally in the period from 2003–2008 melt volumes were above average, with the exception of Hofsjökull and Langjökull in 2005. Below glacier ablation was observed in 2000, 2001, 2013, 2015 and 2017–2018. 2015 was the first year since the glaciological year 1994/95 where net mass balance was reported positive for the glaciers with observed mass balance, identically with the lowest modeled glacier ablation in 2015 (Pálsson, 2020; Þorsteinsson et al., 2017; Pálsson et al., 2020b).

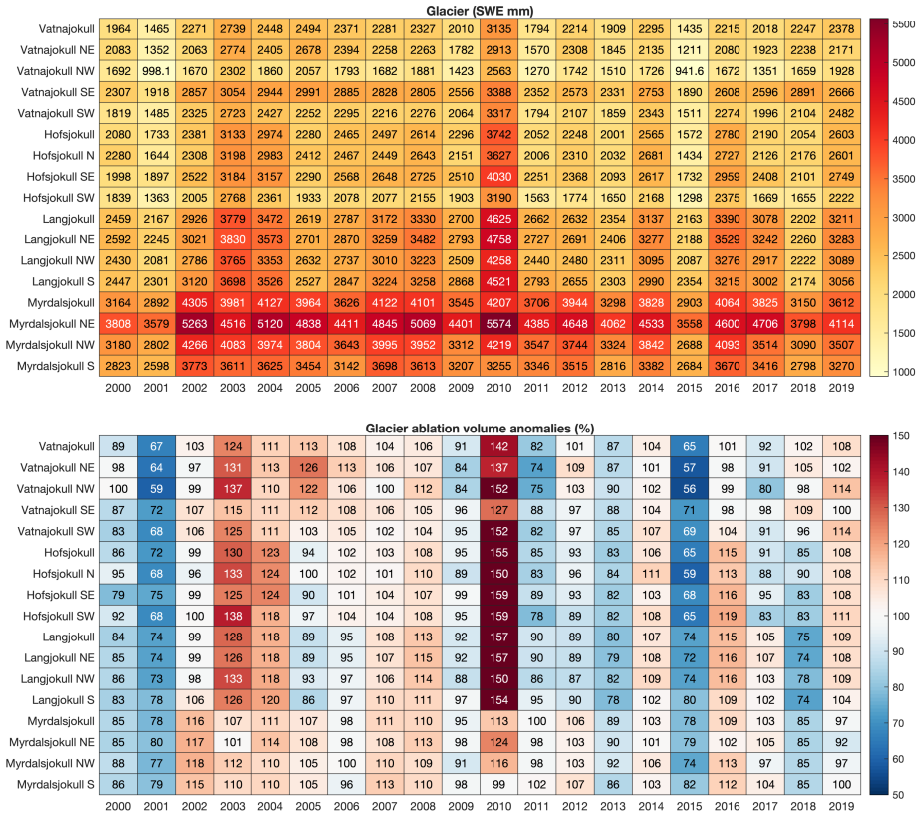

Figure 10. The figure shows melt in mm (upper panel) and melt volume anomalies in percent (lower figure) for the main Icelandic glaciers and their sub-areas. A melt anomaly of 100 % represents the mean for the period form 2000 - 2019 year while values below 100 % represent below average melt and vice versa. Glaciers and their sub-outlets are listed from the lowest average melt (top) to the highest (bottom)

5.3 Trends of melt

Figure 11 shows the spatial pattern of mean melt season (AMJJAS) trends in terms of the total change of a least-square fit to the SWE from 2000-–2019. Statistically significant trends (p>0.05) are shown with stipples. Negative significant trends at the terminus of glaciers were expected due to glacier retreat in recent decades, with associated debris deposits on dead ice (Hannesdóttir et al., 2020). Other significant negative trends were not detected. At the northern outlet glaciers of Vatnajökull, Brúarjökull and Dyngjujöklull, non-significant trends were observed concurrent with an increasing significant albedo trend for the same period (Gunnarsson et al., 2021). These were in the end-of-year equilibrium-line altitude (ELA) area which varies from year to year. This pattern might support changes since 2012 where more winter bass balance has been observed and genereal less summer ablation, pushing the ELA to lower elevations (Pálsson, 2020). For seasonal snow, significant positive trends were observed for most of mountain tops in Austfirðir and Tröllaskagi. These trends align with recent results from the same period from (Gunnarsson et al., 2019), reporting that the snow cover extent was spanning a longer time, i.e., that snow cover was extending further into the spring and summer months. It is noted that only 20 years of data were available when reporting trends.

6 Conclusions

In this study, snow water equivalent was reconstructed using a gap-filled satellite-observed albedo and fractional snow cover data forced with climatological data. Data was calculated at a 500 m spatial resolution from 2000 until 2019 from mid-March out through September spanning spring and summer melt periods.

Energy balance components were thoroughly validated using in situ automatic weather station data with good statistical agreement. For the reconstruction of glacier ablation, long-term extensive in situ data was available of mass balance observations to validate the results. A good statistical agreement was found between model results and observations. For seasonal snow much less in situ data was available to validate the model results although the limited data available shows acceptable performance.

Overall, the results show the annual high variability in seasonal snow and glacier ablation SWE production. For seasonal snow, the majority of melt water production was observed in April and May while high accumulation areas in the highlands retain snow into June and July. Glaciers had limited ablation in April although in proximity to the south coast, high ablation values were observed. The majority of the ablation occurs in June, July and August with increasing bare-ice exposure but lowering solar elevation angles (less availability of short-wave energy), while May and September produce less ablation water on average.

Light absorbing particles (LAPs) produced in volcanic eruptions and from pro-glacial hotspots deposited in the surfaces of glaciers have a strong influence on glacier ablation, clearly depicted in 2010 and 2019. Significant positive trends of SWE were observed in mountainous north and east Iceland while other areas glaciers show a non-significant trend although trends with only 20 years of data should be reported with care.

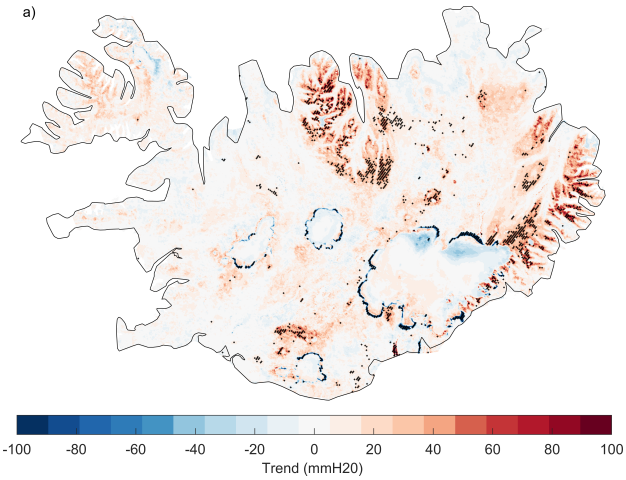

Figure 11. Spatial pattern of mean melt season (AMJJAS) trends in terms of the total change of a least-square fit to the SWE from 2000-–2019

The model pipeline developed can utilized alternative climatological forcing data and the previously adopted methods to produce spatio-temporal gap-filled albedo and fractional snow cover data can be utilized with alternative satellite products allowing the model framework to be adopted to future data sources. Although many complex hydrological and glaciological processes were simplified or omitted in the model, the main strength can be found in the real time usability of remotely sensed albedo and fractional snow cover. As the past years have shown in Iceland, real time assessment on the impact of LAPs from volcanic eruptions or large-scale extensive dust deposits events can provide vital information for operations and optimization of water resource usage.

Appendix A: Automatic weather station statistics

Table A1. Summary of meterological observations sites used for validation. id. refers to location of the site, L for non-glaciated areas and G for glaciated areas. The last three columns, N. T_2 obs., N. SW_{in} obs. and N. LW_{in} obs. indicate the number of usable days for each variable at each site.

Lat.	Lon.	Ele.	Site name	id	N. T_2 obs.	N. SW_{in} obs.	N. LW_{in} obs.
63.979	21.6556	530	Bláfjöll úrk.	L	3313		
63.969	21.666	530	Bláfjöll	L	3617		
63.983	21.649	530	Bláfjallaskáli	L	3359		
64.033	21.366	380	Hellisskarð	L	3412		
64.055	21.253	360	Ölkelduháls	L	3434		
64.056	21.346	597	Skarðsmýrarfjall	L	2451		
64.240	21.463	771	Skálafell	L	3286		
64.490	21.762	480	Skarðsheiði Miðf.	L	1734		
64.452	21.403	500.5	Botnsheiði	L	3264		
65.604	23.990	350	Patreksfjörður	L	861		
65.552	21.825	377	Arnkatla	L	1072		
65.578	21.322	282	Ennishöfði	L	704		
65.656	23.002	510	Þingmannaheiði	L	236		
66.044	23.307	753	Þverfjall	L	3571		
66.075	23.198	550	Seljalandsdalur	L	3410		
66.068	23.210	283	Seljalandsdalur	L	2611		
65.123	20.696	383	Austurárdalsháls	L	1558		
65.062	18.838	785	Sáta	L	3476		
65.222	20.056	509	Grímstunguheiði	L	1203		
65.313	19.847	490	Auðkúluheiði Fri.	L	420		
65.230	19.717	506	Kolka	L	3557	944	944
65.341	17.243	405	Svartárkot	L	2939		
65.748	18.001	580	Vaðlaheiði	L	3593		
65.787	17.003	390	Gæsafjöll	L	1624		
65.891	17.228	350	Sóleyjarflatamelar	L	1640		
65.856	17.201	390	Rauðhálsar	L	721		
65.060	16.210	563	Upptyppingar	L	3447		
65.265	14.032	400	Seyðisfjörður Kb.	L	2280		
65.223	14.258	949	Gagnheiði	L	3461		
65.619	16.976	282	Mývatn	L	3615	2171	0
65.629	16.837	347	Bjarnarflag	L	1503		
65.642	16.128	390	Grímsstaðir á Fjöllum	L	1268		
65.710	16.878	560	Reykjahlíðarheiði	L	376		
65.694	16.774	455	Krafla	L	1436		

Table A1. continued

Lat.	Lon.	Ele.	Site name	id	N. T_2 obs.	N. SW_{in} obs.	N. LW_{in} obs.
65.911	16.976	311	Þeistareykir	L	2535		
65.375	15.883	450	Möðrudalur	L	2786		
64.828	16.089	748	Brúaröræfi	L	2339		
64.816	15.322	750	Innri Sauðá	L	726	554	554
64.798	14.789	590	Líkárvatn	L	1285		
64.728	16.111	845	Brúarjökull B10	L	2365	2392	2392
64.928	15.777	639	Kárahnjúkar	L	3617	527	527
65.108	15.529	373	Brú á Jökuldal	L	3615		
64.815	15.423	655	Eyjabakkar	L	3617		
65.079	14.674	573	Hallormsstaðaháls	L	3617		
65.036	14.571	300	Þórudalur	L	336		
64.995	14.510	300	Brúðardalur	L	2024		
65.000	14.462	500	Þórdalsheiði	L	2360		
65.018	14.453	640	Hallsteinsdalsvarp	L	2111		
65.043	14.162	281	Ljósá í Reyðarfirði	L	734		
65.161	13.688	559	Neskaupstaður	L	2666		
63.775	19.677	870	Tindfjöll	L	2199		
64.098	18.614	675	Lónakvísl	L	3474		
64.025	18.119	555	Laufbali	L	3310		
64.199	19.030	555	Vatnsfell I	L	454		
64.195	19.046	539	Vatnsfell	L	2666		
64.395	18.504	647	Veiðivatnahraun	L	3608	0	0
64.317	18.217	726	Jökulheimar	L	3601	2528	888
64.680	19.282	925	Kerlingarfjöll	L	336		

Table A1. continued

Lat.	Lon.	Ele.	Site name	id	N. T_2 obs.	N. SW_{in} obs.	N. LW_{in} obs.
64.604	19.018	693	Setur	L	3602	512	512
64.581	18.598	620	Þúfuver	L	3617		
64.571	18.111	819	Hágöngur	L	2773		
64.866	19.562	641	Hveravellir	L	3193		
64.933	17.983	820	Sandbúðir	L	3579		
64.133	19.725	279	Haf við Ísakot	L	422		
66.063	18.630	450	Ólafsfjörður	L	2211		
66.168	23.268	500	Bolungarvík	L	2327		
66.152	18.936	546	Fífladalir	L	497		
66.153	18.937	600	Fífladalir	L	38		
66.153	18.935	550	Siglufjörður	L	2126		
64.503	17.234	1689	Dyngjujökull	G	484		
64.538	15.597	1141	Hoff	G	1688	1774	
64.514	20.450	588	L01	G	2246	2254	2254
64.302	17.153	1207	Ske02	G	37	39	39
64.728	16.111	779	B10	G	3224	3296	3215
64.575	16.328	1216	B13	G	2043	2725	2338
64.402	16.681	1526	B16	G	2575	2730	2569
64.417	17.319	1405	Grímsvötn	G	2687	791	
64.182	16.335	528	Br04	G	597	600	
64.368	16.282	1242	Br07	G	395	397	
64.325	18.117	771	T01	G	483	567	567
64.336	17.976	1068	T03	G	1943	2586	2094
64.404	17.608	1466	T06	G	2538	2632	1691
64.639	17.522	1945	Bard	G	1509	898	
64.406	17.267	1724	Grímsfjall	G	2495	1324	
63.611	19.158	1345	MyrA	G	385	413	
64.594	20.374	1095	L05	G	2536	2544	2544
64.770	18.543	840	HNA09	G	292	307	307
64.813	18.648	1235	HNA13	G	294	307	307
64.677	15.581	766	E01	G	106	121	121
64.611	15.615	1190	E03	G	115	122	122

Appendix B: Melt stats

Acknowledgements. The authors would like to thank Sibylle von Löwis of Menar at the Icelandic Met Office for providing automatic land weather station data.

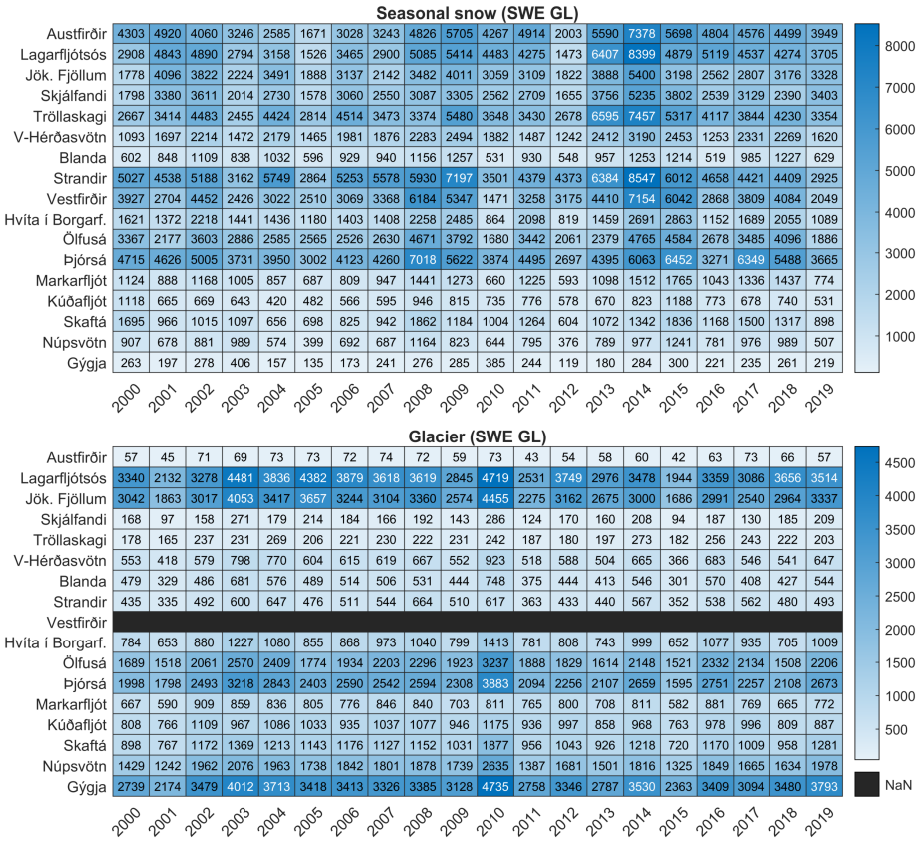

Figure B1. Seasonal snow annual melt volumes for the main catchments for (upper panel) non-glaciated areas and (lower panel) glaciated areas.

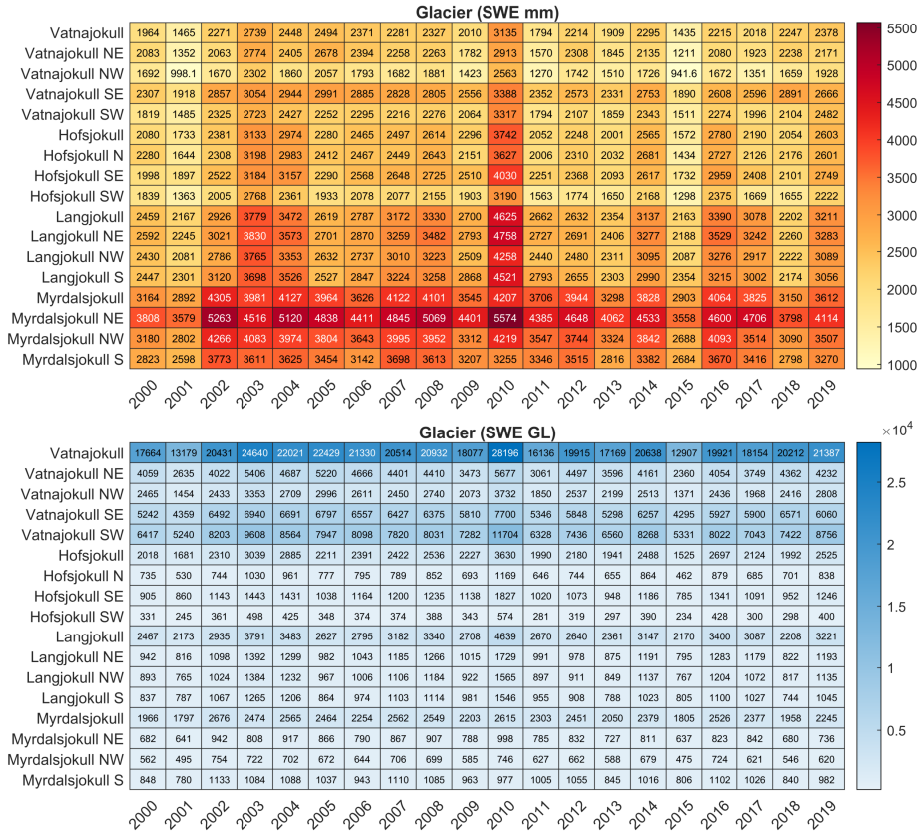

Figure B2. Seasonal snow annual maximum cumulative melt for glaciers (upper panel) and cumulative melt volumes in GL (lower panel).

References

Adam, J. C. and Lettenmaier, D. P.: Adjustment of global gridded precipitation for systematic bias, Journal of Geophysical Research: Atmospheres, 108, https://doi.org/10.1029/2002JD002499, 2003.

Adam, J. C., Clark, E. A., Lettenmaier, D. P., and Wood, E. F.: Correction of Global Precipitation Products for Orographic Effects, Journal of Climate, 19, 15–38, https://doi.org/10.1175/JCLI3604.1, 2006.

Bair, E. H., Rittger, K., Davis, R. E., Painter, T. H., and Dozier, J.: Validating reconstruction of snow water equivalent in California's Sierra Nevada using measurements from the NASA Airborne Snow Observatory, 52, 8437–8460, https://doi.org/10.1002/2016WR018704, 2016.

Bair, E. H., Abreu Calfa, A., Rittger, K., and Dozier, J.: Using machine learning for real-time estimates of snow water equivalent in the watersheds of Afghanistan, The Cryosphere, 12, 1579–1594, https://doi.org/10.5194/tc-12-1579-2018, 2018.

Berrisford, P., Dee, D., Poli, P., Brugge, R., Fielding, M., Fuentes, M., Kållberg, P., Kobayashi, S., Uppala, S., and Simmons, A.: The ERA-Interim archive Version 2.0, ECMWF, p. 23, 2011.

Björnsson, H. and Thorsteinsson, T.: Climate Change and Energy Systems: Impacts, Risks and Adaptation in the Nordic and Baltic Countries, TemaNord, Nordic Council of Ministers, Copenhagen, https://doi.org/10.6027/TN2011-502, 2012.

Björnsson, H., Sigurðsson, B.D., Davíðsdóttir, B., Ólafsson, J. S., Ástþórsson, Ó. S., Ólafsdóttir, S., Baldursson, T., and Jónsson, T.: Loftslagsbreytingar og áhrif þeirra á Íslandi : Skýrsla Vísindanefndar um loftslagsbreytingar 2018., Tech. rep., Veðurstofa Íslands, Reykjavík, 2018.

Björnsson, H.: Hydrology of ice caps in volcanic regions., Reykjavík: Vísindafélag Íslendinga, 1988.

Björnsson, H., Pálsson, F., and Guðmundsson, M. T.: Surface and bedrock topography of the Mýrdalsjökull ice cap, Iceland: The Katla caldera, eruption sites and routes of jökulhlaups, Jökull, 49, 29–46, 2000.

Brubaker, K., Rango, A., and Kustas, W.: Incorporating radiation inputs into the snowmelt runoff model, Hydrological Processes, 10, 1329–1343, https://doi.org/10.1002/(SICI)1099-1085(199610)10:10<1329::AID-HYP464>3.0.CO;2-W, 1996.

Cline, D. W., Bales, R. C., and Dozier, J.: Estimating the spatial distribution of snow in mountain basins using remote sensing and energy balance modeling, Water Resources Research, 34, 1275–1285, https://doi.org/10.1029/97WR03755, 1998.

Cogley, J., Arendt, A., Bauder, A., Braithwaite, R., Hock, R., Jansson, P., Kaser, G., Moller, M., Nicholson, L., Rasmussen, L., and Zemp, M.: Glossary of glacier mass balance and related terms, vol. 86 of *IHP-VII Technical Documents in Hydrology*, International Hydrological Programme, France, 2010.

Crochet, P. and Jóhannesson, T.: A data set of gridded daily temperature in Iceland, 1949–2010, Jökull, 61, 1–17, 2011.

Crochet, P., Jóhannesson, T., Jónsson, T., Sigurðsson, O., Björnsson, H., Pálsson, F., and Barstad, I.: Estimating the Spatial Distribution of Precipitation in Iceland Using a Linear Model of Orographic Precipitation, 8, 1285–1306, https://doi.org/10.1175/2007JHM795.1, 2007a.

Crochet, P., Jóhannesson, T., Jónsson, T., Sigurðsson, O., Björnsson, H., Pálsson, F., and Barstad, I.: Estimating the Spatial Distribution of Precipitation in Iceland Using a Linear Model of Orographic Precipitation, 8, 1285–1306, https://doi.org/10.1175/2007JHM795.1, 2007b.

Dozier, J. and Warren, S. G.: Effect of viewing angle on the infrared brightness temperature of snow, Water Resources Research, 18, 1424–1434, https://doi.org/https://doi.org/10.1029/WR018i005p01424, 1982.

Dragosics, M., Meinander, O., Jónsdóttír, T., Dürig, T., De Leeuw, G., Pálsson, F., Dagsson-Waldhauserová, P., and Thorsteinsson, T.: Insulation effects of Icelandic dust and volcanic ash on snow and ice, Arabian Journal of Geosciences, 9, https://doi.org/10.1007/s12517-015-2224-6, 2016.

Einarsson, M. A.: Climates of the Oceans, H. Van Loon (Ed.). Vol. 15 of World Survey of Climatology, Editor-in-Chief H. E. Landsberg, Journal of Climatology, 5, 673–697, https://doi.org/10.1002/joc.3370050110, 1984.

Elder, K., Dozier, J., and Michaelsen, J.: Snow accumulation and distribution in an Alpine Watershed, Water Resources Research, 27, 1541–1552, https://doi.org/10.1029/91WR00506, 1991.

Elder, K., Rosenthal, W., and Davis, R. E.: Estimating the spatial distribution of snow water equivalence in a montane watershed, Hydrological Processes, 12, 1793–1808, https://doi.org/https://doi.org/10.1002/(SICI)1099-1085(199808/09)12:10/11<1793::AID-HYP695>3.0.CO;2-K, 1998.

Gardner, A. S., Sharp, M. J., Koerner, R. M., Labine, C., Boon, S., Marshall, S. J., Burgess, D. O., and Lewis, D.: Near-Surface Temperature Lapse Rates over Arctic Glaciers and Their Implications for Temperature Downscaling, 22, 4281–4298, https://doi.org/10.1175/2009JCLI2845.1, 2009.

Guan, B., Molotch, N. P., Waliser, D. E., Jepsen, S. M., Painter, T. H., and Dozier, J.: Snow water equivalent in the Sierra Nevada: Blending snow sensor observations with snowmelt model simulations, Water Resources Research, 49, 5029–5046, https://doi.org/10.1002/wrcr.20387, 2013.

Gunnarsson, A., Pálsson, F., Aðalgeirsdóttir, G., Björnsson, H., and Guðmundsson, S.: Monitoring Energy Balance of Icelandic Glaciers for 25 years, Proc. 27th IUGG General Assembly ,Montréal, Québec, Canada., IUGG19-3435, 2019.

Gunnarsson, A., Gardarsson, S. M., Pálsson, F., Jóhannesson, T., and Sveinsson, O. G. B.: Annual and inter-annual variability and trends of albedo of Icelandic glaciers, The Cryosphere, 15, 547–570, https://doi.org/10.5194/tc-15-547-2021, 2021.

Gunnarsson, A., Gardarsson, S. M., and Pálsson, F.: Modeling of surface energy balance for Icelandic glaciers using remote sensing albedo, to be submitted, manuscript in preparation, 2022.

Hannesdóttir, H., Sigurðsson, O., Þrastarson, R. H., Guðmundsson, S., Belart, J. M., Pálsson, F., Magnússon, E., Víkingsson, S., Kaldal, I., and Jóhannesson, T.: A national glacier inventory and variations in glacier extent in Iceland from the Little Ice Age maximum to 2019, Jökull, 12, 1–34, 2020.

Hjaltason, S., Guðmundsdóttir, M., Haukdal, J. Á., and Guðmundsson, J. R.: Energy Statistics in Iceland 2019, Tech. rep., Orkustofnun, 2020.

Hodgkins, R., Carr, S., Pálsson, F., Guðmundsson, S., and Björnsson, H.: Modelling variable glacier lapse rates using ERA-Interim re-analysis climatology: an evaluation at Vestari- Hagafellsjökull, Langjökull, Iceland, International Journal of Climatology, 33, 410–421, https://doi.org/10.1002/joc.3440, 2013.

Huai, B., van den Broeke, M. R., and Reijmer, C. H.: Long-term surface energy balance of the western Greenland Ice Sheet and the role of large-scale circulation variability, The Cryosphere, 14, 4181–4199, https://doi.org/10.5194/tc-14-4181-2020, 2020.

Jennings, K. S., Kittel, T. G. F., and Molotch, N. P.: Observations and simulations of the seasonal evolution of snowpack cold content and its relation to snowmelt and the snowpack energy budget, The Cryosphere, 12, 1595–1614, https://doi.org/10.5194/tc-12-1595-2018, 2018.

Jepsen, S. M., Molotch, N. P., Williams, M. W., Rittger, K. E., and Sickman, J. O.: Interannual variability of snowmelt in the Sierra Nevada and Rocky Mountains, United States: Examples from two alpine watersheds, Water Resources Research, 48, https://doi.org/10.1029/2011WR011006, 2012.

Jóhannesson, T., Aðalgeirsdóttir, G., Björnsson, H., Crochet, P., Elíasson, E. B., Guðmundsson, S., Jónsdóttir, J., Ólafsson, H., Pálsson, F., Rögnvaldsson, Ó., Sigurðsson, O., Snorrason, Á., Sveinsson, Ó. G. B., and Þorsteinsson, Þ.: Effect of Climate Change on Hydrology and Hydro-Resources in Iceland., Reykjavík : Orkustofnun, 2007, Reykjavík, 2007.

Jóhannesson, T. and Sigurðsson, O.: Samantekt um snjómælingar á hálendi Íslands, 2014.

Jónsson, T.: Langtímasveiflur I, Snjóhula og snjókoma, Veðurstofa Íslands, 2002.

Jónsson, T. and Jónasson, K.: Fimmtíu ára snjódýpt á Íslandi, Veðurstofa Íslands, 1997.

Lettenmaier, D. P., Alsdorf, D., Dozier, J., Huffman, G. J., Pan, M., and Wood, E. F.: Inroads of remote sensing into hydrologic science during the WRR era, Water Resources Research, 51, 7309–7342, https://doi.org/doi.org/10.1002/2015WR017616, 2015.

Lingli Wang, Qu, J. J., Xiaoxiong Xiong, Xianjun Hao, Yong Xie, and Nianzeng Che: A new method for retrieving band 6 of aqua MODIS, IEEE Geoscience and Remote Sensing Letters, 3, 267–270, 2006.

Magnússon, E., Belart, J. M., Pálsson, F., Anderson, L. S., Ágúst Þ. Gunnlaugsson, Berthier, E., Ágústsson, H., and Áslaug Geirsdóttir: The subglacial topography of Drangajökull ice cap, NW-Iceland, deduced from dense RES-profiling, Jökull, 66, 1–26, 2016.

Martinec, J. and Rango, A.: Areal distribution of snow water equivalent evaluated by snow cover monitoring, Water Resources Research, 17, 1480–1488, https://doi.org/10.1029/WR017i005p01480, publisher: John Wiley & Sons, Ltd, 1981.

Milly, P. C. D., Betancourt, J., Falkenmark, M., Hirsch, R. M., Kundzewicz, Z. W., Lettenmaier, D. P., and Stouffer, R. J.: Stationarity Is Dead: Whither Water Management?, 319, 573, https://doi.org/10.1126/science.1151915, 2008.

Molotch, N. P., Painter, T. H., Bales, R. C., and Dozier, J.: Incorporating remotely-sensed snow albedo into a spatially-distributed snowmelt model, Geophysical Research Letters, 31, https://doi.org/10.1029/2003GL019063, 2004.

Nawri, N., Björnsson, H., Petersen, G. N., and Jónasson, K.: Empirical Terrain Models for Surface Wind and Air Temperature over Iceland, VÍ, 2012-009, Reykjavík : Veðurstofa Íslands, 2012, 2012.

Ohmura, A.: Physical Basis for the Temperature-Based Melt-Index Method, 40, 753–761, https://doi.org/10.1175/1520-0450(2001)040<0753:PBFTTB>2.0.CO;2, 2001.

Painter, T. H., Rittger, K., McKenzie, C., Slaughter, P., Davis, R. E., and Dozier, J.: Retrieval of subpixel snow covered area, grain size, and albedo from MODIS, 113, 868 – 879, https://doi.org/https://doi.org/10.1016/j.rse.2009.01.001, 2009.

Pálsson, F., Guðmundsson, S., and Björnsson, H.: Afkomu- Og Hraðamælingar á Langjökli Jökulárið 2011–2012., Tech. Rep. LV-2015-076, Institute Earth Science, Univeristy Iceland and Landsvirkjun, 2013.

Perkins, H., Hopkins, T. S., Malmberg, S.-A., Poulain, P.-M., and Warn-Varnas, A.: Oceanographic conditions east of Iceland, Journal of Geophysical Research: Oceans, 103, 21 531–21 542, https://doi.org/doi.org/10.1029/98JC00890, 1998.

Plüss, C. and Ohmura, A.: Longwave Radiation on Snow-Covered Mountainous Surfaces, 36, 818–824, https://doi.org/10.1175/1520-0450-36.6.818, 1997.

Pálsson, F.: Vatnajökull: Mass balance, meltwater drainage and surface velocity of the glacial year 2018–19, Tech. Rep. LV-2020-016, Institute Earth Science, Univeristy Iceland and Landsvirkjun, 2020.

Pálsson, F., Gunnarsson, A., Jónsson, G., Pálsson, H. S., and Steinþórsson, S.: Vatnajökull: Mass balance, meltwater drainage and surface velocity of the glacial year 2014–15, Tech. Rep. LV-2016-031, Institute Earth Science, Univeristy Iceland and Landsvirkjun, 2016.

Pálsson, F., Gunnarsson, A., Jónsson, G., Pálsson, H. S., and Steinþórsson, S.: Vatnajökull: Mass balance, meltwater drainage and surface velocity of the glacial year 2018–19, Landsvirkjun, Reykjavík, RH-01-20 – LV-2020-016, 56, 2020a.

Pálsson, F., Gunnarsson, A., Pálsson, H. S., and Steinþórsson, S.: Afkomu- og hraðamælingar á Langjökli jökulárið 2018–2019, Landsvirkjun, Reykjavík, RH-10-20 / LV-2020-017, 27, 2020b.

Pálsson, F., Gunnarsson, A., Pálsson, H. S., and Steinþórsson, S.: Vatnajökull: Mass balance, meltwater drainage and surface velocity of the glacial year 2020–21, Landsvirkjun, Reykjavík, pp. 1–62, 2022.

Raleigh, M. S. and Lundquist, J. D.: Comparing and combining SWE estimates from the SNOW-17 model using PRISM and SWE reconstruction, 48, https://doi.org/10.1029/2011WR010542, 2012.

Raleigh, M. S., Landry, C. C., Hayashi, M., Quinton, W. L., and Lundquist, J. D.: Approximating snow surface temperature from standard temperature and humidity data: New possibilities for snow model and remote sensing evaluation, Water Resources Research, 49, 8053–8069, https://doi.org/10.1002/2013WR013958, 2013.

Rist, S.: Snjómæling inni á hálendinu. Úrkomumælingar., Vatnamælingar, Raforkumálastjóri, p. 9, 1958.

Rist, S.: Snjómælingar vetur 1965/1966., Vatnamælingar, Raforkumálastjóri, p. 1, 1966.

Rist, S.: Afstæð snjódýptarmæling á hálendinu, Orkustofnun, p. 4, 1981.

Rittger, K., Bair, E. H., Kahl, A., and Dozier, J.: Spatial estimates of snow water equivalent from reconstruction, Advances in Water Resources, 94, 345–363, https://doi.org/https://doi.org/10.1016/j.advwatres.2016.05.015, 2016.

Rögnvaldsson, Ólafur, A.: RÁVII: Tæknileg útfærsla á niðurkvörðun á Íslandsveðri, Tech. rep., Belgingur - Reiknistofa í Veðurfræði, Reukjavik, 2016.

Sandoval-Solis, S.: Water Resources Management in California, pp. 35–44, https://doi.org/10.1007/978-3-030-16565-9_4, 2020.

Schmidt, L. S., Aðalgeirsdóttir, G., Guðmundsson, S., Langen, P. L., Pálsson, F., Mottram, R., Gascoin, S., and Björnsson, H.: The importance of accurate glacier albedo for estimates of surface mass balance on Vatnajökull: evaluating the surface energy budget in a regional climate model with automatic weather station observations, The Cryosphere, 11, 1665–1684, https://doi.org/10.5194/tc-11-1665-2017, 2017.

Schmidt, L. S., Langen, P. L., Aðalgeirsdóttir, G., Pálsson, F., Guðmundsson, S., and Gunnarsson, A.: Sensitivity of Glacier Runoff to Winter Snow Thickness Investigated for Vatnajökull Ice Cap, Iceland, Using Numerical Models and Observations, Atmosphere, 9, https://doi.org/10.3390/atmos9110450, 2018.

Schmidt, L. S., Aðalgeirsdóttir, G., Pálsson, F., Langen, P. L., Guðmundsson, S., and Björnsson, H.: Dynamic simulations of Vatnajökull ice cap from 1980 to 2300, Journal of Glaciology, 66, 97–112, https://doi.org/10.1017/jog.2019.90, 2020.

Schneider, D. and Molotch, N. P.: Real-time estimation of snow water equivalent in the Upper Colorado River Basin using MODIS-based SWE Reconstructions and SNOTEL data, Water Resources Research, 52, 7892–7910, https://doi.org/10.1002/2016WR019067, 2016.

Sigurðsson, F. H., Pálsdóttir, T., and Antonsson, T. K.: Veðurstöð og veðurfar á Hveravöllum á Kili, Rit Veðurstofu Íslands 20, 2003.

Sigurðsson, O.: Fyrirkomulag snjómælinga á hálendi Íslands, Orkustofnun, p. 3, 2002.

Sveinsson, Ó.: Energy in Iceland: Adaptation to Climate Change, UNU-FLORES Policy Briefs, United Nations University Institute for Integrated Management of Material Fluxes and of Resources (UNU-FLORES), Dresden, 2016.

Van den Broeke, M., Reijmer, C. H., and Van De Wal, R. S.: A study of the surface mass balance in Dronning Maud Land, Antarctica, using automatic weather stationS, Journal of Glaciology, 50, 565–582, https://doi.org/10.3189/172756504781829756, 2004a.

Van den Broeke, M., van As, D., Reijmer, C., and Wal, R.: Assessing and Improving the Quality of Unattended Radiation Observations in Antarctica, Journal of Atmospheric and Oceanic Technology, 21, https://doi.org/10.1175/1520-0426(2004)021<1417:AAITQO>2.0.CO;2, 2004b.

Veðurstofa Íslands: Meteorological data from automatic weather stations, 2020.

Ágústsson, H., Hannesdóttir, H., Thorsteinsson, T., Pálsson, F., and Oddsson, B.: Mass balance of Mýrdalsjökull ice cap accumulation area and comparison of observed winter balance with simulated precipitation, Jökull, 63, 91–104, 2013a.

Ágústsson, H., Hannesdóttir, H., Thorsteinsson, T., Pálsson, F., and Oddsson, B.: Mass balance of Mýrdalsjökull ice cap accumulation area and comparison of observed winter balance with simulated precipitation, Jökull, 63, 91–104, 2013b.

Þorsteinsson, Þ., Jóhannesson, T., Sigurðsson, O., and Einarsson, B.: Afkomumælingar á Hofsjökli 1988-2017., Veðurstofa Íslands, Reykjavík, 2017-016, 82, 2017.